Copyright: The author,
Michael K.T. Theodoulides,
2020.

Defining the mechanistic toxicity of metal oxide nanoparticles *in vitro,* under physiologically relevant oxygen concentrations

Swansea University,

Medical School

Cardiff Metropolitan University,

Biomedical Department

Michael K.T. Theodoulides

Submitted to Swansea University in the fulfilment of the requirement for the degree of Doctor of Philosophy

2020

Declarations and Statements

DECLARATION

This work has not previously been accepted in substance for any degree and is not being concurrently submitted in candidature for any degree.

Signed [redacted] (candidate)

STATEMENT 1

This thesis is the result of my own investigations, except where otherwise stated. Where correction services have been used, the extent and nature of the correction is clearly marked in a footnote(s). Other sources are acknowledged by footnotes giving explicit references. A bibliography is appended.

Signed [redacted] (candidate)

STATEMENT 2

I hereby give consent for my thesis, if accepted, to be available for photocopying and for inter-library loan, and for the title and summary to be made available to outside organisations.

[redacted] didate)

This thesis is dedicated to my parents, Constandinos Theodoulides and Petroulla Christodoulou, for their upbringing which can be described by empathy, understanding and development of critical thinking. Without their support I wouldn't be able to get this far in my education.

Abstract

Metal oxide nanoparticles (MONPs) are intended for use in numerous consumer applications, leading to inevitable human exposure. Previous work conducted in hyperoxic cell culture conditions (21% O_2, 5% CO_2) with nanoparticles (NPs) has proven the ability of some material types to induce genotoxicity and inflammatoxicity. Alteration in intracellular calcium [i(Ca^{2+})] signalling is involved in facilitating toxicity through the alteration of signal-transduction pathways, but there is less understanding of the impact of NPs exposure upon changes in such signalling pathways. Furthermore, whilst human cells cultured in ambient air may induce a particular toxicity profile, this may not be the same under the physiologic oxygen conditions experienced in the human body. Therefore, the aim of this study was to assess the impact of anatase TiO_2 (NM-102), Rutile TiO_2 (NM-104) and dextran coated superparamagnetic Fe_3O_4 (dSPIONs) upon monocytes (THP-1), macrophages (dTHP-1) and hepatocarcinoma (HepG2) cells in both an *in vivo*-resembling physioxia environment (5%O_2, 5%CO_2) and hyperoxic cell culture conditions (21%O_2, 5%CO_2). Their impact on i(Ca^{2+}) homeostasis and how it relates to their potential genotoxic potential was also evaluated.

Due to the importance of different physicochemical characteristics for the facilitation of toxicity, all MONPs were characterized. MONPs hydrodynamic diameter (HD) and ζ-potential (ζ) in PBS were identified using dynamic light scattering: NM-102: HD=391.9nm, ζ =7.1±2.0mV; NM-104: HD=255nm, ζ=14.6 +/- 2.1mV; dSPIONs: HD=88.6nm, ζ =10.4±1.3mV. The possible toxic effect of NPs depends on their concentration and duration of their interaction with cells. Therefore, following 24h exposure to dSPIONs (0-100µg/ml), concentration-dependent and cell-type-dependent (dTHP1>THP-1>HepG2) significant increases in NP-cellular interaction were observed, which was significantly greater in the physioxic culture environment. Concurrent, significant loss of dSPION-associated cell proliferation (evaluated using relative population doubling) in all cell lines and significant increases in DNA damage was also identified in HepG2 cells (using the cytokinesis block micronucleus assay), albeit only in physioxia. Exposure to ≥10ug/ml NM-102 and NM-104 resulted in significant, two-fold increases in micronuclei formation in HepG2 in both environments. All MONPs induced a significant increase in tumour necrosis factor-α and interleukin-8 secretion in all cell lines and oxygen culture environments. Increase in the production of the chemokines was correlated with the observed HepG2 cell genotoxicity. In all cell lines and cell culture environments, treatment for up to 5h with NM-102 or dSPIONs triggered cell type specific increases in i(Ca^{2+}) that correlated with the reduction of cellular antioxidant glutathione (measured after 5h treatment with all the MONPs). After pre-treatment of the cell lines with antioxidant trollox in all cell culture environments i(Ca^{2+}) appeared to be increased independently from the change of cellular redox status.

Environment-specific biological interaction and impacts with regard to NP uptake, genotoxic effects, and consequence on cellular signaling mechanisms were only observed with dSPIONs in a physioxic culture environment, while NM-102 and NM-104 induced similar effects in both environments. The results presented in this study allow the conclusion that the environmental oxygen content has an impact on the NP toxicity profiles although it is NP dependent.

Table of Contents

Chapter 1: General Introduction 1

1.0 General Introduction 2

1.1 NP physicochemical properties influencing their uptake and toxicity 4

1.1. 1 Size 4

1.1.2 Shape and Agglomeration 5

1.1.3 Surface Properties 6

1.1.4 Chemical Composition and Purity 8

1.2 Nanoparticle Cellular Uptake 8

1.2.1 Phagocytosis 10

1.2.2 Endocytosis 10

1.2.3 Non-Endocytic Mechanisms 12

1.3 The Toxicological Effects of NPs 13

1.4 DNA Damage and Genotoxicicty 18

1.4.1 Iron Oxide NPs (IONP's) 20

1.4.2 Titanium dioxide polymorphs (Titania NPs/TiO_2 NPs) 25

1.5 Introduction to Ca^{2+} Signalling 30

1.5.1 Altered Ca^{2+} homeostasis, cellular function and the effect of NP treatments 34

1.6 Physioxic Cell Culture Environment 39

1.7 Aims of thesis 42

Chapter 2: General Materials and Methods 43

2.1 Chemicals and Reagents 44

2.2 Particle Preparation and Characterization 44

2.2.2 Dispersion SOP for TiO_2 44

2.2.3 NP Endotoxin Identification 45

2.2.4 TiO_2 NP Sedimentation Studies 46

2.2.5 Light Scattering 46

2.2.6 Determination of Zeta potential using DLS 48

2.2.7 Ultraviolet-Visible spectroscopy (UV-Vis) 49

2.2.8 Scanning Electron Microscopy (SEM) 52

2.2.9 NP protein Corona Purification and identification 52

2.3 Cell culture 55

2.3.1 Oxygen cell Culture Environment 55
2.3.2 Culturing of the different cell lines 56
2.4 Cell section imaging by TEM 56
2.4.1 Cell Preparation and Resin Embedding for TEM 56
2.5 Quantification of dSPIONs-Cell Interaction through identification of Iron concentrations 57
2.6 Investigation of TiO_2 NPs cellular interaction 58
2.7 Pro-Inflammatory cytokine quantification using an Enzyme-Linked Immunosorbent Assay (ELISA) 59
2.8 Intracellular reduced Glutathione 60
2.9 Cell viability assessment 60
2.10 *In Vitro* Cytokinesis Block Micronucleus assay (CBMN) 61
2.10.1 Cell Harvesting and Micronucleus scoring 61
2.10.2 Centromere Staining 62
2.11 Mitotic Spindle analysis 63
2.12 Intracellular Ca^{2+} signalling 64
2.13 Measurement of intracellular Ca^{2+}-antioxidant pre-treatment 65
2.13.1 Determine nation of the effects in different Ca^{2+} organelles 65
2.13.2 Immediate response to changes in intracellular Ca^{2+} homeostasis 65
2.14 Data and Statistical Analysis 67
Chapter 3: Primary and secondary characterization of metal oxide NPs 68
3.1 Introduction 69
3.1.3 Study Aim and objectives 71
3.2 Materials and Methods 72
3.2.1 Particle Preparation and Characterization 72
3.2.2 Dynamic light scattering and NP tracking analysis 72
3.2.3 TiO_2 NP sedimentation Studies 73
3.2.4 Ultraviolet-visible spectroscopy (UV-Vis) 74
3.2.5 NP protein corona purification and identification 75
3.2.6 NP endotoxin identification 75
3.2.7 Statistical analysis 75
3.3 Results 76
3.3.1 Visual identification of sedimentation of Titanium dioxide NPs 76

3.3.2 Hydrodynamic Diameter identification 81
3.3.3 Investigation of suspension stability of Titanium dioxide NPs using UV-Vis spectrophotoscopy 84
3.3.4 Electron microscopy imaging of Anatase (NM-102) and Rutile (NM-104) TiO_2 87
3.3.5 Identification of the hard protein corona in the different suspension liquids 91
3.3.6 LAL Gel Clot Test for Endotoxin Contamination of the different MONPs 93
3.4 Discussion 94
3.4.1 Primary and secondary characterization of dSPIONs and comparison of dynamic light scattering techniques 94
3.4.2 Primary and secondary characterization of TiO_2 NPs 96
3.4.3 Protein Corona and endotoxin contamination of MONPs 100
3.4.4 Summary and Conclusion 102
Chapter 4: Comparison of NP-cell interactions and toxicity under culture environments with distinct oxygen levels. 103
4.1 Introduction 104
4.1.2 Study Aim and objectives 106
4.2 Materials and Methods 107
4.2.1 Cell culture 107
4.2.2 Physioxia (5%O_2) experiments 107
4.2.3 Cell viability assessment 107
4.2.4 Pro-Inflammatory cytokine quantification using an Enzyme-Linked Immunosorbent Assay (ELISA) 108
4.2.5 Intracellular reduced Glutathione 108
2.4.6 Cell Preparation and Resin Embedding for TEM 108
4.2.7 Iron-cell interaction 108
4.2.8 Flow cytometry for identification of cellular interaction with titanium dioxide polymorphs 108
4.2.9 Micronucleus assay 109
4.2.10 Centromere staining 109
4.2.11 Mitotic spindle analyses 109
4.2.12 Statistical analysis 110
4.3 Results 111
4.3.1 Characterization of cellular behaviour in culture environments with differing oxygen content 111

4.3.2 NP-cell interaction 119
4.3.3 Uptake and cell compartmentalization determined by TEM 124
4.3.4 Toxicity assessment of MONPs in different culture environments 132
4.3.5 Centromere Staining 138
4.3.6 Mitotic Spindle Analyses 140
4.4 Discussion 141
4.4.1 Culturing the different cell lines in the different oxygen culture environments 141
4.4.2 NP-Cell Interaction/Uptake and Future work 143
4.4.3 Investigation of the toxicological effects in different oxygen culture environments 146
4.4.4 Summary and Conclusion 148
Chapter 5: Understanding the toxicological mechanisms of the metal oxide NP exert effects. 149
5.1 Introduction 150
5.1.1 Chapter 5 Aim 152
5.2 Materials and Methods 153
5.2.1 Cell culture 153
5.2.2 Physioxia (5%O2) experiments 153
5.2.3 Pro-Inflammatory cytokine quantification using an Enzyme-Linked Immunosorbent Assay (ELISA) 153
5.2.4 Intracellular reduced Glutathione 154
5.2.5. Intracellular Ca^{2+} signalling 154
5.2.6 Statistical analysis 155
5.3 Results 156
5.3.1 Glutathione depletion 156
5.3.2 Quantification of Intracellular Ca^{2+} Concentrations 158
5.3.3 Inflammatory cytokine quantification using an Enzyme-Linked Immunosorbent Assay (ELISA) 176
5.4 Discussion 182
5.4.2 Cellular antioxidants depletion and Oxidative stress 182
5.4.3 Intracellular Ca^{2+} signalling 183
5.4.4 Pro-inflammatory responses 186
5.4.5 Summary and Conclusion of Chapter 5 188

Chapter 6: General Discussion 189
6.1 Fulfilment of the objectives of this Study 190
6.1.1 Objectives and Summary of Chapter 3 190
6.1.2 Objectives and Summary of Chapter 4 193
6.1.3 Objectives and Summary of Chapter 5 196
.....198
6.2 Discussion of NP-Cell Interaction findings, and their Implications 199
6.3 Evaluation of the Cytotoxicity and Genotoxicity of the NPs under investigation 201
6.4 Elucidation of Cellular signalling mechanics triggered following NP exposure 203
6.5 Suggestions for Future Research.....207
6.6 General Conclusion 211
Chapter 7: References 212
Appendix 1: Use of UV-Vis Results for calculation of NP concentration in Suspension.... 246
Appendix 2: Additional results acquired in physioxia for i(Ca^{2+}) Signaling 247
1. Cytosolic Ca^{2+} immediate response to MONPs treatments.....247
2. Intracellular Ca^{2+} responses to GPN/ MONPs treatment.....250

List of Figures

Figure 1.1: A synopsis of the different cellular uptake mechanisms for the internalization of particles at both nano- and macro- scales.. 9
Figure 1.2: A schematic diagram summarizing the formation of ROS from nicotinamide adenine dinucleotide phosphate (NADPH) oxidase and mitochondria and the mechanisms involved in scavenging of ROS. 14
Figure 1.3: Suggested Mechanisms for the induction of Toxicity by Nanoparticles. 15
Figure 1.4: Ca^{2+} "On and Off mechanisms", the cellular calcium transporters and calcium storage organelles.. 32

Figure 3.1: Visual identification of TiO_2 sedimentation after dispersion at a concentration of 1mg/ml over time… 77
Figure 3.2: Visual identification of TiO_2 sedimentation following suspension in cell culture medium 78
Figure 3.3: Visual identification of sedimentation after dispersion of (A) NM-102 and (B) NM-104 at a concentration of 100µg/ml. 79
Figure 3.4: Visual identification of sedimentation in a suspension of TiO_2 in cell culture medium.. 80
Figure 3.5: Hydrodynamic diameter (HD) of Anatase (NM-102) and Rutile (NM-104) dispersed in 0.05% BSA.. 82
Figure 3.6: Size distribution of dSPION following NP tracking analysis (NTA) and Nano ZSizer measurements. 83
Figure 3.7: Whole spectrum screening of 100µg/ml of NM-102 and NM-104 in dispersion buffer at (A) 0h (B) after 2h of incubation and (C) after 24h of incubation. 85
Figure 3.8: Calculated concentration of NM-102 and NM-104 in suspension after incubation for 0h, 2h and 24h. 86
Figure 3.9: SEM images of Anatase (NM-102) TiO_2 prepared using the hang and dry approach on a silicon wafer.. 88
Figure 3.10: SEM images of Rutile (NM-104) TiO_2 prepared using the hang and dry approach on a silicon wafer.. 89
Figure 3.11: Hard protein corona of MONPs separated using SDS-PAGE. 92

Figure 4.1: Relative population doubling (RPD) of THP-1 cells cultured in different oxygen culture environments… 111
Figure 4.2: Relative population doubling and MN concentration of HepG2 in the distinct oxygen culture environments. 112
Figure 4.3: Antioxidant and inflammatory cytokine production in the different oxygen culture environments. 114
Figure 4.4: THP-1 differentiation to dTHP-1 after incubation under hyperoxic and physioxic conditions with 50nmol PMA for the period of (A and D) 24h, (B and E) 48h and (C and F) 72h.... 116
Figure 4.5: Effect of PMA (50nmol) on cell number in a Hyperoxic and a physioxic environment. 117
Figure 4.6: Antioxidant and inflammatory cytokine production in the different oxygen culture environments. 118
Figure 4.7: Iron content of cell lines after treatment with dSPIONs under physioxia and hyperoxia environments 120
Figure 4.8: NM-102-cellular interaction investigated using flow cytometry.. 122
Figure 4.9: NM-104-cellular interaction investigated using flow cytometry 123
Figure 4.10: TEM image of a untreated THP-1 single cell, this is a control image in the untreated control.. 125
Figure 4.11: TEM imaging for the investigation of NM-102 uptake and compartmentalization in THP-1 cells 126

Figure 4.12: TEM imaging for the investigation of NM-104 uptake and compartmentalization in THP-1 cells 127
Figure 4.13: TEM image of an untreated HepG2 single cell 128
Figure 4.14: TEM imaging for the investigation of NM-102 uptake and compartmentalization in HepG2 cells 129
Figure 4.15: TEM imaging for the investigation of NM-104 uptake and compartmentalization in HepG2 cells 131
Figure 4.16: Cell viability of THP-1 after treatment with MONPs under physioxia and hyperoxia: 133
Figure 4.17: Cell viability of THP-1 after treatment with MONPs under physioxia and hyperoxia: 135
Figure 4.18: Cell viability and Genotoxicity after treatment with MONPs under physioxia and hyperoxia 137
Figure 4.19: Aneugenic and clastogenic MN formation determined after centromere staining of HepG2 cells that were blocked during cytokinesis 138

Figure 5.1: Mechanisms resulting in the induction of toxicity by NPs. 151
Figure 5.2: Quantification of the reduction In the natural antioxidant glutathione in the distinct cell lines (1) THP-1, (2) dTHP-1 and (3) HepG2 after treatment with the different metal oxide NPs 157
Figure 5.3: Immediate response of intracellular Ca^{2+} concentrations to treatments of the distinct metal oxide NM, namely, (A) dSPIONs, (B) NM-102 and (C) NM-104 in the Hyperoxic environment. 159
Figure 5.4: Comparison of the immediate response of intracellular Ca^{2+} concentrations in the different cell lines 160
Figure 5.5: 30 min treatments with dSPIONs in the distinct environments with and without Thapsigargin pre-treatment to determine the levels of Ca^{2+} release from the ER. 162
Figure 5.6: 30 min treatments with NM-102 in the distinct environments with and without Thapsigargin pre-treatment to determine the levels of Ca^{2+} release from the ER. 164
Figure 5.7: 30 min treatments with NM-104 in the distinct environments with and without Thapsigargin pre-treatment to determine the levels of Ca^{2+} release from the ER. 166
Figure 5.8: Continuous measurements of intracellular Ca^{2+} concentrations after treatments of the distinct metal oxide NM, namely, (A) dSPIONs, (B) NM-102 and (C) NM-104 and administration of GPN (at 20seconds) in the Hyperoxic environment. 169
Figure 5.9: Comparison of measurements of intracellular Ca^{2+} concentrations after treatments of the different cell lines, namely, (A) THP-1, (B) dTHP-1 and (C) HepG2 to treatments with the distinct metal oxide NM (namely, dSPIONs, NM-102 and NM-104) and the administration of GPN. 170
Figure 5.10: Elevation in cytosolic Ca^{2+} in THP-1 cells after pre-treatment with Trolox 172
Figure 5.11: Elevation in cytosolic Ca^{2+} in dTHP-1 cells after pre-treatment with Trolox 173
Figure 5.12: Elevation in cytosolic Ca^{2+} in THP-1 cells after pre-treatment with Trolox 174
Figure 5.13: Ca^{2+} concentrations in the cytosol after treatment with MONPs for 24h 175
Figure 5.14: Quantification TNF-α production after treatment with MONPs 178
Figure 5.15: Quantification of IL-8 production after treatment with MONPs 181

Figure 6. 1: Suggested mechanism for the induction of DNA damage. 210

List of tables

Table 1.1: A brief description of the major cellular uptake pathways. 12

Table 2. 1: Dispersant characteristics……47
Table 2. 2: Preparation of 4% and 10% stacking and resolving gels for SDS-PAGE……54
Table 2. 3: dSPION, NM-102 and NM-104 volume used for each of the immediate response treatments……66

Table 3.1: True concentrations of an initially prepared 100µg/ml dose of NM-12 and NM-104 after incubation for 0h, 2h, and 24h……..87
Table 3.2: Elemental composition of (A) Anatase NM-102 and (B) Rutile NM-104 TiO_2, based on the results from EDX analyses……..90
Table 3.3: Gel clot assay results for endotoxin contamination of the different MONPs……93

Table 4.1: Aneugenic and clastogenic MN formation determined after centromere staining of HepG2 cells that were blocked during cytokinesis……..139
Table 4.2: Analytical results for mitotic Spindle Analysis. ……140

Table 6. 1: Summary of objectives and Results of Chapter 3, MONPs characterization……192
Table 6. 2: Summary of objectives and Results of Chapter 4……195
Table 6.3: Summary of objectives and Results of Chapter 5……..197
Table 6.4: Summary of objectives and Results of Chapter 5; intreacellular calcium signalling…….198

Chapter 1: General Introduction

1.0 General Introduction

The origin of the prefix “nano” comes from the Greek “nanos” that means “dwarf” and is used to signify the spatial measurement of 10^{-9} meters (nanometers). The origins of the concept of nanoscale manipulations can be traced back to 1959 and Richard Feynman whom discussed the direct manipulation of atoms (Feynman, 1959). The appearance of the branch of nanotechnology might have made nanostructured materials famous, although, nanoparticles (NPs) did not first come into existence with the emergence of nanotechnology.

NPs have been defined by the European Commission as *“A natural, incidental or manufactured material containing particles, in an unbound state or as an aggregate or as an agglomerate and where, for 50 % or more of the particles in the number size distribution, one or more external dimensions is in the size range 1 nm - 100 nm.*

In specific cases and where warranted by concerns for the environment, health, safety or competitiveness the number size distribution threshold of 50 % may be replaced by a threshold between 1 and 50 %.” (696/2011/EU).

By extrapolation from the above, fullerenes, graphene flakes and single wall carbon nanotubes with one or more external dimensions below 1 nm should be considered as NPs. NPs might have either crystalline or amorphous formations which sometimes can act as carriers for liquid droplets or gases. In addition to the solid, liquid, gaseous and plasma states, it is thought that Nano particulate matter should be considered a distinct state of matter due to the large surface area and quantum size effects it has. NPs that have diameter smaller than 100 nm are often called ultrafine particles (UFP) or ultrafine particulate matter.

The design, engineering and application of materials and devices that have been developed at the nanoscale can be defined as nanotechnology. Nanotechnology utilizes the distinctive physico-chemical, mechanical and electrical properties that are the result of the arrangement of matter at the nanoscale. The ultra-small size and unique physico-chemical properties of these new materials are furthering advances previously unattainable in a number of sectors including electronics, aerospace and medicine. NPs can be constructed from vast array of materials including gold, iron oxide, silver, carbon and titanium and they

have very different properties to their bulk micron-sized counterparts. They can come in a variety of different shapes such rods, particles and tubes, in addition to more complex structures including multi-walled tubes, nano peapods and nano cubes.

Numerous pre-existing materials are structured on the nanometer scale and are used in industrial processes to take advantage of the nanoscale phenomena. Nanoscale structures can be found in the natural world such as proteins, bacteria, viruses, or milk proteins (which is a nanoscale colloid). Technological advances have however promoted the research and manufacturing of engineered nano-structured materials. NP potential uses are vast and have already been applied to various different fields, for example the high surface area of many NPs such as titanium dioxide (TiO_2) gives them unique catalytic properties (Chaturvedi et al., 2012). In medicine a range of NPs including iron oxide nanoparticles (NPs) are being applied in tissue engineering, imaging enhancement and drug delivery systems (Cortajarena et al., 2014). Within aerospace and other industries, the low mass and extremely high strength of NPs such as carbon nanotubes makes them ideal for the construction of numerous components (De Volder et al., 2013). Moreover, a variety of NPs are utilised in a number of personal care products including zinc oxide (ZnO) and TiO_2 in sun cream, in addition to products such as moisturiser, foundation and hair colouring (Keller et al., 2014).

The evolution of the nanotechnology industry has led to the introduction of '*nanotoxicology*', which addresses the potential toxic health effects that may be caused through human exposure to engineered NPs (Donaldson *et. al.* 2004, Oberdörster *et. al.* 2005). Over the last decade numerous nanotoxicology studies have been undertaken and various NPs have indeed been shown to cause adverse toxicity. Initially the primary focus in the assessment of NM toxicity was on their ability to promote cytotoxicity (Soto et al., 2007, Jia et al., 2005, Magrez et al., 2006). However, it became increasingly evident that the focus needed to be broadened to investigate the potential of these materials to promote DNA damage. Assessment of a NPs ability to induce genetic damage is critical to consider given that exposure to a mutagenic material could ultimately lead to carcinogenesis (Singh et al., 2009). Also requiring consideration is the ability of NPs to be immunologically reactive.

1.1 NP physicochemical properties influencing their uptake and toxicity

NPs are classified based on their physicochemical characteristics, which are not only important for defining their application, but are also critical influencers on cellular uptake and subsequent cellular responses. The dimensions of engineered materials are measurable in the nanometer scale, but their size fluctuates between those of isolated NPs and the size of NP agglomerates. In contrast to the equivalent bulk material, NPs have distinct physicochemical properties that promote physiological interactions, such as size, surface properties, shape, composition, molecular weight, purity, stability and solubility (Hachani *et. al.*, 2013, Patri *et. al.*, 2006).

The importance of understanding how the different physicochemical characteristics of NPs affect their behaviour and distribution *in vivo and in vitro* must be pointed out. The different techniques used for studying the physicochemical characteristics of NPs have been described and discussed in the review published by Lin (Lin *et. al.* 2014). The following sections highlight each of the physicochemical features that are of importance in governing cell uptake and subsequent biological response.

1.1. 1 Size

Cellular response following exposure to NPs is highly dependent on their size , which also governs their ability to penetrate across the biological barriers (Ferrari 2008, Sunkhanova *et. al.* 2018). On one hand this can be considered to be an advantage and can be used for the development of new nano-medicines for clinical healthcare (Ferrari 2005, Sunkhanova *et. al.* 2018). Although on the other hand an exposure to engineered NPs may have negative effects upon human health.

Cellular uptake is strongly dependent on the size of the NP. NPs can be internalized by several mechanisms, either by using membrane channels (10-30nm wide), via direct transport across the phospholipid bilayer, or energy dependent mechanism such as endocytosis can lead to uptake (further described in Section 1.2). Additionally, NP size has been shown to strongly affect the binding and activation of membrane receptors to trigger receptor mediated endocytosis or alters subsequent signalling pathways (Jiang *et. al.* 2008). For example, the smallest silica NPs have a greater apoptotic effect against certain cell lines,

with greater toxicity exhibited by 20 nm silica NPs than negatively-charged 100 nm silica NPs (Kim *et. al.* 2012, Park *et. al.* 2013). Several NPs are reported to be more toxic than their larger counterparts with the same chemical composition, but there are examples where this is not always easily demonstrated, therefore a consensus has yet to emerge (Karlsson *et. al.* 2009). Therefore, due to the wide variance in the behaviour of different NPs the relationship of size and/or shape to NP toxicity has to be investigated on a case by case basis.

When particle size decreases, there is an increase in both the number of particles per unit of mass and the overall surface area. The dimensions of NPs will also influence the overall surface area, for example octagonal nanostructures will have a slightly bigger surface area than sphere shaped structures of the same size. Due to the unsatisfied high energy bonds of surface atoms that need to be stabilized, the catalytic activity of the material is enhanced; therefore, with bigger surface area the reactivity of a NP is increased (Oberdorster *et. al.* 2005).

1.1.2 Shape and Agglomeration

The shape and morphology of the NP influences its effects on cellular systems by governing cellular uptake, biocompatibility and retention in tissues and organs (George *et. al.* 2012, Jiang *et. al.* 2013, and Sunkhanova *et. al.* 2018). Interestingly, several publications support the fact that the cellular uptake is highly influenced by the shape of a NP. Chithrani and colleagues have shown that protein coated-gold NPs with a spherical shape show higher uptake than nanorods (Chithrani and Chan 2007); this is explained by greater membrane wrapping time required for the elongated particles. In addition, the dimensions of cylindrical shaped materials influence strongly their ability to be internalized; this is observed in particles with high aspect ratio and some symmetry (Granton *et. al.* 2008).

Phagocytosis of NPs by macrophages is also dependent on carrier shape (Decuzzi *et. al.* 2009,Champion and Mitragotri, 2009, Sunkhanova *et. al.* 2018). Ispas and colleagues have shown that spherical nickel NPs had lower levels of toxicity compared to dendrimer NPs with the same composition towards zebrafish embryos (Ispas *et. al.* 2009). In another example, different shapes of silver NPs were tested against *E.coli* and zebrafish embryos; interestingly plate-shaped NPs were more hazardous than rod, spherical, or wire shaped NPs (George *et. al.* 2012).

The state of agglomeration also influences translocation of NPs in the organism (Powers *et. al.* 2009). The tendency of several NPs to agglomerate under physiological conditions is due to their innate hydrophobicity, which is determined by the material the surface consists of. An *in vitro* study of silica NPs revealed that a potential trigger of pulmonary pathogenesis might be shape-driven agglomeration (Brown *et. al.* 2007). The formation of agglomerates is controlled by the chemistry and the charge of the surface, the behaviour depends on their surrounding environment, and in particular factors such as the pH or ionic strength (Jiang *et. al.* 2009).

A major change in free energy occurs in the case of large and elongated NPs; the reason is that only one particle bound by several receptors is transported by one vesicle (Gao *et. al.* 2005, Sunkhanova *et. al.* 2018). This also results in the decreased uptake of other particles due to less available binding sites (Chithrani *et. al.* 2006, Sunkhanova *et. al.* 2018). More time is needed to wrap large (agglomerated) particles (Chithrani and Chan 2007). In contrast multiple small particles can be internalized in one vacuole, the downside is that single attachments per NP are present therefore the energy release is weaker. For endocytosis to be energetically possible a minimum size of a single particle in proportion to the density of a ligand must exist in order for the decrease in the Gibbs free energy to induce membrane wrapping (Yuan and Zhanga 2010, Sunkhanova *et. al.* 2018).

1.1.3 Surface Properties

Interaction between NPs and their surrounding environment are due to their surface functionality, including both the presence of physical surface structures and their molecular or atomic composition (Patri *et. al.* 2006. Powers *et. al.* 2006, Sunkhanova *et. al.* 2018). Several important surface parameters affect interactions with organisms, including surface composition, surface energy, surface charge and species absorbance or adhesion (Ratner *et. al.* 2004, Sunkhanova *et. al.* 2018).

The dissolution/agglomeration status, aggregation and accumulation of NPs are relevant to the surface energy. Surface charge of NPs is estimated via the ζ potential and this regulates the aggregation and dispersion stability of NPs. Surface charge has a possible effect on receptor binding and physiological barrier penetration. The absorbance or adhesion of the

NPs is highly determined by their surface charge due to the ability to alter the surface of NPs, therefore it affects also the interaction with the attached species (Powers *et. al.*, 2006).

Receptor mediated endocytosis is induced when serum proteins are attached on the surface of NPs while they are incubated with cells in media (Khan *et. al.* 2007, Sunkhanova *et. al.* 2018). Xie and colleagues have shown that iron oxide (Fe_3O_4) NPs coated with PEG when incubated in cell culture reduced aggregation and non-specific uptake by macrophage cells (Xie *et. al.* 2007). In another study non-coated Quantum dots were compared with Quantum dots of the same composition but coated with 700 and 6000 MW PEG; interestingly the PEG coated NPs showed a five-fold higher uptake by endocytosis (Chang *et. al.* 2005). However, during the process pores are created in the plasma membrane that may result in cellular toxicity and eventually the disturbance of the normal functions of the cell. This is due to destruction of the transmembrane proteins and the disturbance in the concentration balance of intracellular versus extracellular ions (Baoum *et. al.* 2010. Luyts *et. al.* 2013).

Several studies have shown greater uptake of positively charged NPs into the cell and/or lysosome in comparison with their neutral or negatively-charged counterparts (Baoum *et. al.* 2010, Luyts *et. al.* 2013). One of the explanations for the higher uptake of positively charged NPs is that phospholipids on the outer surface the plasma membrane are negatively charged, as is the intracellular environment, and therefore it is easier and faster for cationic NPs to be endocytosed in comparison to anionic NPs.

Interestingly, positively-charged NPs appear to be more toxic than their negatively charged counterparts. For example, the positively-charged amino-modified polystyrene-formulated NPs induce DNA damage to certain cell lines (Liu *et. al.*, 2011). Positively charged silver NPs (polyethyleneimine coated), were also highly toxic as a result of membrane damage caused to *Bacillus* species (El Badawy *et. al.* 2010). In contrast, negatively charged silica NPs demonstrated enhanced cytotoxicity and reactive oxygen species generation compared with NPs of the same composition but with weaker negative charge (Park *et. al.* 2013). Thus, indicating that surface charge alone cannot always be considered in isolation, when evaluating the potential hazard presented by NP exposure.

1.1.4 Chemical Composition and Purity

An important aspect that influences the toxicity of NPs is their chemical composition (Buzea *et. al.* 2007, Hardman 2006, Sunkhanova *et. al.* 2018). Several types of NPs exist such as carbon nanotubes, quantum dots, titanium dioxide (TiO_2), zinc oxide (ZnO), cerium oxide (CeO_2), iron oxides and silver NPs and others. To form a complex (e.g. capsule, chelate) in biomedical applications two or even more types of NPs are usually needed. Therefore, the difficulty of a chemical composition analysis of the NP complex is not comparable to that of a single entity (Patri *et. al.* 2006, Sunkhanova *et. al.* 2018). In addition, metal contaminants that are left behind by synthesis processes or purification processes (e.g. ultra-sonication, washing) have been shown to either modify the surface of NPs or oxidise them (Sayes *et. al.* 2006, Sunkhanova *et. al.* 2018). For example, NP quantum dots with core metalloids complexes that usually consist of widely used metals (e.g. cadmium, selenium) have been observed to induce cytotoxicity (Hardman 2006).

A number of different NPs with distinct chemical composition have been found to induce oxidative stress, including fullerenes, carbon nanotubes and metal oxides (Bonner 2007). A reactive particle composition is pointed out by a number of researchers as one of the most notable ways for reactive oxygen species (ROS) generation (Schins 2002). To generalise, if the surface is bound with metals and chemical compounds, a ROS response is accelerated (Wilson *et. al.* 2002). Interestingly when either free radicals or oxidants come into contact and bind to a NP's surface, further production of free radicals is observed. Quartz NPs have been identified to produce ROS (e.g. OH and O_2^-) because their surface is bound with SiO· and SiO_2· (Knaapen *et. al.* 2004, Sunkhanova *et. al.* 2018). Oxidative stress is also observed when ambient matter such as ozone and NO_2 are trapped on the surface of a particle (Buzea *et. al.* 2007, Sunkhanova *et. al.* 2018).

1.2 Nanoparticle Cellular Uptake

Cellular uptake of NPs is a key factor that influences toxicity (Hachani *et. al.*, 2013,Patri *et. al.*, 2006). Important mechanisms for cellular uptake of NPs are phagocytosis, endocytosis and diffusion (Lu *et. al.*2009, He *et. al.* 2010, Behzadi et al., 2017), as illustrated in **Figure 1.1**.

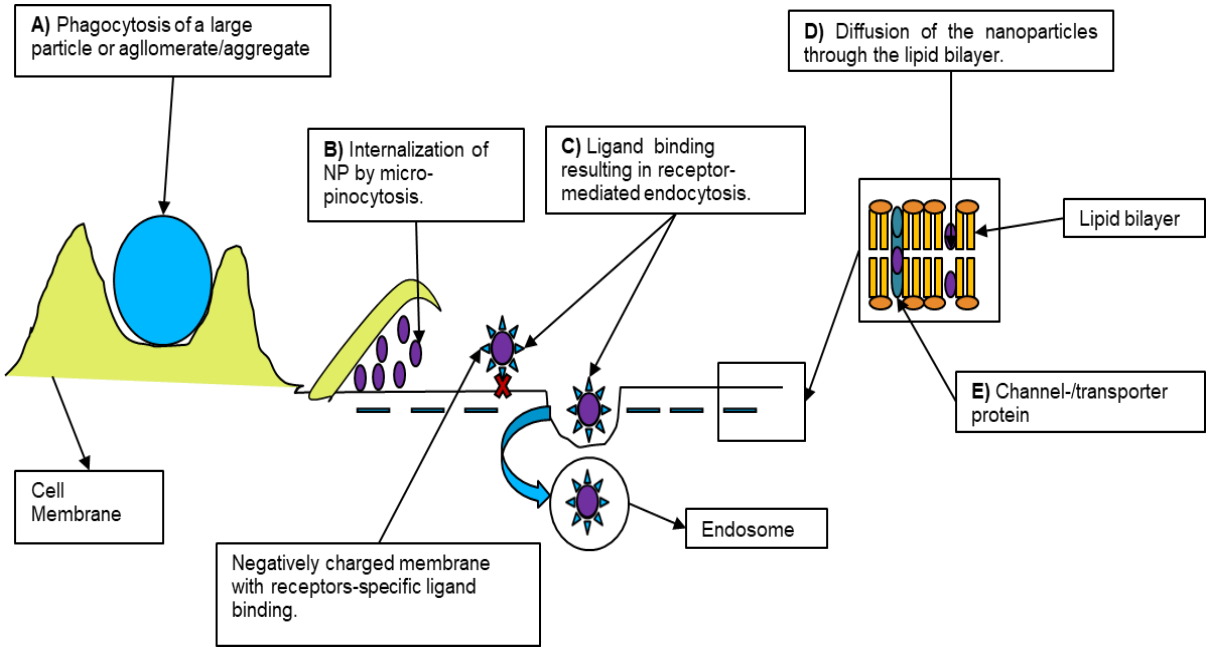

Figure 1.1: A synopsis of the different cellular uptake mechanisms for the internalization of particles at both nano- and macro- scales. A) Uptake of a large particle by phagocytosis. B) Liquid internalization with included particles by micropinocytosis. C) Specific binding of ligands to cell surface receptors and subsequent receptor-mediated endocytosis. D) Diffusion of NPs through the lipid double layer forming the cell membrane. E) Transporter/channel proteins.

1.2.1 Phagocytosis

Phagocytosis is a process by which solid and liquid particles such as proteins and other nutrients are enclosed by the cell membrane into vesicles. Static particles together with pathogenic microorganisms and dysfunctional and apoptotic cells with a diameter between 0.5 µm and 10 µm are engulfed by phagocytes and broken down (Aderem and Underhill 1999, Behzadi et al., 2017).

Clearance of particles smaller than 10µm that are able to reach the alveoli of lungs (Ng *et. al.* 2004, Behzadi et al., 2017) is primarily carried out by macrophage phagocytosis, which are responsible for the physical removal of particles from the alveoli across the alveolar epithelium or mucociliary escalator, to the lymph nodes of the lung (Peters *et. al.* 2006, Behzadi et al., 2017). Phagocytic cells such as the neutrophils (white blood cells) from the circulatory system are recruited to help in the removal of particles when extended exposure occurs.

Small NPs can pass through the epithelium of the alveolus to the interstitial space, since the mechanisms that keep the alveoli clean is not always efficient (Oberdörster *et. al.* 2005). From there the NPs can penetrate the circulation and the lymphatic system and affect other parts of the body (Sioutas *et. al.* 2005, Behzadi et al., 2017). Phagocytes are found at different sites in the body for example in the lungs, liver and spleen, and according to their location are given different names e.g. alveolar macrophages, Kupffer cells and splenic macrophages respectively (Thibodeau and Patton 2003, Behzadi et al., 2017).

1.2.2 Endocytosis

Endocytosis has been characterized as "the *de novo* production of internal membranes from the plasma membrane lipid bilayer" (Doherty and McMahon 2009). The major endocytic pathways are briefly described at **Table 1.1** but are also further analysed in the following paragraphs. Endocytosis and more specifically, pinocytosis is the process used to internalize large amounts of particles in solute form. According to the size of the vesicle and the protein used to form it, the mechanisms of pinocytosis is divided to four different processes (Table 1). The dimensions of vesicles are restricted therefore limited cargo size is internalized (Patel *et. al.* 2007). The assumption of a maximum size of NPs that could be internalized is

based on the size of the vesicles created by each species and cell types (Xu *et. al.* 2009). NPs of 200nm in size are not easily internalized by classical endocytosis (Patel *et. al.* 2007), while those that have a size above 200nm will not be internalized via a single clathrin-coated vesicle (McMahon and Boucrot 2011, Behzadi et al., 2017).

In highly ruffled areas of the cell membrane, a process known as micropinocytosis is continuously occurring regardless of the needs of the cell. In this process surrounding solutes are enclosed by the tips of the ruffles when they bend back toward the cell surface (Pastan and Willingham 1981).

Present in all mammalian cells, clathrin-mediated endocytosis occupies an important process for facilitating cellular entry. The process of regulating the molecular composition of the cell membrane to internalize either nutrients or pathogens is the product of several biochemical activities and the change in shape of the cell membrane (Merrifield 2004, Conner and Schimd 2003). A number of studies in both mammalian and yeast cells using multicolour real-time fluorescence microscopy have proven that the schism of vesicles and membrane invagination in the endocytic site is due to the recruitment of several proteins depending on the type of endocytosis which is taking place (Conner and Schmid 2003. Sun *et. al.* 2006. Merrifield *et. al.* 2006).

When receptors on the cellular membrane interact with NPs, the polymerization on the endocytic site of the cytosolic protein known as clathrin-1 takes place (Rappoport 2008). The NP is wrapped in a clathrin coated vesicle (CCV), which is formed due to the activity of dynamin's GTPase that pinches it off (Pucadyil and Schmid 2009). Which type of endocytosis is going to be used is determined by numerous factors alongside the particle's size (Mercer and Helenius 2009). Some of factors that influence the rate by which the particles are internalized by receptor mediated endocytosis (RME) are the availability of binding site, the rate of receptor diffusion towards the bound particle, wrapping time, the ability of the cell to create more vesicles and most importantly the interplay of energy liberated by bound receptors to drive the cargo into the cell (Gao *et. al.* 2005).

Table 1.1: A brief description of the major cellular uptake pathways.

Type of endocytosis	Brief description	Size of vesicle formed
1) Phagocytosis	Internalization of solid particles such as bacteria and yeast by specialized cells.	Dependent on the particles being engulfed.
2) (A)Pinocytosis **(B) Macro pinocytosis**	Fluid-phase uptake of extracellular molecules. Nonspecific mechanism by which fluid contents are taken up in the same concentration as in the surrounding medium. Multiple pinocytic pathways are possible (classed by size of the resulting vesicles).	(A) >1µm (B) 100 nm-5µm
4) Clathrin-mediated/ Receptor-mediated Endocytosis	Concentration of transmembrane receptors and bound ligands in "coated pits" on the plasma membrane formed by the assembly of cytosolic proteins, the main assembly unit being clathrin.	≈120 nm
5) Caveolae-mediated endocytosis	Flask-shaped invaginations in the plasma membrane that mediate uptake of extracellular molecules into the cell by specific receptor binding.	≈50–60 nm

1.2.3 Non-Endocytic Mechanisms

NPs are also proven to be internalized by non-endocytic mechanisms, such as diffusion or active transport (Lead 2009). Uncharged and hydrophobic molecules (e.g. O_2, CO_2) and lipid soluble substances are able to move from high to low concentration by the process of diffusion. In the process of facilitated diffusion water-soluble molecules pass passively through the membrane via pores. Because molecules with certain electrical charge and size are only allowed through the pores, specialized and/or larger molecules are assisted by carrier molecules to pass actively against the concentration gradient (Alberts *et. al.* 2002, Behzadi et al., 2017).

It was previously demonstrated that the uptake of particles with various sizes, namely 78 nm, 200 nm, and 1000 nm were not bound to the membrane suggesting that the

transport occurred via either pores or diffusion (Geiser *et. al.* 2005). The size of channel pores is 10-30nm; therefore NPs exceeding this size could not pass (Lead 2009). Additionally, charged particles are not able to pass through the cell membrane by diffusion (Lead 2009). The evidence to date however, suggests that cellular uptake of NPs by diffusion is unlikely and active transport mechanisms are more predominant for these materials (Lead 2009, Behzadi et al., 2017).

1.3 The Toxicological Effects of NPs

Several articles in the scientific literature have demonstrated that NPs of different compositions can contribute to the induction of oxidative stress, inflammation, DNA damage and cell death (Johnston *et. al.* 2010, Li *et. al.* 2008, Manke, Wang and Rojanasakul, 2013). In a biological system oxidative stress can be caused as a result of the excessive production of reactivate oxygen species (ROS) and the ability of the organisms to repair the resulting damage or readily detoxify the reactive intermediates; this can have potentially damaging biological responses. Either non- or enzymatic antioxidant systems are utilized by cells to overcome the excessive production of ROS (Sies 1991). Cellular and tissue mechanisms responding to increased oxidative stress include the production of antioxidant enzymes, this is also known as the hierarchical model of oxidative stress (Li *et. al.* 2008). Some of the functions of the antioxidants mentioned is illustrated in **Figure 1.2**. The balance in the generation and the neutralization of ROS by cellular antioxidants is referred to as a reduction-oxidation (redox).

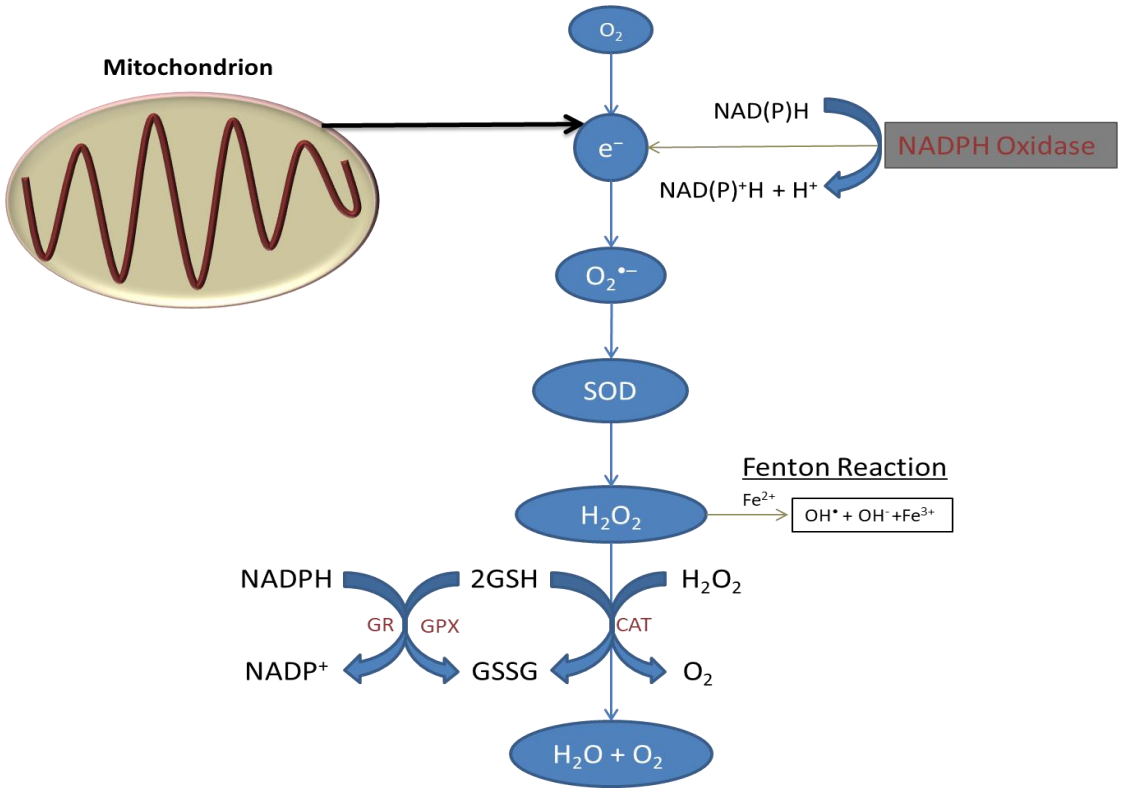

Figure 1.2: A schematic diagram summarizing the formation of ROS from nicotinamide adenine dinucleotide phosphate (NADPH) oxidase and mitochondria and the mechanisms involved in scavenging of ROS. SOD: superoxide dismutase; CAT: catalase; GPX: glutathione peroxidase; e−: electron; GR: glutathione reductase; and GSSG: Glutathione disulphide.

When an organism is presented with conditions of mild oxidative stress, nuclear factor (erythro-derived 2)-like 2 (Nrf2) is induced and activates (via transcription) phase II antioxidant enzymes. At an intermediate level a pro-inflammatory response is initiated, due to the effect of both the nuclear factor kappa-light-chain (Nf-κB) that enhances activated B-cells cascades, and redox-sensitive mitogen-activated protein kinase (MAPK) (Buzea *et. al.* 2007, Manke, Wang and Rojanasakul, 2013). Interestingly, when the levels of oxidative stress are extremely high, electron chain dysfunction and damage of the mitochondrial membrane occur that eventually lead to cell death. The increased production of ROS and the depletion of antioxidants favour the pro-oxidant effects of engineered NPs (Buzea *et. al.* 2007, Manke, Wang and Rojanasakul, 2013). **Figure 1.3** presents a schematic summary of some of the steps involved in oxidative stress that can arise in cells following exposure to NPs.

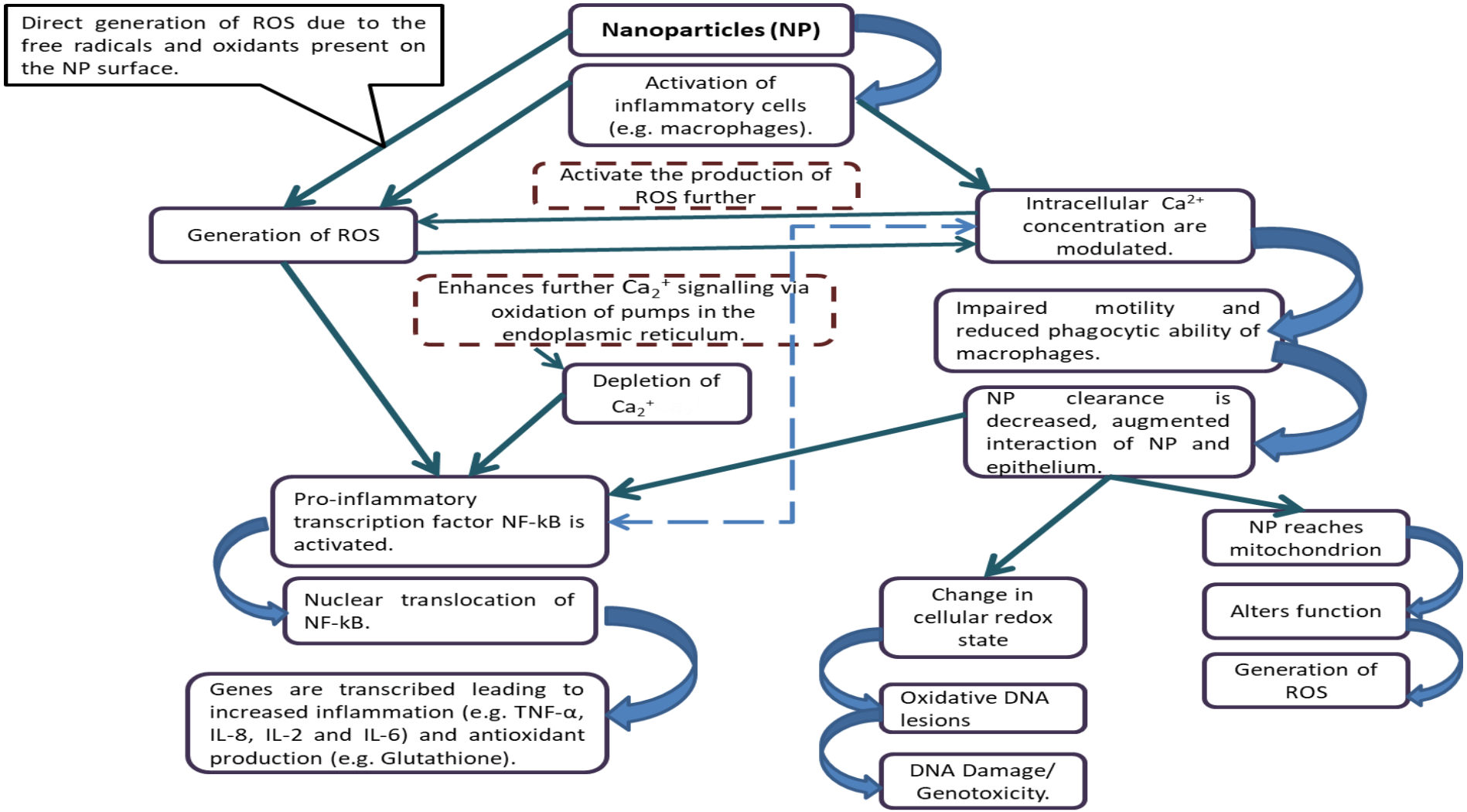

Figure 1.3: Suggested Mechanisms for the induction of Toxicity by Nanoparticles. The molecular incidents that lead to the induction of toxic effects at the cellular level after treatment to NPs.

As previously mentioned, NP physicochemical properties (e.g. size, shape, chemical composition and surface charge) can affect uptake and therefore induce ROS and eventually mediate injury (Shvetova *et. al.* 2012). Signalling pathways result in the increase of the expression of fibrotic and pro-inflammatory cytokines due to oxidative stress caused by carbon nanotubes in the lungs (Li *et. al.* 2010). Oxidative stress signalling cascades are induced when subcellular organelles and the cellular surface are bound by certain types of NPs, namely, titanium dioxide (TiO_2), zinc oxide (ZnO), cerium oxide (CeO_2), IONPs and silver NPs (Buzea *et. al.* 2007 Kennedy *et. al.* 2009, Evans *et. al.* 2017). Some NPs induce production of ROS but the exact underlying cellular mechanism for ROS generation is not fully understood and appears to be NP dependent. A number of mechanisms have been identified for several types of NPs; for example, carbon nanotubes damage the mitochondrion resulting in ROS generation (He *et. al.* 2011), while free radical mediated toxicity is a result of metal-based NPs inducing Fenton-type reactions (Huang *et. al.* 2010, Manke, Wang and Rojanasakul, 2013, Evans *et. al.* 2017). However, numerous studies have reported that toxicity arises following NP exposure without the presence of ROS, suggesting different pathways for the induction of cell death (Wang *et. al.* 2010, Manke, Wang and Rojanasakul, 2013).

NM oxidative stress potential is however not limited to those comprised of transition metals, a number of materials have been shown to catalyse ROS production at their surface in aqueous suspension including silica and carbon nanotubes (Magdolenova et al., 2014b). Furthermore, the mitochondria can be a major NM target, resulting in ROS stimulation via impairment of the electron transport chain and structural damage to NADPH like enzymes (Sioutas et al., 2005). Finally, there is evidence to suggest that NM exposure can cause a reduction in intracellular antioxidants. TiO_2 for instance has been shown not only to promote ROS production in human osteoblast cells but also decreased SOD activity (Niska et al., 2015).

Reactive species of molecular oxygen, for example superoxide anion (O2·−), hydroxyl radical (OH·), hydrogen peroxide (H_2O_2), singlet oxygen ($1O_2$), and hypochlorous acid (HOCl), have a key role in modifying cell signalling cascades. Interestingly ROS can be generated as a result of processes originating inside or outside of the cell. Intracellularly, nicotinamide adenine dinucleotide phosphate oxidase (NADPH oxidase) catalyses the reduction of one electron to produce the primary ROS O_2- , whereas metal catalysed Fenton reaction and dismutase reactions can lead to the production of OH· and H_2O_2 respectively (Thannicka and Fanburg 2000). Extracellularly derived factors such as environmental pollutants and engineered NPs act as inducers of ROS production, often triggering endogenous generation of ROS from sources including microsomes, peroxisomes, mitochondrial respiration, and through an inflammatory response. Thus, transition metal ion-catalysed Fenton-type reactions and mitochondrial respiration generate free radicals as a by-product (Vallyathan and Shi 1997, Manke, Wang and Rojanasakul, 2013); while the oxidative burst is induced by inflammatory phagocytes as a mechanism for defence against environmental pollutants, tumour cells, and microbes. Finally, while ROS production is induced by MONPs and other NPs as a principal mechanism of cytotoxicity via the production of free radicals, NPs can influence signalling processes such as modulation/activation of intracellular Ca^{2+} concentrations, cytokine production and transcription factors (Li *et. al.* 2010, Risom *et. al.* 2005, Manke, Wang and Rojanasakul, 2013).

Nevertheless, increased production of peroxide and free radicals can negatively influence the cell by disrupting proteins, lipid peroxidation or even damaging DNA. Carcinogenesis, loss of cell growth and fibrosis can also be a result of oxidative stress by activating intracellular/extracellular signalling networks (Huang *et. al.* 2010, Manke, Wang and Rojanasakul, 2013, Evans *et. al.* 2017). Oxidative stress from both controlled experimental and occupational exposures with various MONPs (TiO_2, ZnO, CeO_2, SPIONs) lead to airway inflammation and interstitial fibrosis (Donaldson *et. al.* 2006, Manke, Wang and Rojanasakul, 2013). Accordingly, the intracellular signalling systems such as MAPK and NF-κB mentioned earlier are shown to be more active in the presence of metal NPs (Smith *et. al.* 2001). ROS production is also induced endogenously in the mitochondrion, *"via impaired electron transport chain, structural damage, activation of NADPH-xidase like enzyme system, and depolarization of the mitochondrial membrane"* (Sioutas *et. al.* 2005). When murine

macrophages were cultured with cationic polystyrene nanospheres that are able to target mitochondria, apoptosis was induced due to high concentrations of O_2^- (Xia *et. al.* 2006, Manke, Wang and Rojanasakul, 2013). Given the role of NADPH oxidase in generation of ROS during the 'oxidative burst' of immune cells, it is interesting to note that ROS and reactive nitrogen species concentrations are increased with the activation of the immune system, an effect which might occur as a result of NP cell internalization (Knaapen *et. al.* 2004, Risom *et. al.* 2005, Wang and Rojanasakul, 2013, Evans *et. al.* 2017].

Finally, in addition to oxidative damage, reactive nitrogen species (RNS) have been identified in lungs that were exposed with NPs. When particles are deposited in the lung leading to the recruitment of inflammatory cells (e.g. phagocytes), clastogenic factors, RNS and cytokines are produced, in addition to the production of ROS (Bonner *et. al.* 2007). Reactive nitrogen species such as NO and peroxy-nitrite that is produced from the reaction of NO· and O_2 are produced in large amounts by phagocytes and are considered highly genotoxic. The nitric oxide synthase (iNOS) ability of phagocytes may result in DNA fragmentation, lipid oxidation, and protein dysfunction (Pryor *et. al.* 1993). For example, phagocyte influx observed *in vivo* after the exposure of lung tissue to quartz and SiO2 NPs resulted in the highly genotoxic production of RNS (Castranova *et. al.* 1998, Sunkhanova *et. al.* 2018).

1.4 DNA Damage and Genotoxicity

A key area in the toxicity assessment of NPs is its ability to promote DNA damage. If a test NM is capable of causing damage to genetic material it can ultimately result in carcinogenesis or if promoted in germ cells result in reproductive damage or the transfer of defects to subsequent generations (Singh et al., 2009). There are various mechanisms by which a NM could potentially induce genotoxicity, these mechanisms are categorised as either primary (direct or indirect) or secondary.

Direct primary DNA damage can result when a NM directly interacts with DNA. Depending on NP characteristics direct access to DNA maybe gained by penetration though nuclear pores or by simply becoming trapped there during mitosis. The number of studies providing evidence of direct primary DNA damage by NPs is limited in comparison with other mechanisms. However, NM nuclear uptake has been demonstrated in a number of studies; Ahlinder et al (2013) for instance showed via Raman spectroscopy that both α-FeO(OH)

(goethite) and TiO_2 are capable of passing though the nuclear pore (Ahlinder et al., 2013). Similarly, quantum dots have been shown to be able to locate to the nucleus of a human macrophage derived from the THP-1 cell line with subsequent binding to histone proteins (Nabiev et al., 2007).

Indirect primary DNA damage will stem from means other than direct NM-DNA contact. It may be caused by a NM damaging proteins associated with DNA maintenance/cell division or via the induction of oxidative stress through reactive oxygen species (ROS) production (Magdolenova et al., 2014a, Evans et al., 2016). The key mechanism by which NPs may induce indirect DNA damage is via oxidative stress. Transition metal-based NM's such as iron, copper, nickel, cobalt, and zinc may therefore release ions that can take part in the Fenton reaction promoting an increase in intracellular •OH formation. This free radical presents a significant risk for DNA damage as •OH is capable of attacking the DNA backbone and nucleotide bases promoting the formation of DNA lesions. More than 20 oxidative base lesions have been identified, the most notable being 8-hydroxyguanine (8-OH-dG) which frequently mis-pairs with thymine resulting in double stranded breaks and point mutations (Cooke and Evans, 2003). When tested in HepG2 cells Ag NPs promoted increased ROS production (quantified by the DCFDA assay) promoting downstream double stranded DNA breaks (Kim et al., 2009). The interaction of NPs with vital cellular proteins can potentially result in downstream damage. A NP may for instance interact with protein kinases associated with the regulation of the cell cycle. Progression through each phase of the cell cycle requires the completion of the previous phase; during G1 the cell prepares for growth followed by DNA replication in S phase. During G2/M phase essential proteins for division are synthesised and division is promoted resulting in two daughter cells (Norbury and Nurse, 1992). TiO_2 has been shown to be capable of damaging this process by deregulating the PLK1 protein which supports the maturation the centrosome in late G2/early prophase among other mitotic processes (Huang et al., 2009).

With substantial risk of NPs promoting genotoxicity, evaluation of this potential hazard is highly important. Due to the variety of potential mechanisms that can lead to DNA damage there are various *in vivo* and *in vitro* tests available. To fully establish the genotoxicity of a substance a battery of tests need to be undertaken to assess a number of genotoxic end points: point mutations, aneuploidy and chromosomal breakages (Doak et al., 2012). The

guidelines for this assessment include the *in vitro* bacterial reverse gene mutation assay (Ames; OECD 471), an *in vitro* chromosomal aberration or micronucleus assay (OECD 487 and 473) and an *in vitro* mammalian cell gene mutation test such as the (HPRT) assay (OECD 476). The *in vitro* CBMN assay is a OECD approved robust quantitative assay of chromosomal damage induced by a test chemical or material (OECD, 2014). The technique is based on the use of cytochalasin B (Cyto B), a cell permeable mycotoxin that inhibits actin filament polymerisation and blocks the formation of contractile microfilaments (Theodoropoulos et al., 1994). This actin inhibition freezes cell mitosis during anaphase preventing the cell from undergoing more than one round of cell division and results in the formation of binucleated cells. During anaphase small membrane bound nuclei known as micronuclei may become visible; these micronuclei may be the result of aneugenic (whole chromosome gain / loss) or clastogenic (chromosome breakage) damage (Fenech, 2000). Following treatment with a test agent micronucleus quantification in binucleated cells therefore provides an assessment of chromosomal aberration.

1.4.1 Iron Oxide NPs (IONP's)

A major focus of the present study is superparamagnetic iron oxide NPs (SPIONs). SPION's have several applications industrially and have also been proven to be an effective negative contrast agent in clinic imaging technologies such as MRI, optical imaging/MRI and MRI/PEP due to their ability to decrease T2 signals. Interestingly they can also disrupt the homogeneity of a magnetic field by causing a magnetic field gradient that affects water molecules (Clemente-Casares and Santamaria 2014). This magnetic field disruption can not only be viewed by MRI, but can also provide a mechanism that could be used in gene therapy for the tracking of transplanted cells (Maciony *et. al.* 2006, Arias *et. al.* 2018).

Macrophages are extravagated in inflamed tissue, in both the common inflammation process and autoimmune diseases, and as a result of the activation of endothelium in blood vessels. Because SPION's are endocytosed by macrophages the signals of this event can be enhanced when visualized by MRI. This compelling application of SPION's (Ferumoxytol) enhanced the prognosis of active ulcerative colitis, also it was shown to improve the diagnosis of Crohn's disease (D' Arienzo *et. al.* 2001, Maciony *et. al.* 2006, Arias *et. al.* 2018). In comparison to the previously used T1-gadolinium, ferumoxtran was proven to be a

massive improvement for the detection of pancreatic islet inflammation in Type 1A diabetes patients (Velinga *et. al.* 2009, Arias *et. al.* 2018). Additionally, of great importance was the discovery that the previously labeled as normal-appearing white matter in patients with multiple sclerosis was easily identified in USPION-based MRI due to the labelling of larger and better-defined areas (Vellinga *et. al.* 2009, Tourdias *et. al.* 2012, Arias *et. al.* 2018).

Aside from MRI imaging, SPION have been used in other therapeutic forms. For example, treatment with ferumoxytol via intravenous injections has been approved by both the FDA and EC in 2012 as a treatment therapy for iron deficiency for patients with chronic kidney disease; this was also particularly beneficial for patients that were unfit for oral iron treatment (Vadhan-Raj *et. al.* 2014, Hetzel *et. al.* 2014). Additionally, SPION's have been evaluated for use as a solid tumor thermotherapy, usually used after the initial cancer treatment alongside chemotherapy or radiation. To promote the warming of the region to high temperatures, IONPs fluid is administered within the tumor and an alternating magnetic field is applied. Numerous outcomes at both tissue and cellular level are seen when the temperature in the area is raised between 41-46 ºC (Wankhele *et. al.* 2012, Arias *et. al.* 2018). At a cellular level the hyperthermia induces the expression of heat-shock protein in elevated quantities, denatures proteins and finally induces apoptosis. The temperature elevation also affects the organisms at the tissue level in the tumor region in a number of ways such as changes in the pH, and in perfusion that results in oxygenation (Wust *et. al.* 2012). In combination these effects on the tissue for long periods of time may lead to necrosis.

The most common reason for the induction of toxicity and cellular damage by magnetic IONPs is due to the excessive production of ROS (e.g. O_2^-, -OH, H_2O_2) (Shafiri *et. al.* 2011, Singh *et. al.* 2012). Four sources for the creation of oxidative stress as a response to the exposure to IONPs' iron have been demonstrated (Kim *et. al.*2012), namely: generation of ROS from the surface of the IONP's; dissolved iron molecules produce ROS; alteration of the organelle (e.g. mitochondrial) functions; and induction of cell signalling pathways.

The importance of SPIONs size, composition and surface coating has been identified as the main reasons for the generation of toxicity by SPIONs (Rivet *et. al.* 2012, Singh et. Al. 2012, Hong *et. al.* 2011). Cytotoxicity caused by Fe_2O_3 NPs on A349 cells, a human alveolar

epithelial cell line, was identified via trypan blue exclusion; in contrast Fe_3O_4 NPs did result in the same cytotoxic effects (Karlsson *et. al.* 2009). A number of different IONP's coated with polyvinyl alcohol (Mahmoudi *et. al.* 2009) and Fe_3O_4 mesosporous silica composites (Huang *et. al.* 2012) cause minimal to no cytotoxicity when tested in the L-929 cell line. In a similar test where a tetrazolium salt assay was used instead of MTT, IONP's induced significant cytotoxicity in the fibroblast cell line L-929, showing that the test used to detect cytotoxity may influence the assay outcome (Hong *et. al.* 2011). Using trypan blue exclusion assay, the cytotoxic effects of uncoated Fe_3O_4 were compared with oleate-coated Fe_3O_4; the coated NPs were proven to be cytotoxic while in contrast were uncoated ION's were not, but sodium oleate alone was excluded as a cause of toxicity, thus demonstrating the important influence surface coating can have on the subsequent toxic response (Magdolenova *et. al.* 2013). Additionally, a study comparing the cytotoxic effects of IONPs in two cell lines, namely, HeLa and human retinal pigment epithelial cell line (RPE), proved that high concentrations of uncoated IONP induced significant cytotoxicity in both cell lines, whereas low concentrations were only significantly toxic to HeLa cells (Li *et. al.* 2012). A carboxy-dextran coated SPIONs that is already approved for use as an MRI negative contrast was incubated with human mesenchymal stem cells for 24 and 72 hours, but neither the significant toxicity nor successful chondrogenesis were induced (Yang *et. al.* 2011). In a study by Begini and colleagues IONPs coated with carboxy-dextran were used to treat human Amniotic Fluid Cells (hAFC); the internalization of the NPs had no effect on either the metabolism or the cell cycle of the cells (Bigini *et. al.* 2012). The studies perform in the past indicate that IONs with different characteristics such as size, composition and surface coating can have variable effects on the same cell line. In addition, the same IONPs may produce different results dependent upon the cell line used.

As exposure of cells to IONP's often induces cytotoxicity as a result of oxidative stress and ROS generation, several studies have investigated the relationship between antioxidant defense and NP cytotoxicity (Dwivedi *et. al.* 2014, Malvindi *et. al.* 2014). Chinese hamster lung cells were treated with to L-glutamic acid coated Fe_2O_3 for 36 hours and caused ROS induction, plus inactivation of a number of antioxidant enzymes and glutathion depletion, (Zhang *et. al.* 2012). In another example, exposure for 24 hours to magnetite (Fe_3O_4) in the nano-range led to endocytosis by A549 cells, and whilst cytotoxicity was not observed,

production of ROS and increased depolarization of mitochondria was significantly induced (Konczol *et. al.*, 2011).

The ability of iron to change from ferrous to ferric ions by readily accepting and donating electrons makes it important for maintenance of life (Kim *et. al.* 2012), as it has a prominent role in numerous metabolic pathways such as DNA synthesis, mitochondrial oxidative phosphorylation and cytochrome P450 function (Shander *et. al.* 2009). When IONP's are metabolized, the free iron that is produced from the endocytic compartments is incorporated to the cellular iron pool (Soenen and De Cuyper 2010). Excess iron quantities could be extremely toxic, therefore large doses of IONP's should be avoided (Kunzmann *et. al.* 2011). Studies have shown that excess iron targets the mitochondrial genome, therefore organs that have high mitochondrial activity such as the heart or liver have high vulnerability to iron toxicity (Eaton and Qian 2002). In one intriguing study by Malvindi *et. al.* it was shown that when IONP's coated with silica were suspended in an acidic environment that mimic the lysosomal pH~4.5, iron ions were released, whereas when suspended in either ultrapure water and cell culture medium that have neutral pH 7, ions were not observed. This finding suggests that these IONP's must be endocytosed releasing ions (Malvidi *et. al.* 2014). Additionally, the rate of degradation of the iron oxide NP's and therefore their ability to release iron ions is dependent on whether or not the physicochemical properties of the coating allow it (Mahon *et. al.* 2012, Singh *et. al.* 2012).

A key aspect of toxicity of NPs is their ability to induce DNA damage, therefore after reviewing the research published in the literature that explore the genotoxicity produced by IONP's, the most commonly used tests are the *in vitro* comet assay and micronucleus assay (used to test chromosomal aberrations in the cells). A positive genotoxic response after the treatment of A549 alveolar cells with nano-magnetite (Fe_3O_4) was observed using both the comet assay and the micronucleus assay; interestingly when the cell line was either pre-exposed to butylated hydroxyanisole or simultaneously exposed to N-acetylcysteine, both potent antioxidants that would reduce changes in the cellular redox state, the results were significantly reduced (Konczol *et. al.* 2011). When primary human leukocytes and human lymphoblastoid TK-6 cells were treated with oleate-coated nano-magnetite primary and oxidative DNA damage was observed using the comet assay, but interestingly when the cells were treated with uncoated nano-magnetite, no DNA damage was present (Magdolenova

et. al. 2013). This allows the conclusion that the coating reduced the production of transition metals from the surface of SPIONs, hence the reduction of catalyse ROS production and toxicity. In addition, when skin epithelial A431 and lung epithelial A549 cells were treated with nano-magnetite using the comet assay, DNA damage was observed (Ahamed *et. al.* 2012). The effect of nano-hematite was investigated on human IMR-90 lung fibroblasts and human BEAS-2B bronchial epithelial cells, results suggested it was also able to induced DNA damage (Bhattacharya *et. al.* 2009).

In two publications by Karlsson *et. al.* the ability of Fe_2O_3 and Fe_3O_4 to induce primary DNA damage was observed using the comet assay; additionally, increased oxidative stress was observed when A549 cells were treated with Fe_3O_4 NPs (Karlsson *et. al.* 2009). In contrast, the frequency of micronuclei was not increased when human lymphoblastoid cells were treated with uncoated Fe_2O_3 NPs or with either uncoated or dextran-coated Fe_3O_4 (Singh *et. al.* 2012). The exposure of Syrian hamster embryo cells to Fe_2O_3 and Fe_3O_4 NPs similarly did not show any increase in DNA damage or micronuclei formation (Guichard *et. al.* 2012). In a similar study Chinese hamster lung cells were treated with glutamic acid-coated Fe_2O_3, while disturbed cell redox status was observed, interestingly no significant genotoxic response was reported (Zhang *et. al.*, 2012).

Whilst there are many *in vitro* studies in the literature on SPION induced genotoxicity, there are fewer *in vivo* studies as they are more complexity, high in cost, time-consuming and most importantly are associated with ethical concerns surrounding the use of animals. However, a small number of *in vivo* genotoxicity have been performed that have generated important insights. In a study performed on Wistar rats, a single dose of Fe_2O_3 NPs was administered orally and demonstrated the ability of IONP's to penetrate the intestinal barrier (Singh *et. al.* 2013). The NPs were found to accumulate in organs such as the liver, spleen, kidney, heart and bone marrow; interestingly genotoxicity was not induced in leukocytes and the bone marrow cells when evaluated by the comet assay, while the micronucleus assay showed no significant results (Singh *et. al.* 2013). In other studies, mice were exposed to IONP's and significant induction of micronuclei were reported in the bone marrow after either the exposure to magnetite NPs intraperitoneally or polyaspartic acid-coated magnetite NPs following intravenous administration (Freitas *et. al.* 2002, Sadeghiani *et. al.* 2005).

Evaluating the results from the studies mentioned above allows the conclusion that the IONP's ability to induce genotoxicity is due to either oxidative stress-triggered DNA damage or DNA breaks. However, it must be pointed out that this ability is determined by the physicochemical characteristics of the particular IONP used (e.g. size, composition, or type of surface coating). As most studies have focused on oxidative stress induction, further investigation is however needed to determine if other mechanism are involved in DNA damage induction caused following IONPs exposure. Additionally, it is notable that a wide range of cell lines have been used in the scientific literature, which can introduce conflict as they each have varying capacities for cell uptake and sensitives to subsequent damage induced by NPs. Thus, it is important that relevant cell lines are selected, which relate to tissues associated with the primary or secondary (sites of accumulation following translocation) exposure sites in the human body.

1.4.2 Titanium dioxide polymorphs (Titania NPs/TiO_2 NPs)

Widespread use of titanium dioxide NPs (TiO_2 NPs) in both industrial and biomedical applications has resulted in an increasing need for identification and characterization of their effects on human health. Titania NPs are naturally occurring in three distinct polymorphs: rutile, anatase and brooklite. Rutile and anatase have a stable atomic structure/surface that makes them suitable for numerous applications. The two polymorphs form distinct crystalline structures in the form of TiO_6 octachedra chains; interestingly, anatase is known to transform to rutile in high temperatures (Vittadini *et. al.* 1998). The different crystalline structures have been reported to induce distinct biological effects to cells, with both their cytotoxic and genotoxic behaviour previously shown to be mediated by oxidative stress (Petkovic *et. al.* 2011, De Angelis *et. al.* 2012, Shukla *et. al.* 2013).

TiO_2 fine particles (FP) have been previously thought as poorly soluble entities that induce low toxicity, as a result they have been traditionally used as a "negative control" in both *in vitro* and *in vivo* toxicological studies (ACGIH 1992, Zhao *et. al.* 2009). However, based on recent studies this view was questioned. After two years of exposure of rats to high concentrations of TiO_2 FP lung tumours were developed (Lee *et. al.*1985). As a result, the International Agency for Research on Cancer (IARC), classified TiO_2 as a Group 2B carcinogen (possibly carcinogenic to humans) (IARC 2006). In 2017 an opinion was published by the

committee for Risk Assessment of the European Partnership for Chemicals Risk Assessment that suggested a harmonisation of the classification of TiO_2 NPs into a Group 2B carcinogen by inhalation that will come into effect in September of 2021.

The nanoparticulate form of TiO_2 has a greater catalytic activity when compared to TiO_2FPs, and as a result the use of TiO_2 NPs in both industrial and consumer products has greatly increased. The catalytic activity of these NPs has been attributed to their larger surface area per unit mass, which in turn is the result of their smaller sizes. As a result, a great concern was raised, that the same properties of TiO_2 NPs that make them attractive for industrial and consumer use may present unique bioactivity and challenges to human health (Maynard and Kuempel 2005). Due to their high stability, anticorrosive and photocatalytic properties TiO_2 NPs are used widely (Riu *et. al.* 2006, Ziental *et. al.* 2020). The catalytic ability is attributed to the high surface are of TiO_2 NPs, although it is suggested that anatase polymorph has a higher catalytic ability (Warheit *et. al.* 2007). TiO_2 NPs are widely used as a white pigment, this is due to its brightness and high refractive index, and therefore it is one of the most used NPs worldwide (Ortlieb 2010, Shukla *et. al.* 2010).

Among other applications, TiO_2 can be used in paints, coatings, plastics, papers, inks, medicines, pharmaceuticals, food products, cosmetics, and toothpaste (Wolf *et. al.* 2003, Ziental *et. al.* 2020). TiO_2 is also used as a component for articulating prosthetic implants (e.g. hip, knee), but it was observed that a high number of these implants fail, possibly as the result of degradation of the materials in the implant and a chronic inflammatory response to the implant material (Patri *et. al.* 2009, Ziental *et. al.* 2020). It is suggested that these NPs can be a useful tool in advanced imaging and nanotherapeutics. Some of the examples include use in photodynamic therapy as photosensitizers (Szaciłowski *et. al.* 2005, Ziental *et. al.* 2020, Yuan *et. al.* 2010). Interestingly, TiO_2 NPs have also shown antibacterial properties under UV light irradiation (Wiesenthal *et. al.* 2011, Ziental *et. al.* 2020). The unique physical properties of TiO_2 NPs make them ideal for use in various skin care products: accordingly, these NPs are also investigated for treatments for acne vulgaris, recurrent condyloma accuminata, atopic dermatitis, hyperpigmented skin lesions (Wiesenthal *et. al.* 2011). Finally, as was described for IONPs, TiO_2 NPs are functionalized for use as nanocarriers, as they can increase the concentration of drugs in the locations of the body mostly needed (e.g. cancer cells) (Wiesenthal *et. al.* 2011, Ziental *et. al.* 2020).

Titania NPs have been described by multiple studies to exhibit low solubility in different environments, due to their high agglomeration and aggregation status (De Angelis *et. al.* 2012, Andersson *et. al.* 2011, and Baranowska-Wójcik *et. al.* 2019). However, in lower concentrations (e.g. 80μg/ml), the stability of TiO_2 NP suspensions is significantly increased (Shukla *et. al.* 2013). The mechanism for induction of genotoxicity associated with NPs with low solubility, such as TiO_2, is commonly reported to be the result of damage caused by ROS (Shukla *et. al.* 2013).

In vitro assessment of the toxicity induced by NPs, including the expression of inflammatory mediators and activation of intracellular transduction pathways, is strongly correlated with size/agglomeration dependent NP uptake and interaction with distinct cell lines (Andersson *et. al.* 2011, Baranowska-Wójcik *et. al.* 2019).

In the various *in vivo* studies different exposure routes have been used including, inhalation, dermal exposure, intra-tracheal instillation, oral gavage, intragastric application and intraperitoneal or intravenous injection. One of the first articles that reported a greater hazard produced by TiO_2 NPs (21nm) in comparison to TiO_2 FP was produced by Oberdorster and colleagues, whose article reported that when both the particles at the same mass burden were used, greater amounts of TiO_2 NPs entered the alveolar interstitial in the lungs and induced greater pulmonary inflammatory response (Oberdorster *et. al.* 1994). In the work done by Sager and colleagues in a rat model, intra-tracheal instillation of well-dispersed suspensions of a mixed batch of both TiO_2 NP polymorphs (80/20 anatase/rutile; 21 nm, P-25) and TiO_2 FPs (100% rutile; 1μm) were conducted. After administration in an equal mass burden, TiO_2 NPs had a 40-fold greater potency in inducing lung inflammation and damage at both the first and 42nd day post-exposure than TiO_2 FP (Sager *et. al.* 2008).

The results of numerous studies *in vitro* revealed that TiO_2 NPs are more toxic than FPs (Zhao *et. al.* 2009,Fabian *et. al.* 2008, Oberstroder 2001, Baranowska-Wójcik *et. al.* 2019). As shown by Shukla *et. al.*, anatase NPs with a diameter of 192.5nm were internalized by HepG2 cells after a 20h exposure, and interestingly accumulated close to the nuclear region. In addition, in a dose range of 0-80μ/ml an increase of flow cytometric side scattering (cell internal complexity) was observed, which can be correlated with a dose dependent increase in the concentration of internalized NPs (Shukla *et. al.* 2013). Uptake and distribution of different TiO_2 NPs was investigated

using Raman spectroscopy, this allowed both visual identification through the optical micrographs, and analysis of the intensity of the Raman spectra obtained at different locations of A549 cells. Using transmission electron microscopy (TEM), endosomal uptake of both rutile and anatase TiO_2 was observed within a 15min period. Distribution of TiO_2 in the intracellular environment was highly dependent on the dispersion of the NPs in solution. Preferential uptake of equally dispersed titania with a smaller size was observed, whereas the polymorph type had no effect on the extent of uptake. Additionally, Raman mapping showed that small concentrations of anatase were observed in the cellular nuclear region (Anderrson *et. al.* 2011). Finally, De Angeli *et. al.* and colleagues quantified the levels of titanium in colorectal cells after treatment with anatase for 6h using inductively coupled plasma mass spectrometry (ICP-MS): a greater dose dependent increase was identified when CACO-2 cells were cultured with fetal calf serum (FCS) than without (De Angeli *et. al.*2012).

With regard to impact on cell viability, after treatment of HepG2 cells with anatase TiO_2 over a dose range of 0-80µg/ml for both 24h and 48h, showed significant reduction in cell viability using both the MTT assay and neutral red uptake, while apoptosis due to NP exposure was induced via the caspase-dependent pathway(Shukla *et. al.* 2013). Significant genotoxicity was observed using both the comet and cytokinesis block micronucleus assays. Reduction in glutathione levels with concomitant increase in lipid peroxidation and reactive oxygen species generation was observed. Thus, the genotoxic behaviour of anatase TiO_2 is mediated via the induction of oxidative stress (Shukla *et. al.* 2013). In another study by Petrovic and colleagues, both anatase and rutile TiO_2 NPs, were used to treat HepG2 cells for a period of 20h at concentrations of up to 250µg/ml. In contrast to Shukla *et. al.* the cellular viability of the cells was not significantly affected, although no data for the stability of the colloidal suspension were provided at this high concentration. Using the DCFH-DA assay, significant elevation of intracellular ROS formation was identified in all applied concentrations of anatase NPs after a 5h exposure. In contrast, the rutile polymorph showed minimal increase in DCF fluorescence. The results for production of ROS correlated with the results observed for DNA strand breaks and oxidative DNA damage (2, 4, 24h), with anatase being the significantly more hazardous polymorph. Interestingly, mRNA expression of DNA damage responsive genes p53, mdm2, gadd45a and p21, was altered after treatment with the distinct TiO_2 polymorphs (anatase and rutile) (Petrovic *et. al.* 2011). A third study by Andersson and colleagues reported minimal effects on the cellular viability of

A549 cells at concentrations of TiO_2 rutile and anatase lower than 200µg/ml. However, supporting previous research, significant intracellular oxidative stress (as identified using DCF fluorescence) was induced in A549 when treated with all five distinct TiO_2 NP suspensions, 3 Anatase (A14, A60, P25) and 2 Rutile (R5,R9). On the contrary, generation of superoxide anion observed using a nitroblue tetrazolium after a 1h exposure to the cells, showed significant increase only in one of the two larger anatase NPs (A60, P25) that had the most significant uptake. Interestingly, when the NP effects on the production of pro-inflammatory (IL-8 and MCP-1) responses were investigated, rutile NPs showed more significant results than the more-readily endocytosed A60 NPs (Anderson *et. al.* 2011). In a fourth study De Angelis and colleagues however noted that a significant increase in ROS production was observed after 6h that reduced when the CACO-2 cells were exposed for 24h to anatase TiO_2, this was accompanied with no reduction in cellular viability. Despite this, no significant results were observed when IL-8 production was investigated following exposure to the non-soluble TiO_2 (De Angelis *et. al.* 2012).

In synopsis, the hazardous effects observed in distinct cell lines are strongly dependent on the degree of TiO_2 uptake. Uptake is in turn dependent on both the agglomeration status and the colloidal stability of TiO_2 NP in suspension. The technique currently considered as the gold standard for uptake assessment is TEM, which can allow not only the identification of the NP presence but also their localization in the cellular environment. However, a combined application with other techniques that allow quantification is preferable, and such quantitative techniques have shown a dose dependent increase in cellular interaction and uptake (Evans *et. al.* 2016). A certain time point for the exposure of cells must be chosen, or the correlation of the results from different outpoints is not possible. Even though uptake and the induction of oxidative stress are strongly dependent on the agglomeration/dispersion status of the TiO_2 NPs, results suggest that the production of pro-inflammatory responses to be a size dependent effect. To conclude, evidence in the literature suggests that the genotoxic behaviour of titania NPs is induced via the indirect mechanism of genotoxicity. An explanation for the more significantly hazardous effects (oxidative stress) induced by anatase TiO_2 in comparison to rutile, may be related to the reactivity of the surface of the different crystalline structures (Vittadini *et. al.* 1998, Baranowska-Wójcik *et. al.* 2019).

1.5 Introduction to Ca^{2+} Signalling

The actions of both extrinsic and intrinsic signals have been proven to be mediated by the divalent Ca^{2+} ion (Ca^{2+}) which is proven to be a universal intracellular messenger (Bootman *et. al.* 2012). The versatility of the Ca^{2+} controlled biological functions is incredible; among these functions are the ability to move, process information and store memories (Berridge *et. al.* 1998). On the cellular level Ca^{2+} is involved in the process of fertilization/birth, and the monitoring of the differentiation to specialised types (Clapham *et. al.* 2007). The universal effect of Ca^{2+} on cell death should also be pointed out. In general a significant number of the cellular activities that will be mentioned in the following paragraph are moderated by Ca^{2+} (Carafoli 2003). These incredible phenomena are the result of Ca^{2+} acting as an intracellular messenger to regulate the activity of cells by transferring signalling information.

During recent years of research to identify the organelles included in cellular calcium signalling included in has been identified that includes Ca^{2+} channels, Ca^{2+} pumps and cytosolic buffers that control Ca^{2+} levels, additionally a number of proteins whose functions has been found to be managed either directly or indirectly by Ca^{2+} (Beridge *et. al.* 2000). Ca^{2+} signals can be the result of the entry of ions from the extracellular environment through the plasma membrane, or from the release of ions from intracellular stores (Bootman *et. al.* 2012). The precise coordination of a number of functions is strongly dependent on both the flexibility and acute regulation of Ca^{2+} signals. The incredible range of functions that Ca^{2+} can mediate arises through the versatility of Ca^{2+} signals (Berridge *et. al.* 2000). Advanced subcellular imaging techniques, alongside a number of intracellular Ca^{2+} probes (e.g. Fluo-4, Fura 2 etc.) have revealed a complexity in the myriad of Ca^{2+} signalling patterns. The variability of the patterns is due to the changes in Ca^{2+} concentration with regard to either the intracellular space, time or the amplitude (Berridge *et. al.* 1998, Brownlee 2000). The specificity of these complex spatio- temporal patterns is interrelated with the nature of the cellular stimuli (Galione *et. al.* 2003).

Different cell types will not have the same Ca^{2+} transporters, as they are directly correlated with their distinct functions and physiology that links to their unique Ca^{2+} signalling pathways (Berridge *et. al.* 2003). Non-electrically excitable cells have been shown to produce oscillated Ca^{2+} signals repeated within minutes and these oscillations can last for

several seconds (Dupont *et. al.* 2011). In contrast, cells that are required to generate contraction such as cardiac myocytes have been shown to change Ca^{2+} levels within a matter of milliseconds (Bers 2002). Ca^{2+} channels found on the plasma membrane that are voltage operated result in the rapid influx of Ca^{2+} which triggers the release of Ca^{2+} from the SR (Fearnley *et. al.* 2011). Non excitable cells rely on other Ca^{2+} stores, such as the endoplasmic reticulum (ER) and the activation of a protein known as the inositol 1.4.5-triphosphate receptor ($InsP_3Rs$); or the acidic organelles (e.g. lysosomes) where a nicotinic acid adenine dinucleotide phosphate (NAADP)-gated channel operates (Galione 2011). Thus, for the majority of cells, signalling functions are generated when Ca^{2+} concentrations are elevated in the cytosol, and several simultaneous mechanisms that oppose each other are responsible for the control of cytosolic Ca^{2+} levels. A summary of the 'on and off mechanisms' known to be responsible for Ca^{2+} regulation can be seen at **Figure 1.4** (Bootman *et. al.* 2012).

A diversity of Ca^{2+} channels found on the plasma membrane are responsible for both the intake of extracellular Ca^{2+}, and the regulation of a number of Ca^{2+} release channels found on intracellular organelles specialised for Ca^{2+} storage (e.g. ER, SR, Golgi, mitochondria, lysosomes and other acidic vesicles) (Bootman *et. al.* 2012). These intracellular organelles are able to maintain high concentrations of Ca^{2+}, for example the ER has an estimated Ca^{2+} content of ~0.5–2 mM (Burdakov *et. al.* 2005) whereas the cytosolic concentration of Ca^{2+} is as low as ~100nM (Tsien *et. al.* 1992). A number of mechanisms exist to which cells rely on for the reduction of cytoplasmic Ca^{2+} levels. The 'off mechanisms' that are responsible for removing Ca^{2+} from the cytosol are ATPases (PMCA, which pumps Ca^{2+} outside the cells located on the plasma membrane and the SR/ER Ca^{2+} ATPase (SERCA) pumps). Additionally, exchangers such as Na^+/Ca^{2+} (NCX) are able to utilize electrochemical gradients of other ions (Na^+) in order to reduce intracellular Ca^{2+} levels (Bootman *et. al.* 2012). Several protein channels, pumps and co-factors are responsible for the maintenance of cytosolic and organelle concentrations of Ca^{2+}.

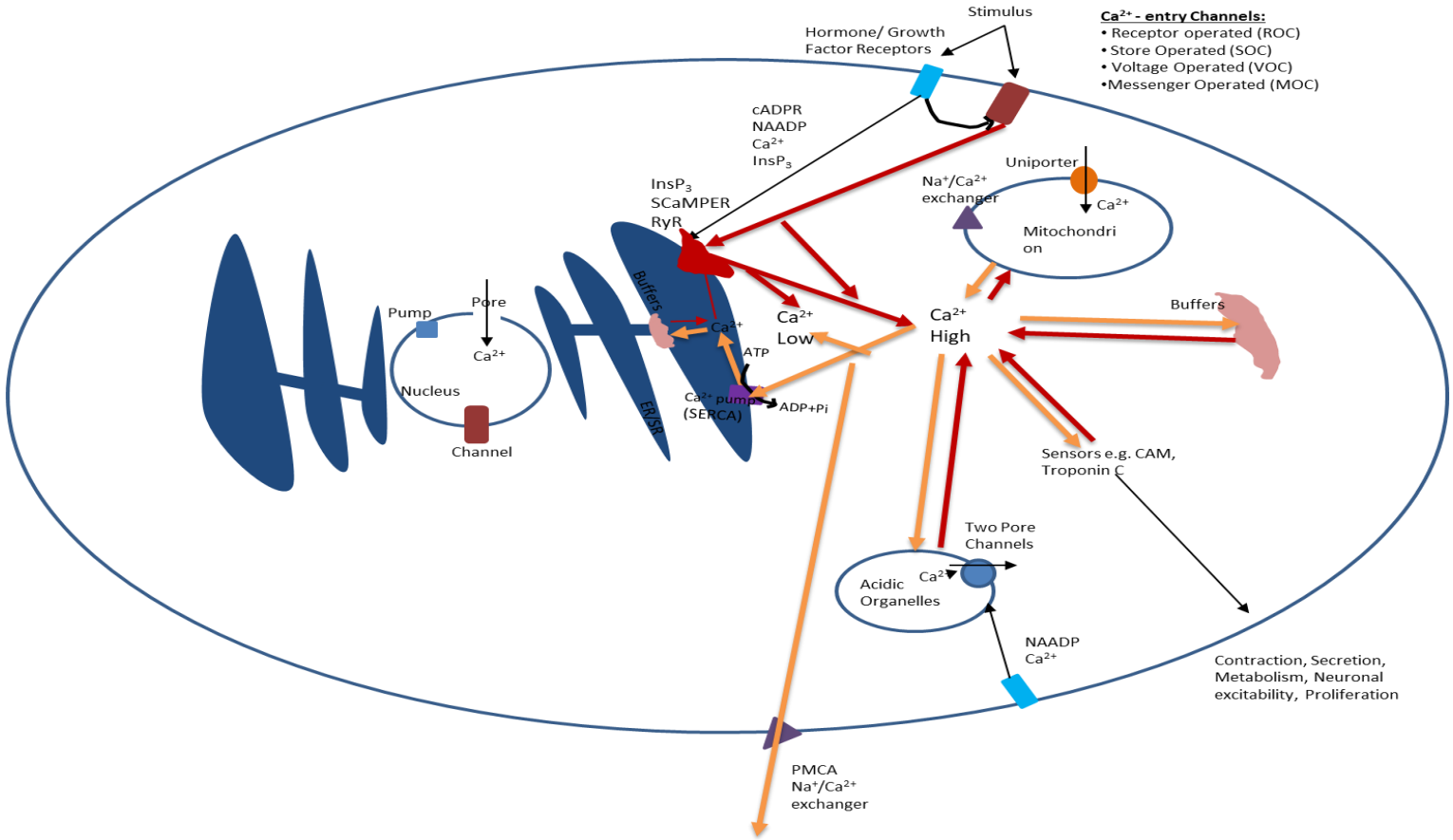

Figure 1.4: Ca^{2+} "On and Off mechanisms", the cellular calcium transporters and calcium storage organelles. The orange color represents the mechanism for reduction of Ca^{2+}, and the red arrows represent the mechanisms for increasing Ca^{2+} levels in a cell. These mechanisms are responsible for the facilitation of the spatio-temporal characteristics of distinct signals. Oxidants cause the influx of Ca^{2+} from either the extracellular environment, SR/ER or other cellular organelles (via: $InsP_3$, RYR etc). Simultaneously the mechanisms that transfer Ca^{2+} out of the cytoplasm (e.g. ATPase pumps, Na^+/Ca^{2+} exchangers) are inhibited by oxidants, leading to further increases in intracellular Ca^{2+}.

A number of other channels release Ca^{2+} in response to ligands such as the intracellular second messengers NAADP, Ins*P*$_3$ and cADPR (cADP-ribose). Responsible for the transfer of Ca^{2+} in the lumen of ER/SR sarco-endoplasmic reticulum is the Ca^{2+}-transporting ATPases also known as SERCA. SERCA transfers Ca^{2+} against its concentration gradient and it reduces cytoplasmic Ca^{2+} antagonizing the function of $InsP_3$. This Ca^{2+} can later be released to the cytoplasm through $InsP_3$ operated channels (Marin *et. al.* 1999, Ermak *et. al.* 2002). Inositol 1.4.5-triphosphate receptors ($InsP_3Rs$) are almost universally expressed in mammalian cells particularly in the ER. $InsP_3Rs$ are responsible for the release of Ca^{2+} into the cytoplasm as a response to external stimuli (Ermack and Davies 2001). Specific receptors on the plasma membrane when bound by a number of hormones and growth factors lead to the activation of phospholipase C that mediates the production of $InsP_3$ by catalysing the hydrolysis of phospholipids. Interestingly even though $InsP_3$ derives from a lipid, it is water soluble, this makes it able to diffuse into the cytoplasm and bind to $InsP_3Rs$ in the ER/SR. After the two are bound the structure of $InsP_3Rs$ changes, as a result the Ca^{2+} that was stored in high concentrations in the ER/SR enters the cytoplasm (Bootman *et. al.* 2012). A number of fundamental biological processes have been found to be either regulated or activated by $InsP_3$, such as fertilization, secretion and gene transcription (Malcuit *et. al.* 2006, Pittersen and Tepikin 2008, Lewis 2001). A pivotal role in the propagation of Ca^{2+} signals in the mitochondria is associated with $InsP_3$ located in the vicinity of mitochondria; depending on the conditions, ATP synthesis could be enhanced or apoptotic signalling can be initiated (Szalai *et. al.* 1999).

An additional store important to cellular Ca^{2+} signalling; that is crucial for numerous cellular functions from fertilization through to cell death are the lysosomes (Babcock *et. al.* 1997). In a number of studies that utilized different Ca^{2+} probes the content of macrophage cell lysosomes was measured to have a content of ~400–600 µM Ca^{2+} (Barrow *et. al.* 2008, Patel and Cai 2015). Results from various studies have shown similar concentration levels of Ca^{2+} to those within the ER, indicating that the lysosome is a substantial Ca^{2+} store (Arnaudeau *et. al.* 2001, Patel and Cai 2015). Two pore channels (TPC) have been recently identified to operate in acidic organelles and NAADP was demonstrated to target TPC. Therefore, molecular evidence presented in numerous articles give proves that NAADP (one of the most potent intracellular Ca^{2+} releasing second messengers) targets acidic organelles (Feng

and Yang, 2016, Galione *et. al.* 2011). As previously described in **Section 1.2,** uptake of NPs is greatly observed to be through endocytic and phagocytic pathways suggesting a great presence of NPs in the lysosomes. Therefore, there is a possibility that NPs may have a negative impact on lysosomal calcium. In a study presented by Lorente and colleagues, lysosomal dysfunction/damage after exposure to NPs decreases their capacity of Ca^{2+} and eventually results in the aberrant regulation of intracellular Ca^{2+} levels (Lorente *et. al.* 2013). In a recent study by Manshian and colleagues the impact of gold and SiO_2 NPs on the lysosomes integrity of human bronchial epithelial cells (BEAS-2B) and mouse mesenchymal stem cells (MSCs) was investigated. In the study, clear evidence have been presented that the NPs reduced lysosomal activity by alkalinisation of the lysosomal lumen (Manshian *et. al.*2018*).* The alteration of lysosomal functions further arouses curiosity on the limited understanding the impact of NPs have on lysosomal calcium concentrations and hence the impact that has on intracellular $Ca2^{+}$ homeostasis. GPN can be used, is cleaved by the lysosomal enzyme cathepsin C which gives rise to osmotic stress and so ruptures lysosomal membranes, as a result lysosomal calcium is released as a result the concentration of lysosomal calcium can be identified (Lloyd Evans *et al.* 2008).

1.5.1 Altered Ca^{2+} homeostasis, cellular function and the effect of NP treatments

Ca^{2+} signalling is able to control numerous processes including gene expression, which results from the merge with other signal-transduction pathways (Dolmetsch 2008). A relevant example of altered Ca^{2+} homeostasis is in cancer development: interestingly, in contrast to all non-carcinogenic eukaryote cells, some tumour cells do not depend on Ca^{2+} signalling to preserve cell proliferation (Cook and Lockyer, 2006). A growing acknowledgment and understanding of how Ca^{2+} signalling pathways are remodelled in carcinogenesis has grown, however it is still debatable whether these changes are fundamental for the facilitation of cancer (Wood *et. al.* 2007).

Interestingly, ROS such as NO or O^{2-} can be produced by the cell as a result of a Ca^{2+} signal, these signals can be initiated by oxidative stress (Brown *et. al.* 2002). Therefore, oxidative stress and the elevation of intracellular Ca^{2+} are interrelated. Mild oxidative stress due to the presence of hydrogen peroxide has been observed to dramatically increase the cytoplasmic Ca^{2+} levels. In ROS stimulated Ca^{2+} signalling, the exact role of $InsP_3Rs$ is yet unclear.

Recently research conducted on three different cell lines HepG2 (human), RBL-2H3 (rat) and DT40 (chicken) have proven that superoxide anion causes oxidation of the $InsP_3Rs$, as a result cytoplasmic Ca^{2+} oscillations are produced that enhance mitochondrial uptake (Bangashi *et. al.* 2014). However, the production of $InsP_3$ is directly affected by oxidants; as a result the release of Ca^{2+} from the ER/SR is directly regulated. For example, in endothelial cells hydrogen peroxides were observed to cause the release of Ca^{2+} from internal stores (Doan *et. al.* 1994). After the addition of thapsigargin one of the many agents that modulate Ca^{2+} homeostasis, the release of Ca^{2+} by H_2O_2 from the stores was shown to decline, this proves H_2O_2 has access to $InsP_3$ regulated stores.

Reactive oxygen species (ROS) stimulate the activation of NF-κB and activator protein-1(AP-1), which in turn can induce the production of inflammatory mediators. Such redox sensitive transcription factors have been observed to be directly activated by intracellular thiol status (Wilhelm *et. al.* 1997). Additionally, other pathophysiological responses such as gene expression or signal transduction are also affected by cellular redox status (Rahman and MacNee 2000). While increase in intracellular Ca^{2+} can be traced back to the elevation of ROS, the cellular chain of protein members of the mitogen activated kinase (MAPK)-pathway are also activated after the phosphorylation of MAPK, and this eventually results in increased gene transcription (Thannickal, and Fanburg 2000). The activation of members of the MAPK-pathway are trans-activating transcription factors, including, c-Jun, activating factor 2 (ATF2), cyclic AMP response element binding protein (CREB)-binding protein (CBP) (Rahman, and MacNee, 2000). These proteins subsequently induce the expression of genes responsible for the regulation of inflammatory responses and chromatin remodelling.

Brown and colleagues published a series of articles where rat alveolar macrophages and a human monocytic cell line were treated with ultrafine carbon particles and polysterene NPs: in these experiments the induction of transcription factor activation and cytokine expression were a result of both the presence of oxidants and observed Ca^{2+} signalling events (Brown *et. al.* 2002). A rapid increase of Ca^{2+} was observed after the exposure of the cells to the particles, interestingly this was not associated with cell death (stone *et. al.* 1998). Thapsigargin (50nM) was used in the experiments to increase the cytosolic Ca^{2+} concentration. Thapsigargin is a known agonist able to increase the cytosolic Ca^{2+} levels by emptying the ER stores, this is achieved by inhibiting the SERCA ATPase pumps (Thastrup

1990). Increases to the response to pre-exposure to thapsigargin in macrophage cells were observed after exposure with ultrafine latex beads (64 nm); in contrast, treatment with fine latex (202 nm) alone did not show a significant effect. Similarly, ultrafine carbon black (CB) induced a significant increase in the response to thapsigargin by 2.6-fold, whereas fine CB alone had no significant effect (Stone *et. al.* 2001). The experiments were repeated in the absence of extracellular Ca^{2+} to support the finding that ultrafine particles in contrast to fine particles with the same chemical structure are able to reverse the current of Ca^{2+} through the plasma membrane, and that this is distinct from any effects which agents such as thapsigargin may exert on ER Ca^{2+} (Stone *et. al.* 2001). Additionally, an increased production of $InsP_3$ as a result of oxidative stress was reported in several cell lines, including, endothelial cells and macrophages (Graier 1998). When the antioxidants nacystelin (NAL) and manitol were used, alongside to the exposure of carbon black NPs and thapsigargin, no significant elevation of cytosolic Ca^{2+} was observed (Stone *et. al.* 1998). These results suggest that oxidative stress plays a principal role in the elevation of intracellular Ca^{2+}.

The effects of ZnO NPs (20nm) on the induction of oxidative stress, cytotoxicity and Ca^{2+} homeostasis were observed in Human bronchial cells (Huang *et. al.* 2010). Cytotoxicity was eliminated when the antioxidant N-acetylcysteine (NAC) was used. Interestingly, intracellular Ca^{2+} was partially reduced when cells were exposed to NAC and ZnO NPs for 6 hours, whereas no immediate response was observed after the exposure. The use of nifedipine allows the assumption that a portion of Ca^{2+} is imported from the extracellular environment; the peroxidation of membrane lipids may play a role in this Ca^{2+} influx (Huang *et. al.* 2010). In contrast, a correlation between the levels of oxidative stress and intracellular Ca^{2+} was not observed when macrophage cells were treated with organic Quantum dots (QT), or COOH and PEG coated QT. Interestingly, organic QT (which had the most significant increase in cytosolic Ca^{2+}) induced the mildest oxidative stress in comparison to the other QTs (Clift *et. al.* 2010). Similarly, intracellular Ca^{2+} could not be linked to increases in either ROS levels or lysosomal damage, when endothelial cells were exposed to several polystyrene and silica NPs. In addition, differences between the changes in Ca^{2+} levels were observed when non-cytotoxic membrane damage and severe membrane damage occurred (Meindl *et. al.* 2015). Recently, Gilardino and colleagues suggested that the oscillatory changes in intracellular Ca^{2+}, after the exposure of neuronal cell in silica NPs,

were a result of interactions in the cell membrane, with influx from the extracellular environment being the only pathway responsible (Gilardino *et. al.* 2015). In the presences of NPs the levels of intracellular Ca^{2+} return to their baseline in about 4h (Miletto *et. al.* 2010, Gilardo *et. al.* 2015).

The exposure of rat macrophages and human derived monocytes to carbon black NPs induced increased production of tumour necrosis factor-α protein (TNF-α) after only 4h of exposure (Brown, Donaldson and Stone 2002). Interestingly, the production of TNF-α was the result of modifications in Ca^{2+} signals. The involvement of Ca^{2+} in the increased production of TNF-α was supported by an inhibited response (to calcium signalling); a result of cells treated with an intracellular Ca^{2+} chelator a BAPTA-AM and the Ca^{2+} antagonist verapamil (Brown, Donaldson and Stone 2002, Duffin *et. al.* 2002). Additionally, when the antioxidants NAL and trollox were used, a partial inhibition of the production of TNF-α and Nf-κβ was observed (Brown *et. al.* 2002).

Chen and associates observed that mast cells exposed to a mixture of anatase and rutile TiO_2 NPs produced oxidative stress that led to both the opening of L-type Ca^{2+} channels and the influx of extracellular Ca^{2+} by permeation of the plasma membrane (Chen *et. al.*, 2012b). In contrast, histamine secretion was observed as a result of the sustained elevation in cytosolic Ca^{2+}, achieved by releasing of Ca^{2+} from the ER (Chen *et. al.* 2012a). Epithelial cells treated with TiO_2 NPs exhibited both extracellular Ca^{2+} influx and release of Ca^{2+} from the ER that leads to the stimulation of mucin secretion (Chen *et. al.*, 2011). Glioblastoma cells and human lung fibroblasts were exposed *in vitro* to Ag NPs; these were mainly internalized through endocytosis, and measurements of intracellular Ca^{2+} revealed significant increase in both cell lines after exposures of 4h, 24h and 48h. Therefore, the toxicity of Ag NPs was concluded to be a result of changes in Ca^{2+} signalling; interestingly this also resulted in mitotic arrest (Asharani *et. al.*, 2009). The effects ZnO NPs (20nm) on the induction of oxidative stress, cytotoxicity and Ca^{2+} homeostasis were evaluated on Human bronchial cells. Cytotoxicity levels were eliminated when the antioxidant N-acetylcysteine (NAC) was used. Interestingly, intracellular Ca^{2+} was partially reduced when cells were exposed to NAC and ZnO for 6 hours, with no immediate response was observed after the exposure. The use of nifedipine allows the assumption that a portion of Ca^{2+} can enter from the extracellular environments, the peroxidation of membrane lipids may also play a role in the Ca^{2+} influx

(Huang *et. al.* 2009). A correlation between the levels of oxidative stress and intracellular Ca^{2+} was not observed when macrophages cells were treated with organic quantum dots, COOH and PEG coated quantum dot NPs (QT). Interestingly, organic QT that had the most significant increase in cytosolic Ca^{2+} induced the mildest oxidative stress in comparison to the other QT (Clift *et. al.* 2009).

In literature a lot of evidence has been presented that connect NP treatments with the rapid increase of intracellular Ca^{2+} (iCa^{2+}) concentrations, but not a lot of work has been done to identify the effect of NPs on iCa^{2+} for extended periods of time. Varied are the results suggesting a strong connection between oxidative stress and increase in iCa^{2+}. Different antioxidants have been used prior to treatments to identify if a reduction in the increase in Ca^{2+} after treatment with NPs. A partial reduction was identified suggesting that iCa^{2+}increase are not only affected by changes in the redox state of the cells, whereas concurring increase in cytokines and chemokines remained increased. As it was previously mentioned the connection between changes in iCa^{2+}homeostasis and changes in the production of chemokines and chemokines is well established. The link between Ca^{2+} increase and inflamatotoxicity should be further investigated. In order to do that the origins of the identified increase of iCa^{2+}should be investigated in different Ca^{2+} storages organelles (e.g. ER, lysosomes) for extended periods of time where oxidative stress is more potent.

1.6 Physioxic Cell Culture Environment

In aerobic life forms oxygen is utilized and distributed to various organs and tissues by a complex respiratory system. Ambient atmospheric oxygen is 21%O_2, which is the equivalent of 150mm/Hg. However, after inhalation, O_2 levels decrease as it reaches the various internal organs, where it presents at different concentrations. In humans, under physiological conditions, the arterial blood pressure of O_2 is 100mm/Hg (14% O_2), while the pressure in the different organs such as the lungs and kidneys vary, ranging between 1-14% O_2 (Miller *et. al.* 2010, Muller *et. al.* 1998). The concentration of O_2 in the liver has been recorded at 5.6%, which is substantially lower than ambient levels (Brooks *et. al.* 2007, Leary *et. al.* 2002). Oxygen tension in certain pathological conditions has been documented to vary, examples include hyperoxia associated lung injury and hypoxia in cancer and wound healing (Ames *et. al.* 1993).

Although, traditional *in vitro* cell culture is performed under ambient oxygen levels (21% O_2, hyperoxia (21% O_2), this is substantially higher than the oxygen levels that cells in the human body experience under normal physiological conditions (Atkuri *et. al.* 2007). Interestingly, numerous studies have observed that when cultured under physiological oxygen conditions (physioxia) the replicative life span of the cells is increased (Ithana *et. al.* 2003, Parinello *et. al.* 2003). The non-physiological consequences of culturing immortalized cells under hyperoxia (21% O_2) have been overlooked. Evidence in the scientific literature suggests that the physiology of cells cultured under hyperoxia are greatly affected due to elevated ROS and the induction of oxidative stress associated with the high oxygen levels. This, in turn may have a subsequent effect on experimental outcomes when using cells cultured under these conditions (Halliwell 2014).

The majority of cellular ROS are generated by the mitochondrial respiratory chain and is modulated by the rate of electron flow. It was previously reported that 1-4% of the oxygen consumed by the mitochondria is diverted for the formation of ROS. Considering the amount of oxygen utilized by each cell is ~ 2.5 × 10–18 mol/s, then almost a billion ROS are being produced every day *in vivo* (Wagner *et. al.* 2011). This can be increased greatly when the cells are cultured *in vitro* under hyperoxic conditions compared to physiological conditions (10–13% O_2).

Excessive production of ROS for an extended period of time contributes to reduced antioxidant capacity and ultimately chronic inflammation (Sesti *et. al.* 2012). It was previously observed that freshly isolated peripheral blood monocytes (PBMCs) cultured under hyperoxia (21%O_2) produced inflammatory signals resembling those produced during an infection. When the same cells were cultured under lower oxygen concentrations (5% and 10% O_2), production of inflammatory signals was also identified but at considerably lower levels (Atkuri *et. al.* 2005, Atkuri *et. al.* 2007). After treatment of PBMCs with mitogen in under both hyperoxia (21% O_2) and physioxia (5% O_2), a significant increase in conA and CD3/CD28 crosslinking alongside the increase in production of NOS and reduction of GSH was identified under the hyperoxia condition as compared to physioxia (Atkuri *et. al.* 2005, Atkuri *et. al.* 2007). After culturing primary T-cells under hyperoxia (21% O_2) compared to physioxia (8% O_2), an increase in the expression of cell death/repair and stress responses were identified, indicating an increase in the response to oxidative stress (Haddad *et. al.* 2004).

After rat liver sinusoidal cells (LSECs) were cultured under physioxia (5% O_2) a reduction of the production of the pro-inflammatory mediator, interleukin-6 (IL-6) and increased production of the anti-inflammatory cytokine, interleukin-10 (IL-10) were observed compered to hyperoxia (21% O_2). Additionally, improved survival of LSECs was identified alongside the increase in scavenger receptor-mediated endocytic activity (Martinez *et. al.* 2008). Following the isolation of primary hepatocytes from C57BL/6 mice, they were cultured under both hyperoxia (21% O_2) and physioxia. Guo and colleagues were able to prove that when the primary hepatocytes were cultured under hyperoxia (21% O_2), they undergo epithelial-to-mesenchymal transition in addition to obtaining fibroblast-like morphology and decreased hepatic functions. On the contrary, when the primary hepatocytes were cultured under physioxia (5% O_2) they maintained many of the cellular functions for up to five days. More importantly, a reduction in the presence of oxidative stress was identified alongside the decrease of the levels of DNA damage in the physioxic environment when compared with hyperoxia (Gao *et. al.* 2017).

Given that culturing cells in a more physiological culture environment can alter their cellular functions in comparison to culturing them in a hyperoxic environment, it can by hypothesised that cell interaction and/or uptake and toxicity arising as a result of NPs

exposure could be altered when treatments take place in the physioxic culture environment (5% O_2). In recent years, gold NPs have emerged as one of the novel agent for cancer therapies, studies have therefore focused upon their ability to interact with cells in an oxygen environment that represents the levels observed in tumours *in vivo* (hypoxia*;* less than 0.7%) (Jain *et. al.* 2014, Neshatian *et. al.* 2015). For example, studies on breast cancer cells (MCF-7 and MDA-MB-231) and cervical cancer cells (HeLa) demonstrated that changes in oxygen culture conditions can greatly alter the uptake and interaction of gold NP with different cell lines in hypoxic oxygen culture conditions (Jain *et. al.* 2014, Neshatian *et. al.* 2015). Whilst these studies provide evidence to suggest that the cell culture environment has a significant impact on biological interactions between NPs and cells, the research in this area is highly limited. There is therefore an urgent need to expand our knowledge on the role that oxygen tension has on hazard evaluations following NPs exposure to ensure that *in vitro* toxicological studies are more representative of the *in vivo* situation.

1.7 Aims of thesis

The overarching aim of this thesis was to investigate and understand the potential of different MONPs (dextran coated-SPIONs, Anatase-TiO_2 and Rutile TiO_2) to exert toxic (genotoxic, cytotoxic and proinflammatory) effects on human cells and the associated damage mechanism. All the experiments in this thesis were conducted in both in hyperoxia (21% O_2) and physioxia (5% O_2) in mono-cultures of hepatocellular carcinoma cells (HepG2), primary monocytes (THP-1) and differentiated-THP-1 macrophages resembling cell line (dTHP-1), to investigate the impact of varying environmental oxygen content on MONPs toxicity profiles.

To achieve this aim in **Chapter 3**, a series of experiments in which physicochemical characterisation of the NPs in question was carried out prior to cell treatments. Characterization of the behaviour the different MONPs exhibit under experimental conditions was a vital undertaking because the toxicological profile of a NP is strongly dependent on its physico-chemical characteristics. A secondary aim of this chapter was to compare a range of technical approaches to define the hydrodynamic diameter of the MONPs agglomerates.

The second objective contributing to the thesis aim was the assessment and comparison of the ability the MONPs to induce toxicity in the hyperoxic and physioxic culture environments, evaluated in **Chapter 4**. The possible toxic effect of NPs depends on their concentration and duration of their interaction with cells. Therefore, the level of interaction and uptake of MONPs with the cells was investigated in both hyperoxic and physioxic culture environments. The ability of MONPs to promote toxicity and chromosomal DNA damage in HepG2 cells was then quantified and compared in the different culture environments.

The final objective of this thesis that is described in **Chapter 5** was to investigate the mechanisms underlying the MONPs toxicity identified in Chapter 4. Evaluation of pro-inflammatory response of the test materials was undertaken as the induction of an immune response may lead to cytotoxicity and genotoxicity. The effects of MONPs treatments under hyperoxia and physioxia on the induction of oxidative stress were investigated by identifying depletion of the cellular antioxidant glutathione. Furthermore, their ability to alter iCa^{2+} signalling was investigated.

Chapter 2: General Materials and Methods

2.1 Chemicals and Reagents

All chemicals and reagents were purchased from Sigma-Aldrich (UK), unless otherwise stated. Flasks and pipettes used were acquired from Greiner Bio-One (Gloucester, UK). Roswell Park Memorial Institute 1640 (RPMI), Dulbecco's Modified Eagle Medium (DMEM), foetal bovine serum (FBS), L-glutamine, antibiotics (streptomycin 100 mg/ml-1/penicillin 100 IU/ml^{-1}) and Trypsin/ Ethylenediaminetetraacetic acid (EDTA) were purchased from Gibco, UK.

2.2 Particle Preparation and Characterization

Dextran-coated Fe_3O_4 NPs (dSPIONs) were purchased from Liquids Research (Bangor, UK). The stock of dSPIONs prior to cell treatments was vortexed for 10s and then suspended in the appropriate growth media [RPMI 1640 or Dulbecco's modified medium (DMEM)]. dSPIONs were used to treat the cell lines in concentrations of 0, 2, 4,8,10,50 and100µg/ml. The TiO_2 NPs were supplied from the joint research centre (JRC) NPs repository in dry powder. Furthermore, their secondary characteristics have been identified in a dispersion buffer "0.05% BSA dH_2O_2"(DB) (Rasmussen *et. al.* 2014). The two different types of titanium dioxide NPs (TiO_2 NPs) were used for this study were anatase (NM-102) and rutile (NM-104), they were used to treat the cell-lines in concentrations of 0,2,4,8,10 and 50µg/ml. Characterization of the distinct metal oxide NPs (MONPs) (dSPIONs, NM-102 and NM-104) was investigated; the techniques applied are described in the following sections.

2.2.2 Dispersion SOP for TiO_2

Dispersion buffer was produced by diluting sterile filtered bovine serum albumin (BSA) (Sigma Aldrich, UK) in deionized/distilled water (ddH_2O) in the volume of 6.25ml into in 50ml flat bottom centrifuge tube followed by 0.125g BSA, to reach a concentration of 1% w/v. An additional 6.25ml of ddH_2O was added and the flask. Following a 24h incubation at 4°C, the solution was transferred in Class II tissue culture hoods (Scanlaf Mars, Denmark) where a 0.2um sterile disposable filter ware (Corning incorporated, UK) was used to sterile filter the solution, producing the Dispersion Buffer "0.05% BSA dH_2O_2 " (DB).

TiO_2 NPs (NM-102 & NM-104) were weighed to stock samples of 1.5-2g within Eppendorf tubes. Depending on the weight of the NPs in the scintillation vessel, the calculated amount of ethanol (EtOH) was added at a concentration of 0.0015mg/ml (*e.g.* 2mg NPs diluted in 3µl EtOH) and the vial was gently mixed by tapping the top. The final concentration of the stock was 1mg/ml in EtOH & "0.05% BSA Water"). Dispersion buffer ("0.05% BSA Water") was added along the sidewalls of the scintillation vessel using a pipette in order to wash down NPs that have adhered to the sidewalls. The sonicating water bath was filled with water and ice to keep the temperature constant the vial that contained the diluted NPs was placed in a mixture of ice (80%) and water (20%) in the sonicating water bath. Sonication of the NP suspensions commenced for the period of 1h at a frequency of ~30Hz, which produced the final product for characterization

2.2.3 NP Endotoxin Identification

The *Limulus Amebocyte* Lysate (LAL) PYROGENT™ (Lonza, UK) was used to determine the presence of endotoxin in all stock NP samples. On three independent occasions (n=3), the protocol followed was that as described in the manufacturers kit manual. For each replicate three vials containing Control Standard Endotoxin (CSE) which was diluted from 1.0 EU/ml to give the final product of 0.5 EU/ml were used as positive controls. Test samples include, the negative control, LAL Reagent Water. The NPs were tested by diluting them with LAL free water in their higher concentration under investigation dSPIONs (100µg/ml) and both TiO_2 NP types (50 µg/ml). Preparation of the samples to be tested was carried out by adding 0.10 ml of the reconstituted lysate provided in the kit which was followed by mixing the content of the tube thoroughly. The samples were then incubated in a tissue culture incubator at 37°C for a period of 60 min. The assay was carried out as a positive/negative outcome test. After the incubation the samples where then carefully removed from the incubator and invert in a 180°. Positive reactions were characterized by the formation of a firm gel that remains intact momentarily when the tube is inverted. The reaction in each tube was recorded as either positive or negative.

2.2.4 TiO_2 NP Sedimentation Studies

Visual identification of the TiO_2 NP sedimentation as a result of agglomeration was investigated in different concentrations and time points. Photographs (seen in **Section 3.3.1**) of the sample were taken for each of the steps and different concentrations described below:

- The samples were imaged following the dispersion of the TiO_2 NPs (as described in **Section 2.1.1)** at a concentration of 1mg/ml. Pictures of the samples were taken after incubation for 2h in 37°C. The NPs that remained in suspension were used to prepare three samples. The first sample is 400µl of the supernatant (NPs in suspension). Sample two and three are 200µl of the supernatant in 800µl of the distinct medium used for cell culture as described in **Section 2.2**.

- The dispersed sample (1mg/ml) was used to prepare a sample with a concentration of 100ug/ml. The sample was incubated for 2h and as with the previous experiment the supernatant was used to prepare three samples.

2.2.5 Light Scattering

The theory of Brownian motion dictates that NPs randomly move in a suspension due to forces applied by macromolecules. Brownian motion, also known as pedesis, suggests that the larger the NP the slower it moves. Based on the formula of the Stoke-Einstein equation, DLS and NTA allow the correlation of the movement to calculate the hydrodynamic diameter of agglomerates (Equation 3.1). This equation also requires temperature and solvent viscosity (Konan *et. al.*, 2002).

Equation 2.1 2D Stokes- Einstein equation: $(\mathrm{x},\mathrm{y})2 = \frac{\mathrm{KT}}{3\pi\mathrm{nD}}$

k = Boltzmann's constant

T = Absolute Temperature

η = Dynamic viscosity

D = translational diffusion coefficient

To identify the hydrodynamic diameter of the distinct MONPs, two distinct light scattering methods incorporating the use of the Malvern ZetaSizer nano ZS (Malvern instruments Ltd., UK) and the Malvern Nanosight LM-12 (Malvern instruments Ltd., UK), were used.

The dispersant characteristics used to set-up the method for all measurements in both Malvern ZetaSizer nano ZS and Malvern Nanosight LM-12 can be seen in table 2.1. The DLS method was set-up according to each of the instruments operating manual; it is also important to note that the set-up requires the input dispersant properties outlined in each of the NPs optical parameters.

Table 2. 1: Dispersant characteristics

	PBS and ddH_2O	**0.05% BSA in ddH_2O**
Density (g/cm^3)	1.0040	1.0095
Dynamic Viscosity (cP)	0.6963	0.7228
Refractive Index	1.3402	1.3414

2.2.5.1 Sample preparation for each of the NPs

- Dilution of dSPIONs at the concentration used for the treatment of cell lines (100ug/ml) was carried out in PBS (Sigma-Aldrich, UK) and distilled-deionized H_2O (ddH_2O).

- Hydrodynamic diameter of TiO_2 polymorphs was monitored for 24h, prior to the experiment all the samples were prepared as mentioned in **Section 2.1** and further diluted in the dispersion buffer "0.05% BSA ddH_2O". The initial concentration in suspension was 100ug/ml, and it was measured in the dispersion buffer "0.05% BSA ddH_2O". Due to the sedimentation of the NP in suspension the original concentration was reduced. After determination of the concentration using UV-Vis (as seen in **Section 2.1.6**) measurements of the highest concentration used to treat the cells (50ug/ml) were also carried out.

The Malvern ZetaSizer nano ZS measures the dynamic light scattering intensity of the particles to identify their hydrodynamic diameter (HD). In DLS the speed the NPs move in a diluent is determined by passing a laser through and determining the fluctuations of intensity of the scattered light. The lack of randomness in the fluctuations is presented as a correlation coefficient. The correlation coefficient is then plotted against time resulting in a correlation curve. The samples (100µl) were pipetted into micro cuvettes (Sigma-Aldrich, UK) and inserted into the instrument. The same sample is measured for 3 times in the period of 2 min. All the measurements were undertaken at a temperature of 37°C. The instrument attenuator was set to automatic and analysis of the resulting data was conducted using the ZetaSizer software (Malvern, UK).

The nanosight allows visualization of the NPs and the identification of their every movement therefore the name of the technique is NP Tracking Analysis (NTA). NTA was programmed to measure the sample for 60 seconds for five repeats; the temperature of the sample is manually measured and adjusted in the software. The measurements were undertaken at room temperature. The prepared samples were loaded into a 1ml syringe and loaded into the machine. The samples were measured in a static and not using a flow the reason is that pressure applied on the liquid suspension further induced agglomeration of the NPs in suspension.

2.2.6 Determination of Zeta potential using DLS

When NPs are suspended in a solution a two part layer of liquid surrounds them. In the first layer that sits on the outside the ions are weakly associated. In the inner layer the ions are strongly bound forming a stable entity with the particle. The ions within this perimeter will move with the particle when a particle moves under Brownian motion. The hydrodynamic shear at the surface is also known as the ζ-potential (Malvern, 2011, Kirby 2010). Essentially, the ζ-potential is the difference between the bulk solution and the static layer of fluid adhered to the particle. Therefore, this strongly determines the charge of a particulate solution.

The charge can be identified by applying an electrical field. Due to the presence of these charges the particles will interact with the electrical field, charged particles will move

towards the electrode of the opposite charge. Viscous forces of the fluid will oppose this movement and when equilibrium is reached NPs will move at constant velocity. This velocity is known as electrophoretic mobility and zeta potential is related to it by the Henry equation (Equation 3.2) (Shaw, 1992). The ζpotential values of the NP's were determined by a Zetasizer 2000 (Malvern instruments Ltd., UK.

Samples were prepared as described in **Section 2.1.3.1**. A total of 500 µl of particle suspension was then injected into a Folded Capillary Cell (Malvern, UK) using a 1 ml syringe. The capillary cell was placed into a ZetaSizer (Malvern, UK) and allowed to equilibrate for 2 min before the measurement process. The z-potential values presented are the average of 3 scans; the experiment was done in a triplicate.

Equation 2.2 $\boldsymbol{Electroporetic\ Mobility} = \frac{2\ \varepsilon\ z\ f(\kappa a)}{3\eta}$

ε = Dielectric constant

Z = Zeta potential

f(κa) = Henry's function

H = Dynamic viscosity

2.2.7 Ultraviolet-Visible spectroscopy (UV-Vis)

2.2.7.1 Acquiring UV-Vis Data

Following dispersion of TiO_2 NPs, as it was described in **Section 2.1.1**, the suspension of 1mg/ml was further diluted to a concentration of 100µg/ml. Measurements of the optical absorbance at the whole light spectrum of the NPs was measured. Measurements were undertaken immediately after dispersion (0h) and also following by incubations at 37°C in a NU-5510 DHD Autoflow incubator (Nuaire, UK) for the periods of 2h and 24h. UV–Vis absorption spectra were recorded using a U3310 spectrophotometer (Hitachi). All the measurements were carried 3 times for each of the samples; the experiment was carried out in a triplicate. All measurements were made at 37°C in square cuvettes (Sigma- Aldrich, UK) with a one cm light path.

2.2.7.2 Background theory applied to acquire NP concentration in solution

Unlike molecular solutions, the state of the NP suspensions dictates if it will absorb or scatter light (or both) in distinct wavelengths (Buhren and Huffman 1983). Scattering of radiation, of wavelength (λ), by small particles, of diameter (d) [(d)/(λ) < 0.1], was analyzed by Rayleigh. Mie's scattering adaption for larger spherical particles, took into account interference between light scattered from different points on the particle surface (Metwally, Mensah and Baffou 2015). Mie showed that light scattering depends on both the ratio [(d)/(λ)], and on the refractive index. Refractive index is a complex quantity with real (n) and imaginary light scattering (k); these respectively represent the refraction and the attenuation of the wave (Bohren and Huffman 1983).

Therefore, the A (λ) of particulate suspensions is calculated using **Equation (2.3)**. The extinction coefficient (q) of the particle colloidal suspension is the sum of the coefficients of scattering (q_{sca}) and absorption (q_{abs}), **Equation (2.4)**. It is often convenient to express both scattering and absorption on a unit-volume or mass basis.

Equation 2.3 $\log I_\lambda / I_\lambda^0$= q.c.l

Equation 2.4 $q_{abs} = q_{ext} - q_{sca}$

When a particle is illuminated by a plane wave of angular frequency $\omega = 2\pi c/\lambda_0 = kc/n_m$ (the wave vector). The extinction, scattering, and absorption cross sections of a spherical particle with radius (r_0) embedded in a medium with dielectric permittivity $\varepsilon_m = n_m^2$ at a wavelength (λ) can be represented by the **formulas (2.5)** and **(2.6)** (Haiss *et. al.*2007, Metwally, Mensah and Baffou 2015).

$$k = 2\pi \frac{\sqrt{\varepsilon_m}}{\lambda}$$

2.5. $$q_{ext} = \frac{2\pi}{k^2} \sum_{j=1}^{\infty} (2j+1)\, Re(a_j + b_j)$$

2.6. $$q_{sca} = \frac{2\pi}{k^2} \sum_{j=1}^{\infty} (2j+1)\ (a_j{}^2 + b_j{}^2)$$

Based on the Ricatti-Bessel functions the scattering coefficients can be produced following the **equations** provided at **(2.7)** and **(2.8)** (Haiss *et. al.*2007, Metwally, Mensah and Baffou 2015).

$m = n/n_m$

$v = k\, r_0$

$w = m\, v$

2.7. $$\alpha_j = \frac{m\psi_j(w)\psi_j^{'}(v) - \psi_j(v)\psi_j^{'}(w)}{m\psi_j(w)\xi_j^{'}(v) - \xi_j(v)\psi_j^{'}(w)}$$

2.8. $$\alpha_j = \frac{\psi_j(w)\psi_j^{'}(v) - m\psi_j(v)\psi_j^{'}(w)}{\psi_j(w)\xi_j^{'}(v) - m\xi_j(v)\psi_j^{'}(w)}$$

Data from experiments produced with different NPs suggests that the absorbance and scattering cross section is strongly affected by multiple parameters, such as the size, shape, composition, concentration and the dielectric environment (Haiss *et. al.* 2007, Metwally, Mensah and Baffou 2015). Consequently the experimental estimation of the amount of radiation absorbed by a particulate suspension is not straightforward. Both scattering and absorption depend on the particles diameter, NPs in suspension almost always forms aggregates or agglomerates; therefore the optic of an aqueous suspension is not relevant to the size of primary particles. As a general rule, smaller particles will have a higher percentage of extinction, due to their greater ability to absorb light (Haiss *et. al.* 2007).

Based on the Mie theory and with results acquired using UV-Vis spectroscopy, methods to calculate the diameter of NPs suspended in a known and stable concentration are developed (Zook *et. al.*2011). When the analytical relations between the extinction efficiency (q_{ext}) and diameter, acquired by other techniques such as dynamic light scattering (DLS) or electron microscopy (EM) (e.g. Transmission EM or Scanning EM), are established, a determination of the particle concentration (c) can be also accomplished (Paramelle *et. al.* 2014). Optical quantification methods provided by UV-Vis spectroscopy received a great popularity with gold and silver NP, this is mainly due to the techniques ability to monitor passivation (e.g. oxidation), and over-time degradation of a sample through aggregation (Paramelle *et. al.* 2014, Haiss *et. al.* 2007). The MatLab coding used to utilize the results from UV-Vis in order to get the concentration of NPs in suspension can be seen in **Appendix 1.**

2.2.8 Scanning Electron Microscopy (SEM)

The suspension of Titanium dioxide NPs were prepared as described in **Section 2.1.1** and further diluted to 100µg/ml prior to use for the preparation of the samples. The samples were prepared on silicon mounts (Agar Scientific, UK), 2µl of each of the NPs in suspension were drop-cast on a silicon wafer that was positioned at a 45° angle and were left to dry for 24h at room temperature. The imaging was carried out on an ultra-high resolution FE-SEM S-4800 (Hitachi, Japan), in the following magnifications, 10.3 x 6.00K SE(U),10.3 x 35.00K SE(U),10.3 x 60.00K SE(U) and 10.3 x 180.00K SE(U).

2.2.8.1 Energy-Dispersive X-ray spectroscopy (EDX)

Elemental composition of the sample was identified by EDX. Each element emits specific energy X-rays, the electron diffraction spectrometer (EDS detector (Oxford Instruments, UK) is used to separate the characteristic X-rays of different elements, that information are analysed by the Integrated Calibration and Application Tool (INCA) software (OXFORD Instruments, UK).

As with SEM, TEM can also provide the ability to determine the presence of the element in sample by energy dispersive X-ray spectroscopy (EDX). EDX is an analytical technique for chemical characterisation and can create an elemental composition map of a selected sample area. In principle the technique works by the incident beam exciting an electron in an atomic inner shell, this removes it from that shell creating an electron hole. This hole will be filled by an electron from an outer higher energy ring, this means that the difference in energy between the higher and lower energy shell can be released in the form of an X-ray. An energy-dispersive spectrometer within the TEM can measure the number and energy of the X-rays. This energy will be characteristic of the difference in the energy between the electron shells and hence the atomic structure of the element. From this a multiple channel analyser is able interpret the X-ray data and produce an elemental spectrum (Lawes, 1987).

2.2.9 NP protein Corona Purification and identification

Hard protein corona identification of MONPs within biological media and dispersion buffer was performed by using the steps outlined in the following paragraphs. Initially all MONPs

at the maximum concertation used for cell treatments and toxicity tests (for dSPIONs was 100µg/ml and for both titanium dioxide NPs it was 50µg/ml), suspensions were incubated in 1.5ml Eppendorf tubes with 1ml of DMEM or RPMI with FBS at a concentration of 10%, MONPs were also incubated with the developed suspension buffer mentioned in **Section 2.1.1** The diluted NP suspensions were thoroughly vortexed for 30s. Samples were then placed into an orbital shaker at 250g for 1h. Following the above step in order to isolate the NP hard corona the sample tubes were centrifuged for 45min at 18000g at 37°C and the supernatant was removed via gentle pipetting.

Following the isolation of a pellet containing the NP-hard protein corona complex a serious of washes with PBS were carried out. In order for the washes to be performed the pellet was resuspended in 1ml of PBS by gentle pipetting and centrifuging the samples at 18000RCF for a period of 20min. This step was then repeated at a total of 3 times in order to remove any traces of the lightly bound to the agglomerates soft protein corona.

The resultant pellet was prepared for Sodium Dodecyl Sulphate Polyacrylamide Gel Electrophoresis (SDS-PAGE). The NP-hard protein corona complexes were suspended in 20µl of SDS-Page loading buffer which consisted by nine parts loading buffer (Cell signalling technologies, UK) one part dithiothreitol (DTT) (Sigma-Aldrich, UK). The final product was then heated at 100°C for the period of 5min in a heat block. Construction of SDS-PAGE gels was undertaken using 4% stacking gel and a 10% resolving gel as presented at table. SDS-PAGE gels were constructed of a 4% stacking gel and a 10% resolving gel as in **Table 2.2**. Initially 1.5 mm glass plates were washed with ethanol and assembled in a casting stand. The resolving gel was cast first (with a 2 cm gab left), gel was overlaid with isopropanol and allowed polymerise for 1h. The isopropanol was then removed and the stacking gel applied with a comb to allow well formation and left to polymerise for 1h. The comb was removed and gels placed into an electrode assembly/clamping frame and filled with running buffer (25 mM Tris, 192mM glycine, 0.1% SDS). A protein sizing ladder (BioRad Dual colour standard, BioRad, UK) 3.2.9.1 was loaded in to the first gel (2 µl) well followed by each sample (15µl) into individual wells. Gel was run at 120v until the dye had reached the bottom of the gel.

Visualization of the of the SDS-PAGE protein bands was carried out using the Pierce® Silver Stain Kit (Thermo scientific, UK). All the washing and staining steps that follow were carried out in glass staining trays. Initially the gels were washed twice using ddH_2O for the period of 5min. Gels were then fixed using 30% ethanol and acetic acid solution overnight. Fixative was washed twice using 10% ethanol with and two washes with ddH_2O followed. The gel was then washed with silver stain sensitizer solution that consisted by 1-part silver stain sensitizer 500 parts ultrapure water. Staining was performed using a 30min wash with that consisted by 1-part silver stain enhancer 50 parts silver stain. Staining was subsequently visualised by addition of developer solution until bands were clear but not over developed (developing was stopped by the addition of 5% acetic acid).

Table 2. 2: Preparation of 4% and 10% stacking and resolving gels for SDS-PAGE

	Stacking gel (4% SDS)	Resolving gel (10% SDS)
1. 30% Acrylamide (ThermoFisher)	650 µl	5 ml
2. ddH2O	3 ml	6 ml
3. 1.5M Tris (Sigma-Aldrich, UK)		3.75 ml
4. 1M Tris	1.25 ml	
5. 10% Sodium dodecyl sulphate (SDS) (Sigma-Aldrich, UK)	50 µl	150 µl
6. 10% ammonium persulfate (APS) (Sigma-Aldrich, UK)	25 µl	75 µl
7. Tetramethylethylenediamine (TEMED)(ThermoFisher, UK)	5 µl	µl

2.3 Cell culture

All newly prepared cell culture medium was sterility tested and the cell line routinely tested for Mycoplasma using the MycoAlert detection kit (Lonza, Slough, UK).

All cell types were adjusted to a suspension of 2×10^5 cells/ml in complete medium (different for each of the cell lines and is described in section 2.3.2) and used for all subsequent experiments and passaging. Cell concentrations were determined using a Z1 Coulter Counter (Beckman Coulter, UK), 50µl of cell suspension were placed in 50ml of diluent (Beckman Coulter, UK). Events were counted at a size range 10 – 17 µm and cell concentrations were established using **Equation 2. 1**:

$$Volume\ of\ stock\ cells\ required = \left(\frac{\text{Concentration required}}{\text{Concentration of stock cells}}\right) \times New\ volume\ of\ cells\ required$$

Cell culture examination to assess cell health and confluence was undertaken using an Axiovert light microscope (Carl Zeiss, Cambridge, UK). Long term cell storage of both cell lines used in this study was undertaken by suspending cells at a concentration of cells/ml in a solution of one part dimethyl sulfoxide (DMSO) (Sigma, UK) to nine parts FBS in cryovials (Elkay Lab Products, Basingstoke, UK). Cells were then frozen at -80°C overnight in a vessel containing isopropanol. Cryovials were then transferred to liquid nitrogen for long-term storage.

2.3.1 Oxygen cell Culture Environment

Hyperoxic environment (21% O_2, 5% CO_2) experiments were carried out in A Class II tissue culture hood (Scanlaf Mars, Denmark) that was UV sterilised and cleaned with 70% ethanol prior to cell culture. A NU-5510 DHD Autoflow incubator (Nuaire, UK) was used to maintain cells at a temperature of 37°C in a 5% CO_2 atmosphere. Prior to cell culture the reagents were pre-warmed to a temperature of 37°C in a water bath in an ambient oxygen environment (21% O_2).

Physioxic environment (5% O_2, 5% CO_2) experiments were carried out in a Invivo$_2$ physiological cell culture workstations (Ruskinn International, UK). Prior to use all culture reagents and media were acclimatised for 48h in the physioxic culturing environment. All

cell lines were cultured for 48h at a temperature of 37°C in a 5% O_2, 5% CO_2 atmosphere prior to any investigated endpoint described in the physioxic environment.

2.3.2 Culturing of the different cell lines

The hepatocellular carcinoma cell line HepG2 was purchased from the European Collection of Authenticated Cell Cultures (ECACC) and cultured in DMEM supplemented with 10% FBS, 1% L-glutamine and antibiotics. The cells were grown to at least 80% confluence at 37°C in a 5% CO_2 atmosphere. Flasks at >80% confluence required splitting; media was removed and cells washed twice PBS (Sigma, UK), following the second wash cells were then treated with trypsin, and afterwards transferred to a 15ml centrifuge tube and centrifuged at 230 g for 4 min. Cells were reseeded at $1x10^5$ cells/ml and passaged for at least two weeks prior to use following resurrection from liquid nitrogen. Passaging of cells was undertaken every 2-3 days.

The monocyte cell line THP-1 was purchased from American Tissue Culture Collection (ATCC) and cultured in RPMI 1640 containing 10% FBS, 1% L-glutamine and antibiotics. Cell were passaged every 2-3 days by re-suspending in complete medium after to centrifugation at 800rpm for 5 min. THP-1 were differentiated to the non-proliferating adherent cell line dTHP-1, a macrophage resembling cell line, by addition of PMA at 50nmol for 48h, and a recovery period for 24h.

2.4 Cell section imaging by TEM

Prior to imaging by TEM, cell samples destined for NP uptake analysis required embedding in epoxy resin and ultra-sectioning to 70 nm thick sections.

2.4.1 Cell Preparation and Resin Embedding for TEM

Following NP treatment, cells were washed and trypsin was used for 5 min to detach the cells from the tissue culture flask also known as a trypsinization process (trypsinized), cells were then re-washed in maintenance buffer (Table 2.7) and placed into 0.5 ml Eppendorf tubes. Cell pellets were resuspended in 100 mM phosphate buffered 2.5% glutaraldehyde fixative (Table 2.7) for 15 min at 37°C, cells were then pelleted (230 g for 10 min) and re-

suspended in fresh glutaraldehyde fixative for 4h at 4°C. Fixative was aspirated and 0.5 ml of maintenance buffer placed over cell pellets, samples were then left overnight.

Following overnight incubation, cells were pelleted (230 g for 10 min) and washed once in maintenance buffer. Cells were then post fixed in 1% osmium tetroxide fixative (Table 2.7) for 1.5 h at 4°C in the dark on a rocker. After secondary fixation cells were re-pelleted at 230 g speed for 10 min and the fixative aspirated off. At this stage the TAAB Premix resin kit (TAAB Laboratory and Microscopy Reagents, UK) was prepared by the addition of the hardener to the resin and placed on a roller for 1h, after 1h accelerator component was added. Prior to adding resin to cell pellets dehydration stages were undertaken; cells were placed in 10% ethanol for 10 min, 70% ethanol for 30 min and then twice in 100% ethanol for 20 min, all dehydration stages were undertaken under gentle agitation. Cell samples were place into 100% propylene oxide for 20 min (twice), then placed in 1:1 ratio of resin and propylene oxide for 90 min, finally cells were placed into 100% resin overnight at 4°C (resin was stored at -20°C). Resin was pre-warmed at room temperature on a roller, and then the cell sample resin replaced with 100% fresh resin). Cell samples were then placed in an oven at 60°C for 24h with the caps left open (to allow any residual propylene oxide to evaporate).

2.5 Quantification of dSPIONs-Cell Interaction through identification of Iron concentrations

The Ferrozine assay was used to measure the amount of iron internalized by each cell line after a 24h exposure to the selected range of doses (Riemer *et. al.* 2004). The procedure was adapted from Singh *et. al.* (2012). The reagents used in this experiment potassium permanganate ($KMnO_4$), Neocuproine, Ascorbic acid (Sigma, UK), 3-(2-Pyridyl)-5, 6-diphenyl-1,2,4-triazine-*p*,*p*'-disulfonic acid monosodium salt hydrate (Ferrozine), Ammonium acetate and Ethylenediammonium sulphate (EAS) (Sigma, UK). Three replicates were carried out for each cell line and for every culture environment.

Prior to the experiment the reagents were prepared. Reagent A was made with the following ingredients; 1.8g $KMnO_4$ + 20ml H_2O, 20 ml 2.4M HCl, 2.5 ml of each solution was mixed in new bottle to create reagent A. Reagent B was made with the following

ingredients; 0.042g neocuproine in 1 ml methanol (13.1mM), 0.8g ascorbic acid, 0.049g ferrozine in 1 ml d.H_2O (6.5mM) *Reagent B was made in a separate bottle (final volume of 1.961 ml = ~2ml): 1.3 ml ammonium acetate, 131 µl neocuproine, 500 µl dd$H_2$0, 130 µl ferrozine, 0.8g ascorbic acid. Standards were made with the following ingredients; mixture of 100 µL of $FeCl_3$ standards (0–300 µM) in 10 mM HCl, 100 µL 50 mM NaOH, 100 µL releasing reagent, and 30 µL detection reagents.

Frozen cell pellets were first re-suspended in 200 µl 0.01M HCl (Sigma, UK). 100 µl of Reagent A was added to pellets and standards and incubated at 60°C for two hours (Belly Dancer water bath). Samples and standards are then removed and left to cool to room temperature. 50 µl of Reagent B is then added to standards and samples, a colour change of brown to purple was observed upon vortexing. If samples appear clear this indicates no iron uptake. Samples and standards (100 µl) were loaded later added to a 96 well plate and the absorbance measured by a plate reader at 570nm. Preparation of ferrozine standards: 0.2g ferrous ethylenediammonium sulphate (EAS) was dissolved in 2 ml 0.01M HCl. Distinct concentrations (of the standards were prepared by further dilution using 0.01M HCl. Depending on volume of standards reduce amount of reagents accordingly (*e.g.* if 100µl use 50µl of reagent A and 10µl reagent B).

2.6 Investigation of TiO_2 NPs cellular interaction

The laser beam (488 nm) illuminates cells in the sample stream which go through the sensing area. The laser light scattered at narrow angles to the axis of laser beam is called forward-scatter(ed) (FS) light. The laser light scattered at about a 90° angle to the axis of the laser beam is called side-scatter(ed) (SS) light. The intensities of FS and SS are proportional to the size of cells and the intracellular density, respectively. Increase in cellular-NP interaction was correlated with the shifting/increase of side scattering (SS), which suggests an increase in cellular granularity.

Investigation of cellular interaction of the distinct cell lines with the polymorphs of TiO_2 NPs (NM-102 and NM-104) was carried out with the use of flow cytometry. The experiment was based on the paper Zucker and colleagues (2010) that detection of interaction was based on light scattering principles. Measurements were carried out after a 24h treatment of the

distinct cell lines in the different oxygen culturing environments. After treatment of the cell lines for the period of 24h with the NPs, the cells were collected and washed with PBS twice. The cells were re-suspended in flow cytometry liquid and measurements were carried out. To identify changes in granularity the results were plotted as histograms of the SS against the forward scattering (FS). The extent of the increase in granularity and therefore the interaction of NPs with the different cell lines the measurements were plotted as count against SS. Statistical comparisons were carried in order to determine if the increase granularity/cellular interaction were significant when compared with the negative control.

2.7 Pro-Inflammatory cytokine quantification using an Enzyme-Linked Immunosorbent Assay (ELISA)

Following a 24h treatment of the cells with the mentioned NPs, supernatants were collected and stored in -20C°. Quantification of TNF-α (DTA00C) & IL-8 (CXCL8) was carried out using ELISA Kits that were purchased from R&D, UK. Capture antibody was diluted in a concentration of 4 µg/ml and loaded in 96-well plates (Corning incorporated, UK) at a volume of 100 µl. Following loading the plate was covered with parafilm and it was incubated at room temperature overnight. Cytokines standards were prepared as described according to manufacturer's instructions; all supernatant samples were diluted 1 in 10. After a 1h incubation with the blocking buffer the plate was washed 3 times with wash buffer and 100 µl of standards and samples were loaded and the plate was incubated for 2h. Dilution of the detection antibody in a concentration of 20ng/ml in 4ml of reagent diluent was carried out. After incubation samples and standards were removed and the wells were washed 3 times with wash buffer; 50 µl per well of detection antibody was then added to the plate followed by 2h incubation. Removal and washing of the wells was repeated, 100 µl of streptavidin-HRP (1:200 dilution of stock) was added to each well and the plate was incubated in the dark for 20 min at room temperature. The plate was washed for one more time after incubation with 100 µl of SureBlue™ substrate solution (KPL Inc., USA) in the dark until the colour had sufficiently developed. The reaction was stopped by the addition 38 µl of 50 1M HCl. Finally, the optical density (absorbance) of the samples was determined by using a FLUOstar Omega Multimode microplate reader (BMG LABTECH Ltd, UK) set to 450 nm. Optical density of the standards was used to generate a standard curve which was used to determine concentrations in the unknown samples. Three replicates of ELISA cytokine

analysis were performed for each cell type (THP-1, dTHP-1 and HepG2), each dose and for each of the culture environments (hyperoxic and physioxic).

2.8 Intracellular reduced Glutathione

The Glutathione Detection Assay (fluorometric) (AbCam, UK) was used for the determination of glutathione concentration. After a 5h treatment with NPs at the concentrations described in **Section 2.1.2**, $1x10^6$ cells in 1ml for each of the treatments were harvested and washed twice using PBS. All centrifugation steps were carried out at a speed of 250g. After a 5min centrifugation with PBS the pellets were re-suspended in 100µl Cell Lysis buffer and incubated in ice for 10min. The samples were centrifuged for 10min at 4°C; the supernatant was collected and transferred in a clean tube. The samples were kept on ice, a deproteinization of the samples step was initiated by adding 1 volume of ice cold 100% (w/v) trichloroacetic acid (TCA) (Sigma Aldrich, UK) into 5 volumes of sample, each of the tubes was then vortexed for 30seconds and incubated on ice for 10min. The samples were then neutralised by adding sodium bicarbonate (Sigma Aldrich, UK) drop by drop till the pH equals 4-6. The samples were then centrifuged for 15min at 4°C and the supernatant was collected. Standards were prepared in concentration of 0-1µg/well. A black bottom 96 well assay black plate with clear bottom (Corning incorporated, UK) was loaded with 100µl of sample and standard. The wells were then loaded with 2µl of each the dye monochlorobimane and GST reagent. Fluorescence was measured using a Clariostar pate reader (BMG Labtech, Germany) at excitation 380nm and emission 461nm. Three replicates were performed for each cell type (THP-1, dTHP-1 and HepG2), each dose and for each of the culture environments (hyperoxic and physioxic).

2.9 Cell viability assessment

RPD was used to calculate the cellular viability for HepG2 and THP-1 cells, after counting cell numbers using a Z™ Series COULTER COUNTER® (Beckman Coulter, UK). An initial cell count was undertaken prior to NPs treatment which was used as the initial cell count number in Equation 2.8. After treatment for the period of 24h with NPs and standard (Mitomycin-C at 0.05µg/ml) the effects on cell viability were identified using the relative population doubling (RPD) (**Equation 2.8**).

dTHP-1 stop dividing after exposure to PMA (**Section 2.2**). Therefore, the numbers of live / dead cells were determined both prior and after treatment using Trypan blue (0.4% solution) and a haemocytometerThe measurements were used to produce a relative increase in cell count (RICC). The formulas used for the calculations of RPD and RICC were found in Lorge *et. al.* (2008) and are presented below:

Equation 2.8: RPD= $\frac{\text{No. of population doublings in treated cultures}}{\text{No. of population doublings in control cultures}} \times 100$

Equation 2.9: RICC= $\frac{\text{Increase in number of cells in treated cultures (final – starting)}}{\text{Increase in number of cells in control cultures (final – starting)}} \times 100$

2.10 *In Vitro* Cytokinesis Block Micronucleus assay (CBMN)

HepG2 cells were cultured as described in **Section 2.2** and were seeded in 25cm^3 flasks at a concentration of 2x10^5 cells/ml that were incubated for 24h. Cell treatments of all NPs were then undertaken for a period of 24h in the concentrations mentioned in **Section 2.1.2.** The concentration of the NPs were used to treat the cells in this study are relevant to the dosages employed in clinical trials, and were adopted from Singh *et. al.* 2012. Mitomycin-C (Sigma Aldrich, UK) was chosen as the assays positive control, it was used at a concentration of 0.05µg/ml. After treatment for a period of 24h the cells were washed three times with PBS and clean medium was added. Cell cycle arrest was achieved by exposing the cells to cytochalasin B 0.5µg/ml (Sigma Aldrich, UK) for 24h. NP treated HepG2 cells were washed with PBS twice, 2ml of trypsin/EDTA solution was added to detach adhere cells from the flasks. After detaching the cells 5ml of PBS was added and the cell suspension was transferred in 15ml centrifuge tube and centrifuged for 5min in 230xg.

2.10.1 Cell Harvesting and Micronucleus scoring

All centrifugation steps that follow were performed for 10 min at a speed of 230xg and a temperature of 4°C. The supernatant was discarded and the cells were re-suspended with

hypotonic solution (KCl 0.56%) and centrifuged. The supernatant was removed and the cell pellet was re-suspended in **Fixative 1** {methanol: acetic acid: 0.9%NaCl (5:1:6 parts)} and centrifuged. Four washes with **Fixative 2** {methanol: acetic acid (5:1)} were performed by centrifuging and re-suspending the cells. After the fourth wash the cells were incubated at 4°C overnight. Prior to slide preparation the slights were incubating in Fixative 2 at 4°C overnight and washed once by rinsing with ddH_2O. Slides were prepared by pipetting 100µl of the cell suspension. The slides were dried for 24h and stained by applying 30µl of 40,'6-diamidino-2- phenylindole (DAPI) (Vectashield, UK) for the period of 15min. The scoring of the cell was carried out using the METAFER automated analysis system (MetaSystems, Carl Zeiss Ltd). 6000 binucleated cells were scored for each of the doses (after three replicates of 2000). Following automated scoring a manual check was performed of the image gallery to ensure all micronuclei had been appropriately identified by the software.

2.10.2 Centromere Staining

Buffers used for the experiment **include, 10*SSC:** 43.8g NaCl and 22.05gSodium Citrate in 500ml in ddH_2O, **Reagent A** made by70% Formamide and 2*SSC and **Reagent B made** 0.4*SSC with 0.3%Tween20.

Supernatant was removed and the pelletized treated HepG2 were re-suspended in 90% Methanol. Density of the cells in suspension was checked under a microscope and adapted after visual investigation. Cytospin harvesting commenced, 150µl of the cell suspensions was dispensed into a Megafunnel ™ and centrifuged at 1,000 rpm for 5min using a cytospin (Thermofisher, USA). The slides where then removed and left to dry for 24h. A mini-oven (Hybaid Limited, UK) was prepared at a temperature of 42°C, a tray of PBS was added to keep the min-oven humid. Prior to staining **Reagent A** and **Reagent B** were prepared. Star*FISH© Human Chromosome Pan-Centromeric Probes (Cambio, UK) were defrosted by keeping them at room temperature for 15 minutes. The Slides were transferred into the prepared mini-oven and incubated for 10 minutes. Chromosome denaturation was performed by incubating the slides for 2 minutes in a coplin jar filled with **Reagent A** in a 70°C water bath. 8.5µl of the pan-centromeric probe was applied to each of the slides; they were then covered with cover slips and incubated for 5min at room temperature. The probe was denatured in a mini-oven providing dry heat, which was set at a 70°C for 15 minutes,

then the temperature was reduced to 42°C and the slides were incubated for 20h. After incubation the cover slips were removed and the slides were agitated in a coplin jar filled with **Reagent B** for 2 minutes. A coplin jar filled with Reagent A at room temperature was used for a 2 min wash of the slides. Lastly the slides were stained with 10µl of 40,'6-diamidino-2- phenylindole (DAPI)/ Vectashield (Vector Laboratories, USA) and the cells were scored using the metafer automated analysis system (MetaSystems, Carl Zeiss Ltd).

DAPI was excited at a wavelength of 360nm, and FITC which the centromeres were labelled with, was excited at a wavelength 500nm. Further information on what a centromere positive and centromere negative micronuclei looks like can be found in **Section 4.3.5.** Clastogenic responses were deemed when no centromeres were identified in a formed MN, and aneugenic responses where labelled as such when a centromere was identified in a formed MN. 100 bi-nucleated cells with present micronuclei (33 from each of the 3 replicates) were scored for each of the treatments, which allowed the identification of aneunogenicity and clastogenicity.

2.11 Mitotic Spindle analysis

HepG2 cells were cultured as described in **Section 2.2** and were seeded in 25cm^3 flasks at a concentration of 2x10^5 cells/ml that were incubated for 24h. Treatments of HepG2 cells were carried out only in concentrations of 100µg/ml of dSPIONs, 10µg/ml of NM-102 TiO_2 and 10µg/ml of NM-104 TiO2 and a negative control as mentioned in **Section 2.1.2**.

For staining microtubules, cells were fixed with 3% paraformaldehyde in PBS for 30 min and permeabilized with 0.1% Triton X-100 in PBS for 10 min in room temperature (Triton-X, Sigma-Aldrich). All solutions applied directly to slides used a volume of 200 ml per slide. Slides were incubated in blocking solution (0.3% Triton-X, 1% Bovine Serum Albumin, diluted in PBS) for the period of 20 min at room temperature. This was followed by an overnight incubation at 4℃ in Anti-alpha Tubulin antibody [DM1A] - Microtubule Marker (AbCam, UK) at a 1:100 concentration diluted in the blocking solution. After rinsing in 1× PBS, sections stained by applying 30µl of 40,6-diamidino-2- phenylindole (DAPI) (Vectashield, UK) for the period of 15min in room temperature. Scoring of dividing cell was carried out on fluorescent microscope. Three replicates of 100 mitotic cells were investigated (total of 300

cells) and allocated to each of the following categories; monopolar spindle, bipolar Spindle (normal) and multipolar Spindle.

2.12 Intracellular Ca^{2+} signalling

Following treatment with the distinct NPs in the different culture oxygen environments for the periods of 30min, 5h and 24h with the concentrations described in **Section 2.1.2** investigations on the effects of Ca^{2+} intracellular levels was carried out. All cell lines were seeded in a 96 well assay black plate with clear bottom (Corning incorporated, UK) at a concentration of $2*10^5$ cells/ml. lines (*e.g.* THP-1 cells). All the measurements were carried at a temperature of 37°C. All physioxic culture measurements were carried at the mentioned environment (5% O_2, 5% CO_2) the measuring chamber of the plate reader was calibrated to resemble that environment. All measurements were carried out using Clariostar Multimode microplate reader (BMG LABTECH Ltd, UK).

An aliquot of FLUO-4AM (Thermofisher Scientific, USA) was diluted in DMSO stock solution to a concentration of 2.5mM. The non-ionic detergent Pluronic™ F-127 (20% Solution in DMSO) (Thermofisher scientific, USA) was added to assist in the dispersion of the non-polar AM ester in aqueous media. An equal volume of 20% (w/v) Pluronic in DMSO was mixed with the aliquot of AM ester stock solution before dilution into the loading medium, making the final Pluronic concentration about 0.02%. The stock solution was further diluted in full medium used for the culture of each cell line at a final concentration of FLUO4AM to be 2.5µM. The organic anion-transport inhibitors probenecid (Thermofisher Scientific, USA) at a concentration of 2.5 mM was added to the cell medium to reduce leakage of the de-esterified indicator. Stock solutions of probenecid are necessarily quite alkaline; it is therefore important to readjust the pH of media to which they have been added. All cell lines were incubated with the mixture mentioned above for the period of 45min. The minimum dye concentration required to yield fluorescence signals with adequate signal to noise was used.

Before any fluorescence measurements took place cells were washed 2 times using PBS by spinning them down to remove any dye and then re-suspended in indicator-free phenol red

medium. Cells were then incubated for a further 20 minutes to allow complete de-esterification of intracellular AM esters.

2.13 Measurement of intracellular Ca^{2+}-antioxidant pre-treatment.

All cell lines were pre-treated with 25 mM of the hydrophobic antioxidant Trolox, diluted in DMSO for the period of 24h prior to treatment with the distinct NPs for 5h. Control cells received either cell medium only (complete medium in the absence of phenol red) (control) and complete medium (in the absence of phenol red) supplemented with either Trolox (antioxidant control). After treatment to NPs staining with FLUO-4AM and measurements were carried out as described in **Section 2.10**. Investigation into the effects of exposing cells pre-treated with either Trolox was repeated a total of three (n = 3) times.

2.13.1 Determination of the effects in different Ca^{2+} organelles

- Following treatment as described in **Section 2.10** the effects of NP treatment had on the Endoplasmic reticulum Ca^{2+} levels (ER Ca^{2+}) were determined using thapsigargin. Thapsigargin stimulates release of Ca^{2+} from the endoplasmic reticulum (ER). All the cells were then stimulated with 100 nM of Thapsigargin diluted in DMSO, for the period of 20min, this was carried out during the final step of staining mentioned in **Section 2.10**.

- Determination on the effects 30min treatments with the distinct NPs had on lysosomal Ca^{2+} levels was determined using GPN. After treatment and staining with FLuo4-AM (as mentioned in **Section 2.10**) the black plate with clear bottom (Corning incorporated, UK) with the cells was loaded in a clariostar Multimode microplate reader (BMG LABTECH Ltd, UK). The software was programmed to perform a continuous measurement for the period of 80s. An injection of Glycyl-L-phenylalanine 2-naphthylamide (GPN) was administered using the needle/syringe of the machine after a period of 10. Final concentration of GPN (Sigma-Aldrich, UK) varied depending for each of the cell lines 50µM for THP-1, 100µM for dTHP-1 and 200µM GPN for HepG2.

2.13.2 Immediate response to changes in intracellular Ca^{2+} homeostasis

The immediate effects of treatments with the distinct NPs on the intracellular Ca^{2+} homeostasis were investigated using the injection system of the clariostar multimode

microplate reader. The different cell lines were seeded and stained as described in **Section 2.10** above.

The injection machinery (tow provided pumps) of the plate reader was primed using two diluted Eppendorf tubes for each of the NPs. The two tubes were at concentrations seen at table 2.8 a, the volumes used for the treatment of the cells and the final concentration of NPs in the well can be found in **Table 2.3**. The measurements were carried for the period of 300seconds in total. The injection of the NPs and the positive control were carried out after measurement for 30s. As soon all the replicates (n=3) were carried out for the NP treatments, the pumps were then primed with full medium (pump 1: negative control, complete medium), and the positive control used for this experiment, the ionophore known as A23187 (Sigma-Aldrich, UK) at a concentration of 0.5 nmol/mg (Pump 2).

Table 2. 3: dSPION, NM-102 and NM-104 volume used for each of the immediate response treatments. *Only used with dSPIONs

Pump used:	Volume injected (µl)	Concentration of NP in well (treatment) (µg/ml)	
Pump 1 (70 µg/ml)		5.5	2
Pump 1 (70 µg/ml)		11.5	4
Pump 1 (70 µg/ml)		23	8
Pump 1 (70 µg/ml)		29	10
Pump 2 (500µg/ml)		20	50
Pump 2 (500µg/ml)*		40 *	100*
Pump 1 Negative control (Complete medium)		40	0

2.14 Data and Statistical Analysis

GraphPad Prism 6 was used for the plotting and the statistical analysis of all the results. All data is presented as mean and standard error (SEM). Normality of the data was performed using the D'Agostino-Pearson normality test. The choice of a parametric or non-parametric test depended on the outcome of the normality test which was performed using the software GraphPad PRISM (USA). Two-way ANOVA and Tukey's multiple comparisons test were used to compare the results in all cell lines between each dose, the untreated controls and the different oxygen environments. All of the statistical analyses of the acquired data we were completed with *a* $p \leq 0.05$ considered as significant. Unless otherwise stated all experimental data were gathered in in three replicates unless it is stated otherwise.

Chapter 3: Primary and secondary characterization of metal oxide NPs

3.1 Introduction

The physicochemical characteristics of engineered NPs influence the distinct behaviour they will have in a biological environment, as discussed in detail in **Section 1.2**. Thus, evaluation of the physicochemical characteristics of NPs is necessary prior to toxicological studies in order to understand their ability to interact with cells and potentially induce toxicity (Rivera-Gil *et. al.* 2010).

When the nanotoxicology field was at an early stage, the importance of the assessment of NPs physicochemical characteristics prior to toxicological screening was not well understood. Consequently, reports in the literature were highly contradictory when apparently investigating the same material. However, it became increasingly evident that differences in NM properties, such as size/agglomeration status, surface charge, shape and chemical composition could affect the outcome of the toxicological endpoints (Hall *et. al.* 2007). For example, when different sized TiO_2 and carbon black were tested in rat lung tissue for inflammatory responses, the researchers suggested that the bulk material was non-toxic whereas the nano-sized materials demonstrated toxic potential, and that the carbon NPs were more toxic than the TiO_2 (Renwick *et. al.* 2004). Whereas, in a different study, nano-sized TiO_2 and carbon black induced similar behaviour when exposed to lung alveolar L-2 type II cells (Barlow *et. al.* 2005). The limited characterization provided in studies for materials that are seemingly the same and in similar concentrations, does not allow detailed comparisons to better understand the different toxicological results.

Characteristics of NPs are divided in to primary and secondary features. NM characterization conducted following their synthesis is deemed as the primary characterisation. Primary NM characteristics include size, morphology, surface area, composition/purity, surface charge, surface chemistry and potentially endotoxin contamination (Saves and Warheit, 2009). Secondary characterisation of the NPs is conducted after their exposure to a test system (e.g. biological environment, experimental environment); these may include assessment of agglomeration state, suspension stability, dissolution and protein corona formation (Johnston *et. al.* 2012). It is of critical importance to consider both primary and secondary physico-chemical features as they can substantially differ from each other. NM behaviour under experimental conditions, such as their agglomeration status and stability of their

dispersion in different diluents, can be very different from the primary particle features as previously discussed in detail within **Section 1.2.2,** therefore characterisation remains critical in truly understanding the biological impact of NM exposure (Johnston *et. al.* 2012). Evaluation of both primary and secondary NM characteristics is thus a core component of any nanosafety orientated study, as it allows the comparison of data generated across the scientific field.

Despite, the critical need of thoroughly evaluating the physico-chemical features of NM applied in nanosafety studies, a wide range of approaches exist for the characterization of NM primary and secondary characteristics. Depending on the NM under investigation certain techniques are not appropriate. For example, in terms of agglomerate sizing DLS and NTA are some of the most widely used measurement techniques (Filipe *et. al.* 2017). Although, one may not be the most appropriate depending on the NM under investigation and the diluent used for dispersion, this will be further discussed based on the results produced in this chapter. Better understanding and application of characterization techniques is required in the field of nanotoxicology in order to archive correct identification of NM primary and secondary characteristics.

3.1.3 Study Aim and objectives

The aim of this Chapter was to characterise the physico-chemical properties, namely, agglomerate status, hydrodynamic diameter, elemental composition and morphology/shape of the mental oxides NPs (MONPs) under investigation: NM-102 (Anatase TiO_2), NM-104 (Rutile TiO_2) and dFe_3O_4. Undertaking detailed and robust characterisation of the test NPs was necessary to fully understand the biological and toxicological behaviour of the NPs used throughout this thesis. The primary characteristics of the NM under investigation in this study were thoroughly described through previous studies (Evans *et. al.* 2016 and Singh *et. al.* 2012, Rasmussen *et. al.* 2014). Thus, the focus of this Chapter was to evaluate the secondary characteristics of the test NPs following dispersion in the range of diluents to be applied in the later toxicological studies in the thesis: 0.05% BSA, 10%FBS DMEM and 10% FBS RMPI. These characteristics evaluated included the determination of the stability, concentration of NM in suspension and the rate of their sedimentation to identify correct concentrations for exposure regimes, the formation of a protein corona and endotoxin contamination in the samples. In addition, comparison of different techniques used for agglomeration assessment of NPs, namely, DLS, NTA and SEM, was applied in order to determine the best combination of approaches to evaluate NM behaviour in an *in vitro* environment.

3.2 Materials and Methods

3.2.1 Particle Preparation and Characterization

Dextran-coated Fe_3O_4 NP's (dSPIONs) were purchased from Liquids Research (Bangor, UK). A stock of dSPIONs were vortexed for 10s and then suspended in the appropriate growth media (10% FBS RPMI or 10% FBS DMEM) prior to cell treatments. Two different types of titanium dioxide (TiO_2) NPs were used for this study, NM-102 and NM-104. The TiO_2 were supplied from the Joint Research Centre (JRC) repository and were supplied as a dry powder (Rasmussen *et. al.* 2014).

3.2.1.1 Dispersion process for TiO_2

Dispersion buffer was produced by using sterile filtered bovine serum albumin (BSA) (Sigma Aldrich, UK). After sterile filtrations, the final concentration of the Dispersion Buffer was "0.05% BSA dH_2O_2". TiO_2 NP powders were dispersed at a concentration of 1mg/ml (in the dispersion buffer). The NP suspension was sonicated for the period of 1h at a frequency of ~30Hz as described in **Section 2.2.2.**

3.2.2 Dynamic light scattering and NP tracking analysis

To identify the hydrodynamic diameter (or radius) of the dSPIONs, NM-102 and NM-104 different light scattering techniques were used. These include utilization of the widely used Malvern ZetaSizer Nano ZS (Malvern instruments Ltd., UK) and the Malvern Nanosight LM-12 (Malvern instruments Ltd., UK). Further information on the background and the set up according to each of the instruments operating manual can be found in **Section 2.2.4**. Three replicates were carried out for each experiment.

- Dilution of dSPIONs at the concentration used for the treatment of cell lines (100µg/ml) was carried out in PBS (Sigma-Aldrich, UK) and distilled-deionized H_2O (ddH_2O).

- The hydrodynamic diameter of TiO_2 polymorphs was monitored for 24h, prior to the experiment all the samples were prepared as mentioned in **Section 2.1** and further diluted in the dispersion buffer "0.05% BSA ddH_2O". The initial concentration in suspension was 100ug/ml.

3.2.2.1 Determination of Zeta potential using DLS

The z-potential values of the NP's were determined by a Malvern ZetaSizer Nano ZS (Malvern instruments Ltd., UK). Samples were prepared as described in **Section 3.2.2** and 500 µl of particle suspension was injected into a Folded Capillary Cell (Malvern, UK) using a 1 ml syringe. The capillary cell was placed into a Malvern ZetaSizer Nano ZS (Malvern instruments Ltd., UK) and allowed to equilibrate for 2 min before the measurement process. The z-potential values presented are the average of 3 scans and the experiment was performed in a triplicate.

3.2.3 TiO_2 NP sedimentation Studies

Visual identification of the TiO_2 NPs sedimentation as a result of agglomeration was investigated at different concentrations and time points. For the two experiments that follow images of the sample were taken for each of the steps as described below:

- The samples were imaged following the dispersion of the TiO_2 NPs (as described in **Section 3.2.1)** at a concentration of 1mg/ml. Pictures of the samples were taken after incubation for 2h in 37°C. The particles that remained in suspension were used to prepare three samples. The first sample was 400µl of the supernatant (particles in suspension). Sample two and three were 200µl of the supernatant in 800µl of the medium used for cell culture as described in **Section 3.2.1.**

- The dispersed sample of the TiO_2 NPs (as described in **Section 3.2.1)** at a concentration of 1mg/ml was further diluted in dispersion buffer to prepare a sample with a concentration of 100ug/ml. The sample was incubated for 2h in 37°C. As previously described for the experiment above, the supernatant was used to prepare three samples. The first sample was 400µl of the supernatant (particles in suspension). Sample two and three were 200µl of the supernatant in 800µl of the medium used for cell culture as described in **Section 3.2.1.**

3.2.4 Ultraviolet-visible spectroscopy (UV-Vis)

Following dispersion of TiO_2 NPs, as described in **Section 3.2.1**, the suspension of 1mg/ml was further diluted to a concentration of 100µg/ml. Measurements of the optical absorbance by the NPs over the whole light spectrum was measured. Measurements were undertaken immediately after dispersion (0h) and also following incubations at 37°C in a NU-5510 DHD Autoflow incubator (Nuaire, UK) for the periods of 2h and 24h.

UV–Vis absorption spectra were recorded using a U3310 spectrophotometer (Hitachi, Japan). All measurements were made at 37°C in square cuvettes (Sigma- Aldrich, UK) with 1 cm light path. All the measurements were carried in triplicate.

The results were used to calculate the concentration of the NPs in suspension after incubation. Based on the Mie theory and with results acquired using UV-Vis spectroscopy, methods to calculate the diameter of NPs suspended in a known and stable concentration have been developed and were applied in this study (Zook *et. al.*2011). When the analytical relations between the extinction efficiency (q_{ext}) and diameter, acquired by other techniques such as DLS are established, a determination of the particle concentration (c) can also be accomplished (Paramelle *et. al.* 2014). More information on the theoretical background for the analysis and computing of the results to identify the NP concentration in suspension is described in **Section 2.2.7.**

3.2.4 Scanning electron microscopy (SEM) and energy-dispersive X-ray spectroscopy (EDX)

The suspension of Titanium dioxide NPs (NM-102 and NM-104) were prepared as described in **Section 3.2.1.1** and further diluted to 100µg/ml prior to use for the preparation of the samples. The samples were prepared on silicon mounts (Agar Scientific, UK); 2µl of each of the NP's in suspension were dropped on a silicon wafer that was positioned at a 45° angle and were left to dry for 24h at room temperature. The imaging was carried out at an ultra-high resolution using a FE-SEM S-4800 (Hitachi, Japan).

Elemental composition of the sample was identified by EDX. Each element emits specific energy X-rays; the EDS detector (OXFORD Instruments, UK) is used to separate the characteristic X-rays of different elements, which is analysed by the INCA software (OXFORD

Instruments, UK). The technique can also be used in Transmission Electron Microscopy (TEM), therefore the techniques theoretical approach is further explained at **Section 2.2.8**.

3.2.5 NP protein corona purification and identification

Identification of the hard protein corona surrounding MONPs following incubation in biological media and dispersion buffer was performed**.** MONPs were incubated in tubes with 1ml of DMEM or RPMI with FBS at a concentration of 10% and suspension buffer as described in **Section 3.2.1**. The diluted NP suspensions were vortexed for 30s. Samples were then incubated for 1h. Following this step and in order to isolate the NP hard corona, the samples tubes were centrifuged for 45min at 18000xg at 37°C and the supernatant was removed gently.

Following the isolation of a pellet containing the NP-hard protein corona complex, a serious of washes were carried out. Further information on preparation, running and visualization of protein bands by Sodium Dodecyl Sulphate Polyacrylamide Gel Electrophoresis (SDS-PAGE) can be found in **Section 2.2.9**. The experiment was conducted in triplicate and images of the gels were obtained immediately after staining. Quantification of the gel protein bands was undertaken using ImageJ (NIH, USA).

3.2.6 NP endotoxin identification

The MONPs suspensions were all investigated for the presence of endotoxin using Limulus Amebocyte Lysate (LAL) PYROGENT™ (Lonza, UK). The protocol for the endotoxin gel-clot assay is further described in **Section 2.2.3**.

3.2.7 Statistical analysis

GraphPad Prism 6 was used for the plotting and statistical analysis of all the results. All data is presented as mean and standard error (SEM). Normality of the data was performed using the D'Agostino-Pearson normality test. Two-way ANOVA and Tukey's multiple comparisons test were used to compare the results. For all statistical analyses, $p \leq 0.05$ was considered as significant. Unless otherwise stated all experimental data were gathered in three replicates.

3.3 Results

The physicochemical properties of the dry powder form of the two different types of NM-102, NM-104, were thoroughly investigated prior to delivery by the JRC NPs repository, and the results were presented by Rasmussen and colleagues in 2014 (Rasmussen *et. al.* 2014). NM-102 and NM-104 were provided in the form of powder therefore some of the primary characteristics had to be investigated to compare and confirm the nature of the NPs. However, their secondary characteristics after application of the optimised dispersion protocol had to be identified and were thus the focus of this Chapter.

Similarly, the form of dSPIONs used in the present study was previously used in the *In Vitro* Toxicology Group's laboratory and thorough investigation of their properties has been previously conducted (Evans *et. al.* 2016 and Singh *et. al.* 2012). Nonetheless, their secondary characteristics had to be investigated as part of the focus of the present Chapter, to define their secondary characteristics in the experimental environments applied during this study.

3.3.1 Visual identification of sedimentation of Titanium dioxide NPs

Following the dispersion of the dry powder of TiO_2 NPs (NM-102 and NM-104) in the dispersion liquid (0.05% BSA water) at a concentration of 1mg/ml, their stability in different suspension buffers was investigated.

The stability of the TiO_2 NP suspensions was investigated in the dispersion liquid (0.05% BSA water). As is seen in **Figure 3.1**, immediately after dispersion the NP suspensions of both NM-102 and NM-104 at a concentration of 1mg/ml seemed to be homogenous with no visible sediment at the bottom of the tube (**Figure 3.1 A & E**). After a 2h incubation of the dispersed NPs at 37°C a layer of sediment was visible in both NP suspensions, in which was more prominent with the NM-102 (**Figure 3.1 B & F**). To identify whether the NP suspension continued to sediment after the 2h incubation, 400µl of the supernatant was removed and placed in a new tube. As is seen in **Figure 3.1 D & H** the sedimentation after a 24h incubation at 37°C continued, with the greatest level identified in NM-102 where the original milky white suspension turned to a clear liquid and a layer of agglomerated NPs

could be clearly seen at the bottom of the tube. Through visual identification it was evident that NM-102 sedimented to a much greater extent than NM-104.

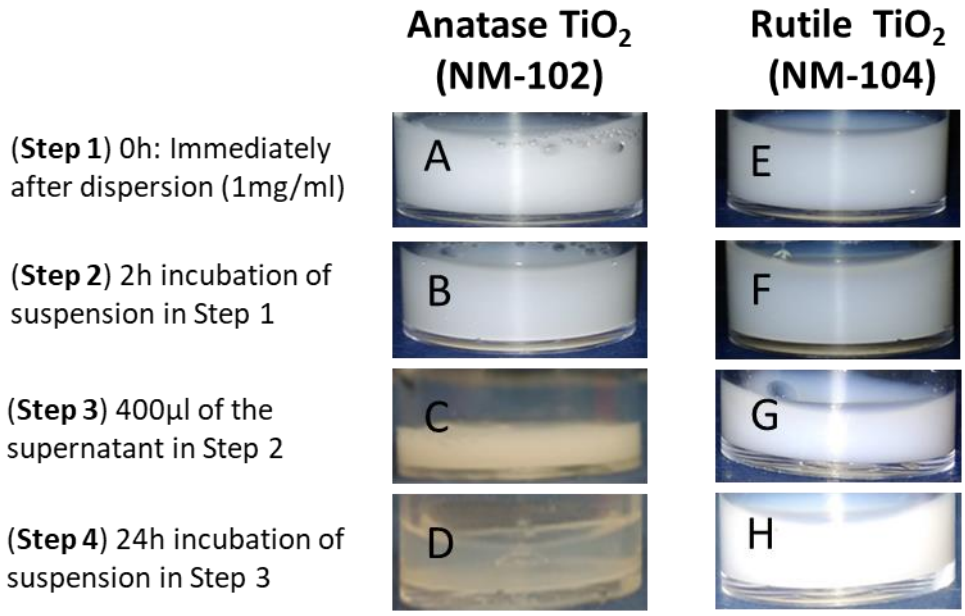

Figure 3.1: Visual identification of TiO_2 sedimentation after dispersion at a concentration of 1mg/ml over time. Immediately after dispersion for (A) NM-102 and (E) NM-104. Incubations were carried for 2h for (B) NM-102 (F) NM-104. After the 2h incubation, 400µl of the supernatant of for (C) NM-102 and (G) NM-104 in Step 2 was removed and added in a new container that was incubated for the period of 24h resulting in the final sedimentation product for (D) NM-102 and (H) NM-104. (n=3)

The next stage of this study involved suspending the two test materials in 800ul of the cell culture medium used for cell culture, namely, 10%FBS-RPMI and 10%FBS-DMEM. As illustrated in **Figure 3.2**, a white colored homogenous suspension was observed after dilution of both TiO_2 NPs in 10%FBS-RPMI (**Figure 3.2 A &B**). A milky pink color was identified after dilution of both TiO_2 NPs in 10%FBS-DMEM, (**Figure 3.2 C & D**). After a 24h incubation of the suspension at 37°C, NM-102 NPs formed a clearly visible white sediment at the bottom of the incubation tube and the liquids took on a clear pink colour (**Figure 3.2 E & F**). After incubation of NM-104 for 24h at 37°C, sediment was visible in both incubation tubes (**Figure 3.2 G & H**). The colour of the liquid after incubation turned into a cloudy pink

in both tubes resembling the colour of the original diluent (**Figure 3.2 G& H**). From the results it is evident that NM-104 showed a promising stability in suspension while, NM-102 nearly completely sediments out over the time period of 24h.

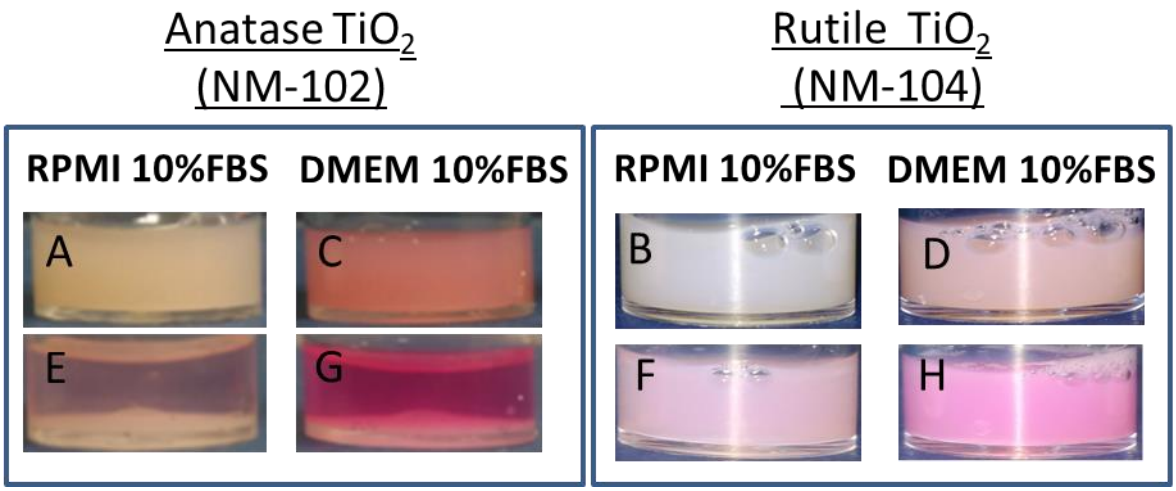

Figure 3.2: Visual identification of TiO_2 sedimentation following suspension in cell culture medium, 200µl supernatant from Figure 3.1 (D) NM-102 and Figure 3.1 (H) NM-104 was diluted immediately after dispersion in 800µl RPMI 10%FBS (A) NM-102 and (B) NM-104. 200µl supernatant from Figure 3.1 (D) NM-102 and (H) NM-104 was also diluted immediately after dispersion in 800µl DMEM 10%FBS (C) NM-102 and (D) NM-104. Images of the samples were taken after incubation for the period of 24h as is seen in (E) for NM-102 and (F) for NM-104 in RPMI 10%FBS and (G) for NM-102 and (H) for NM-104 in DMEM 10%FBS. (n=3)

To identify whether the sedimentation was the result of the large concentration of NPs, the suspension was further diluted by ten-fold (100µg/ml) in the dispersion liquid and the same procedure followed. As is seen in **Figure 3.3 B & F** after the initial incubation of 2h, sediment was still visible at the bottom of the tube for both NP suspensions. In contrast, NM-104 remained in suspension in a higher concentration. When the supernatant was moved into fresh tubes and incubated for 24h, a layer of sediment was not identified at the bottom of the tubes, although the original cloudy white suspension became a cleared transparent colour (**Figure 3.3 D & H**). From the results it is evident that NM-104 showed a promising

stability in suspension although a great amount of the NPs in suspension formed a sediment, while, NM-102 nearly completely sedimented out over the time period of 24h.

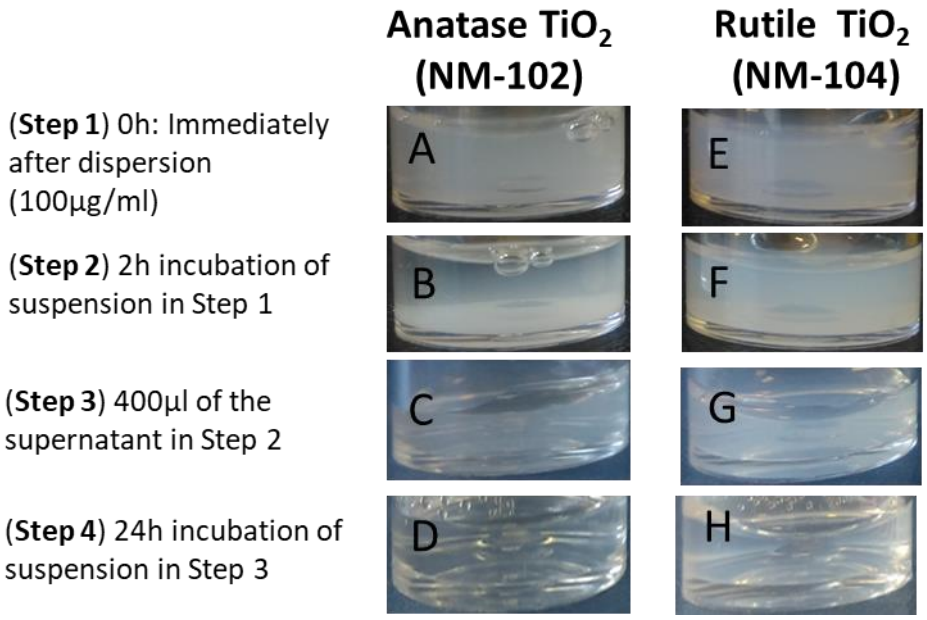

Figure 3.3: Visual identification of sedimentation after dispersion of (A) NM-102 and (B) NM-104 at a concentration of 100µg/ml. Incubations were carried out for 2h for **(B)** NM-102 **(F)** NM-104. After the 2h incubation 400µl of the supernatant of for **(C)** NM-102 and **(G)** NM-104 in Step 2 was removed and added in a new container that was incubated for the period of 24h resulting in the final sedimentation product for **(D)** NM-102 and **(H)** NM-104. (n=3)

As is seen in in **Figure 3.4**, 200ul of supernatant (**Figure 3.3 B&F**) were diluted in 800ul of the different cell culture medium used in this study, namely, 10%FBS-RPMI and 10%FBS-DMEM. No distinct changes were identified in the color of the diluents after the addition of the NPs. After a 24h incubation at 37°C, no changes were identified in terms of the color of the dispersion. Additionally, no layer of sediment was identified at the bottom of the tubes (**Figure3.4 E & F & G & H**). From these results we can conclude that both of the NPs do sediment even in concentrations as low as 100µg/ml after 2h incubation. Use of the NPs that remain in suspension after 2h incubation show increased stability in the dispersion liquid (0.05%BSA water); however the concentration of NPs remaining in suspension at this time point needs to be established due to the earlier initial sedimentation.

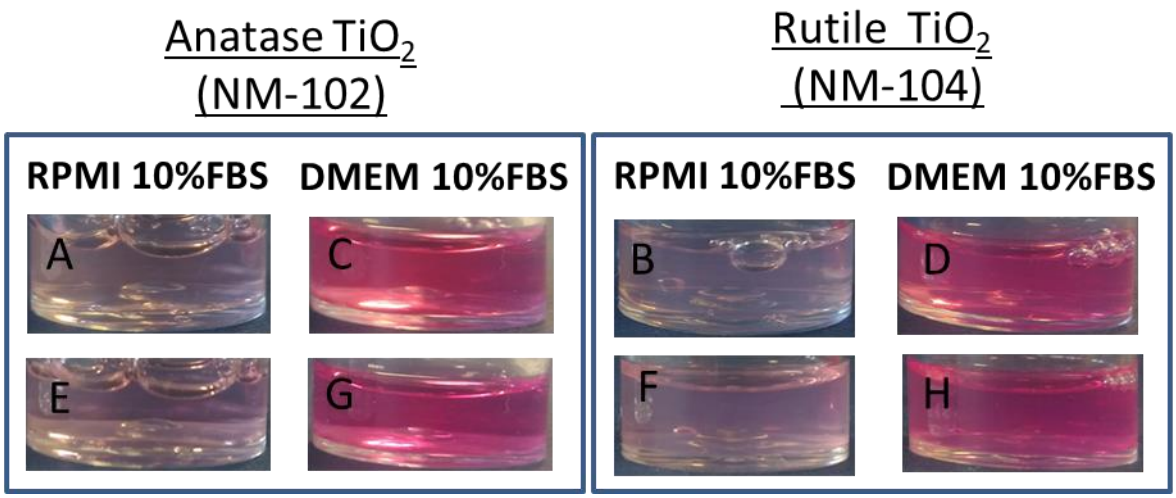

Figure 3.4: Visual identification of sedimentation in a suspension of TiO_2 in cell culture medium, 200µl supernatant from **Figure 3.3 (D)** NM-102 and **(H)** NM-104 was diluted in immediately after dispersion in 800µl RPMI 10%FBS **(A)** NM-102 **and (B)** NM-104. 200µl supernatant from **Figure 3.3 (D)** NM-102 and **(H)** NM-104 was also diluted in immediately after dispersion in 800µl DMEM 10%FBS (**C)** NM-102 and **(D)** NM-104. Images of the samples were taken after incubation for the period of 24h as is seen in **(E)** for NM-102 and **(F)** for NM-104 in RPMI 10%FBS and (**G)** for NM-102 and **(H)** for NM-104 in DMEM 10%FBS. (n=3)

3.3.2 Hydrodynamic Diameter identification

3.3.2.1 Identification of Hydrodynamic diameter using dynamic light scattering

Measurements of the hydrodynamic diameter (HD) of the TiO_2, namely, NM-102 and NM-104, were undertaken using DLS. The average (n=9) of the median HD obtained by DLS was plotted against time, and the results are presented in **Figure 3.5**.

As is seen in **Figure 3.5** the agglomerates of the Anatase TiO_2 NPs (NM-102) found in suspension initially had a median diameter of 540nm. The HD measured under DLS then gradually reduced with time. After incubation of the suspension for the period of 600min, the HD reduced to a median HD of 284nm. For the remainder of the incubation, the median HD reduced to 260nm, which was not different as compared with the measurement made at 600min. ζ-potential of the NP suspension fluctuated during the 24h incubation. Although no significant changes were observed with the NM-102 NP suspension, where the median was 12.4 +/- 3.2mV.

The agglomerates of the Rutile TiO_2 NPs (NM-104) found in suspension immediately after suspension and for a period of 24h during their incubation are also illustrated in **Figure 3.5.** Initially the NPs in suspension had a median HD of 255nm. ζ-potential of the NP suspension fluctuated during the 24h incubation. However, no significant changes were observed in the NM-104 NP suspension, where the ζ-potential was 14.6 +/- 2.1mV.

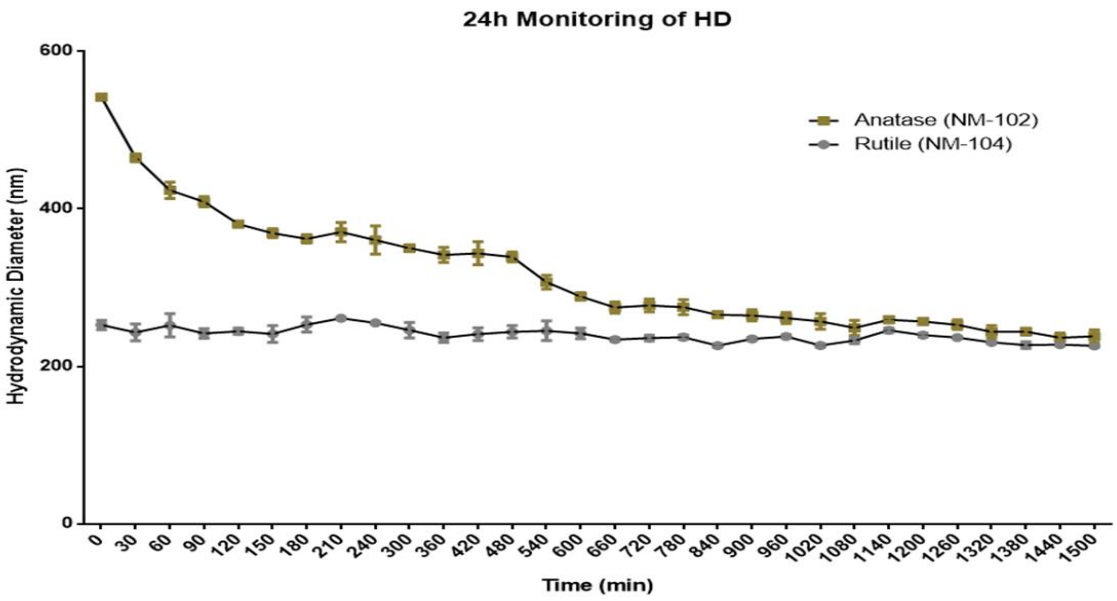

Figure 3.5: Hydrodynamic diameter (HD) of Anatase (NM-102) and Rutile (NM-104) dispersed in 0.05% BSA. Anatase HD reduces throughout the 24h period, whereas agglomerates formed by Rutile NPs have a stable HD for 1500min. The data were plotted as the median measurements per time point (n=9).

3.3.2.2 Measurements of the Hydrodynamic diameter of dSPIONs using NTA and NanoZSizer

Comparison of the two different techniques used for the determination of hydrodynamic diameter was applied using dSPIONs. Given that dSPIONs were stable in suspension no changes would be identified in the HD, therefore no measurements were undertaken over time.

The median (n=9) HD of dSPION produced by NTA were 82.75nm in ddH_2O and 89.45nm in PBS. The mean of the size range identified for dSPIONs of all the replicates (n=9) in NTA is presented in **Figure 3.6A**; the two diluents produced almost identical results, ranging from 54.1-126.8nm in ddH_2O and 31.8nm-123.6nm in PBS.

The most commonly used technique DLS was also applied to evaluate the median size of the dSPION sample. The median size of dSPIONs (n=9) in ddH_2O was 88.56nm and in PBS was 88.73nm. The size range of dSPION in the different diluents had a range from 29.7-457 nm in ddH_2O and 43.8-463nm in PBS (**Figure 3.6B**). ζ-potential was also measured and it was neutral at 10.4 +/- 1.3mV (n=3).

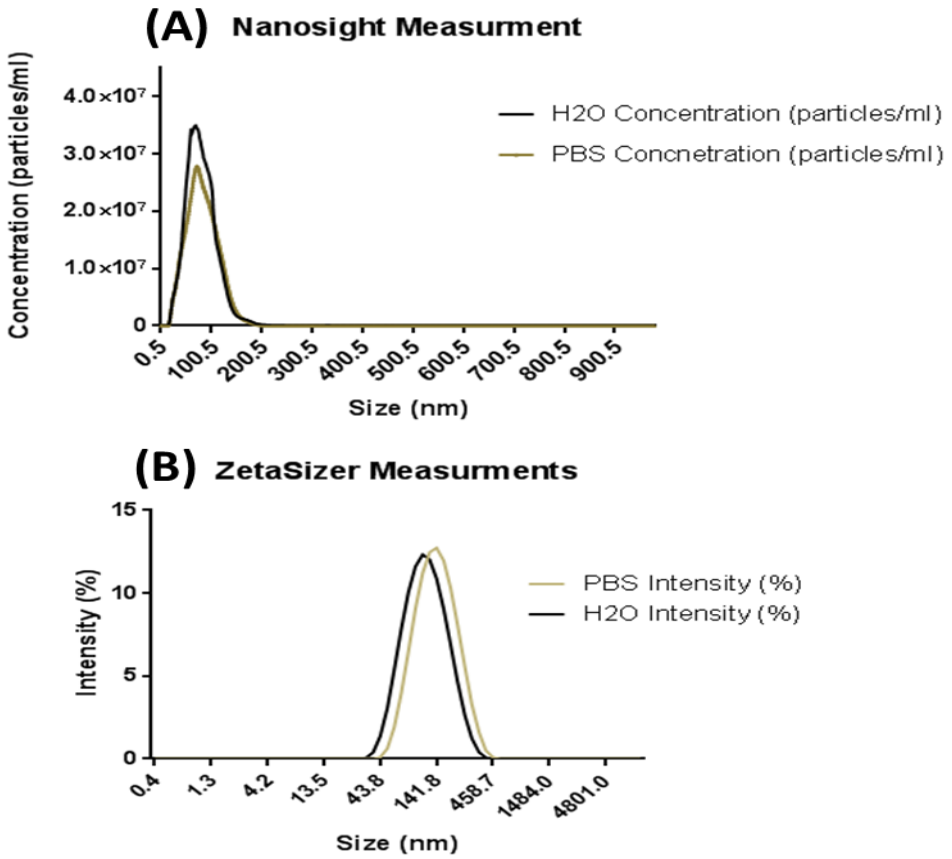

Figure 3.6: Size distribution of dSPION following NP tracking analysis (NTA) and Nano ZSizer measurements. A)_Nanosight: 100ug/ml of dSPION in ddH_2O and PBS (n=3). **B)** Malvern Zetasizer dSPION 100ug/ml of dSPION in ddH2O and PBS (n=9)

3.3.3 Investigation of suspension stability of Titanium dioxide NPs using UV-Vis spectrophotoscopy

Measurements of the extension light that was absorbed in the ultraviolet-visible light spectrum by the TiO_2 NPs, namely, NM-102 and NM-104, were undertaken using UV-Vis spectroscopy. Measurements were undertaken every 0h, 2h and 24h starting immediately after their dispersion as was previously described in **Section 3.1.1** following dilution to 100µg/ml. The average (n=9) of the measurements of absorbed light was plotted against the wavelength (nm) and the results are presented in **Figure 3.7** for each of the incubation periods.

The distorted peaks in both the NM-102 and NM-104 samples identified at 300nm were due to the protein used to prepare the dispersion liquid (0.5%BSA in ddH_2O) for the TiO_2 NPs. This is based on the results produced for the dispersion liquid alone at all incubation periods (**Figure 3.7 A-C**). Peaks of the NPs absorbing light can be seen at approximately at 330nm. Anatase TiO_2 NPs (NM-102) had an absorption that initially was 0.3 (a.u), during the incubation period absorption reduced to 0.2 (a.u) shown with a red line over the period of 24h (**Figure 3.7 A & C**). Rutile TiO_2 NPs (NM-104) had an absorption that initially was 1.3 (a.u), but after the incubation period reduced further to 0.8 (a.u) as is clearly visible shown with a green line (**Figure 3.7 A & C**).

Based on the measurements of absorbance of each sample in the distinct incubation periods, the concentration of the NPs in suspension was calculated. As is seen in **Figure 3.8** the concentration of both polymorphs of TiO_2 in suspension, namely, NM-102 and NM-104 reduced after 2h and 24h of incubation in a similar manner.

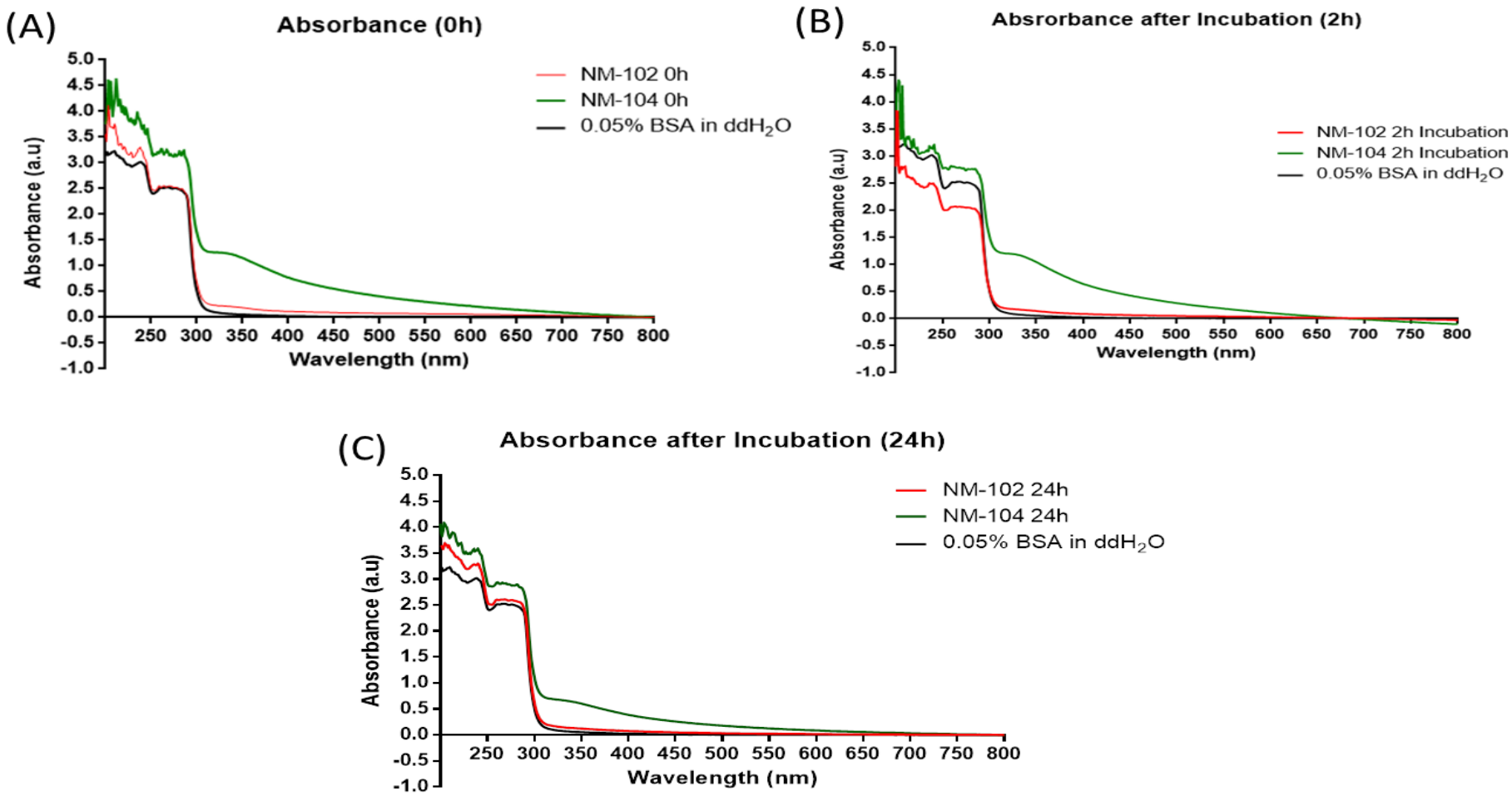

Figure 3.7: Whole spectrum screening of 100µg/ml of NM-102 and NM-104 in dispersion buffer at (A) 0h (B) after 2h of incubation and (C) after 24h of incubation. In all of the graphs the each of the samples are presented with different colours. Black is the diluent used to disperse the NPs, the red line is anatase NM-102 and the green line is rutile NM-104 (n=9).

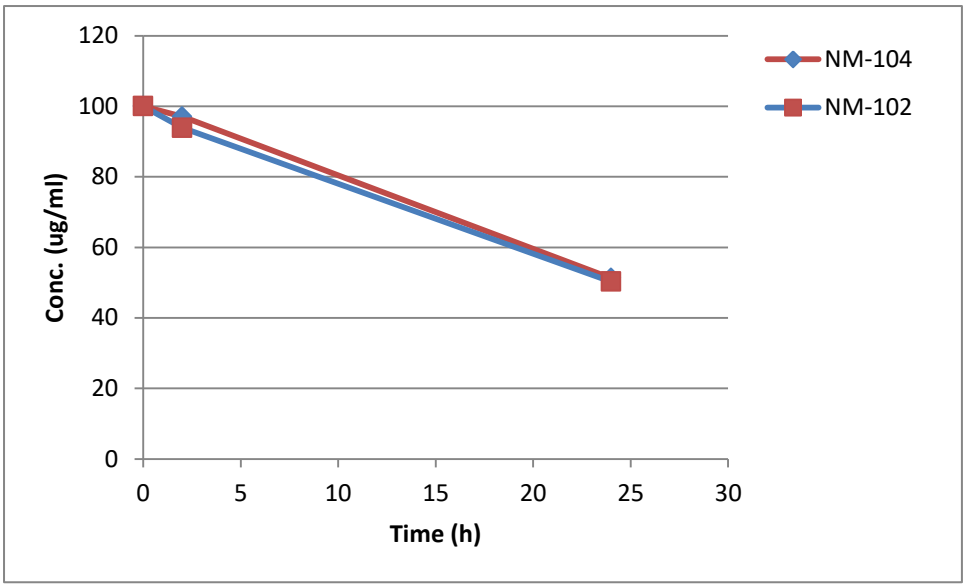

Figure 3.8: Calculated concentration of NM-102 and NM-104 in suspension after incubation for 0h, 2h and 24h. Reduction in concentration of NPs through time was identified using the UV-Vis results presented in **Figure 3.7**.

The concentrations of NM-102 and NM-104 in suspension calculated from the UV-vis data after 0h, 2h and 24h is summarised in **Table 3.1.** The reduction in concentration of NPs remaining in suspension was greater for NM-104. The rutile polymorph reduced to a concentration of 93.88 µg/ml after 2h incubation; after a 24h incubation, the concentration was reduced to 50.24 µg/ml of NPs in suspension**.** With respect to the anatase NPs NM-102 remaining in suspension after 2h incubation, the concentration reduced slightly to 97.08 µg/ml and after a 24h incubation the concentration reduced further to 51.27 µg/ml.

Table 3.1: True concentrations of an initially prepared 100µg/ml dose of NM-12 and NM-104 after incubation for 0h, 2h, and 24h. The concentration of each of the NPs in suspension was calculated using the results observed by UV-Vis analysis.

Incubation period (h)	**Concentration of NM-102 in suspension (µg/ml)**	**Concentration of NM-104 in suspension (µg/ml)**
0	100	100
2	97.08	93.88
24	51.27	50.24

3.3.4 Electron microscopy imaging of Anatase (NM-102) and Rutile (NM-104) TiO_2

The images of theTiO_2 presented in this section of this thesis, were produced after the NPs samples were prepared using the hang and dry approach that was described in **Section 3.2.6**. Images of dSPION are not concurrently illustrated in this Section as their morphology were previously characterised using TEM and are presented in Singh *et. al.* 2012.

Anatase TiO_2 (NM-102) samples were observed to be polydispersed (**Figure 3.9)**. Variation in the size of the agglomerates was identified. Based on the topography of the materials and their structures, smaller agglomerates as low as 150nm were identified, but the majority of the particles formed large agglomerates (700nm-1µm). A representative image of the agglomerate of the NM-102 samples investigated can be seen in **Figure 3.9B** which was taken at a magnification of x60k. Higher magnification images (**Figure 3.9D)** at x180K indicated that the NPs formed agglomerates which had crystalline structures.

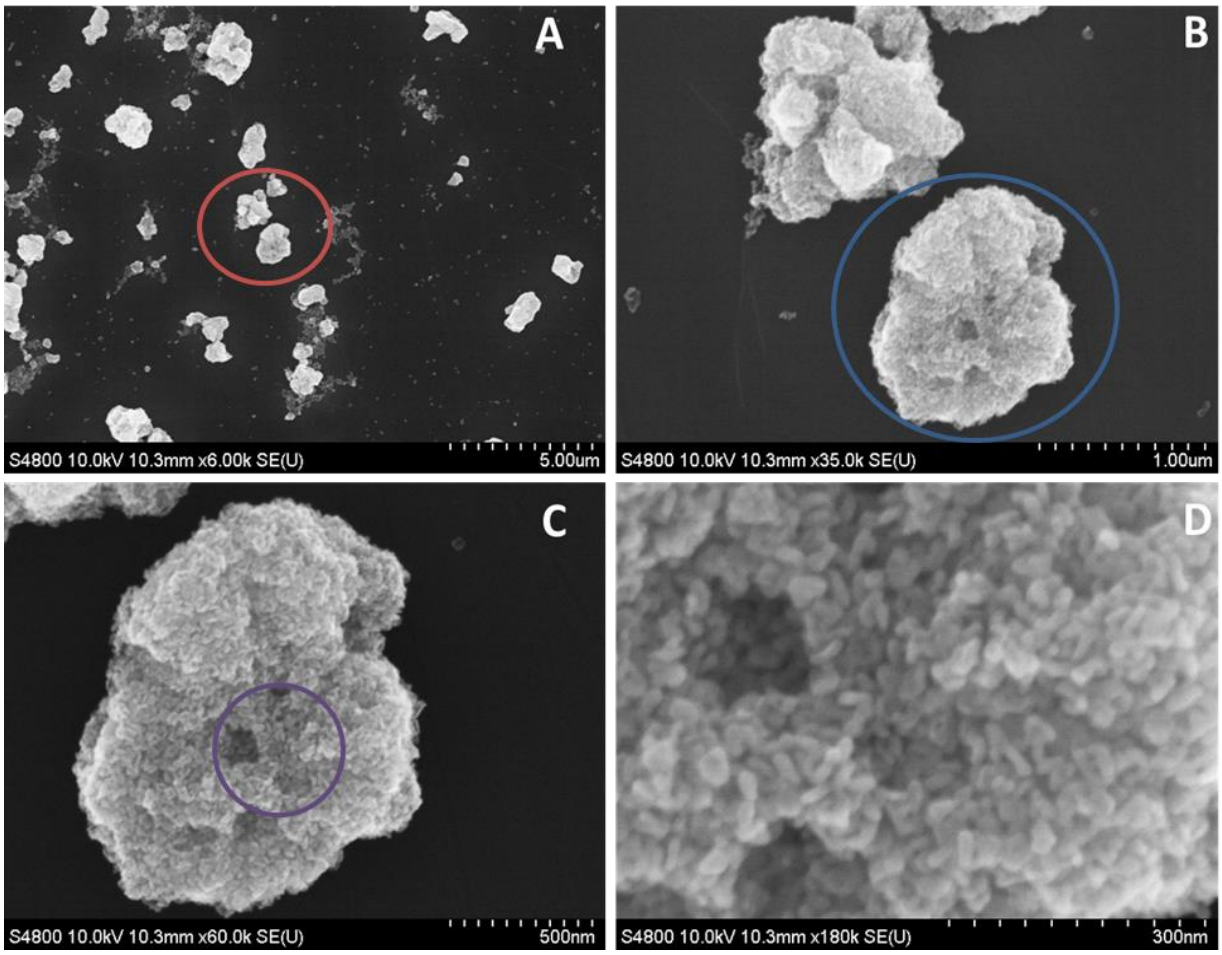

Figure 3.9: SEM images of Anatase (NM-102) TiO_2 prepared using the hang and dry approach on a silicon wafer. The images are of the same sample area evaluated at different magnifications. The agglomerates represent in both size and structure the majority of agglomerates formed by the anatase NPs when they were dispersed in dH_2O. **(A)** Low magnification image that represents the agglomerate size variability. The indicated with red circle area is magnified in **(B)** these agglomerates represent the size and form of the majority of the particles when suspended in H_2O. The indicated with blue circle area is magnified in **(C)** Higher magnification of the NPs topography and structure. The indicated with purple circle area is magnified in **(D)** Higher magnification illustrated the surface structure of the agglomerates, where the individual particles within the large agglomerate can be seen.

After Rutile TiO_2 (NM-104) were used to prepare the samples using the hang and dry approach, SEM imaging suggested that they were polydispersed **(Figure 3.10)**. A variation in the size of the agglomerates formed was identified based on the topography of the materials and their structures in the SEM images. Individual particles and smaller agglomerates were present in the sample, with the majority of the sample being formed by agglomerates within the size range of 170-300nm. As is seen in **Figure 3.10 C&D** that were taken at **x100k** and **x301K,** the sample consisted of rod-shaped NP's that mostly formed small agglomerates.

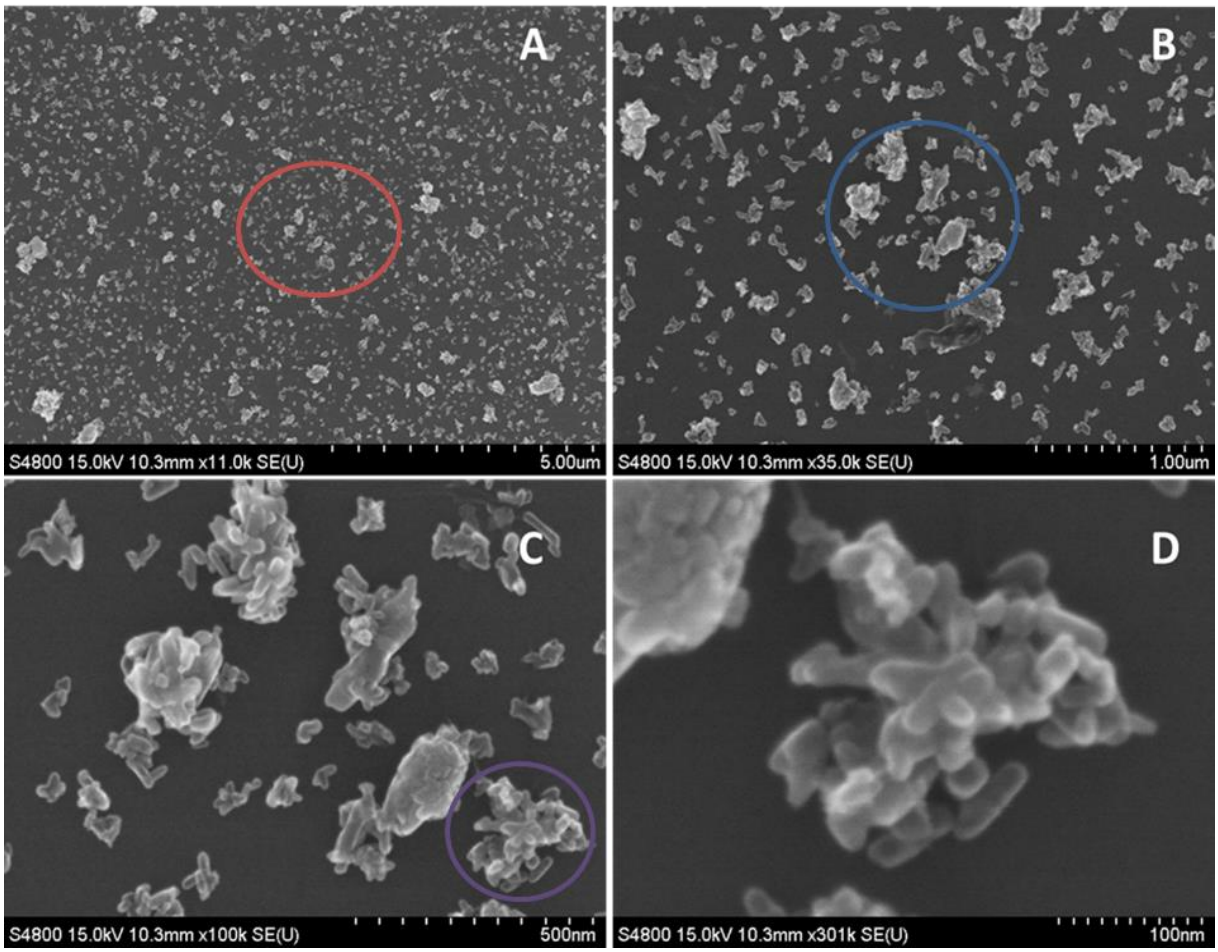

Figure 3.10: SEM images of Rutile (NM-104) TiO_2 prepared using the hang and dry approach on a silicon wafer. The images are of the same sample area evaluated at different magnifications. The agglomerates represent in both size and structure the majority of agglomerates formed by the rutile NP's when they are dispersed in dH_2O. **(A)** The picture represents the agglomerate size variability. The indicated with red circle area is magnified in **(B)** these agglomerates represent the size and form of the majority of the particles when suspended in H_2O. The indicated with blue circle area is magnified in **(C)** Higher magnification of the NPs topography and structure. The indicated with purple circle area is magnified in **(D)** Higher magnification illustrated the surface structure of the agglomerates, where the individual particles within the large agglomerate can be seen.

3.3.4.1 Elemental analysis of the samples using Electron diffraction X-Ray spectroscopy (EDX)

The images presented in **Figure 3.9 and 3.10** were investigated using an analytical technique known as EDX in order to identify the elemental composition of each of the samples evaluated. Large amounts of carbon and silicon were identified as they are the core elements of the wafer on which the samples were prepared. As is seen in **Table 3.2** large amounts of both titanium and oxygen were also identified. The atomic percentage of titanium is slightly higher in the anatase (NM-102) polymorph in comparison to NM-104. Although several impurities were identified, they were at very low (negligible) concentrations.

Table 3.2: Elemental composition of (A) Anatase NM-102 and (B) Rutile NM-104 TiO_2, based on the results from EDX analyses. The results presented here are in atomic% and derived from measurements of the samples presented in Figures 3.9 and 3.10. The atomic% of Carbon and Silicon originated from the silicon wafer and not the particles. (n=30)

	Atomic %						
TiO_2 NP	**C**	**Si**	**Al**	**Br**	**S**	**Ti**	**O**
(A) NM-102	26.22 (±-3.695)	38.493 (±5.37)	0.0072~	ND*	0.0491 (±0.982)	5.7 (±2.327)	31.618 (±10.47)
(B) NM-104	30.766 (±4.175)	39.79 (±11.89)	0.008~	0.0061 (±0.024)	0.403 (±0.362)	2.788 (±1.287)	26.232 (±8.05)

Carbon (C), Silicone (Si), Aluminium (Al), Bromine (Br), Sulfur (S), Titanium (Ti), Oxygen (O)
~Only detected in one of the replicates
*** ND (Non-Detectable).**

3.3.5 Identification of the hard protein corona in the different suspension liquids

The protein that forms the hard corona in the different diluents used in this study, namely, DMEM-10% FBS, RPMI-10%FBS and the dispersion buffer 1%BSA, were isolated. As illustrated in **Figure 3.11,** the hard protein corona was comprised of one protein (represented by a single band) for all the MONPs in the three different media (10%FBS RPMI, 10% FBS DMEM and 1%BSA). When compared with the protein ladder all the sample protein bands were approximately 66kDa. These results suggest that the same protein constitutes the hard corona of the NPs regardless of the different diluents applied. It is safe to assume that the protein is BSA, as the only protein present in 1% BSA (**Figure 3.11 A3**) is bovine serum albumin. Protein bands with a fading color were identified in all the samples that the NPs were dispersed in, although in the dispersion buffer that contains 1% BSA were less evident, this is due to the lower amount of protein that accumulates around the NP agglomerates (**Figure 3.11A3**). A similar concentration of BSA in the hard corona was identified in all the NPs when suspended in media. Although, NM-102 appeared to have a greater affinity for BSA than the other NPs when in the 1% BSA solution (**Figure 3.11B**).

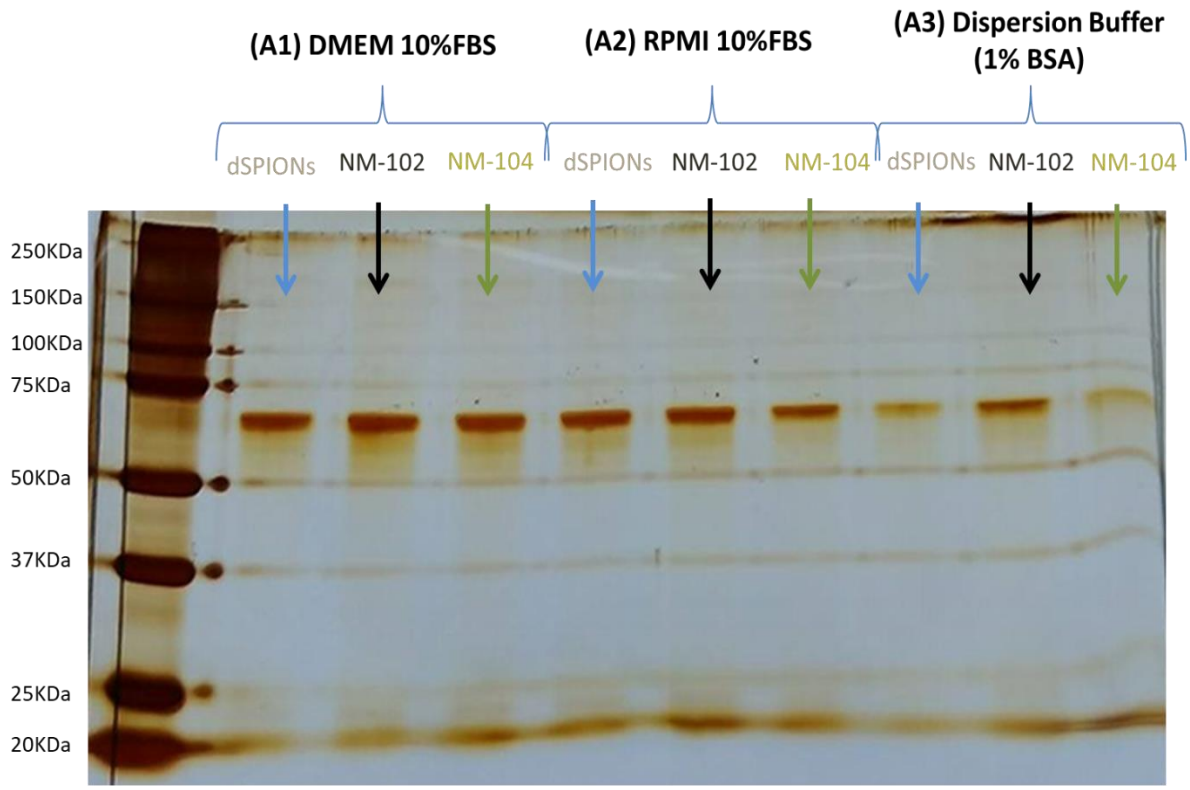

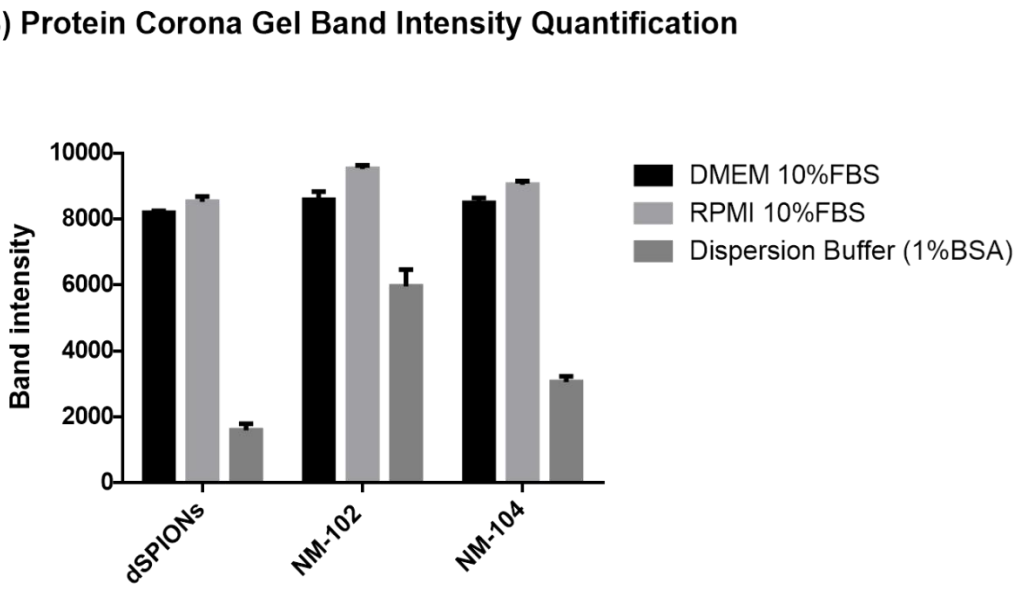

Figure 3.11: Hard protein corona of MONPs separated using SDS-PAGE. **(A)** Visualisation of the protein band forming the hard protein corona of MONPs on an SDS page gel after they were dispersed in **(A1)** DMEM 10% FBS **(A2)** RPMI 10%FBS **(A3)** Dispersion Buffer (1%BSA). **(B)** Hard protein corona gel band quantification using ImageJ (n=3).

3.3.6 LAL Gel Clot Test for Endotoxin Contamination of the different MONPs

During the manufacturing process of a NM there is substantial risk of endotoxin contamination (Dobrovolskaia *et. al.*, 2013). MONPs samples, namely, dSPIONs and the TiO_2 NPs (NM-102 and NM-104) suspended in 0.05% BSA in ddH_2O were investigated for endotoxin contamination. The NP suspensions were all investigated for the presence of endotoxin using the Limulus Amebocyte Lysate (LAL) PYROGENT™ (Lonza, UK). As is seen in **Table 3.3** the results were marked as positive or negative depending on the coagulation of the gel; positive means that there is presence of endotoxin. The level of the contamination cannot be identified due to the NPs interacting with the chromogenic KITs. As is seen at the table below (**Table 3.3**) all the NPs in suspension were positive for endotoxin.

Table 3.3: Gel clot assay results for endotoxin contamination of the different MONPs. The results of the endotoxin test indicate the presence of endotoxin in the NP stock (n=6).

Sample	Constituents	Result
Positive Control	50 µl LPS + 50 µl dH_2O	**Positive (+)**
Negative Control	100 µl dH_2O	**Negative (-)**
Dextran coated-Fe_3O_4 (100µg/ml)	50 µl Fe_3O_4 + 50 µl dH_2O	**Positive (+)**
0.05% BSA in ddH_2O	50 µl Fe_3O_4 + 50 µl dH_2O	**Negative (-)**
TiO_2 Anatase (NM-102) (100µg/ml)*	50 µl NM-102 + 50 µl dH_2O	**Positive (+)**
TiO_2 Rutile (NM-104) (100µg/ml)*	50 µl NM-102 + 50 µl dH_2O	**Positive (+)**

*The NPs were dispersed using the protocol previously provided in **Section 3.2.1.1**. NM-102 and NM-104 were in a concentration of 100µg/ml in 0.05% BSA / ddH_2O.

3.4 Discussion

Understanding the physico-chemical characteristics of NM is vital for nanotoxicology studies in order to interpret the toxicological profile of the NM under investigation. As previously discussed in **Section 1.2,** the evaluation of the physicochemical characteristics of NPs is necessary prior to toxicological studies in order to understand their ability to interact with cells and induce toxicity (Rivera-Gil *et. al.* 2010). Characteristics of NPs are divided in to primary and secondary features. NM characterization conducted following their synthesis is deemed as the primary characterisation. Primary NM characteristics include size, morphology, surface area, composition/purity, surface charge and surface chemistry (Saves and Warheit, 2009). This chapter aimed to identify the physicochemical characteristics of NM-102, NM-104 and dSPIONs in comparison to future toxicological studies and others in the literature that have used these materials. The physicochemical properties of the dry powder form of the two different types of titanium dioxide (TiO_2) NPs NM-102, NM-104, were thoroughly investigated prior to delivery by the JRC NPs repository, and the results were presented by Rasmussen and colleagues in 2014 (Rasmussen *et. al.* 2014). The form of dSPIONs used in the present study was previously used in the *In Vitro* Toxicology Group's laboratory and thorough investigation of their properties has been previously conducted, with the results located in Evans and colleagues 2016 (Evans *et. al.* 2016, Singh *et. al.* 2012). This chapter therefore focused on evaluating the secondary physico-chemical characteristics of the materials under study. In addition, comparison of different techniques used for agglomeration assessment of NPs, namely, DLS, NTA and SEM, was applied in order to determine the best combination of approaches to evaluate NM behaviour in an *in vitro* environment.

3.4.1 Primary and secondary characterization of dSPIONs and comparison of dynamic light scattering techniques

The evaluation of the size and the agglomeration status of NPs is necessary in order to understand their ability to interact with cells, become internalised and interpret their subsequent biological impact on the cells under investigation (Rivera-Gil *et. al.* 2010, Johnston *et. al.* 2012). In a previous study, the dSPIONs applied in the present Chapter were

investigated using drop cast technique by TEM, where the size, shape and agglomeration status of the NPs was identified (Evans *et. al.* 2016, Singh *et. al.* 2012). The material was found to have a primary size of ~8nm, was cubic in shape and formed chain like agglomerates (Evans *et. al.* 2016). The small primary NP size would allow entry to cells via diffusion across the cellular membrane and present a large potentially highly reactive surface area able to interact with biological components within the cell (Singh *et. al.*, 2009). However, it is well understood that NPs agglomerate when they are placed into liquid environments; this tends to happen due to relatively large van der Waals forces of attraction (Boyd *et. al.*, 2011). Therefore, the agglomeration status of dSPIONs was investigated using both DLS and NTA. Both techniques are based on the formula of the Stoke-Einstein equation that allows the correlation of the movement to calculate the hydrodynamic diameter of agglomerates (**Equation 3.1**). This equation also requires knowledge on temperature and solvent viscosity (Konan *et. al.*, 2002). The Malvern ZetaSizer nano ZS measures the dynamic light scattering intensity of the particles to identify their HD. In DLS the speed the NPs move in a diluent is determined by passing a laser through and determining the fluctuations of intensity of the scattered light. The non-randomness in the fluctuations are presented as a correlation coefficient (Filipe, Hawe and Jiskoot 2010). On the other hand the Nanosight system allows visualization of the particles and the identification of their every movement, therefore the name of the technique is NP Tracking Analysis (NTA) (Filipe, Hawe and Jiskoot 2010).

When comparing the output of the DLS and NTA for dSPIONs, similar results were produced using both techniques. The hydrodynamic diameter was found to be ~88nm and the different diluents (I.e. ddH_2O and PBS) seem not to have any effect on the sample agglomeration. A larger radius range was produced by DLS when compared to NTA. While DLS provide an insight into a materials' agglomeration state, the resulting data has the potential to be seriously flawed when evaluating samples that have a wide range of variation in agglomerate size. This is because during DLS measurements the ability of a particle to scatter light is proportional to its diameter to the sixth power (Boyd *et. al.*, 2011). This means that the greater degree of light scattering by larger agglomerates is capable of masking the scattering by smaller ones and hence smaller agglomerates may not be accurately represented in the generated size dispersant peak(s). Moreover, DLS is unable to

discriminate between NPs and background matter; hence proteins in biological media can be measured in addition to NPs, consequently skewing the resulting data as these often are present in great excess as compared to the test NP. Although, NTA allows the visualization of the NPs Brownian motion, the concentration measurements of the technique are imprecise due to the inability of the microscope to focus in on all the NP agglomerates and limitation in the software to track them. This was also identified in a study that used polystyrene beads to compare the two techniques, DLS and NTA (Filipe, Hawe and Jiskoot 2010).

Agglomeration and aggregation status of a NPs in a suspension strongly depends on the ζ-potential; the range of strong agglomeration is considered to be ≤-10mV and ≥10mV (Riddick, 1968, O'Brien, 1990, Buzea *et. al.* 2007). From the observed ζ-potential results (10.4 +/- 1.3mV) in this study, it is suggested that dSPIONs would form agglomerates in solution. When compared with previous studies on dSPIONs the results are similar, suggesting that the surface charge of dSPIONs would have been greatly affected by their dextran coating (Singh *et. al.,* 2012, Easo and Mohanan, 2016, Saraswathy *et. al.*, 2014, Remya *et. al.*, 2016). Other surface coatings for SPIONs were previously observed to result in different surface charges. Such as the polyethylene glycol (PEG) and polyvinylpyrrolidon (PVP) co-modified SPIONs that led to a completely neutral surface charge (Yang *et. al.*, 2016). Thus, this demonstrates that the application of different SPION surface coating allows for a degree of control over the materials surface charge, agglomeration status and hence their colloidal stability. As previously discussed by Xie and colleagues, PEG coated Fe_3O_4 NPs when incubated in cell culture reduced agglomeration and thereby resulted in a greater uptake by macrophage cells (Xie *et. al.* 2007). Furthermore, Singh and colleagues demonstrated that the formation of larger agglomerates reduced the reactive surface area that is eventually able to interact with biological components within the cell and thus, lower agglomeration results in greater cellular damage (Singh *et. al.*, 2009).

3.4.2 Primary and secondary characterization of TiO_2 NPs

Agglomeration status of the different TiO_2 NPs polymorphs was investigated with SEM and DLS. Use of the NTA for measurements of non-spheroid, unequally dispersed NP's (based on the visible observation of sedimentation), such as the TiO_2, is not recommended (Boyd *et.*

al., 2011). SEM images of the sample were not representative of the agglomerates formed by the particle in suspension for two reasons; firstly, the particles were dispersed in ddH_2O, and secondly the drying step in preparation for SEM imaging can induce further agglomeration. The dispersion buffer from Jensen *et. al.* 2011 cannot be used for the preparation of samples for SEM imaging because a high level of image distortion occurs due to the presence of protein. Agglomerate size of NM-102 formed in the conditions described for SEM sample preparation reached ~1um. NM-102 were observed to have a crystalline shape. In contrast, NM-104 was more evenly distributed, in the samples prepared both here for SEM and in JRC's TEM images provided in previous studies (Rasmussen *et. al.* 2014). This might be due to the organic coating deposited on the outside layer of the NM-104 (2% of dimethicone) (Rasmussen *et. al.* 2014). This also explains why the agglomeration state identified in SEM for NM-104 was similar with the data obtained using DLS. NM-104 were observed under SEM to homogeneously be rounded and rod shaped; this agrees with previous characterization studies under TEM imaging (Rasmussen *et. al.* 2014). Primary particle size was not observed under SEM, although in a previous study was found to be ~25nm for both NM-102 and NM-104 (Rasmussen *et. al.* 2014). Since a high degree of agglomeration was identified with both NM-102 and NM-104, this is likely to result in reduced cellular uptake. As Clithrani and Chan observed, more time is needed to wrap large particles during phagocytosis than smaller materials, while active uptake and diffusion of large agglomerates in non-phagocytic cells is highly limited (Chithrani and Chan 2007).

Photographing the visual colloidal stability of NM-102 and NM-104 after incubation for a period of 24h at 37°C in different diluents and concentrations of protein demonstrated that the majority of the particles rapidly sediment. This led to further investigation of the colloidal stability through DLS, ζ-potential and UV-Vis. HD measurement using DLS allowed the monitoring of agglomeration status in NM-102 and NM-104 over time. Results provided by Jensen and colleagues indicated that the HD of NM-102 was 545 +/- 14nm; a similar radius was observed in the present study immediately after dispersion, where the HD was 544 nm (Jensen *et. al.* 2011). In contrast, results for NM-102 in other studies deviate slightly, ranging from 366nm-550nm (Geraets *et. al.* 2014, Tavares *et. al.*2014, Rasmussen *et. al.* 2014). The HD measurement reported by Jensen and colleagues for NM-104 was 234 +/- 4nm, whereas in the present study a slightly higher measurement was recorded at 260.6nm.

The difference in the measurements identified in other studies might be due to changes in the dispersion protocol; for example, not all studies used a probe sonicator for the preparation of the samples. Instability of the colloidal suspensions when TiO_2 NP's were dispersed in 0.05% BSA dH_2O is attributed to the rapid agglomeration, which leads to sedimentation, particularly of the larger agglomerates (Li and Sun 2011, Alluni *et. al.* 2009). In DLS if the colloidal suspension is not stable then the larger agglomerates will precipitate and as a result will remain un-measured, therefore a higher concentration of smaller agglomerates will be measured affecting the median hydrodynamic radius. Measurements of hydrodynamic radius represent the agglomerates that stay in suspension, a sedimentation trend was observed in the DLS measurements overtime (24h) for NM-102. Due to the formation of the large agglomerates and the surface reactivity associated with the crystalline structure of the anatase NM-102 polymorph, it is expected to be highly genotoxic. In contrast, the smaller agglomerates formed by the rutile isomorph NM-104, in addition to the lower reactivity of its crystalline structure suggests that are not expected to induce significant genotoxicity (Magdolenova *et. al.* 2012). The fact that different degrees of agglomeration of NPs may cause different biologic responses is now something that has been well understood for over 10-years, with early studies demonstrating this phenomenon in a carbon nanotube cytotoxicity study (Wick *et. al.* 2007). The TiO_2 NPs used in the present study have been previously used in other investigations to examine how the agglomeration state (using two dispersion protocols) may affect the kinetics of cellular binding/uptake and ability to induce cytotoxic responses in THP1, HepG2 and A549 cells (Lankoff *et. al.* 2012). The agglomeration size depended on the molecule size used for the preparation of a dispersion buffer (Lankoff *et. al.* 2012). Cellular binding/uptake showed no straight relation of the particle size, but rather a complex relation of particle and cell type properties (Lankoff *et. al.* 2012).

Both NM-102 and NM-104 are unstable in suspension, although NM-102 sediments at a higher rate because larger agglomerates are formed. ζ potential, low measurements were identified throughout the 24h for both of the NM's, indicating that the colloid is not electrically stable and that NP agglomeration is occurring. Both NP's (NM-102 and NM-104) were observed to be unstable in suspension when other diluents were used (e.g. dH_2O, HNO_3 10-2 M) (Rasmussen *et. al.* 2014). As it was previously mentioned the agglomeration

and aggregation status of a NPs in a suspension strongly depends on the ζ-potential; the range of strong agglomeration is considered to be ≤-10mV and ≥10mV (Riddick, 1968, O'Brien, 1990, Buzea *et. al.* 2007). In previous studies on colloidal chemistry it was found that surface charge can affect the colloidal stability of the NM in suspension. The incipient instability of the ζ potential that was identified in both of the TiO_2 NPs (NM-102 and NM-104) samples could be one of the reasons for the agglomeration and sedimentation observed visually and by DLS. Furthermore, ζ potential has a possible effect on receptor binding and physiological barrier penetration, absorbance or adhesion; therefore it has an important impact on the interaction of NPs with cells (Powers *et. al.* 2006).

As sedimentation of the initial TiO_2 preparations clearly occurred rapidly, it became obvious that the initial sample concentration applied to cells would not be an accurate representation of the delivered dose. Thus, to more accurately identify the concertation of the NPs in suspensions, measurements of the change in absorbance were required. The absorbance can be correlated with concentration of the particles in suspension using the Beer-Lambert Law as described in **Section 2.2.7**. Absorbance in UV-Vis measurements was reduced through time for both NPs, therefore the concentration of dispersed NP's was reduced, which also supported the fact that the NP suspensions were agglomerating and as a result sedimenting. Visibly when pictures were taken during a 24h period of incubation, NM-102 appeared to sediment to a greater extent than NM-104. However, results from the UV-Vis analysis suggest that the rate of sedimentation between NM-102 and NM-104 was not significantly different and the visual variation was due to the greater size in agglomerates of NM-102, which made them more visible to the naked eye when in suspension. Similar absorbance results were obtained when NM-104 was dispersed in Luria Britani medium and artificial waste water, where absorbance peaks were identified at 325.1nm and 340.5nm respectively (Mallevre, Fernandez and Aspray 2014). The concentration of the NP's that remain in suspension after incubation of 2h in the 0.05% BSA ddH_2O diluent was identified and an optimal dose range for both TiO_2 NP's was developed based on the data. The concentration range selected for future studies in this thesis using TiO_2 were therefore 0-50 µg/ml.

3.4.3 Protein Corona and endotoxin contamination of MONPs

Cellular uptake and interaction is greatly affected by the attachment of protein on the NP surface. What is important about the formed NP protein corona is that it changes the biological identity; this is because the corona will initially come in contact with biological components such as the cell surface, rather than the particle itself (Walczyk *et. al.*, 2010). As a result of the attachment of BSA on the surface of NPs, its ability to enter the cell could be enhanced. In multiple cell lines a number of albumin receptors were identified on the cell surface, these can act as cellular uptake mediators by increasing the interaction with the protein attached on the NP surface (Merlot *et. al.*, 2014). As previously observed, receptor mediated endocytosis was greatly induced when serum proteins are attached on the surface of NPs while they are incubated with cells in media (Khan *et. al.* 2007). In another study by Fleischer and Payne, it was observed that BSA coated polystyrene NPs had an increased binding with the cellular scavenger receptors (Fleischer and Payne, 2014).

In all the diluents applied in this Chapter, the hard protein corona of dSPIONs and both TiO_2 polymorphs was formed by BSA. The biological entity of the NP's is therefore altered when suspended in different diluents that include BSA. The hard protein corona infers the identity of the NPs within a biological environment, therefore in this study, the environment was the biological cell culture medium used during cell toxicity treatments and the dispersion diluent. The presence of a protein corona had an impact on the dispersion of the TiO_2 polymorphs; this was evident in both the visual and DLS media results. This has previously been demonstrated to be the case with ZnO NPs where corona formation resulted in electrostatic repulsion and hence smaller agglomerates developing (Wells *et. al.*, 2012). It is well documented that the presence of protein in the dispersion buffer interferes with both DLS and NTA (Bai *et. al.* 2017). In this study the buffer was sterile filtered prior to dispersion of the different NPs; Bai and colleagues showed that no interference was identified after filtering the dispersion buffer in both DLS and NTA (Bai *et. al.* 2017). The identified protein corona in this study on all three of the NPs (dSPIONs, NM-102, NM-104) may therefore influence agglomerate size and aid in the cellular uptake of the materials, increasing the potential for toxicity to be induced.

NMs and NPs can easily become contaminated with endotoxin, which is a wide-spread contaminant (Evans *et. al.* 2016). The NPs used in this study were provided for research purposes from the JRC, but also bought through the public sector (dSPION), thus providing a real life scenario of the form in which NPs are provided to both researchers and consumers. Furthermore, these materials have been actively applied in a range of other toxicological studies in the literature (Kermanizadeh *et. al.* 2013, Farcal *et. al.* 2015, Louro *et. al.* 2014, Mallevre *et. al.* 2014). Endotoxin contamination assessment showed that dSPION, NM-102 and NM-104 tested positive for the presence of endotoxin as low as in the picomolar range. The observed contamination with endotoxin was vital to understand due to its high immunostimulatory potential (Dobrovolskaia and McNeil, 2013). Thus, the observed presence of endotoxin may result in inflammatory response in follow up studies. However, a disadvantage of the gel-clot assay for endotoxin detection is that the extent of endotoxin presence of endotoxin could not be quantified. Identification of the concentration of endotoxin in samples is possible with the use of chromogenic detection kits, but the presence of nano-particulate matter makes the use of such kits unreliable due to interference during the measurement and quantification of endotoxin (Li *et. al.* 2017). The reason for the interference is due to the absorbance of light by the NPs at the wavelength of absorbance or excitement of the different test. Thus, a challenge remains in accurately quantifying endotoxin presence in NM samples. Whilst the samples provided for this study clearly demonstrated some endotoxin contamination, this was important information to take forward when interpreting the outcome of further toxicological analyses using these materials, particularly inflammatory response.

3.4.4 Summary and Conclusion

As previously mentioned in Chapter 1, primary and secondary physico-chemical characteristics that differ between the NPs under investigation, such as the chemical composition, shape and the agglomeration status, may have an effect on their cellular uptake/interaction and eventually their toxicity. This Chapter therefore focused on establishing those characteristics for the test materials under study. Through extended characterisation analysis, dSPIONs were found to have a spherical morphology, their primary particle size was ~ 8nm, and they had near neutral charge (in both ddH_2O and PBS) and were not endotoxin free, which may have implications with immunological testing. Agglomeration was observed for dSPIONs by both DLS and NTA, with agglomerates being ~88nm in PBS and ddH_2O. Both TiO_2 polymorphs were found to have a primary particle size of ~25nm. NM-102 and NM-104 under SEM were observed to be rod shaped, but with a variation in agglomeration size and shape. The suspensions of both the polymorphs were not endotoxin free. Whilst, the formation of a BSA protein corona led to a more stable suspension of both TiO_2 NPs, this did not fully inhibit agglomeration and sedimentation, which were observed visually, and using DLS and UV-Vis. NM-102 resulted in the formation of non-homogenous, large agglomerates with a median size of 540nm, while NM-104 resulted in the formation of a non-homogenous suspension of agglomerates with a median size of 250nm in size. The concentration after sedimentation was identified and a dose range was developed for both TiO_2 polymorphs for future toxicological studies. From the defined characteristics we can conclude that each of the MONPs under evaluation have distinct physico-chemical features that may highly influence their capacity for cellular internalisation and toxicity potential.

Chapter 4: Comparison of NP-cell interactions and toxicity under culture environments with distinct oxygen levels.

4.1 Introduction

The physiological oxygen environment (physioxia) of mammalian cells that reside at locations distant from blood vessels *in vivo* typically ranges from 0.5-10% (Brahimi-Horn *et. al.*..2007). In humans under physiological conditions, the arterial blood pressure of O_2 is 100mm/Hg (14% O_2), while the pressure in the different organs such as the lungs and kidneys varies in a range of 1-14% O_2 (Miller *et. al.*.. 2010, Muller *et. al.*.. 1998), while the concentration of O_2 in the liver is 5.6% (Brooks *et. al.*. 2007, Leary *et. al.*.. 2002). A standard *in vitro* Mammalian cell culture is normally carried out under humidified air supplemented with 5% CO2, resulting in an environment containing approximately 18.6% O_2, which is substantially higher than cells experience *in vivo*.

The culture of different types of human originated cell lines under a hyperoxic environment (21% O_2) has been previously identified to lead to phenotypic changes to cells when compared with *in vivo*. The absence or excess of oxygen in the culture of cells may lead to the production of reactive oxygen species (ROS) which in turn leads to the induction of oxidative stress (Jagannathan *et. al.* 2016). Changes to the redox status of the cells cultured under hyperoxia or hypoxia may lead to an altered cell proliferation, migration and invasion (Jagannathan *et. al.* 2016). It is therefore evident that a distinct cellular behaviour is observed when cells are cultured in different oxygen culture environments, in order to identify a more accurate toxicological profile and cell interaction of NPs and rule out external stimuli. As is noted a stimulus of significant importance would be oxygen levels. Therefore, culturing cells in physiological resembling oxygen culture environments would allow more precise insight on NPs toxicological profiles. The ability of the NPs under investigation in this chapter to be uptaken and interact and their toxicological profiles was thoroughly investigated in the literature. Although, no previous studies were able to characterize identify, characterize and eventually compare the ability of these MONPs to cause toxicity in a more physiological culture environment. These will increase the validation of *in vitro* studies and will allow them a greater comparability to future *in vivo* studies.

An important parameter for the assessment of potential toxicity induced by NPs is the ability of interaction and uptake with the exposed cell systems. These strongly depend on the physicochemical characteristics identified and described in **Chapter 3.** Cells are naturally

permeable, larger macromolecules or other objects are transported via energy dependent mechanisms such as phagocytosis or endocytosis. The assumption of a maximum size of NPs that could be internalized is based on the size of the vesicles created by each cell type (Xu *et. al*... 2009). The dimensions of vesicles are restricted therefore limited cargo size is internalized (Patel *et. al*... 2007). The mechanisms involved in NP uptake by cells were extensively discussed in **section 1.2.1.** Based on the previously observed alteration of cellular behaviour in different culture environments, questions arise if the ability of cells to interact and internalise NPs will be also altered, and if yes in what exact way.

The SPIONs ability to induce toxicity is well researched and documented in scientific literature; an extensive review can be found in **section 1.5.1**. Based on the previous studies we can conclude that a mild to non-existent ability of SPIONs to induce cell toxicity is due to the alterations in the cellular redox status (Singh *et. al.* 2012). The ability of distinct iron oxide NPs to induce oxidative stress depends on the extent of the NPs uptake and interaction with the cells, and the redox status of the NPs therefore uptake and interaction of iron oxide NPs strongly depends on the coating and its size (Evans *et. al.* 2017). Iron oxides ability to induce toxicity is well documented, in literature under hyperoxic culturing environment but was never previously identifies in a physioxic culture environment.

Titanium dioxide NPs have been described by multiple studies to exhibit low solubility in different environments, due to their high agglomeration and aggregation status (De Angelis *et. al.* 2012, Andersson *et. al.* 2011). The mechanism for induction of genotoxicity associated with NPs with low solubility, such as Titanium dioxide, is commonly reported to be the production of reactive oxygen species (ROS) (Shukla *et. al.* 2013). As it was shown by Shukla and colleagues anatase NPs with a diameter of 192.5nm were internalized by HepG2 cells after a 20h exposure, and interestingly accumulated close to the nuclear region (Shukla *et. al.* 2013). In addition, in a dose range of 0-80ug/ml an increase of the side scattering (cell granularity) in flow cytometry was observed, which can be correlated with a dose dependent increase in the concentration of internalized NPs (Shukla *et. al.* 2013). Shukla and colleagues after treatment of HepG2 with anatase in a dose range of 0-80ug/ml for both 24h and 48h showed significant reduction in cell viability using both the MTT assay and neutral red uptake. Significant genotoxicity was observed using both the comet and cytokinesis block micronucleus assays. Reduction in glutathione levels with concomitant

increase in lipid peroxidation and reactive oxygen species generation was observed. This resulted in the conclusion that the genotoxic behaviour of anatase Titanium dioxide is mediated via the induction of oxidative stress (Shukla *et. al.* 2013). Both anatase and rutile Titanium dioxide were used to expose HepG2 cells for a period of 20h and concentrations of up to 250µg/ml. In contrast to Shukla *et. al.* the cellular viability was not significantly affected, although, no data for the stability of the colloidal suspension were provided at these high concentrations. In summary, the hazardous effects observed in different cell lines are strongly dependent on titanium dioxide degree of uptake. Uptake is in turn dependent on both the agglomeration status and the colloidal stability of Titanium dioxide NP in suspension. As two of the most thoroughly investigated material in nanotoxicological studies titanium dioxides NPs will allow great comparability when results are observed in a more physiological oxygen culture environment.

4.1.2 Study Aim and objectives

The aim of this chapter was to assess the effect of oxygen content in the culture environment on cellular interaction/uptake and toxicity of the distinct MONPs. Anatase Titanium dioxide, Rutile Titanium dioxide and dSPIONs were studied in monocultures of hepatocellular carcinoma cells (HepG2), THP-1 monocytes and macrophages derived from the THP-1 cell line (dTHP-1). The cytotoxicity, genotoxicity and cellular interaction/uptake of MONPs were investigated under physioxic (5%O_2) and hyperoxic (21%O_2) culturing conditions.

Cellular uptake in the distinct environments was investigated prior to any toxicological studies. Cellular uptake was analysed by the ferrozine assay, flow cytometry and TEM imaging. Finally, the ability of MONPs to promote chromosomal DNA damage in HepG2 cells was quantified by the CBMN assay. Kinetochore staining was also applied to investigate the ability of the distinct MONPs to induce either clastogenicity or aneugenicity. The effects of the MONPs on the mitotic spindle were also investigated.

4.2 Materials and Methods

Unless it is stated otherwise all the cell treatments in this chapter were for dSPIONs were used to treat the cell lines in concentrations of 0-100µg/ml. The two different types of titanium dioxide NPs (TiO_2 NPs) were used for this study are Anatase (NM-102) and Rutile (NM-104); they were used to treat the cell lines in concentrations of 0-50µg/ml. The cells were cultured in 25cm^3 flasks at a concentration of 2x10^5 cells/ml that were incubated for 24h before treatments. Unless is stated otherwise all the experiments were conducted in 3 replicates (three distinct occasions with cells seeded at the same passage number, following the same procedure and analyses).

4.2.1 Cell culture

The cell lines used for this study were the hepatocellular carcinoma cell line (HepG2) that was purchased from ECACC and the monocyte cell line (THP-1) that was purchased from ATCC. Further information on cell culture of the primary cell lines and the differentiation of THP-1 to the macrophages resembling cell line dTHP-1 can be found in **Section 2.1.**

4.2.2 Physioxia (5%O_2) experiments

All experiments were carried out in an Invivo$_2$ physiological cell culture workstation (Baker Ruskin Ltd, UK). Cells were characterised after culture in two different oxygen environments; physioxia (5% O_2, 5% CO_2) and hyperoxia (21% O_2, 5% CO_2). Further information on experiments carried out under physioxia can be found on **Section 2.2.**

4.2.3 Cell viability assessment

The relative population doubling (RPD) was calculated for HepG2 and THP-1 after counting using a Z™ Series COULTER COUNTER® (Beckman Coulter, UK). Cell viability for dTHP1 was determined using Trypan blue (0.4% solution) and a haemocytometer, the measurements were used to produce a relative increase in cell count (RICC). Further information can be found **Section 2.8.**

4.2.4 Pro-Inflammatory cytokine quantification using an Enzyme-Linked Immunosorbent Assay (ELISA)

Following a 24h treatment of the cells with the mentioned NPs, supernatants were collected and stored in -20C°. Quantification of IL-8 (CXCL8) was carried out using ELISA KITs that were purchased from R&D, UK. More information can be found in **section 2.7.**

4.2.5 Intracellular reduced Glutathione

The Glutathione Detection Assay (fluorometric) (AbCam, UK) was used for the determination of glutathione concentration. After a 5h treatment with NPs at the concentrations described at **Section 2.1.2**, $1x10^6$ cells in 1ml for each of the treatments were harvested and washed twice using PBS. More information can be found in **section 2.8.**

2.4.6 Cell Preparation and Resin Embedding for TEM

Following NP treatment the cells were washed and trypsinized, cells were then re-washed in maintenance buffer (Table 2.7) and placed into 0.5 ml Eppendorf tubes. Cell pellets were resuspended in 100 mM phosphate buffered 2.5% glutaraldehyde fixative. The cells were then stained using post fixed in 1% osmium tetroxide fixative and embedded in resin. Prior to imaging by TEM, cell samples destined for NP uptake analysis required embedding in epoxy resin and ultra-sectioning to 70 nm thick sections. More information of the technique can be found in **section 2.4.1.**

4.2.7 Iron-cell interaction

A ferrozine assay was used to measure the amount of iron internalized by each cell line after 24h exposure to the selected dose of NP (Riemer *et. al.*.. 2004). The procedure was followed as described in **Section 2.3.** Three replicates were conducted; each replicate was the average of three measurements.

4.2.8 Flow cytometry for identification of cellular interaction with titanium dioxide polymorphs

Investigation of cellular interaction of the distinct cell lines with the polymorphs of Titanium dioxide NPs (NM-102 and NM-104) was carried out with the use of flow cytometry. The

experiment was based on the paper Zucker and colleagues published in 2010, where detection of interaction was based on light scattering principles. Further information of the method applied for this experiment can be found in **Section 2.6.**

4.2.9 Micronucleus assay

The sequential cytokinesis-blocked micronucleus (CBMN) assay is described here briefly, more information can be found at **section 2.9.** .After treatments were carried out for 24h, cell cycle arrest was achieved by exposing the cells to cytochalasin B 0.5µg/ml (Sigma Aldrich, UK) for 24h. More information on fixing of the cells, harvesting and staining with 40,6-diamidino-2- phenylindole (DAPI) (Vectashield, UK) was performed was described in **Section 2.9**. The cell scoring was carried using the metafer automated analysis system (MetaSystems, Carl Zeiss Ltd); the presence of micronuclei (MN) was evaluated in 6000 binucleated cells scored from three replicates (2000 cells per replicate*3) of the distinct NP doses.

4.2.10 Centromere staining

Centromere staining was performed using Star*FISH© Human Chromosome Pan-Centromeric Probes (Cambio, Cambridge, UK). The protocol used for staining is further described in **Section 2.10.2**. In total, 35 micronucleated cells were evaluated from 3 replicates, and scored for the presence of both positive and negative signals representing aneugenicity and clastogenicity respectively. Only doses with a significant increase in MN were evaluated by centromere staining.

4.2.11 Mitotic spindle analyses

After a 24h treatment of HepG2 cells with the distinct MONPs their ability to affect the mitotic spindle was investigated. HepG2 cells were cultured as described in **Section 2.2** and were seeded in 25cm^3 flasks at a concentration of 2x10^5 cells/ml that were incubated for 24h. **T**he doses of MONPs that produced significant genotoxic results were investigated for their ability to disrupt the mitotic spindle by evaluating 300 mitotic cells (altering the spindle from a normal polarity to either monopolar or multipolar). Treatments of HepG2 cells were carried out only at concentrations of 100µg/ml of dSPIONs, 10µg/ml of NM-102 Titanium

dioxide and 10µg/ml of NM-104 Titanium dioxide and a negative control as described in **Section 2.11.**

4.2.12 Statistical analysis

GraphPad Prism 6 was used for the plotting and the statistical analysis of all the results. Two-way ANOVA and Tukey's multiple comparisons test were used to compare the results in all cell lines between each dose, the untreated controls and the different oxygen environments. All of the statistical analysis of the acquired data we were completed with a $p \leq 0.05$ considered as significant. Further information on the statistical analysis can be found in **Section 2.14.**

4.3 Results

4.3.1 Characterization of cellular behaviour in culture environments with differing oxygen content

Before exploring the impact of NP exposure to cells under environments with varying oxygen content, it was important to evaluate and compare the cellular behaviour under physioxia versus hyperoxia conditions. Cellular behaviour would include the growth characteristics (relative population doubling and genotoxicity) cellular antioxidant production and production of pro-inflammatory cytokines (IL-8).

Relative population doubling of the cell lines, namely, THP-1 and HepG2 in the physioxic and hyperoxic culture environments was characterized over a period of 120h. A continuous increase in cell number was identified over this time period in both the cell lines. As is seen in **Figure 4.1** no increase in cellular number of THP-1 was identified after 24h incubation in physioxia in comparison to hyperoxia in both of the cell lines as is seen in **Figure** 4.1. Increase in the numbers of THP-1 cells in the time period between 72-120h was almost identical in the two environments. The cellular number of HepG2 cells followed the same trend observed in **Figure** 4.2 in THP-1. The cell number of HepG2 was similar in physioxia to hyperoxia.

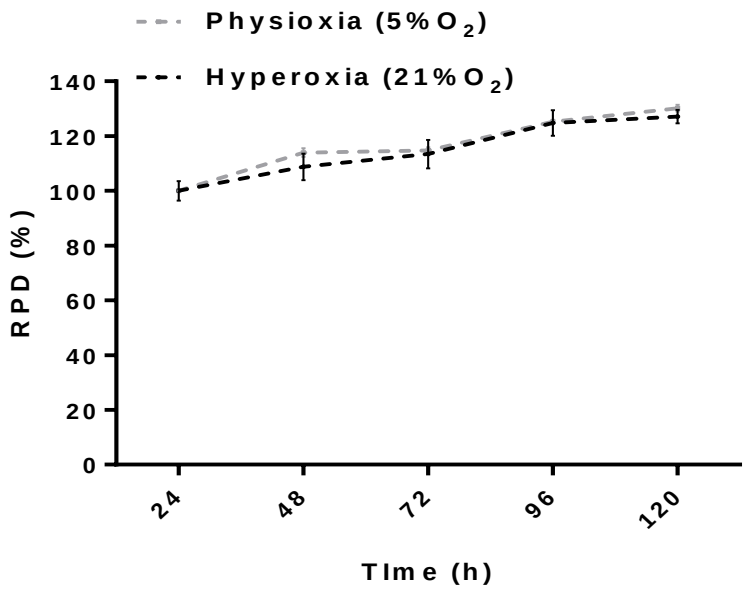

Figure 4.1: Relative population doubling (RPD) of THP-1 cells cultured in different oxygen culture environments. (n=3).

The background levels of DNA damage of cells cultured the different oxygen culture environments were investigated after incubation of HepG2 over 120h. No statistical significance was identified in the induction of micronuclei by untreated HepG2 regardless of the oxygen content of the culture environment. Although, the number of micronuclei in the cells was slightly lower in physioxia, this difference was not significant (**Figure 4.2**).

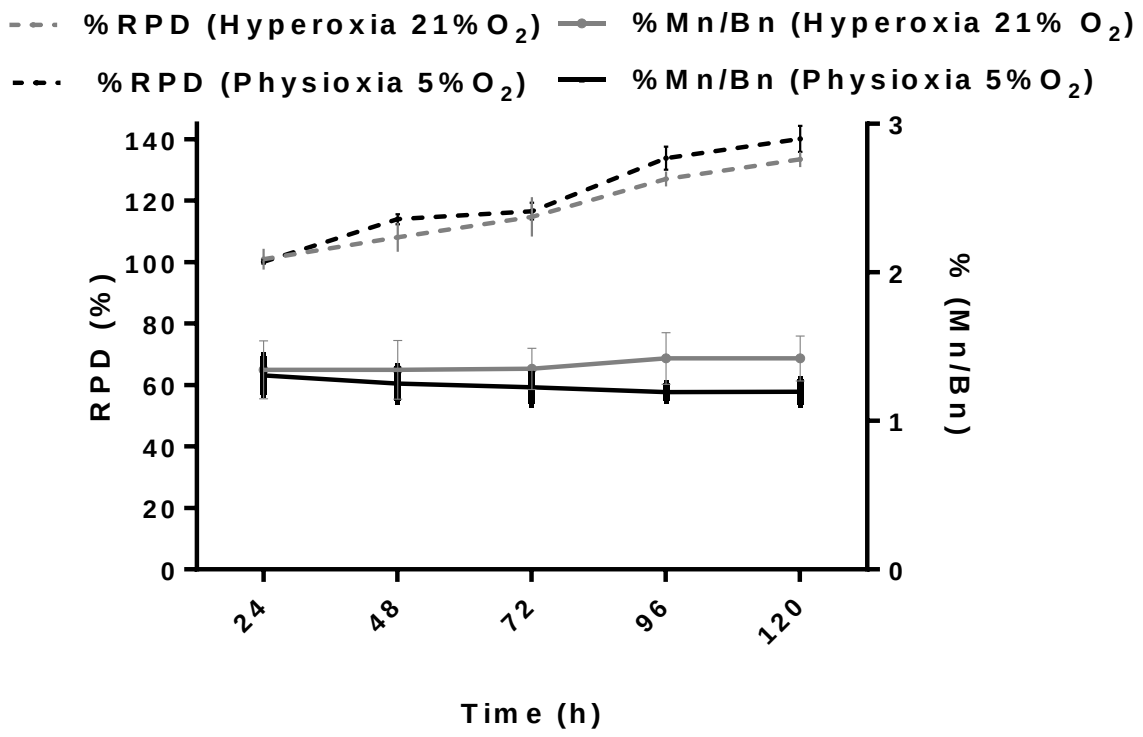

Figure 4.2: Relative population doubling and MN concentration of HepG2 in the distinct oxygen culture environments. Results were gathered over a 120h incubation and induction of micronuclei in HepG2 in the different oxygen culturing environments. (n=3)

The concentrations of glutathione (GSH) after 72h incubation in the two distinct culture environments with varying oxygen content were also investigated. As is seen in **Figure 4.3A** the concentration of GSH in both the cell lines, namely, HepG2 and THP-1 was slightly higher in the physioxic (5%O_2) environment. The concentration of GSH in the distinct environments was not, however significantly different in any of the cell lines. In both cell lines and environments GSH was similar at 24h compared to 72h. There was however, a slightly greater level of GSH measured in the monocytic cell line (THP-1) than in HepG2.

The levels of the pro-inflammatory cytokine, IL-8 was measured in cell culture supernatants for HepG2 and THP-1 after culture for 24h and 72h under physioxia and hyperoxia, as presented in **Figure 4.3B**. In hyperoxia HepG2 secreted more IL-8 than when cultured in the physioxic environment. Under both conditions, there was very little difference in the levels of IL-8 secretion at 72h culture in comparison with 24h. The difference between the secretions of IL-8 was significantly greater in the hyperoxic environment.

With respect to THP-1 cells, there were no differences in the concentration of IL-8 in across culture times. However, as is seen in **Figure 4.3 B** a significant increase was identified in the production of IL-8 in hyperoxia when the results were compared with the same time point in physioxia.

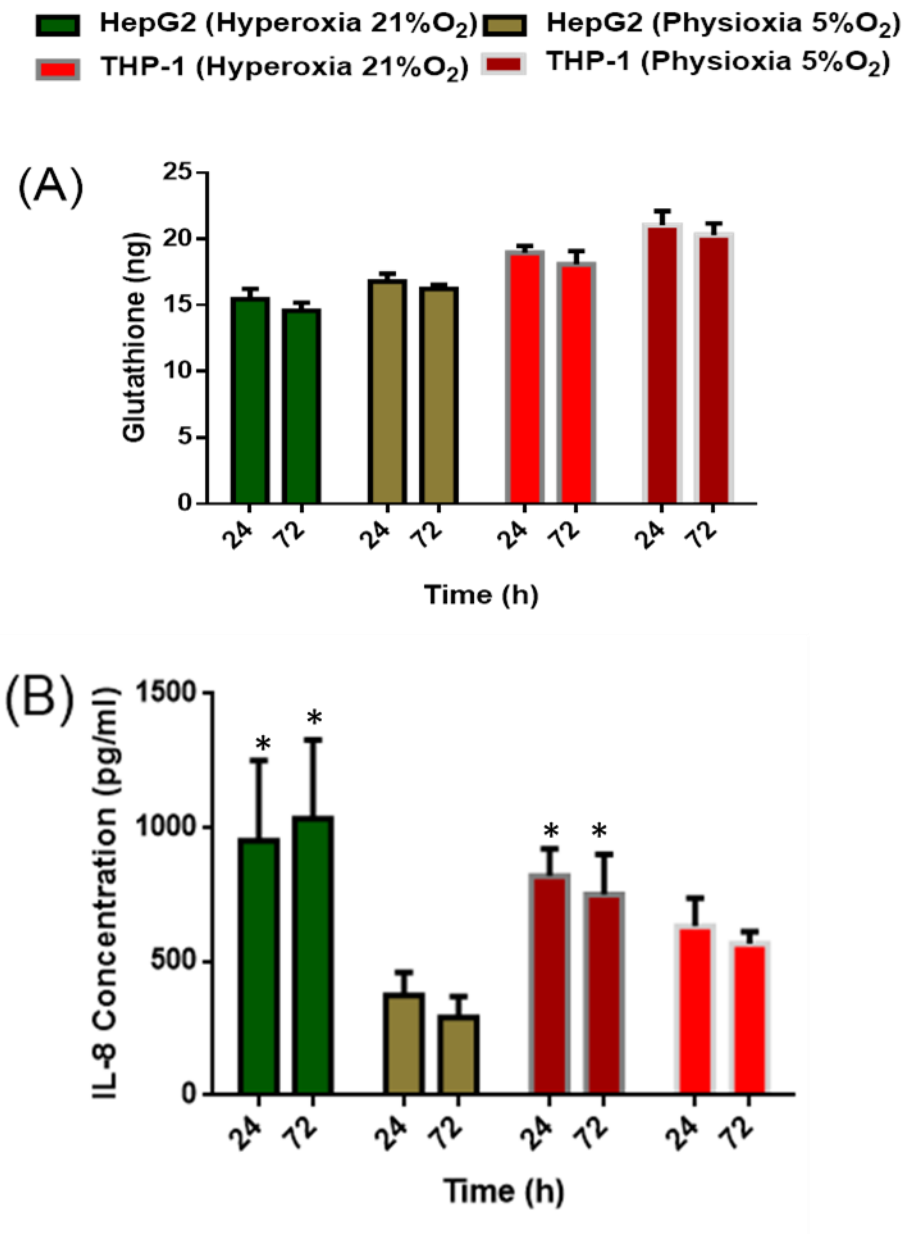

Figure 4.3: Antioxidant and inflammatory cytokine production in the different oxygen culture environments. (A) Glutathione production after incubation in the both a hyperoxic and physioxic oxygen culture environment (n=3) **(B)** Production of IL-8 in THP-1 and HepG2. (n=3) * comparison of the incubation with the same incubation period in the different environment *P≤0.05*

4.3.1.1 Characterization of THP-1 differentiation to dTHP-1

Before exploring the impact of NP exposure to cells, it was important to evaluate and compare the cellular behaviour and optimise the differentiation of THP-1 cells to d-THP-1 using PMA under physioxia versus hyperoxia conditions. Cellular behaviour would include cellular morphology, growth characteristics (relative population doubling) cellular antioxidant production and production of pro-inflammatory cytokines (IL-8).

The behaviour of the macrophage-resembling cell line dTHP-1 using 50nmol PMA was investigated in the different oxygen culture environments over a period of 72h. The morphology of the cells was studied by light microscopy. After visual identification within the first 24h, cells treated with PMA in hyperoxia were slightly inflated with no morphological changes identified (**Figure 4.4A**). When treated with PMA in physioxia more cells developed macrophage like morphological characteristics than those treated with PMA in physioxia (**Figure 4.4D**).

After 48h of incubation with PMA the cells morphologically differentiated into macrophages in both of the environments. No further differences on cellular morphology were observed after the first 48h of culture in the two oxygen culture environments (**Figure 4.4 B and E**).

After 72h culture in the presence of PMA the membrane of dTHP-1 cells in the physioxic culturing conditions seemed to forming blebs, suggesting the cells were undergoing apoptosis (**Figure 4.4F**). This blebbing was not observed in cells cultured in physioxia.

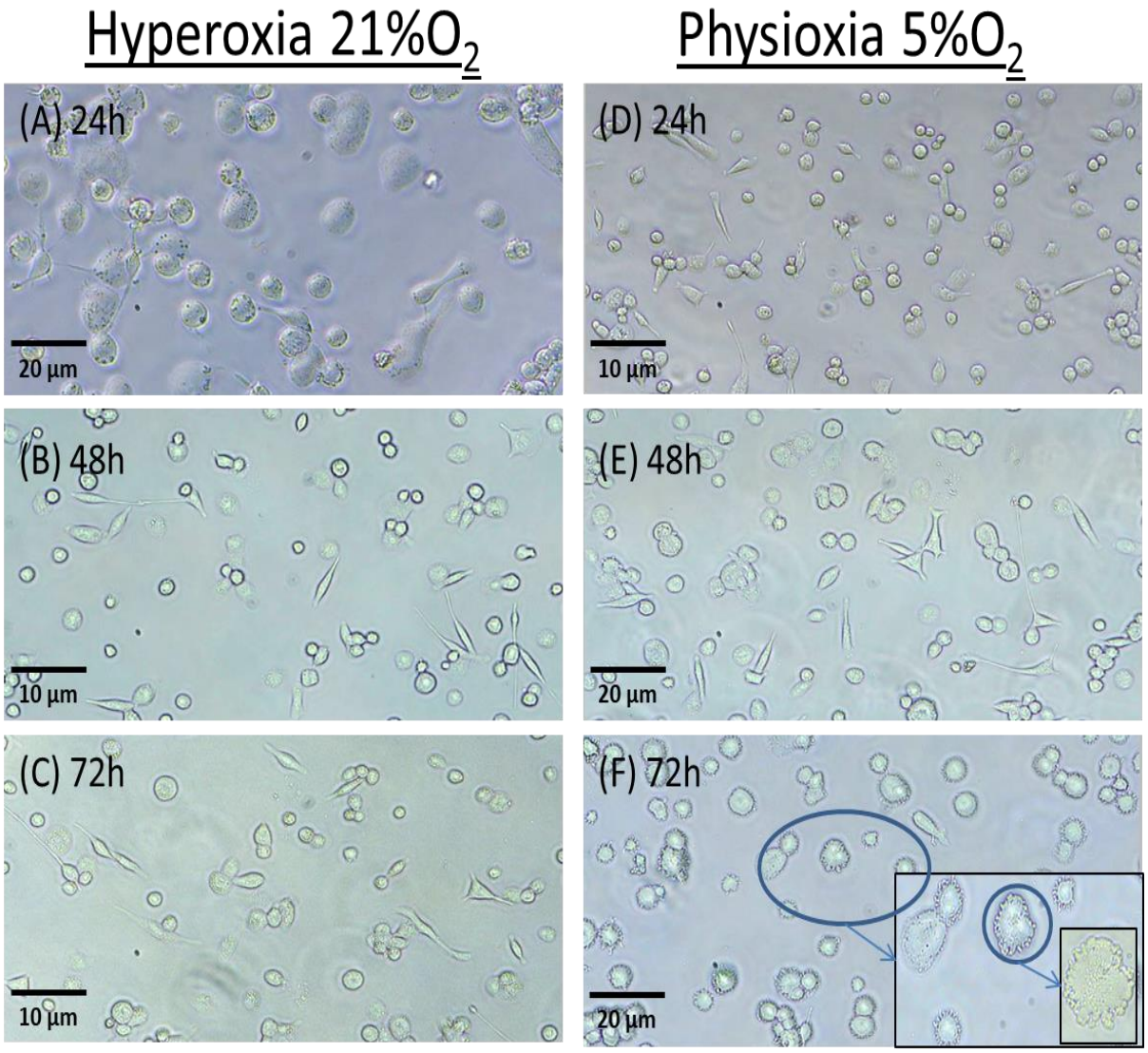

Figure 4.4: THP-1 differentiation to dTHP-1 after incubation under hyperoxic and physioxic conditions with 50nmol PMA for the period of (A and D) 24h, (B and E) 48h and (C and F) 72h.

The effects of the different oxygen culturing environments on the cellular viability of THP-1 cells undergoing differentiation using 50nmol of PMA were determined over a period of 72h using RICC. As is seen at **Figure 4.5** no significant difference in the cell number was identified in the two environments. The cell number over the period of the first 48h remains constant, but was reduced slightly after 72h, no statistical significance was identified.

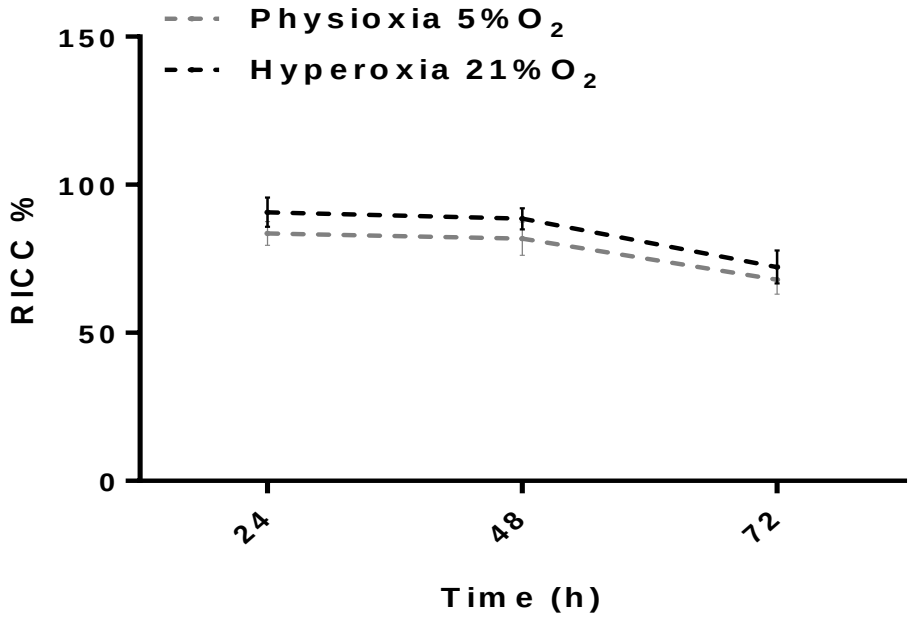

Figure 4.5: Effect of PMA (50nmol) on cell number in a Hyperoxic and a physioxic environment. (n=3).

Glutathione concentrations, after 48h incubation with 50nmol PMA, were investigated in the physioxic and hyperoxic environments. As is seen in **Figure 4.6 A** after the differentiation of THP-1 monocytes to the macrophage resembling cell line dTHP-1, a greater reduction in glutathione concentration was identified in the hyperoxic environment. The reduction was not found significantly greater.

The cells were also investigated for changes in the production of the pro-inflammatory chemokine IL-8. A significant increase was identified in both environments over the period of the incubation (72h), which was significantly greater in the hyperoxic environment. As is seen in **Figure 4.6B** after a 48h and 72h incubation with 50nmol the presence of IL-8 was found to be significantly greater in the physioxic environment.

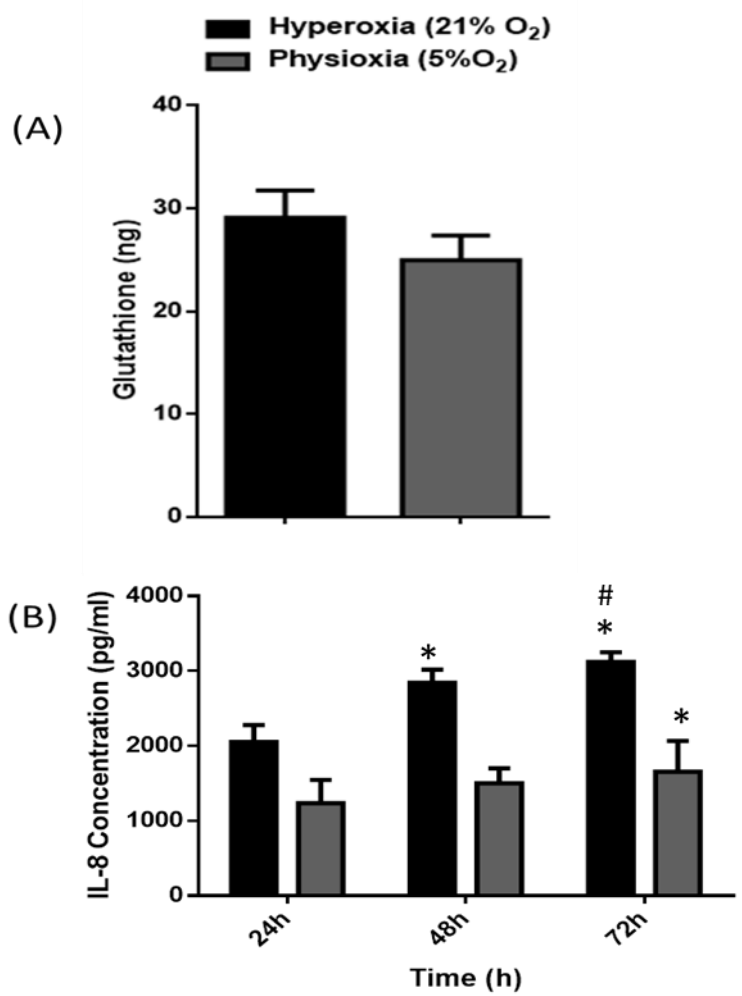

Figure 4.6: Antioxidant and inflammatory cytokine production in the different oxygen culture environments. (A) Glutathione concentration after incubation of THP-1 with 50nmol of PMA for the period of 48h. (B) 50nmol PMA effects in different environments on the production of pro-inflammatory chemokine IL-8. (n=3) * comparison of the incubation time with results on the same environment at 24h # comparison of the results at the same time point in the different environments *P≤0.05*

4.3.2 NP-cell interaction

4.3.2.1 Ferrozine Assay-dSPION cell interactions

In order to identify cellular interaction with dSPIONs after treatment to different concentrations the ferrozine assay that allows identification of Fe concentration in the cells was applied. After treatment for 24h with the NPs the cultured cells were investigated for their interaction with distinct MONPs. Interaction of cells with dSPIONs was investigated using the ferrozine assay. As is seen in **Figure 4.7A** a dose dependent significant increase in Fe concentration was identified in both THP-1 and dTHP-1 cells in both environments. A dose dependent increase was identified in both hyperoxia across doses 10-100µg/ml and in physioxia across doses 8-100µg/ml in both immune cell lines (THP-1 and dTHP-1). The identified increase was generally greater in the physioxic environment; however this difference was only significantly greater at the top dose of 100µg/ml in THP-1 when compared with the Fe concentration in the hyperoxic environment. In contrast, no increase in dSPION-HepG2 interaction was identified in the hyperoxic environment at any of the doses when compared with the negative control (0µg/ml). Yet, a dose dependent increase in the Fe concentration was identified in HepG2 cells treated with dSPIONs under physioxia. Doses over 8µg/ml were significantly greater than the negative control. In summary a distinct interaction with dSPIONs was identified in all of the cell lines with the greater being identified in dTHP-1 and the lowest being identified in HepG2.

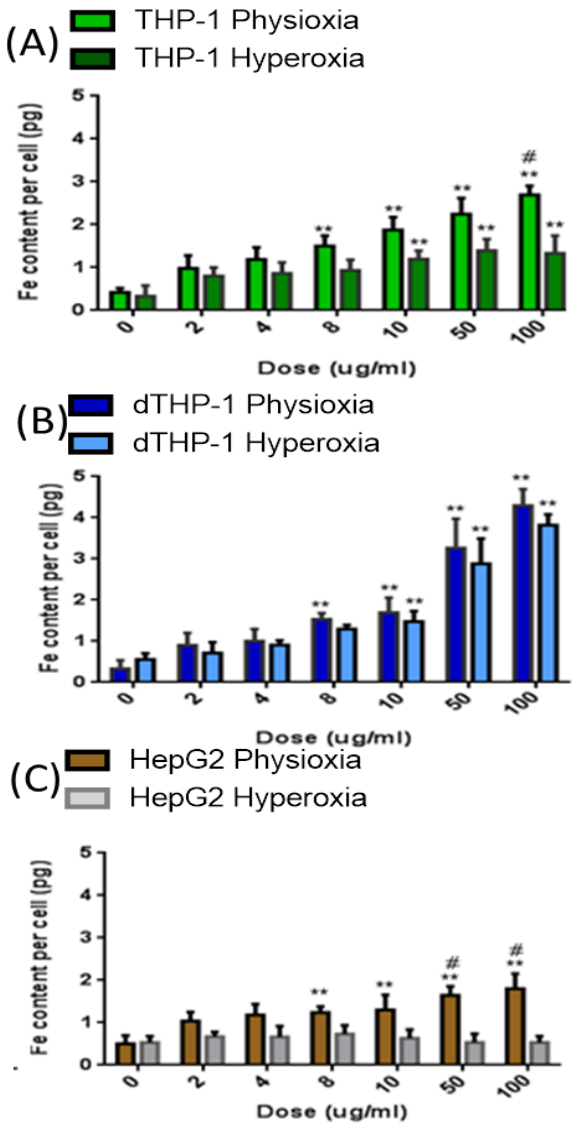

Figure 4.7: Iron content of cell lines after treatment with dSPIONs under physioxia and hyperoxia environments; (A) THP-1 cells (B) dTHP-1 cells and (C) HepG2 cells. (n=3) ** Comparison of the dose with results at 0µg/ml in the same environment # comparison of the results of the same in the different environments

4.3.2.2 Identification of Titanium dioxide-Cell interaction through flow cytometry

Cellular interaction of TiO_2 NPs was investigated using flow cytometry after a 24h treatment. The increase of the interaction was identified by a shifting/increase in the cellular side scattering which indicated changed granularity of the cells. This change in granularity suggested an increase in the interaction with the NPs (either attachment to the cell membrane, free in the cytoplasm or in encapsulated intracellular vesicles). The results presented here indicate that in the physioxic environment for both NM-102 and NM-104, no differences were identified in the NP-cell interaction between the treatments in the distinct environments. All the negative controls in **Figure 4.8 and 4.9** were presented with the colour red whereas the highest NP doses (50µg/ml) were presented with blue. Only data for the highest dose are illustrated as the doses of 2-10µg/ml for both NM-102 and NM-104 did not result in a significant increase in interaction (data not presented here).

As is seen in the flow cytometry dot plots presented in **Figure 4.8 A1, B1and C1,** NM-102 were able to increase the side scattering in all the cell lines when the cells were compared with the negative control. The greatest shift in side scattering was identified in the immune cell lines (dTHP-1>THP-1). The results were also expressed using histograms (**Figure 4.8 A2, B2 and C2**). There is a large increase in cells with high granularity in the dTHP-1 following treatments but only minor changes in cellular granularity in the HepG2 cells.

The NM-104 material induced a similar response to NM-102. As illustrated in **Figure 4.9 A1, B1 and C1,** NM-104 increased the side scattering in all the cell lines when the cells were compared with the negative control. The largest shift in side scattering according to the dot plots was identified in the macrophages resembling cell line dTHP-1. When the results were expressed in histograms (**Figure 4.9 A2, B2 and C2**), the count of cells that increased in granularity after treatments were highest in dTHP-1 and the lowest was in HepG2, suggesting of highest cellular interaction in the immune cell lines when compared to HepG2.

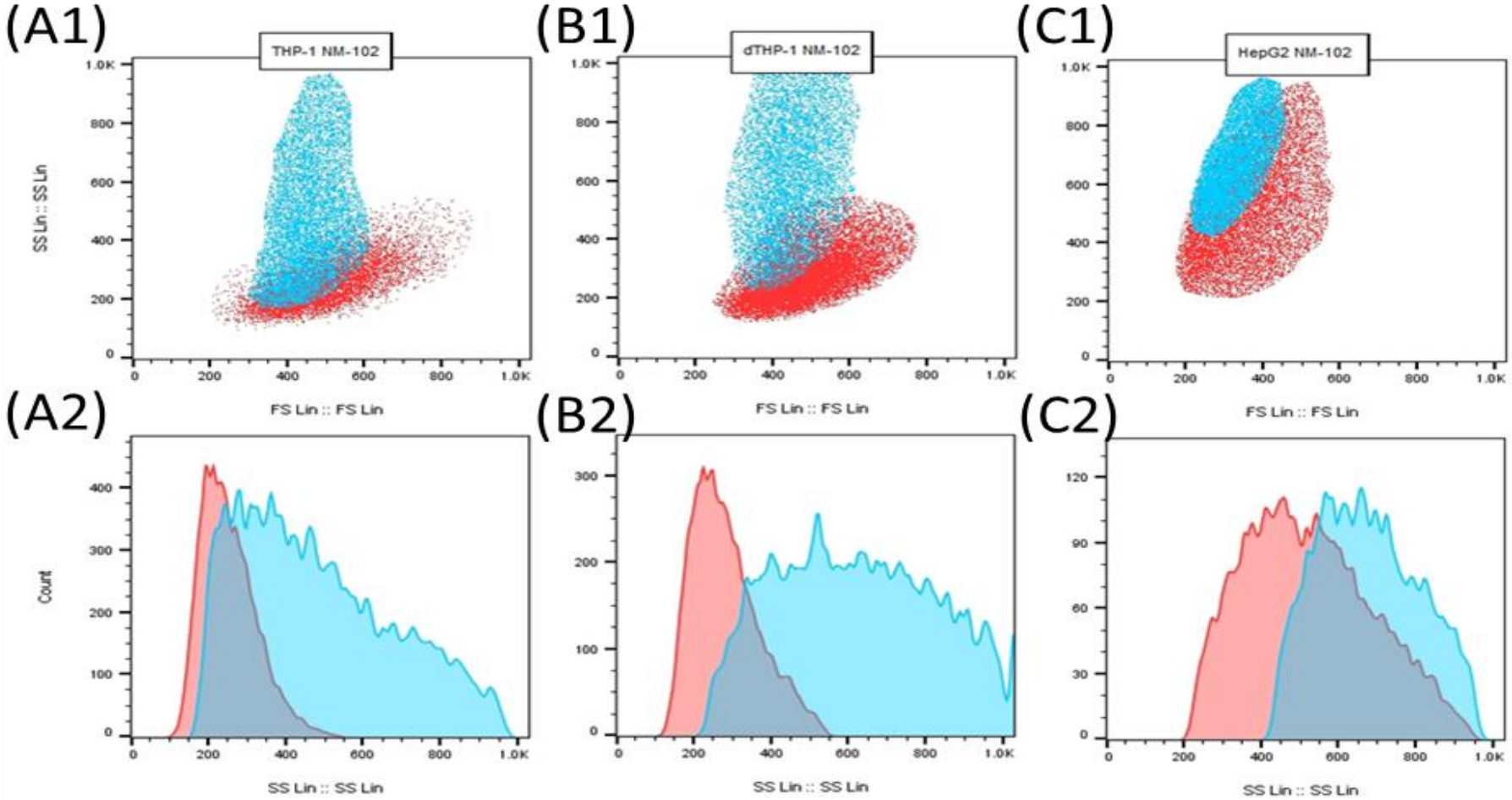

Figure 4.8: NM-102-cellular interaction investigated using flow cytometry. (A1 and 2) THP-1; (B1and 2); dTHP-1 (C1and 2); HepG2 (n=3). In A1, B1and C1 the results are represented by flow cytometry dot plots. The data has also been converted into histograms in A2, B2 andC2. TIO red is the 50 µg/ml of NM-102 and in blue is the negative control of 0µg/ml.

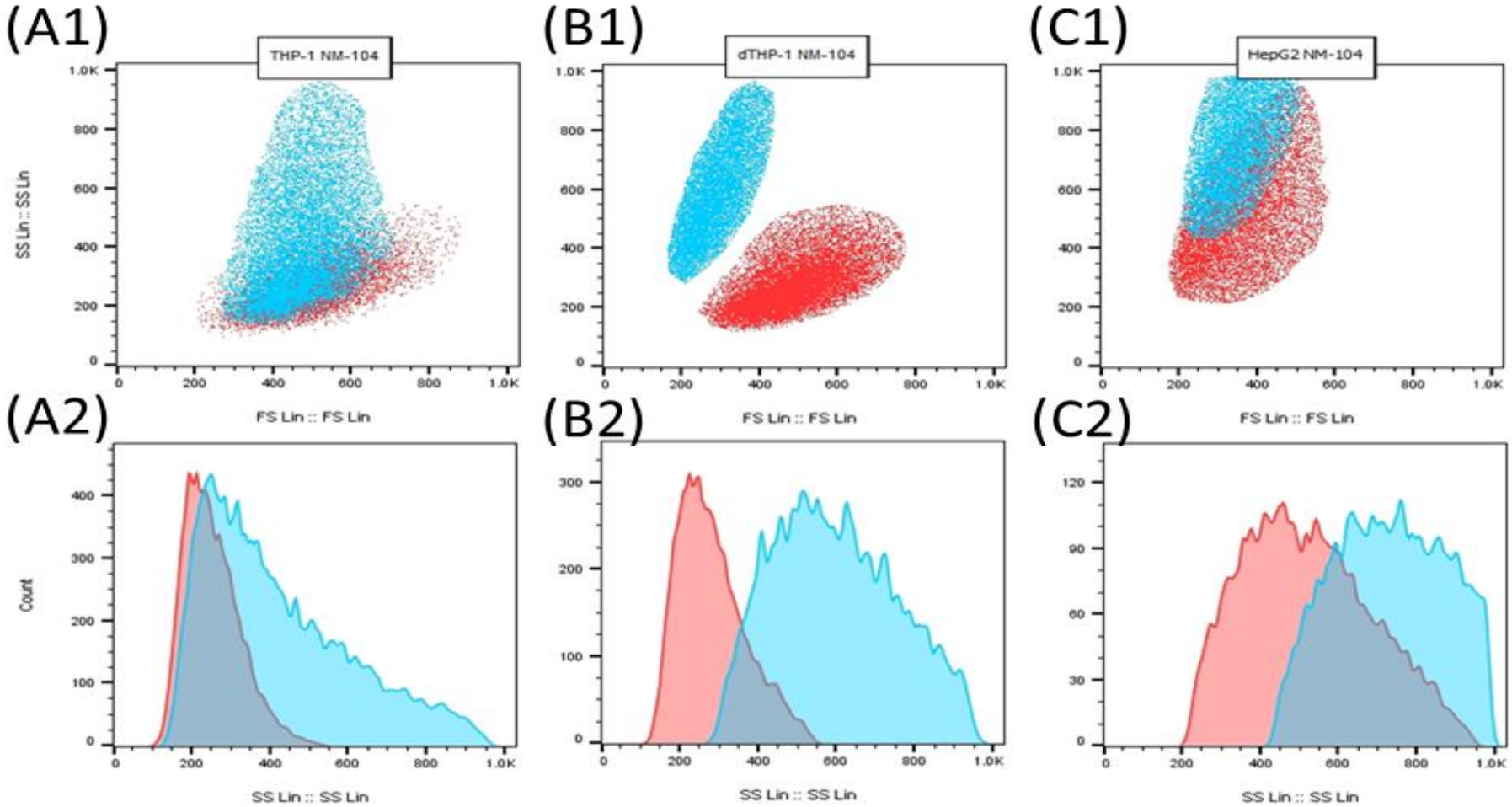

Figure 4.9: NM-104-cellular interaction investigated using flow cytometry (A1and 2) THP-1 (B1and 2) dTHP-1 (C1and 2) HepG2 (n=3). In A1, B1 and C1 results were presented in the flow cytometry dot plots. The results were also presented in histograms A2, B2, C2. In red is the 50 µg/ml of NM-14 and in blue is the negative control of 0µg/ml.

4.3.3 Uptake and cell compartmentalization determined by TEM

After exposure of THP-1 and HepG2 for 24h in the physioxic environment, to the maximum concentration for each of the NPs (for dSPIONs 100µg/ml and for the Titanium dioxide polymorphs 50µg/ml), cellular interaction, uptake and compartmentalization/localization were investigated by TEM. Images of the cells were taken to determine the ability of the different cell lines to internalise the NPs being investigated.

Only one oxygen environment was investigated, this choice was based on previously obtained results in other experiments that have shown a greater NP-cell interaction in the physioxic environment. Due to time limits, the expenses for this technique and the small number of dTHP-1 cells obtained after the cells underwent treatment with the NPs and prepared for imaging samples for were not obtained. Instead THP-1 monocytes were chosen as a representative immune cell line for the experiment.

4.3.3.1 Cellular Uptake and compartmentalization in THP-1 (primary monocyte)

A representative control immune cell, monocytic THP-1, is presented in **Figure 4.10** where THP-1 cells exhibit a large, round, single-cell morphology with a visibly lobulated nucleus.

After treatment of THP-1 cells with dSPIONs at a concentration of 100µg/ml for the period of 24h in the physioxic environment, no visual interaction or uptake was identified. Cells were investigated in a total of 6 sample grids that were prepared after treatment for two distinct replicates. The results observed in the samples treated with dSPIONs were no different with what is presented in the control illustrated in Figure **4.10**.

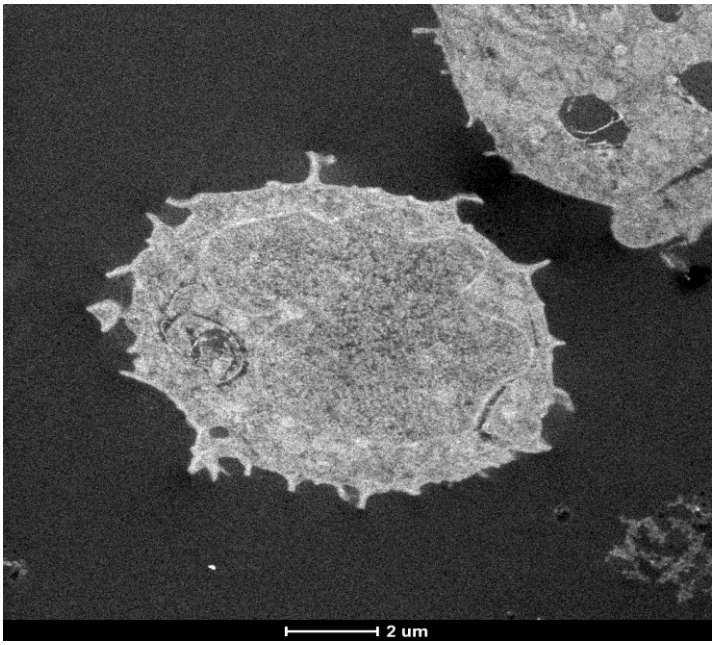

Figure 4.10: TEM image of a untreated THP-1 single cell, this is a control image in the untreated control. THP-1 were observed to have a large, round, single-cell morphology. As is seen the ability of the cells to produce pseudopodia was identified in the control image.

As is seen in **Figure 4.11 A and B**, exposure of THP-1 cells to NM-102 NPs resulted in uptake after a 24h treatment, with the internalised material enclosed in a cellular vesicle. As is seen in the images at figure 4.11 A and B agglomerates of NM-102 varied in size after uptake, sizes were in the range of 200-500nm. To confirm the observed NP agglomerates were indeed titanium dioxide, EDX was applied in the image at **Figure 4.11B**. As is seen in **Figure 4.11C,** EDX mapping on the identified internalised entities indicated that they mainly consisted of titanium, shown in red colour. The analyses of the whole spectrum presented in **Figure 4.11C** can be seen in **Figure 4.11D** where Ti is identified as the highest concentration in the area. Osmium peak was identified as well that was greater than titanium. This is due to the staining procedure the cells underwent with osmium.

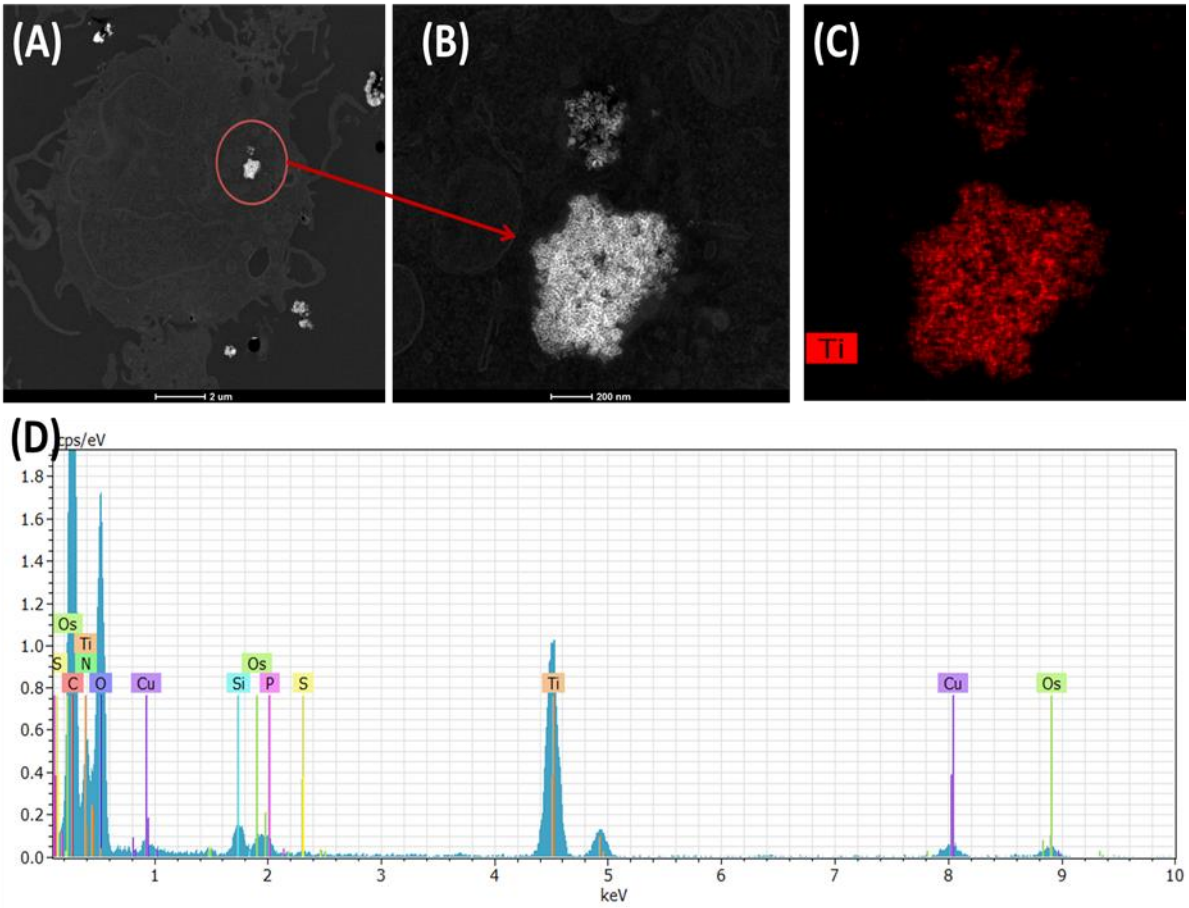

Figure 4.11: TEM imaging for the investigation of NM-102 uptake and compartmentalization in THP-1 cells (A)Internalised NM-102 agglomerate, and compartmentalization.(B) A greater magnification of (A) of the internalised NP agglomerate(C) EDX mapping on the area of the agglomerate indicated by the red circle in (A), where the red colour represents elemental titanium internalised in the cell. (D) Spectrum analysis of the EDX mapping, peaks were identified in Titanium, Oxygen and Osmium.

Electron micrographs presented in **Figure 4.12 A and B** demonstrate the interaction, uptake and localization of NM-104 NPs by THP-1 cells after a 24h treatment. Agglomerates of NM-104 varied in size, 50-250nm, after uptake. NP agglomerates in different amounts were seen to be enclosed in cellular vesicles within the cell. EDX was applied on the image in **Figure 4.12B** in order to determine if the observed uptaken body consist by titanium and hence NM-102 that was used to treat the cells. From the image presented in Figure **4.12 C,** it is

evident that the bodies uptaken by the cell mainly consisted by titanium, shown in red colour. Whole spectrum analyses of the area presented in **Figure** 12C can be seen at **Figure 4.12 D**, where Ti is identified at the highest concentration on the area. Osmium peak was identified as well that was greater than titanium. This is due to the staining procedure the cells underwent with osmium.

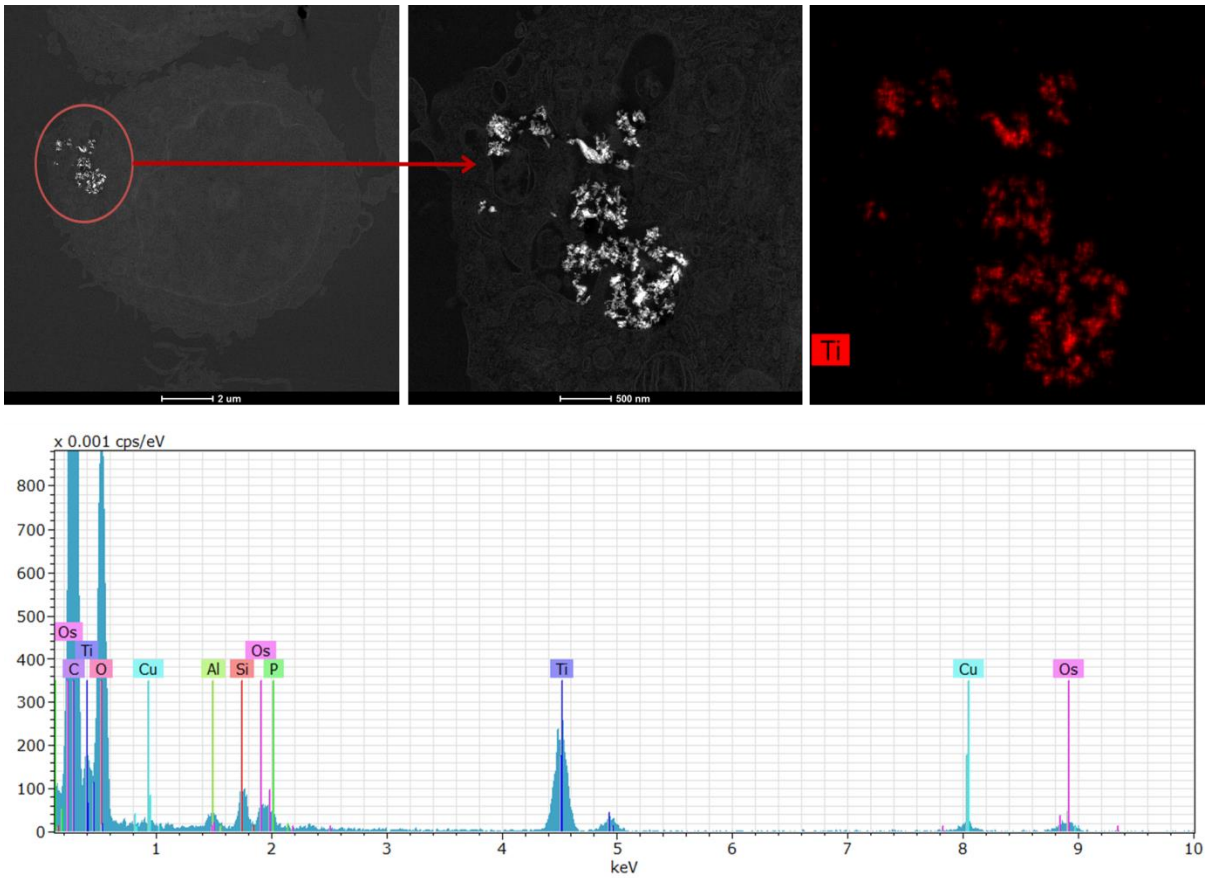

Figure 4.12: TEM imaging for the investigation of NM-104 uptake and compartmentalization in THP-1 cells (A)Internalised NM-104 agglomerate, and compartmentalization.(B) A greater magnification of (A) of the internalised NP agglomerate(C) EDX mapping on the area of the agglomerate indicated by the red circle in (A), where the red colour represents elemental titanium internalised in the cell. (D) Spectrum analysis of the EDX mapping, peaks were identified in Titanium, Oxygen and Osmium.

4.3.3.2 Cellular Uptake and compartmentalization in Hepatocellular carcinoma cell line (HepG2)

A representative untreated Hepatocellular Carcinoma cell (HepG2) is presented in **Figure 4.13;** under TEM an epithelial morphology was observed. HepG2 were found to be polygonal in cell shape and nucleus (**Figure** 4.13).

After treatment of HepG2 cells with dSPIONs at a concentration of 100µg/ml for the period of 24h in the physioxic environment no visual interaction or uptake was identified. These were investigated in the total of 6 sample grids that were prepared after treatment for two distinct replicates. The results observed in the samples treated with dSPIONs were no different with what is presented in the control illustrated in **Figure** 4.13.

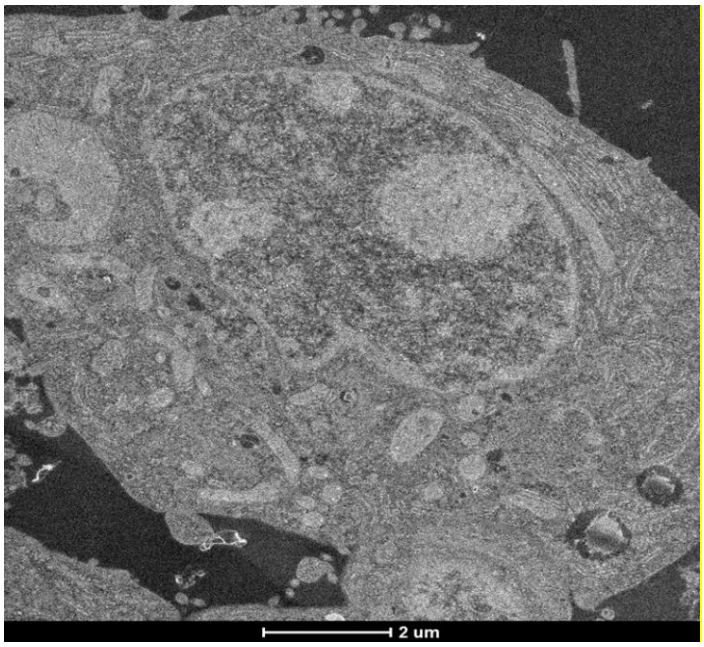

Figure 4.13: TEM image of an untreated HepG2 single cell, this is a control image in the untreated control. HepG2 were found to be polygonal in cell shape and nucleus shape.

After treatment of the hepatic epithelial cells HepG2 under physioxic environmental conditions for the period of 24h internalised NM-102 (50µg/ml) agglomerates were observed. As is seen in the example image in **Figure 4.14A and B**, the observed agglomerates after uptake retained a size of500nm, but variability in size was observed 200-

500nm but various. The observed agglomerates were not enclosed in by cellular bodies. Confirmation that the observed internalized agglomerates in **figure 4.14B** consist by titanium dioxide EDX was applied. After EDX mapping analyses was applied to the area of the observed agglomerates their elemental composition was confirmed to be mainly Ti. Areas with elemental Ti are coloured with red as is seen in **Figure 4.14C**. The analyses of the whole spectrum of the area presented in Figure 14C can be found in **Figure 4.14D**, where Ti is identified at the highest concentration on the area. Osmium peak was identified as well that was greater than titanium. This is due to the staining procedure the cells underwent with osmium.

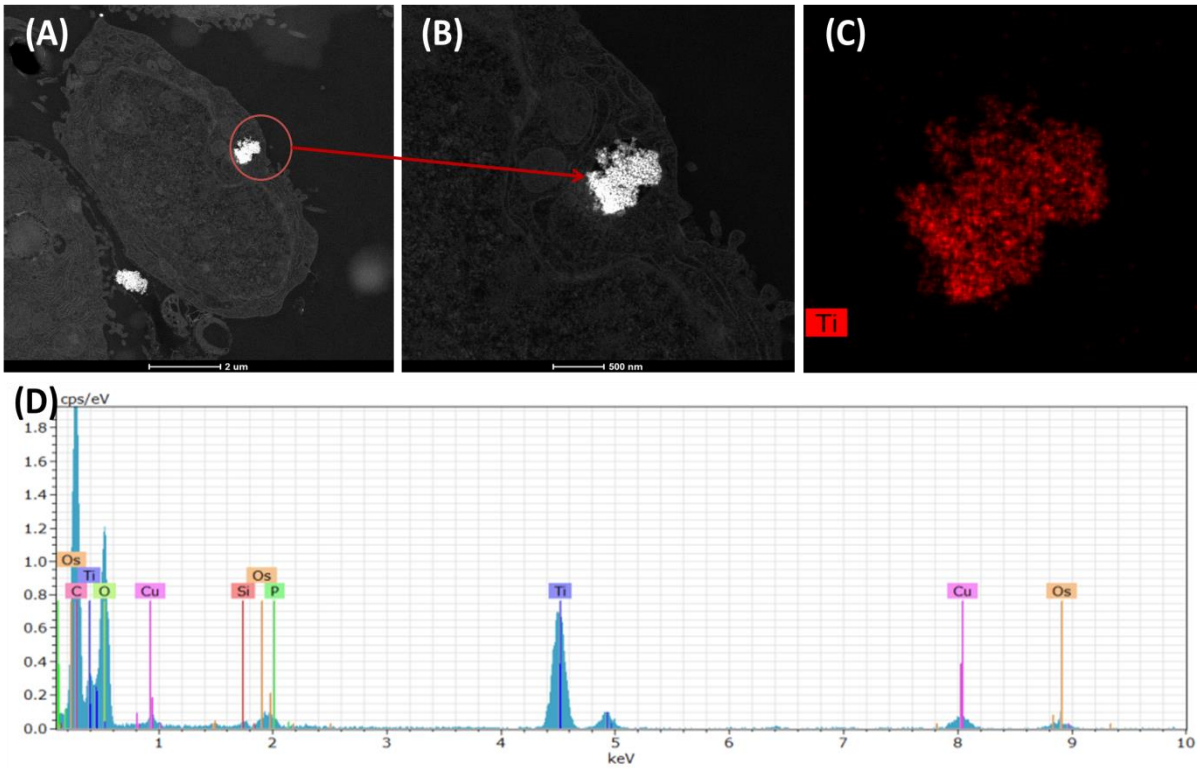

Figure 4.14: TEM imaging for the investigation of NM-102 uptake and compartmentalization in HepG2 cells (A)Internalised NM-104 agglomerate, and compartmentalization.(B) A greater magnification of (A) of the internalised NP agglomerate(C) EDX mapping on the area of the agglomerate indicated by the red circle in (A), where the red colour represents elemental titanium internalised in the cell. (D) Spectrum analysis of the EDX mapping, peaks were identified in Titanium, Oxygen and Osmium.

After treatment of the hepatic epithelial cells HepG2 under physioxic environmental conditions for the period of 24h internalised NM-102 (50µg/ml) agglomerates were observed. As is seen in the example image in **Figure 4.15A and B**, the observed agglomerates after uptake retained a size of500nm, but variability in size was observed 200-500nm but various. The observed agglomerates were not enclosed in by cellular bodies. EDX was applied in order to determine if the observed NP agglomerates consist of Ti. In **Figure 4.15C** EDX mapping on internalised agglomerates by the cell proves that they mainly consist of titanium, shown in red colour. Whole spectrum analyses of the area presented in **Figure** 15C can be seen at **Figure 4.15D**, where Ti is identified as the highest concentration on the area. Osmium peak was identified as well that was greater than titanium. This is due to the staining procedure the cells underwent with osmium.

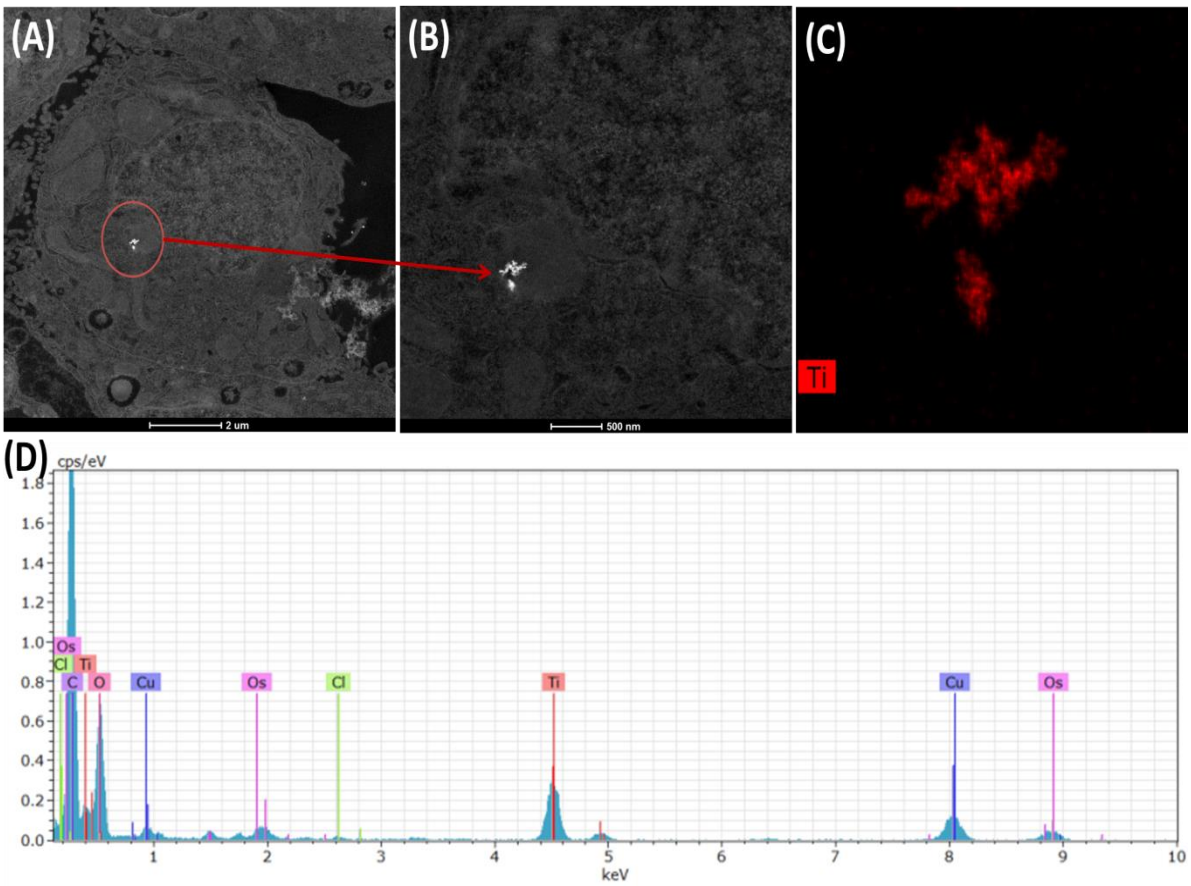

Figure 4.15: TEM imaging for the investigation of NM-104 uptake and compartmentalization in HepG2 cells (A)Internalised NM-104 agglomerate, and compartmentalization.(B) A greater magnification of (A) of the internalised NP agglomerate(C) EDX mapping on the area of the agglomerate indicated by the red circle in (A), where the red colour represents elemental titanium internalised in the cell. (D) Spectrum analysis of the EDX mapping, peaks were identified in Titanium, Oxygen and Osmium.

4.3.4 Toxicity assessment of MONPs in different culture environments

4.3.4.1 Assessment of cellular viability of monocyte THP-1 cells after treatment with MONPs

The effects of the distinct MONPs to reduce the cellular viability of THP-1 cells was investigated using the RPD analysis in both hyperoxic and a physioxic culture environment. As is seen in **Figure 4.16A** after the exposure to a dose range of 0-100µg/ml dSPIONs no significant reduction in cellular viability of THP-1 was identified in the hyperoxic environment. However, a significant reduction in the %RPD was identified at 50 and 100µg/ml under the physioxic culturing conditions when compared with the negative control (0 µg/ml). A greater significant reduction on THP-1 cellular viability after treatment with dSPIONs 100µg/ml was identified in the physioxic environment when compared with the hyperoxic environment. Results for the effects of the Titanium dioxide isomorphs on the cellular viability of THP-1 are presented in both **Figure 4.16 B and Figure 4.16C.** After treatment with NM-102 and NM-104 at 0-50µg/ml, no significant reduction in viability was observed and there was also no significant difference between the toxicity when comparing the two distinct oxygen culture environments.

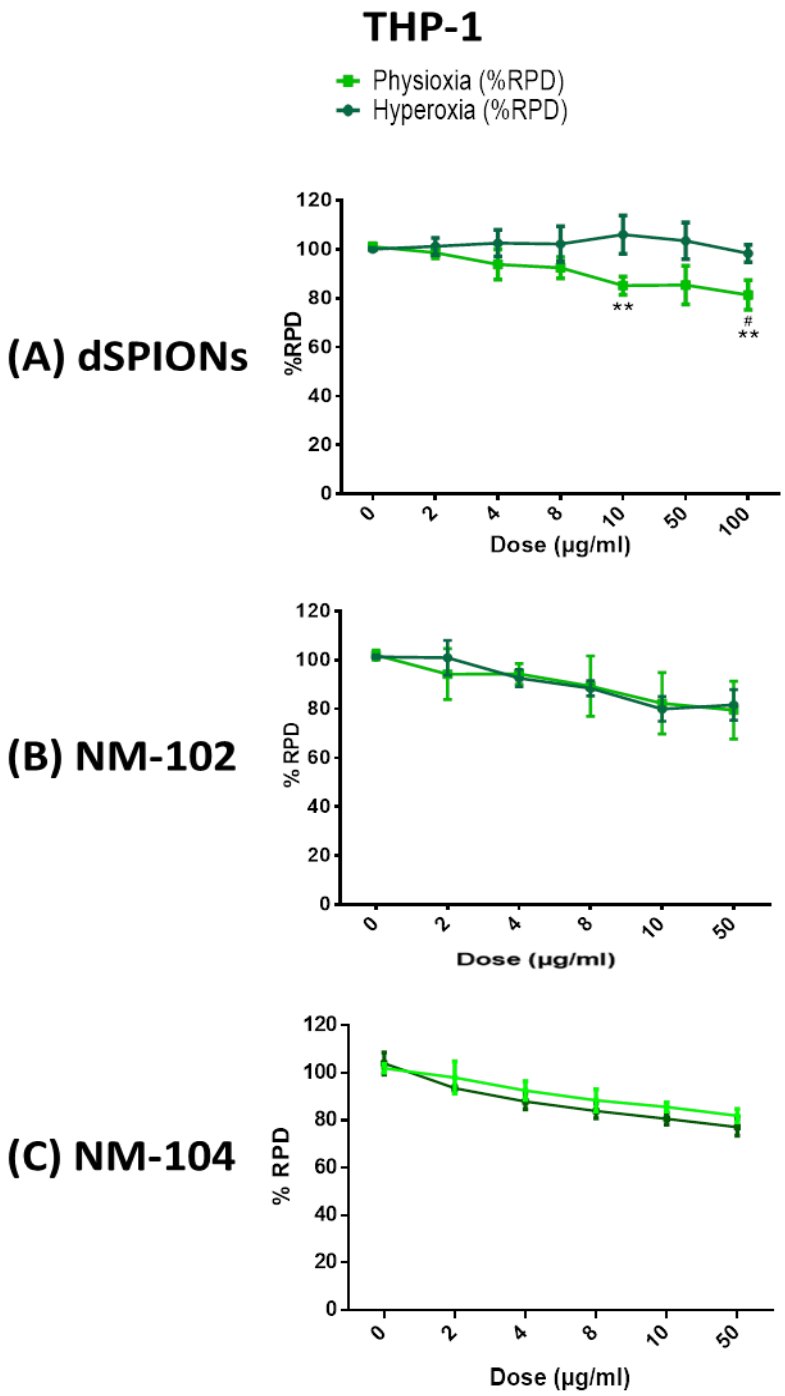

Figure 4.16: Cell viability of THP-1 after treatment with MONPs under physioxia and hyperoxia: Treatments of the cell lines were carried for the period of 24h with (A) dSPIONs (B) NM-102 (C) NM-104. (n=3) **Dose compared to 0µg/ml. # Dose compared to the same treatment in different environment.*P≤0.05*

4.3.4.2 Assessment of cellular viability of macrophages resembling dTHP-1 after treatment with MONPs

The effects on the cellular viability of the macrophages resembling dTHP-1 cells after treatment with the distinct MONPs for a period of 24h was investigated in both a hyperoxic and physioxic environments. As is seen in **Figure 4.17 A,** dSPIONs were not able to induce a significant reduction of cellular viability after a treatment for 24h in the hyperoxic environment. In the physioxic environment, a significant reduction in cellular viability of dTHP-1 was identified at both 10and 100µg/ml when the results were compared with the negative control in the same environment. Additionally, it was notable that 100µg/ml of dSPION were able to induce a significantly greater cytotoxic behaviour in the physioxic environment when compared to response in hyperoxia. The ability of both NM-102 and NM-104 to induce toxicity were investigated in the distinct oxygen-content environments. As is seen in both **Figure 4.17 B and Figure 4.17C** after treatment with the Titanium dioxide isomorphs no significant reduction in cellular viability was identified in either culture environment.

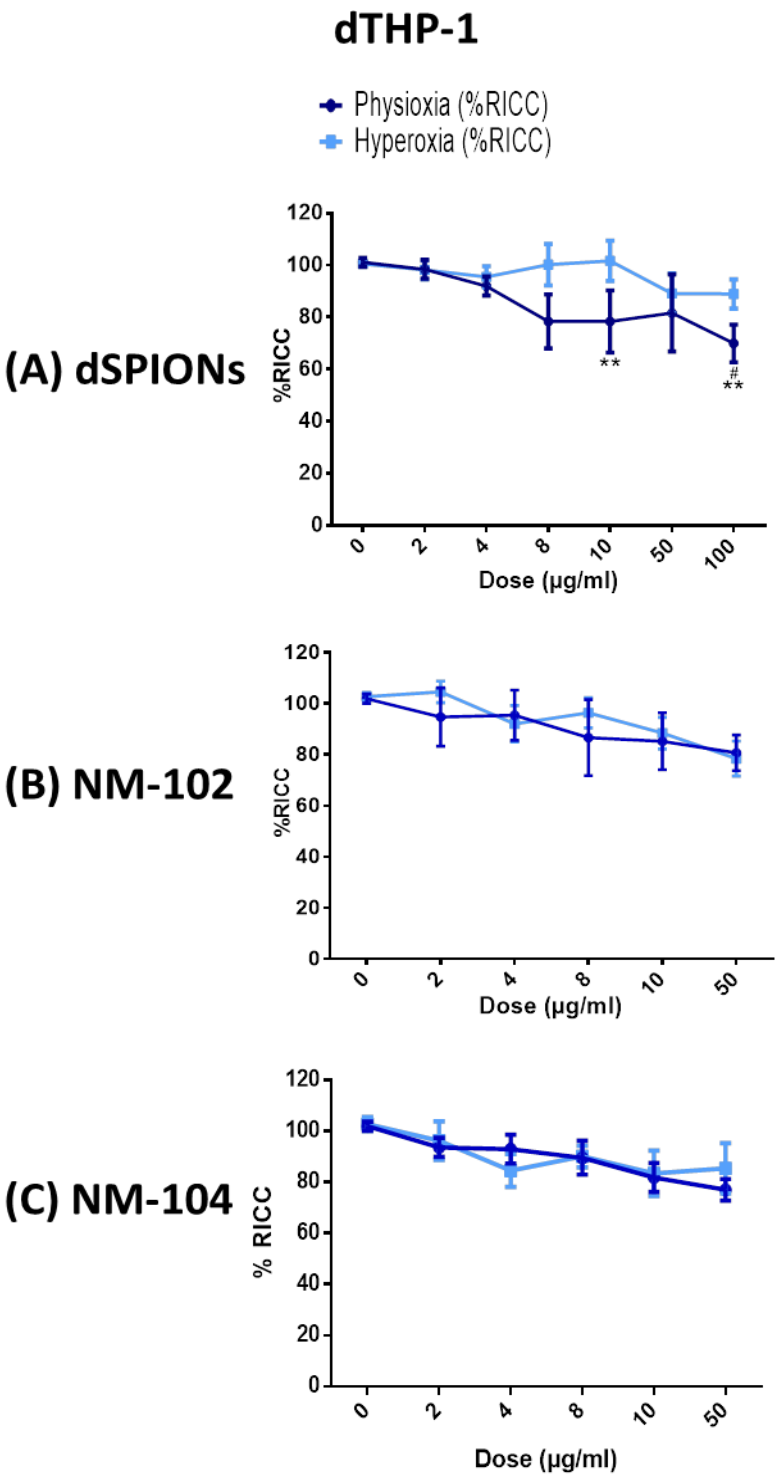

Figure 4.17: Cell viability of THP-1 after treatment with MONPs under physioxia and hyperoxia: Treatments of the cell lines were carried for the period of 24h with (A) dSPIONs (B) NM-102 (C) NM-104. (n=3) **Dose compared to 0µg/ml. # Dose compared to the same treatment in different environment**.** *P≤0.05.*

4.3.4.3 Assessment of cellular viability and genotoxicity in hepatocellular carcinoma HepG2 after treatment with MONPs

Chromosomal damage and cell viability assessment of HepG2 cells exposed to dSPIONs (0-100µg/ml) for 24h was investigated in both physioxic and hyperoxic environments. As from the results presented in **Figure 4.18 A,** dSPIONs were unable to induce significant reduction in cellular viability when compared with the negative control (0µg/ml). A slight reduction was identified in the physioxic environment, but this did not reach significance.

The ability of dSPIONs to induce chromosomal damage was investigated using the CBMN assay. After scoring 6000 cells for each of the doses administered to HepG2 cells, no significant induction of genotoxicity was identified in the hyperoxic environment when compared with the negative control (0µg/ml). In contrast, in the physioxic environment, a significant dose-dependent increase in micronuclei were observed over a range of 8-100µg/ml (**Figure 4.18 A**).

NM-102 was investigated in the distinct environments for its ability to reduce cellular viability of HepG2. As is seen in **Figure 4.18 B** a gradual dose dependent reduction in cellular viability was identified in both physioxia and hyperoxia. In both environments, the dose of 50µg/ml of NM-102 induced a significant reduction of cellular viability. Results for the effects of NM-102 on their ability to induce chromosomal damage were also investigated under physioxia and hyperoxia; where in both cases a gradual increase in the induction of MN up to a dose of 10µg/ml was identified. Results in both environments were found to be statistically significant when compared to the negative control only at a dose of 10µg/ml.

The effect of NM-104 on the cellular viability of HepG2 cells was investigated after a 24h treatment. As is seen in **Figure 4.18 C,** doses of 8-50µg/ml were found to significantly reduce viability in both environments. Additionally, NM-104 were investigated for its ability to induce chromosomal damage, but no significant induction of MN was identified in either of the two environments after HepG2 were treated for a period of 24h.

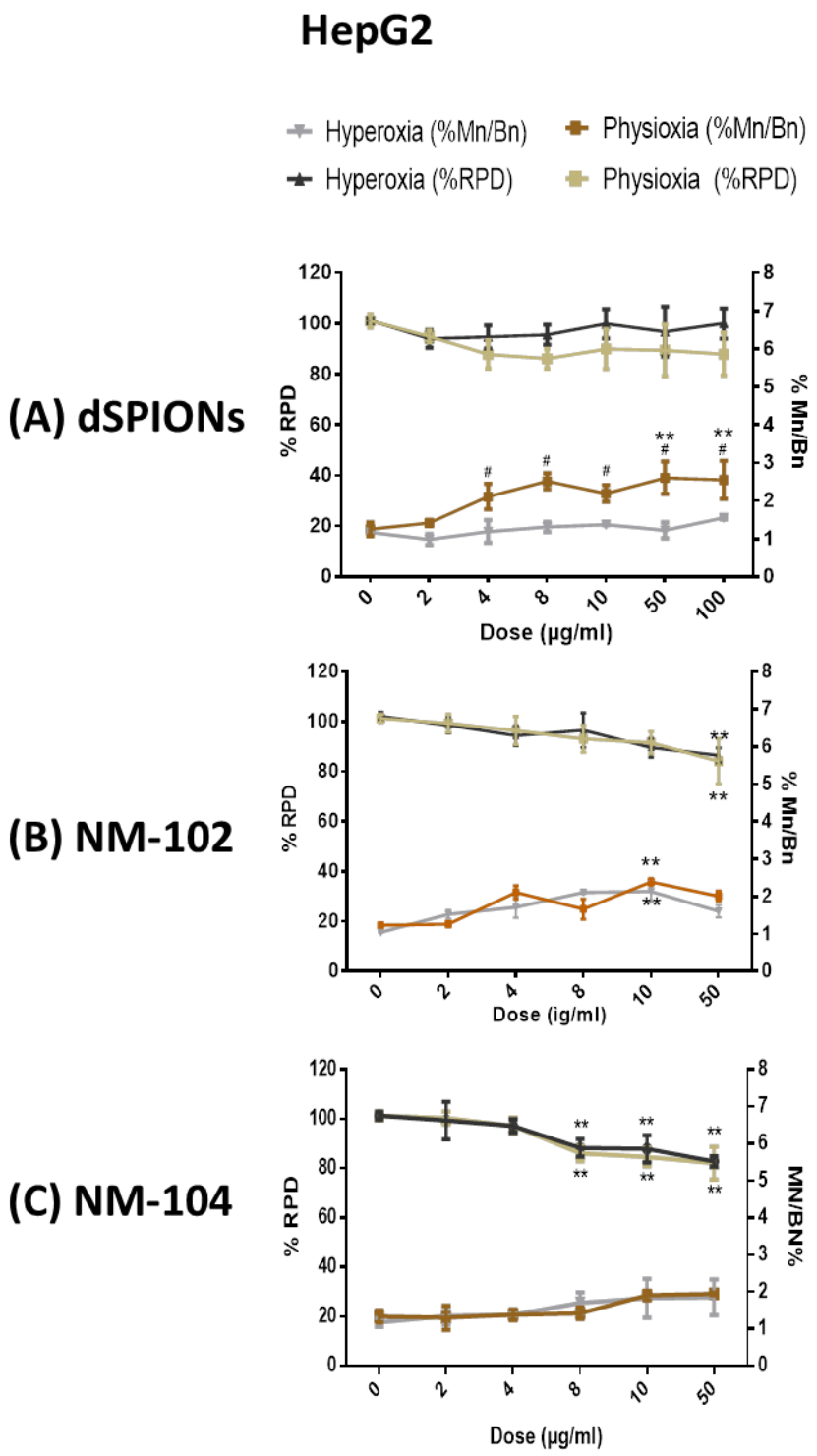

Figure 4.18: Cell viability and Genotoxicity after treatment with MONPs under physioxia and hyperoxia: Effects of MONPs in the cell viability and their ability to induce MN in HepG2 cells. Treatments of the cell lines were carried for 24h with (A) dSPIONs (B) NM-102 (C) NM-104. **Dose compared to 0µg/ml. # Dose compared to the same treatment in different environment. *P≤0.05*

4.3.5 Centromere Staining

The NP doses observed to be significantly genotoxic after the application of the CBMN assay were investigated to determine if the genotoxicity induced were the result of either aneugenic or clastogenic mechanisms. In **Figure 4.19** representative images of the applied centromere stain can be seen. These include a centromere stained binucleated cell without the presence of a MN at **Figure 4.19A**, a clastogenic response with no centromere-signals identified in the MN in **Figure 4.19B** and finally an aneugenic response with multiple centromeric signals in a MN (centromere numbers in the MN varied) in **Figure 4.19C**.

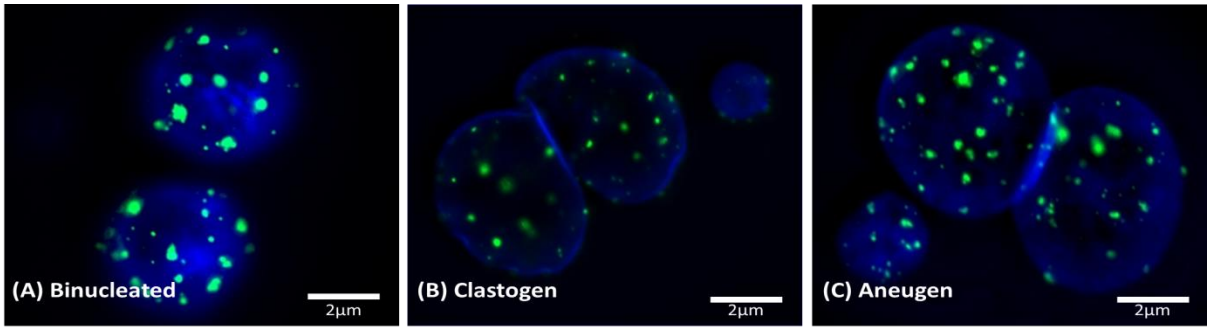

Figure 4.19: Aneugenic and clastogenic MN formation determined after centromere staining of HepG2 cells that were blocked during cytokinesis: (A) Binucleated cell without a micronuclei present cells; (B) Binucleated cell containing no centromeric signal within the micronucleus; (C) Centromere positive cell, indicating the MN was formed by an aneugenic response.

In **Table 4.1** the results for aneugenic clastogenic results are presented. The results include treatments of the NP doses that were found to be significantly genotoxic, untreated cells which acted as a negative control and carbendazim which acted as a positive control for aneugenicity. Statistical comparison of the result obtained for treated cells with the negative control obtained in the equivalent oxygen culture environment were carried out with no significant statistical difference identified. Only NM-102 showed the ability to induce a minor aneugenic response, the response was identified in both oxygen culture environments, was not significant however. In the majority of NM-102 positive results multiple centromeres were observed in the formed MN.

Table 4.1: Aneugenic and clastogenic MN formation determined after centromere staining of HepG2 cells that were blocked during cytokinesis. The average percentages of the number of cells scored (35 cells each replicate, n=3) were classified as centromere positive or centromere negative. Results are presented as a %mean and a %standard error of the mean. (n=3) *Dose compared to 0µg/ml. *P≤0.05*

	Centromere-negative MN (%)		**Centromere-positive MN (%)**	
	Mean % (Cells)	SEM %	Mean %(Cells)	SEM %
(A) Control (-) Hyperoxia	60.95	±3.44	39.05	±3.44
(B) Carbendazim (8uM) Hyperoxia	30.47	±3.43	69.53*	±3.43
(C) NM-102 (10ug/ml) Hyperoxia	57.14	±5.95	42.86	±5.95
(D) Control (-) Physioxia	59.66	±4.95	40.34	±4.66
(E) Carbendazim (8uM) Physioxia	31.42	±1.65	68.58*	±1.65
(F) NM-102 (10ug/ml) Physioxia	56.18	±3.43	43.82	±3.44
(G) dSPIONs 50ug/ml) Physioxia	50.19	±2.06	49.81	±2.06
(H) dSPIONs (100ug/ml) Physioxia	44.76	±5.30	55.24	±5.30

4.3.6 Mitotic Spindle Analyses

After a 24h treatment with the distinct MONPs their ability to disrupt the mitotic spindle was investigated. Staining of the microtubules allowed the identification of changes in the formation of the mitotic spindle following exposure.

As is seen in **Table 4.2** the ability of the previously identified, significantly genotoxic MONPs doses were investigated for their ability to disrupt the mitotic spindle by evaluating 300 mitotic cells. When dSPIONs (100µg/ml) were used to treat HepG2 in physioxia a slight increase in the presence of both monopolar spindle and multipolar spindle were identified, but this did not reach significance.

An increase was identified in the presence of monopolar spindle formation after treatment with NM-102 (10µg/ml) by 3% although it was not a significant elevation when compared with the negative control. Additionally, a slight increase in multipolar spindle was also identified for NM-102 although this too was not significant.

Table 4.2: Analytical results for mitotic Spindle Analysis. The average percentages of the number of cells scored (100 cells each replicate, n=3) were classified as monopolar spindle, bipolar spindle and multipolar and negative results. Results are presented as a %mean and a %standard error of the mean. (n=3) *Dose compared to 0µg/ml. *P≤0.05*

	Monopolar Spindles (%)		**Bipolar Spindles (normal) (%)**		**Multipolar spindles (%)**	
	Mean (%) (Cells)	SEM **(%)**	Mean **(%)** (Cells)	SEM **(%)**	Mean **(%)** (Cells)	SEM **(%)**
(A) 0ug/ml Physioxia	0.33	+/- 0.33	74.66	+/-0.88	25.00	+/-1.15
(B) dSPIONs (100ug/ml) Physioxia	1.000	+/- 0.58	72.33	+/-1.86	26.67	+/-1.45
(C) NM-102 (10ug/ml) Physioxia	3.33	+/- 0.67	66.66	+/-0.33	29.33	+/-0.88

4.4 Discussion

The assessment of NM genotoxicity and cytotoxicity *in vitro* is primarily undertaken in an ambient oxygen culturing environment (Hyperoxia 21% O_2); this has been proven to provide useful data. Although as it has been previously discussed cells cultured in a more physiologically representative environment, with respect to oxygen content have been previously observed to better express the cellular behaviour identified *in vivo* (Costa *et. al...* 2017). Important was the finding that absence or excess of oxygen in the culture of cells may lead to the production of reactive oxygen species (ROS) which in turn leads to the induction of oxidative stress (Jagannathan *et. al...* 2016). These results are of particular interest based on the array of nanotoxicological studies that suggest NP toxicity arises from alteration of the cellular redox state (Shafiri *et. al...* 2011, Anderrson *et. al...* 2011, Singh *et. al.* 2012). Therefore, the purpose of this chapter was to compare the ability of several MONPs to induce genotoxicity and impact on cellular viability in the commonly used hyperoxic culturing environment, as compared to a more physiologically representative (physioxic) oxygen culture environment (5%O_2). This study was applied in different cell lines, two immune cell lines, namely, primary monocyte cell line THP-1 and the macrophage cells dTHP-1 were chosen to represent the reactions of the immune system. The hepatocellular carcinoma cell line was chosen as a representative of the liver where NPs have been previously found to accumulate (Kim *et. al.* 2016.).

4.4.1 Culturing the different cell lines in the different oxygen culture environments

Prior to any investigation of the effects the MONPs have on the different cell lines, the cellular behaviour including cell proliferation, glutathione depletion and production of IL-8 were investigated for both of the immortalized cell lines, namely, HepG2 and THP-1 were characterized under hyperoxia (21%O_2) and physioxia (5%O_2). Investigation of cellular genotoxicity in the different oxygen culture environment was also investigated. The background levels of micronuclei in the two environments was also investigated for HepG2, to determine if the assay could be applied to evaluate genotoxicity under physioxia.

Oxidative stress due to generation of reactive oxygen species (ROS) in cells cultured at higher than physiological oxygen levels is implicated in a multitude of deleterious effects

including DNA damage and genomic instability (Cadet *et. al.*.. 2012). In addition, oxidative stress activates redox sensitive transcription factors related to inflammatory signalling (e.g. IL-8 production) and apoptotic signalling. The mammalian system is naturally equipped to deal with oxidative stress. Antioxidants, including glutathione (GSH), vitamins C and E and antioxidant enzymes such as catalase, superoxide dismutase (SOD) and various peroxidases help to maintain the cellular redox environment (Chakravarthi *et. al.*.. 2018). Evidence suggests that lower availability of antioxidants including Vitamin E, C and selenium in cell culture medium could affect the cell's ability to efficiently scavenge ROS (Leist *et. al.*. 1996). The redox effects of varying oxygen content in the culture environment were therefore investigated by identifying any reduction in the concentration of cellular glutathione levels.

Culturing the immortalized cell line, THP-1, in the different oxygen environments resulted in important changes in cell growth characteristics. Cellular viability was not affected by the oxygen content of the culture environment. Glutathione concentration seems to reduce over time in both of the environments. The observed decrease in GSH seem to be associated with the significantly greater production of IL-8 identified in the hyperoxic environment in THP-1 cells. The observed results with reports in the literature focused on freshly isolated peripheral blood monocytes (PBMCs), where cells isolated in a hyperoxic (21%O_2) environment sent out inflammatory signals that were significantly reduced when the cells were grown at lower oxygen levels (5% and 10% O_2) (Atkuri *et. al.*.. 2005, Atkuri *et. al.*.. 2007).

When comparisons were made in HepG2 cells in the distinct oxygen culture environments, similar results were observed in both cell proliferation and the presence of MN. A slight decrease in the presence of GSH identified in hyperoxia when compared to physioxia and a significantly greater production of IL-8 also identified in the hyperoxic environment. When rat liver sinusoidal endothelial cells (LSECs) were cultured at 5% O_2 and 21% O_2, an improved survival of Liver sinusoidal endothelial cell (LSECs) was identified in 5% O_2 (Martinez *et. al.* 2008). Interestingly in addition, the production of the pro-inflammatory mediator interleukin-6 was reduced, the production of the anti-inflammatory cytokine interleukin-10 was increased and the production of endogenous hydrogen peroxide was decreased (Martinez *et. al.*.. 2008). Under physiological conditions approximately 1–4% of the oxygen

consumed by mitochondria is diverted for the formation of ROS (Wagner *et. al.* 2011). This can be multiplied several fold under *in vitro* culture conditions at 21% O_2. This explains the greater decrease in the presence of the antioxidant GSH, in addition to the effects such as, the reduction in the cellular viability and the increased production of IL-8 in a hyperoxic oxygen culture environment in all the cell lines.

The differentiation of the immortalized monocytic cell line THP-1 to the macrophage-resembling cell line dTHP-1 was investigated in under physioxia and hyperoxia. Through the different incubation periods (24-72h) and oxygen culture environment, the concentration of PMA applied in this experiment was 50nmol. The choice of PMA concentration and the methodology was based on a previous study applied in the hyperoxic (21%O_2) environment (Evans *et. al.* 2017). The study demonstrated the visual physical differentiation of THP-1 cells, but most importantly the ability of an immune response to be induced by dTHP-1 when treated with LPS (Evans *et. al.* 2017). Similar effects on the differentiation of THP-1 cells with PMA were observed in the two distinct oxygen culturing environments. In both environments a 48h incubation with PMA led to the cells full morphological differentiation. After a 72h treatment with PMA, dTHP-1 formed apoptotic blebs in the physioxic environment. In addition, a reduced viability was identified in both environments after a 72h incubation. 48h incubation with 50nmol of PMA was therefore selected as the optimal period for differentiation in both physioxia and hyperoxia. After 48h of incubation with PMA, low concentrations of the antioxidant GSH identified along the greater presence in the concentration of IL-8 in the hyperoxic environment.

4.4.2 NP-Cell Interaction/Uptake and Future work

Cellular interaction and uptake of the distinct NPs was investigated with different techniques. Several techniques have been developed in order to identify the level of NP-cell interaction and the determination of its nature. Certain techniques such as the ferrozine assay and inductively coupled plasma mass spectrometry (ICPMS), allow the determination of changes in the levels of an element that the NPs used for cell treatment consist of (Uboldi *et. al.* 2016). The changes in the concentration of an element correlate with NP-cell interaction. Similarly, flow cytometry allows the identification of changes in NP-cellular interaction by investigating the granularity of the cells after treatment (Zucker *et. al.*2010).

Flow cytometry and the ferrozine assay allow identification of the increase in MONPs interaction with the different cell lines. That being said, these techniques do not allow determination of the nature of the interaction. In order to identify if the different MONPs are internalised by the cells or if they are stuck on the cell membrane TEM imaging was applied. TEM imaging is very high resolution, but low content; it therefore allows determination of sub-cellular localisation of NPs that have been internalised, but it does not support quantification of the internalised materials.

In order to identify the level of interaction of dSPIONs with the different cell lines in the distinct oxygen culture environments the Ferrozine assay was applied. This colorimetric assay provides a sensitive, cheap, and reliable method for the quantitation of intracellular iron and for the investigation of iron accumulation in cultured cells (Riemer *et. al.* 2004). For quantification of the interaction of titanium based polymorphs, namely, anatase (NM-102) and Rutile (NM-104) with human cells, a flow-cytometry based technique was utilized instead. From the results presented in this chapter, the cellular interaction was clearly increased in dose dependent manner in all the cell lines and NPs in both the hyperoxic and physioxic environment. The highest interaction was identified in the macrophage-resembling cell line dTHP-1 and the lowest in HepG2 cells. The difference in uptake capacity between HepG2 and the other cell lines was due to the proficient phagocyte ability present in THP-1 and dTHP-1.

In the TEM experiment THP-1 was chosen as a representative immune cell line. This choice was due to time limits, the expenses for this technique and the small number of dTHP-1 cells obtained after treatment with the NPs and sample preparation for TEM imaging. Instead THP-1 monocytes were chosen as a representative immune cell line for the experiment. No visible interaction was identified after treatments with dSPIONs (of both THP-1 and HepG2 cell lines) in the physioxic environment for the period of 24h. These results contradict the data observed with the Ferrozine assay. This is due to the difference in the ability of the techniques, the ferrozine assay does not discriminate between NPs inside the cells or if is stuck to the outer surface. In the scientific literature, THP-1 cells exposed to dSPIONs under hyperoxic conditions were previously observed to internalize the material by TEM, with dSPIONs agglomerates located within membrane bound vesicles and free within the

cytoplasm (Evans *et. al.* 2017).The results of this study do not correlate with the literature, although it has to be highlighted that results here were obtained in the physioxic culture environment whereas results in literature were obtained in the hyperoxic environment. Obtained results suggest that, when the titanium polymorphs were evaluated by TEM following exposure to THP-1 cells, the NPs were internalised as agglomerates with variable sizes enclosed in membrane bound vesicles. This suggests that a form of endocytosis is the primary pathway for uptake of the titanium dioxide NPs in the immune cell line THP-1.

To conclude, dSPIONs were the only NP that had an increased interaction in the physioxic environment when compared with the results identified in the hyperoxic environment. Previous work done on LSECs would suggest that the observed results are due to the improved scavenger receptor-mediated endocytic activity identified in a physioxic representative environment (Martinez *et. al.*.. 2008). Increased NP-cell interaction in the physioxic environment was only identified with dSPIONs, indicating that the observed results were NP specific. However, it has to be taken into account that the measurements were acquired using different techniques. Flow cytometry based techniques due to their nature allow single cell measurements in contrast to the ferrozine assay, which is a bulk cell measurement with lower sensitivity.

Immune cell lines proficient in phagocytic capacity are able to recognize molecules that do not belong in the surrounding environment, due to the presence of dedicated receptors expressed solely on the surface of proficient phagocyte cells, hepatocellular cells also possess the ability of phagocytosis although they are less proficient (Aderem and Underhill 1999). Based on the size of the NP agglomerates under investigation endocytosis could occur with all the different pathways mentioned in **table 1.1**. Further investigation on the endocytic and phagocytic ability of the different cells should be conducted in future work. The results of interaction and uptake (e.g. flow cytometry and the ferrozine assay and TEM images) suggest that the different cell lines utilize a distinct uptake pathway and at a different extent to interact and internalize the NPs that were under investigation. It also seems that increase in interaction in the physioxic environments might be the result of alterations in the phagocytic ability of the cells. In order to further investigate the uptake pathways utilized for each of the cell lines when treated with the different NPs pathway

inhibitors can be used. Such blockers were previously described in Kuhn *et. al.* 2014, it is suggested that the use of different blockers will allow the determination of the extent the four different endocytic uptake mechanisms, namely, phagocytosis, micropinocytosis, clathrin- and caveolin-mediated endocytosis, are involved in uptake of the different NPs. This will allow a more precise determination why a greater uptake/interaction is identified in the different cell lines and when cells were cultured in the physioxic environments.

4.4.3 Investigation of the toxicological effects in different oxygen culture environments

The identified toxicological effect of the investigated MONPs under hyperoxia and physioxia suggests a close relation with NP-cell interactions. Cellular interaction with dSPIONs identified using the ferrozine assay correlate with the further decrease in cellular viability in all immune cell lines (THP-1, dTHP-1) across the dose range applied in the physioxic environment (5%O_2). This also agrees with the greater increase in MN concentration identified in HepG2 cells with multiple doses being identified as significant in the physioxic environment (21%O_2). A slight trend towards aneugenicity was observed in the results, although spindle analysis suggested that damage to the spindle machinery is unlikely to be associated with the genotoxicity observed. As previously mentioned in **Section 1.5**, substantial evidence in literature suggest that DNA damage as a result of both dSPIONs and Titanium dioxide is the result of endogenous mechanisms such as production of oxidative stress (Shafiri *et. al*... 2011, Anderrson *et. al*... 2011, Singh *et. al.* 2012). Evidence point to change in the cellular redox status in the physioxic environment, which in turn could result in a greater oxidation of bases and generation of DNA strand interruptions from excessive reactive oxygen species (Jagannathan *et. al.* 2016). Further investigation on the mechanism for the induction of genotoxicity of the MONPs under investigation will follow in **Chapter 5.**

As it was previously mentioned in **Section 4.4.2** dSPIONs were observed to have a greater interaction with the different cell lines in the physioxic culture environment. Interestingly this correlates with the greater toxicity identified in all cell lines when cultured in a more physioxic culture environment. In literature the majority of the studies have been conducted in a hyperoxic culture environment, these results would suggest that the scientific field may be underestimating the (geno)toxicity induced by NPs. As mentioned in **Section 1.5.1.2,** numerous studies conducted in the hyperoxic environment have

demonstrated the inability of dSPIONs (dextran-Fe_3O_4) to induce cytotoxic or genotoxic effects although dextran-Fe_2O_3 have been previously demonstrated to induce genotoxicity (Singh *et. al.* 2012). It is of particular interest that dSPION have been demonstrated to degrade forming Fe^{2+}/Fe^{3+}, this effect occurs at a faster rate when exposed to a more acidic environment such of that of an endosome (Singh *et. al.*, 2012). With that information in mind these results arouse curiosity on whether an endocytic pathway was increased in the physioxic environment which in turn allowed the elevated presence of free iron radicals that resulted in the observed toxicity.

The ability of the distinct Titanium dioxide polymorphs to induce cytotoxic and genotoxic behaviours was investigated in both a hyperoxic and physioxic environment. In contrast to dSPIONs, both Titanium dioxide NPs induced an almost identical behaviour in the two environments. No toxicity was identified in the immune cell lines. Although, both Titanium dioxide polymoprhs were able to reduce the cellular viability in HepG2, interestingly only anatase (NM-102) was able to increase the frequency of MN indication after treatment. The results of this study agree with the results of a recent study that observed anatase titanium dioxide caused less severe necrosis and lysosomal membrane permeabilization than rutile titanium dioxide (Li *et. al.* 2017). Anatase Titanium dioxide NPs were previously found to have a greater toxic potency than rutile Titanium dioxide NP, this was due to an increased surface reactivity of anatase Titanium dioxide that results in a greater ability to induce ROS accumulation, which governs their cytotoxic and inflammatory potential (Johnston *et. al.*.. 2009). Observed results of the two polymorphs are not solely associated with their crystalline structure; the results also depend on their distinct size, agglomeration status and solubility.

4.4.4 Summary and Conclusion

This chapter has demonstrated differences between the behaviour of the cells lines (THP-1, dTHP-1 and HepG2) in the different oxygen-content culture environments. Greater production of GSH was identified in the physioxic environment, which correlates with the reduced IL-8 levels identified. Experiments investigating cellular morphology, during the differentiation of monocyte cell line THP-1 to the macrophages resembling cell line dTHP-1 suggest that 48h incubation with 50nmol of PMA was sufficient for the differentiation of THP-1 in both oxygen culture environments.

The ability different MONPs [including, dSPIONs, Anatase Titanium dioxide (NM-102) and Rutile Titanium dioxide (NM-104)] to promote cyto- and genotoxicity with the mentioned cell lines was investigated under physioxia and hyperoxia. All MONPs were found to interact with the cell lines under both oxygen-content culture environments. Only dSPIONs showed a greater cell interaction in the physioxic culturing environment when compared to the hyperoxic culture environment, suggesting NP dependent uptake is altered in the lower-oxygen content environment. The observed NP-cell interaction correlates with the results for cytotoxicity and genotoxicity, where the greater the amount of NP-cell interaction, the higher the identified hazardous effect. Further investigation of the mechanisms underlying the NPs toxicity are however required to more fully understand the differences observed in the physioxic versus hyperoxic culture environments.

Chapter 5: Understanding the underlying toxicological mechanisms of metal oxide NPs.

5.1 Introduction

As has been extensively discussed health hazards associated with human exposure to NPs remains of heightened concern. Primary exposure to NM's is mostly through the skin, gastrointestinal tract and most importantly from the lungs (Papp *et. al.* 2008). Although it is widely accepted that these are the primary exposure sites, distribution of particles via the bloodstream to other tissues is observed as secondary exposure (Eisner *et. al.* 2012). For example, a study recently carried out using different JRC titanium dioxide NP's proved that after oral exposure increased concentrations of titanium were detected in the liver and mesenteric lymph nodes (Geraets *et. al.* 2014).

As it was extensively discussed in **Section 1.3** generation of excessive amount of reactive oxygen species (ROS) is the most frequent pathway NPs have for the induction of toxic actions (Manke *et. al.* 2013). Induction of oxidative stress via excessive ROS levels was reported to lead to oxidative DNA damage and micronucleus formation in response to different metal oxide NP's (Singh *et. al.*2012, Shukla *et. al.* 2011). The ability of different MONPs, namely, TiO_2, ZnO, Fe_3O_4 and Fe_2O_3, CuO, to induce the alteration of cellular redox state and lead to cellular toxicity in different cell lines (HepG2, A549) has been identified in several studies in the past (Li *et. al.* 2008, Singh *et. al.* 2012, Karlsson *et. al.* 2015).

It should be noted that oxidative stress induced by the excessive amounts of ROS that are produced due to the presence of either ambient or engineered NPs, may give rise to the expression of pro-inflammatory responses via the activation of iCa^{2+} signals (Ermak & Davies, 2002). Involvement in iCa^{2+} signalling in the response to MONPs exposure, and the effects increase in ROS levels can have on iCa^{2+} signalling have been extensively discussed in **Section 1.6**. In addition to the known roles of acidic organelles, (such as autophagy and degradation of intracellular molecules) they have been also identified as one of the most important intracellular stores of iCa^{2+}; and by their controlled release and uptake of Ca^{2+} the acidic organelles are crucial for the regulation of numerous cellular functions (Lloyd-Evans *et. al.* 2010). NP treatments may induce membrane and organelle damage, with the membranes of acidic organelles (particularly lysosomes) being particularly sensitive to this (Olsson *et. al.,* 1989). If lysosomal disruption occurs in addition to increase in cytosolic Ca^{2+} a further increase in the levels of ROS is observed (Sabella *et. al.* 2014). Moreover, a study

conducted on three different cell lines [HepG2 (human), RBL-2H3 (rat) and DT40 (chicken)] have proven that superoxide anion causes oxidation of the InsP3Rs, as a result cytoplasmic Ca^{2+} oscillation is produced that enhances mitochondrial uptake (Bangashi *et. al.* 2014).

Thus the induction of oxidative stress and the activation of iCa^{2+} signals by MONPs may lead to expression of pro-inflammatory responses (Ermack and Davies 2002). Therefore, it is possible the MONP induced increases of iCa^{2+} oxidative stress and the production of pro-inflammatory responses may coexist with the cytotoxic and genotoxic effects identified in **Chapter 4**. The scheme presented in **Figure 5.1** summarises all the different parameters that may be the outcome of the exposure to NPs, and also how these effects may interconnect. Importantly, in order to identify and understand the cellular, biochemical & molecular basis by which NP's exert their toxic effects an investigation of all of these end points must be carried out.

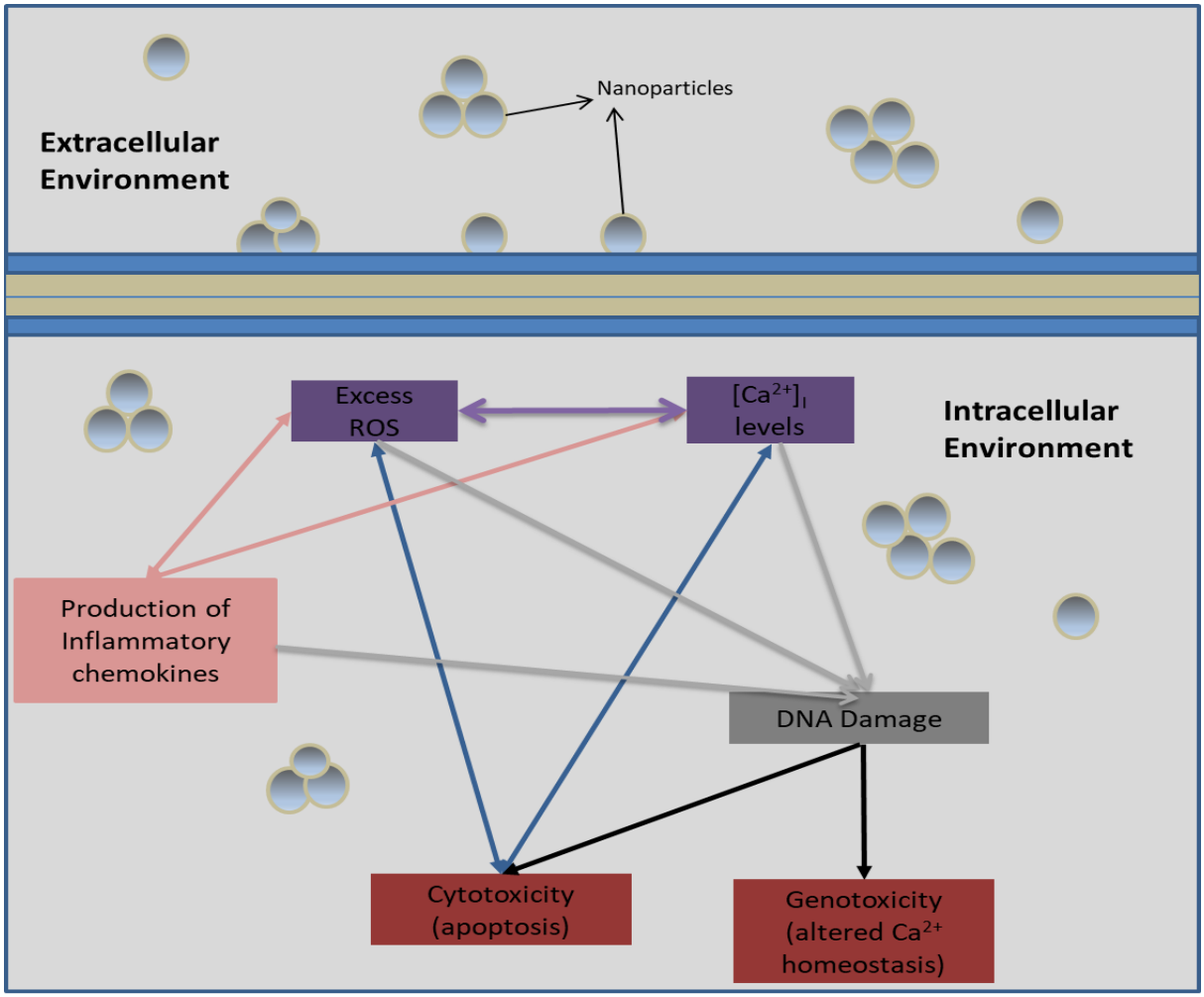

Figure 5.1: Mechanisms resulting in the induction of toxicity by NPs.

5.1.1 Chapter 5 Aim

An investigation of the different MONPs will be carried out in order to evaluate the different cellular responses induced. Although the toxic effects of the various MONPs currently under investigation were previously investigated in **Chapter 4**, the toxicological mechanisms were not. The aim of this chapter is therefore to investigate the different mechanisms that may lead to the previously identified cytotoxicity and genotoxicity. Responses to exposure to the different MONPs that are going to be monitored include among others, the reduction in the presence of cellular antioxidant glutathione (as a marker of oxidative stress), changes in the concentration of iCa^{2+} (as determined using the Ca^{2+}-activated fluophore Fluo-4), and production of inflammatory chemokine IL-8 and cytokine TNF-α (as determined via ELISA). How these mechanisms interact with each other to result in the toxic effects previously identified will be investigated as well the difference in the mechanism in a physiologically resembling oxygen culture environment versus a hyperoxic culture environment.

In order to achieve this, the cell lines were exposed to the MONPs over a dose range of 0-100ug/ml for a period of 0-24h to explore the toxicological mechanism triggered by dSPION and the two TiO_2 polymorphs (NM-102 and NM-104). As it was described in previous chapters the cells selected for this study included the monocytic cell line (THP-1), hepatic cell line (HepG2) and macrophages (dTHP-1) in order to evaluate the biological impact of these particles on both inflammatory and liver cells in a hyperoxic (21% O_2) and physioxic (5% O_2).

5.2 Materials and Methods

Unless stated otherwise all the cell treatments in this chapter were; (a) dSPIONs were used to treat the cell lines in concentrations of 0-100µg/ml. (b) The two different types of titanium dioxide NPs (Titanium dioxide NPs) used for this study [i.e. Anatase (NM-102) and Rutile (NM-104)], they were used to treat the cell lines in concentrations of 0-50µg/ml. The cells were cultured in 25cm^3 flasks at a concentration of 2x105 cells/ml that were incubated for 24h before treatments. Unless stated otherwise all the experiments were conducted in 3 replicates.

5.2.1 Cell culture

The cell lines used for this study were the hepatocellular carcinoma cell line (HepG2) that was purchased from ECACC and the monocyte cell line (THP-1) that was purchased from ATCC. Further information on cell culture of the primary cell lines and the differentiation of THP-1 to the macrophages resembling cell line dTHP-1 can be found in **Section 2.1.**

5.2.2 Physioxia (5%O2) experiments

All experiments were carried out in an InvivO2 physiological cell culture workstation (Baker Ruskin Ltd, UK). Cells were characterised after culture in two different oxygen environments; physioxia (5% O_2, 5% CO_2) and hyperoxia (21% O_2, 5% CO_2). Further information on experiments carried out under physioxia can be found on **Section 2.2.**

5.2.3 Pro-Inflammatory cytokine quantification using an Enzyme-Linked Immunosorbent Assay (ELISA)

Following a 24h treatment of the cells with the mentioned NPs, supernatants were collected and stored in -20C°. Quantification of IL-8 (CXCL8) or TNF-α was carried out using ELISA KITs that were purchased from R&D, UK. More information can be found in **section 2.7.**

5.2.4 Intracellular reduced Glutathione

The Glutathione Detection Assay (fluorometric) (AbCam, UK) was used for the determination of glutathione concentrationας as an indicator of oxidative stress. After a 5h treatment with NPs at the concentrations described at **Section 2.1.2**, $1x10^6$ cells in 1ml for each of the treatments were harvested and washed twice using PBS. More information can be found in **Section 2.8.**

5.2.5. Intracellular Ca^{2+} signalling

Following treatment with the distinct NPs in the different culture oxygen environments for the periods of 0-30min, 5h and 24h with the concentrations described in **Section 2.1.2,** investigations on the effects of iCa^{2+} levels was carried out. All cell lines were seeded in a 96 well assay black plate with clear bottom (Corning incorporated, UK) at a concentration of $2*10^5$ cells/ml. lines (e.g. THP-1 cells). All the measurements were carried at a temperature of 37°C. All physioxic culture measurements were carried at the mentioned environment (5% O_2, 5% CO_2) with the measuring chamber of the plate reader being calibrated to resemble that environment. All measurements were carried out using clariostar Multimode microplate reader (BMG LABTECH Ltd, UK) λ=490nm λ=520nm. Information for the staining the cells with FLUO-4AM (Thermofisher scientific, USA) were described in **Section 2.12.** In some cases measurement of iCa^{2+} were carried out after pre-treatment with the antioxidant Trolox for 24h at a concentration of 25mM. Further information on the procedure can be found in **Section 2.12.** The immediate effects of treatments with the distinct NPs on the iCa^{2+} homeostasis were investigated by injecting MONP suspensions directly onto the cultured cells using the injection system of the clariostar multimode microplate reader. More information on the procedure and the dilutions used for the pumps during treatments can be found in **Section 2.12**.

Investigation of the effect NP treatments had on two different Ca^{2+} storage organells (namely, ER and the lysosomes) was carried out. In order to identify the effects the NP treatment had on the Endoplasmic reticulum Ca^{2+} levels (ER Ca^{2+}) were determined using thapsigargin (100nM) used to stimulate the release of Ca^{2+} from the ER. Further information on thapsigargin pre-treatments can be found in **Section 2.12.**

Determination on the effects 30min treatments with the distinct NPs had on lysosomal Ca^{2+} levels was determined using pre-treatments with NPs, followed by inection of GPN that triggers immediate release of Ca^{2+} from the lysosomes. The cell lines were treated with 50µM GPN for THP-1, 100µM GPN for dTHP-1 and 200µM GPN for HepG2, further information can be found on **Section 2.12**.

5.2.6 Statistical analysis

GraphPad Prism 6 was used for the plotting and the statistical analysis of all the results. Two-way ANOVA and Tukey's multiple comparisons test were used to compare the results in all cell lines between each dose, the untreated controls and the different oxygen environments. All of the statistical analysis of the acquired data we were completed with a $p \leq 0.05$ considered as significant. Further information on the statistical analysis can be found in **Section 2.14.**

5.3 Results

5.3.1 Glutathione depletion

In order to determine the oxidative stress effects exerted by the NPs under investigation, depletion of the levels of the antioxidant glutathione were investigated in the distinct cell lines, namely, HepG2, THP-1 and dTHP-1. Quantification of intracellular glutathione levels was carried out in both a hyperoxic (21% O_2) and a physioxic (5% O_2) environments after treatment of the cells for a period of 5h.

As is seen in **Figure 5.2 (A)** concentrations of glutathione after treatment with dSPIONs (0-100µg/ml) showed a dose dependent decrease in both oxygen culture environments. Glutathione depletion was found to be significant [when compared with the negative control (0µg/ml)] in various doses for THP-1 (8 µg/ml -100µg/ml), dTHP-1 (50 µg/ml & 100µg/ml). In HepG2 8-100µg/ml significant depletion was identified only in the physioxic environment. Interestingly, greater decreases in concentration of glutathione were identified in the physioxic environment (5% O_2) than the hyperoxic environment (21%O_2) after treatment with dSPIONs in THP-1 and HepG2, but the results were found to be significantly different in the different oxygen culture environments only in HepG2 (100µg/ml).

Treatments of the different cell lines with anatase TiO_2 (NM-102) (0-50µg/ml) for periods of 5h were also investigated for the resulting reduction of glutathione. As is seen in **Figure 5.2 (B)** a dose dependent decrease in glutathione was observed in both immune cell lines (THP-1 and dTHP-1). A slight non-significant decrease was identified in the higher doses in HepG2 (**Figure 5.2B2**). After treatment of all the cell lines with rutile TiO_2 (NM-104) (0-50µg/ml) for the period of 5h, the concentration of glutathione was quantified. As is seen in **Figure 5.2 (C)** concentration of glutathione showed a dose dependent decrease in THP-1 and dTHP-1 and a non-significant decrease after treatments in HepG2. As for dSPIONs greater glutathione depletion was identified in the physioxic culture environment than in the hyperoxic environment, with this effect achieving statistical significance at 10-50µg/ml in dTHP-1 cells and at 50µg/ml NM-104 in THP-1 cells (**Figure 5.2B2 and Figure 5.2C1**).

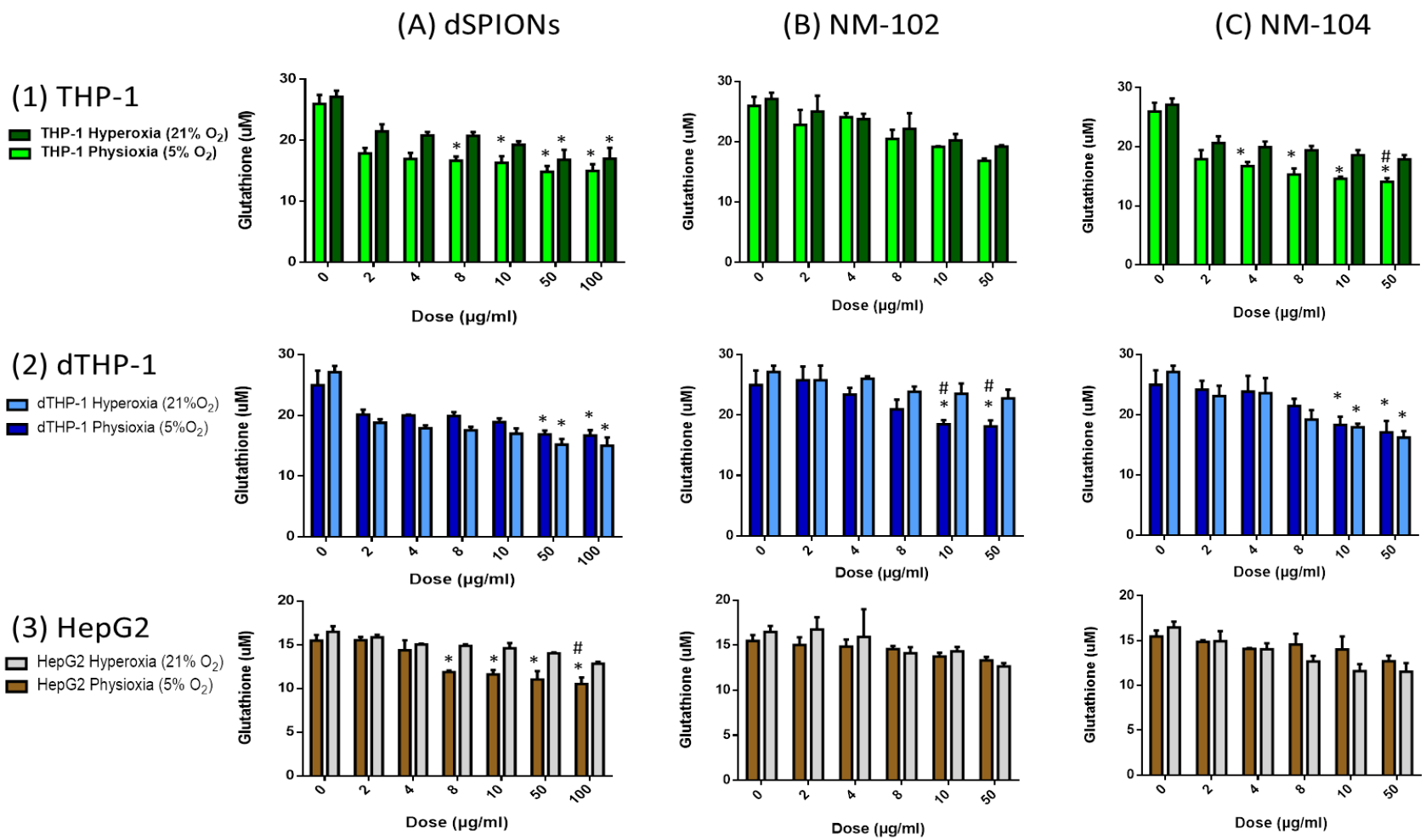

Figure 5.2: Quantification of the reduction In the natural antioxidant glutathione in the distinct cell lines (1) THP-1, (2) dTHP-1 and (3) HepG2 after treatment with the different metal oxide NM, namely, **(A)** dSPIONs, **(B)** NM-102 and **(C)** NM-104 after treatment for the period of 5h. *comparison with 0µg/ml #comparison between environments. *P≤0.05* (n=9).

5.3.2 Quantification of Intracellular Ca^{2+} Concentrations

5.3.2.1 Cytosolic Ca^{2+} immediate response to MONPs treatments

Immediate response to the exposure of the distinct MONPs was investigated in all the cell lines. As is seen in **figure 5.5** in the hyperoxic culture environment (21% O_2) exposures were carried in the full range of the NPs (e.g. for dSPIONs in concentrations of 0-100µg/ml, for NM-102 in concentration of 0-50µg/ml and for NM-104 in concentration of 0-50µg/ml). In the physioxic culture environment (5% O_2) exposures were carried only for 2 concentrations for each of the NPs, for dSPIONs in concentrations of 0, 10, 100µg/ml, for NM-102 or NM-104 in concentration of 0 µg/ml, 10 µg/ml and 50µg/ml (these results are presented in **Appendix 2**).

The results in both of the oxygen culture environments and for all the cell lines and NPs showed a dose dependent elevation of intracellular Ca^{2+} immediately after administration of the NPs (which occurred after 30s of measurements) (**Figure 5.3**). Some variation of intracellular Ca^{2+} elevation (immediately after treatment with MONPs) was identified between the different cell lines and the distinct NPs; also as is seen in **Figure 5.4,** the oxygen culture environments. The elevation intracellular Ca^{2+} was maintained for the period of 5min after treatment in all the experiments.

Comparison of the response in elevation of intracellular Ca^{2+} immediately after treatment with the top doses of each of the NPs, in each of the cell lines and the distinct cell culture environments was carried out and can be seen in **Figure 5.4.** Both the negative control (0µg/ml) and the positive control Ca^{2+} ionophore A23187, produced similar results in both oxygen culture environments in all the cell lines. The top doses of all the NPs were able to induce a significant increase in the concentration of intracellular Ca^{2+} in all the cell lines when the results were compared with the negative control (0µg/ml) in each of the distinct cell lines. In all the NPs and cell lines, greater increase in the elevation of intracellular Ca^{2+} were identified in the physioxic oxygen culture environments (5% O_2) than at hyperoxia (21%O_2); statistical analysis revealed that significantly greater responses were found for at the physioxic environment THP-1 after treatment with dSPIONs and NM-102 for dTHP-1 with dSPIONs and NM-104; and for HepG2 with dSPIONs and NM-102.

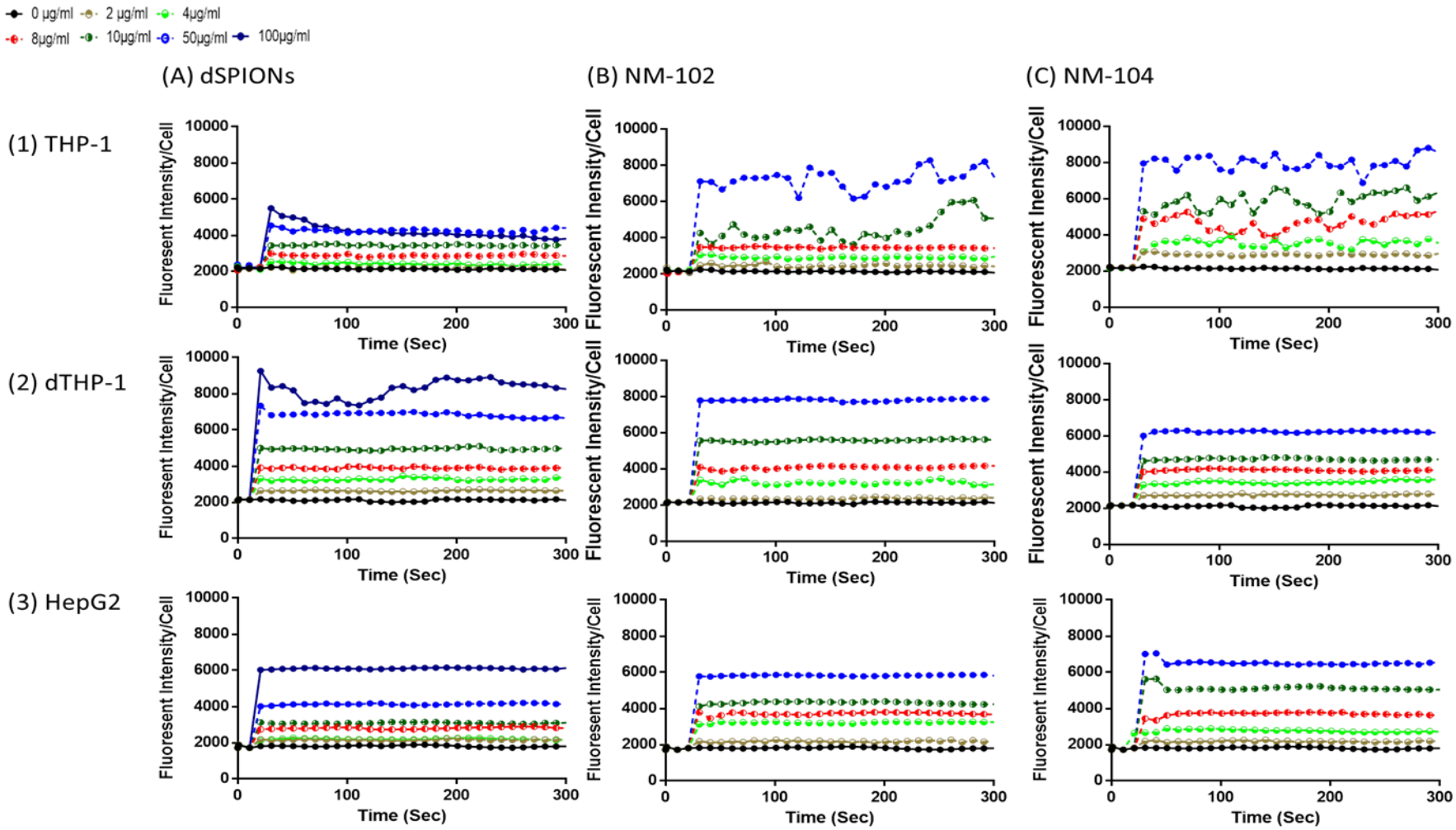

Figure 5.3: Immediate response of intracellular Ca^{2+} concentrations to treatments of the distinct metal oxide NM, namely, (A) dSPIONs, (B) NM-102 and (C) NM-104 in the Hyperoxic environment. Continuous measurements were carried for the period of 300s (5min), woth the NPs being injected after 10s, in the distinct cell lines under investigation, namely, (1) THP-1, (2)dTHP-1 and (3) HepG2. (n=9)

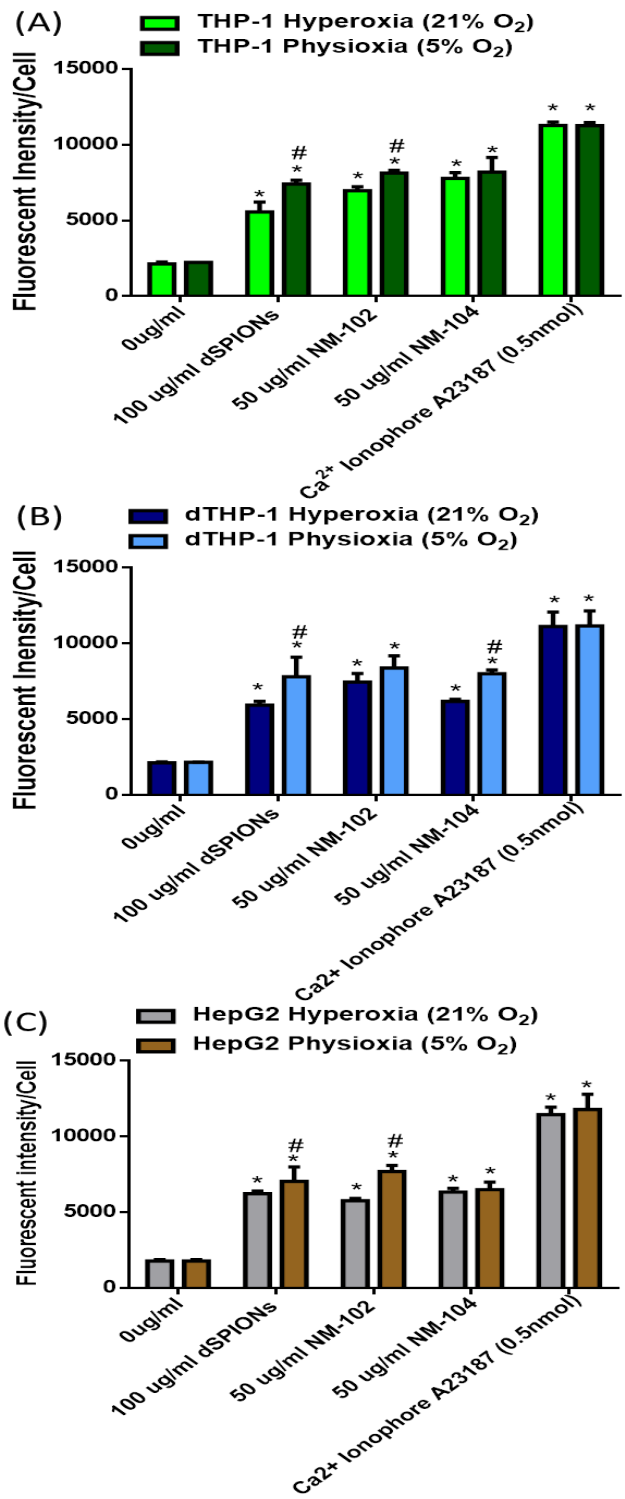

Figure 5.4: Comparison of the immediate response of intracellular Ca^{2+} concentrations in the different cell lines, namely, (A) THP-1, (B) dTHP-1 and (C) HepG2 to treatments (immediately after injection at 10s) with the distinct metal oxide NM (namely, dSPIONs, NM-102 and NM-104) in the different oxygen culture environments. *comparison with 0µg/ml #comparison between environments *P≤0.05* (n=9)

5.3.2.2 Investigating intracellular Ca^{2+} in the distinct organelles after a 30min treatments

5.3.2.2.1 Thapsigargin pre-treatments

As can be seen in **Figure 5.5** the pre-treatment of all the cell lines and oxygen culturing environments with thapsigargin resulted in the depletion of the ER from Ca^{2+}, as the yellow and red braces are consistently higher than the blue and green braces. In contrast, similar results were identified with thapsigargin untreated cells in the two oxygen culture environments. A dose dependent increase in fluorescent intensity was identified in all thapsigargin untreated cells after treatment with dSPIONs for 30min; although this was more visible in the immune cell lines (THP-1 and dTHP-1) (**Figure 5.5 A&B**). Significantly greater increases were identified in the fluorescent intensity (e.g. the concentration of Ca^{2+}) when THP-1 and dTHP-1 cell were treated with dSPIONs after comparison with the negative control (0µg/ml) at concentrations of 50 µg/ml or 100µg/ml.

As seen in **Figure 5.5,** when samples had been treated with thapsigargin, greater fluorescent intensity was observed in physioxia (5% O_2) when compared with hyperoxia (21% O_2) in THP-1 or dTHP-1 (**Figure 5.5 A&B**). Which suggested that more Ca^{2+} is released from the ER by thapsigargin under physioxic conditions.This was observed throughout the dose range of dSPIONs (0 µg/ml -100µg/ml) after treatment for 30min. Significant results were identified when THP-1 and dTHP-1 cells were treated with both thapsigargin and dSPIONs at concentration of 100µg/ml. Significantly greater increase was identified when THP-1 cell were treated with thapsigargin and 100µg/ml of dSPIONs in the physioxic environment in comparison to the increase identified in the hyperoxic environment (**Figure 5.5 A**). Differences between each thapsigargin negative values and the corresponding thapsigargin positive values decrease as the dSPION concentration increases [suggesting that Ca^{2+} released by thapsigargin and the Ca^{2+} released by dSPION is largely from the same source].

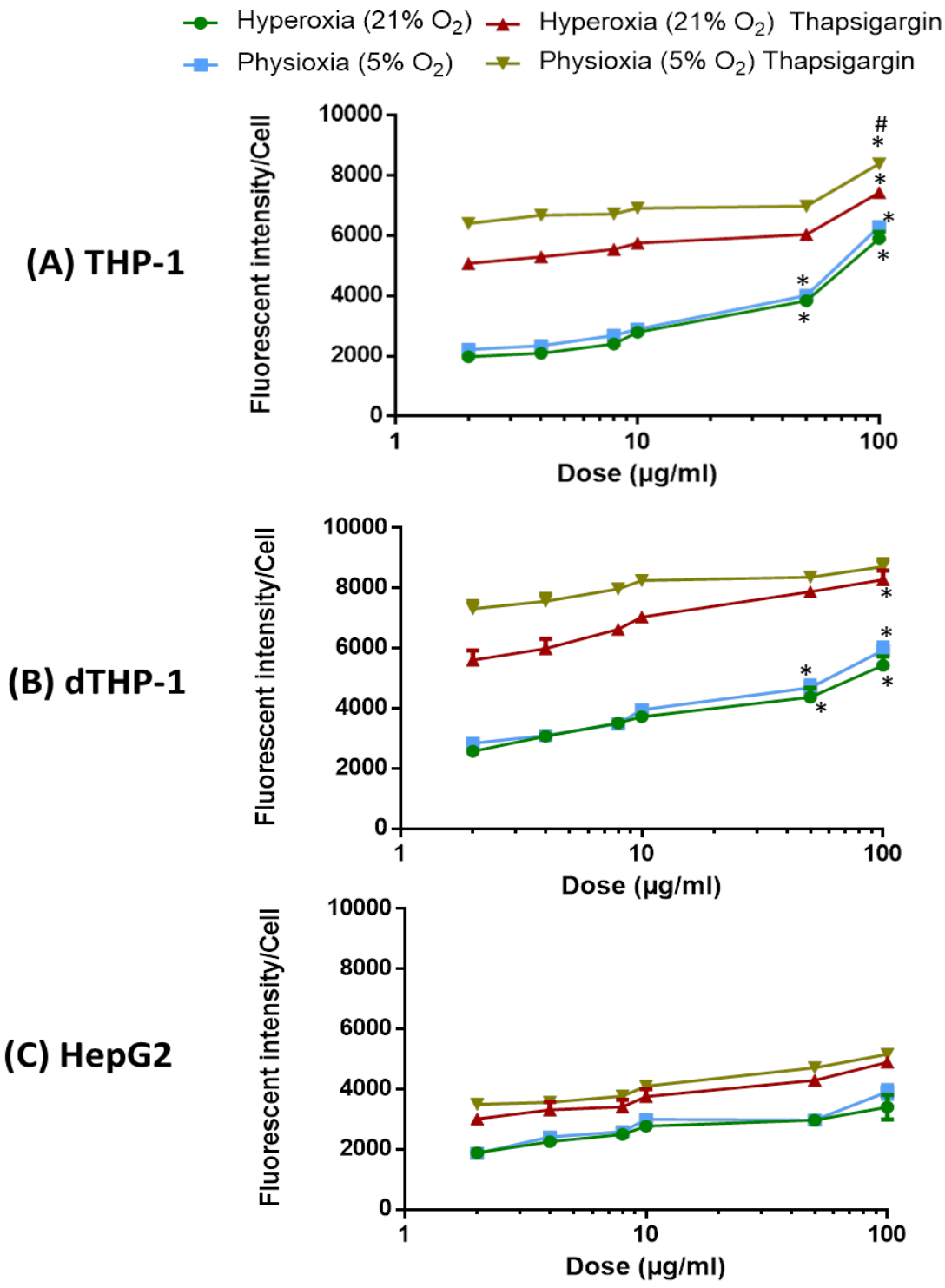

Figure 5.5: 30 min treatments with dSPIONs in the distinct environments with and without Thapsigargin pre-treatment to determine the levels of Ca^{2+} release from the ER. This was performed in the distinct cell lines **(A)** THP-1 **(B)** dTHP-1 and **(C)** HepG2 and the different oxygen culture environments. *comparison with 0µg/ml #comparison between environments *P≤0.05* (n=9).

The effects of NM-102 on the intracellular Ca^{2+} levels after a 30min treatment were investigated. Similar results were identified with thapsigargin untreated cells in both oxygen culture environments in all the cell lines (**Figure 5.6**). In untreated with thapsigargin samples a dose dependent increase in Ca^{2+} dependent fluorescence were identified after treatment with NM-102; but this was only found to be significantly significant in dTHP-1 cells treated with the maximum dose (50µg/ml) in both oxygen environment (**Figure 5.6 B**).

As is seen in **Figure 5.6 A&B** after treatment of the immune cell lines THP-1 and dTHP-1 with thapsigargin greater fluorescent intensity per cell was identified in the physioxic culture environment in both the negative control (0µg/ml) and the after treatment with NM-102 (2-50µg/ml) indicating that either thapsigargin alone or a combination of thapsigargin positive NM-102 elicit release into the cytoplasm. Significantly greater results in fluorescent intensity per cell were identified in dTHP-1 cells in the hyperoxic culture environments when treated with 50µg/ml when compared with the negative control (0µg/ml). Significantly greater increase was identified when dTHP-1 cells were treated with thapsigargin and 50µg/ml of NM-102 in the hyperoxic environment in comparison to the increase identified in the physioxic environment (**Figure 5.6B**).

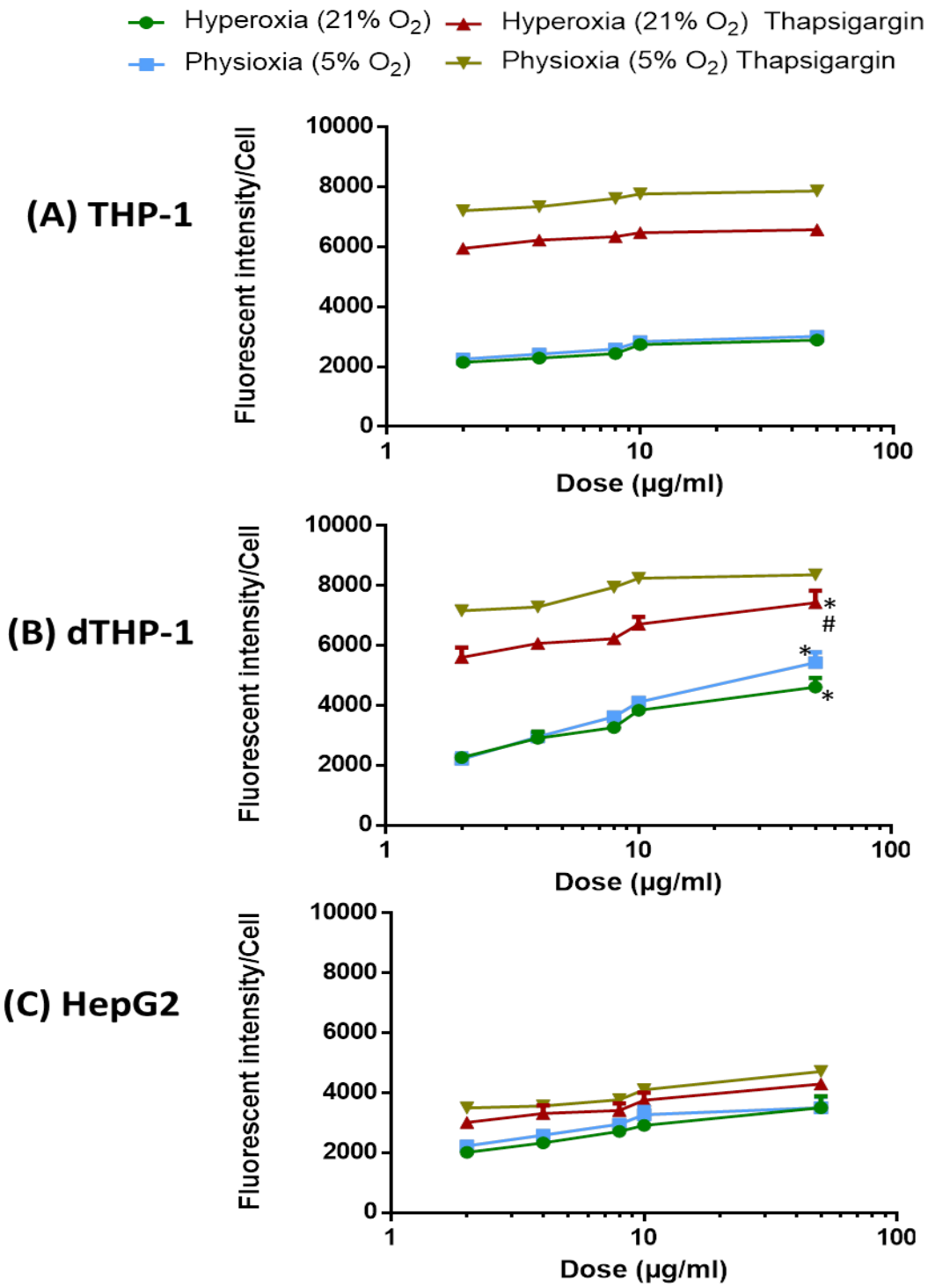

Figure 5.6: 30 min treatments with NM-102 in the distinct environments with and without Thapsigargin pre-treatment to determine the levels of Ca^{2+} release from the ER. This was performed in the distinct cell lines **(A)** THP-1 **(B)** dTHP-1 and **(C)** HepG2 and the different oxygen culture environments. *comparison with 0µg/ml #comparison between environments *P≤0.05* (n=9).

Similar results were identified with thapsigargin untreated cells in the two culture environments in all the cell lines (**Figure 5.7**). A dose dependent increase in fluorescent intensity was visible when all the cell lines were treated with NM-104 for 30min without thapsigargin pre-treatments. Significant results were identified in the fluorescent intensity when THP-1 and dTHP-1 cell were treated with NM-104 after comparison with the negative control (0µg/ml) at concentrations of 10 µg/ml &50µg/ml (**Figure 5.7 A&B**).

Significantly higher fluorescent intensity values were observed in physioxia (5% O_2) when compared to hyperoxia throughout the dose range of NM-104 (0 µg/ml -50µg/ml) when the cells were pre-treated with thapsigargin. In contrast no significant increases were identified in thapsigargin pre-treated samples in either of the environments after NM-104 treatments.

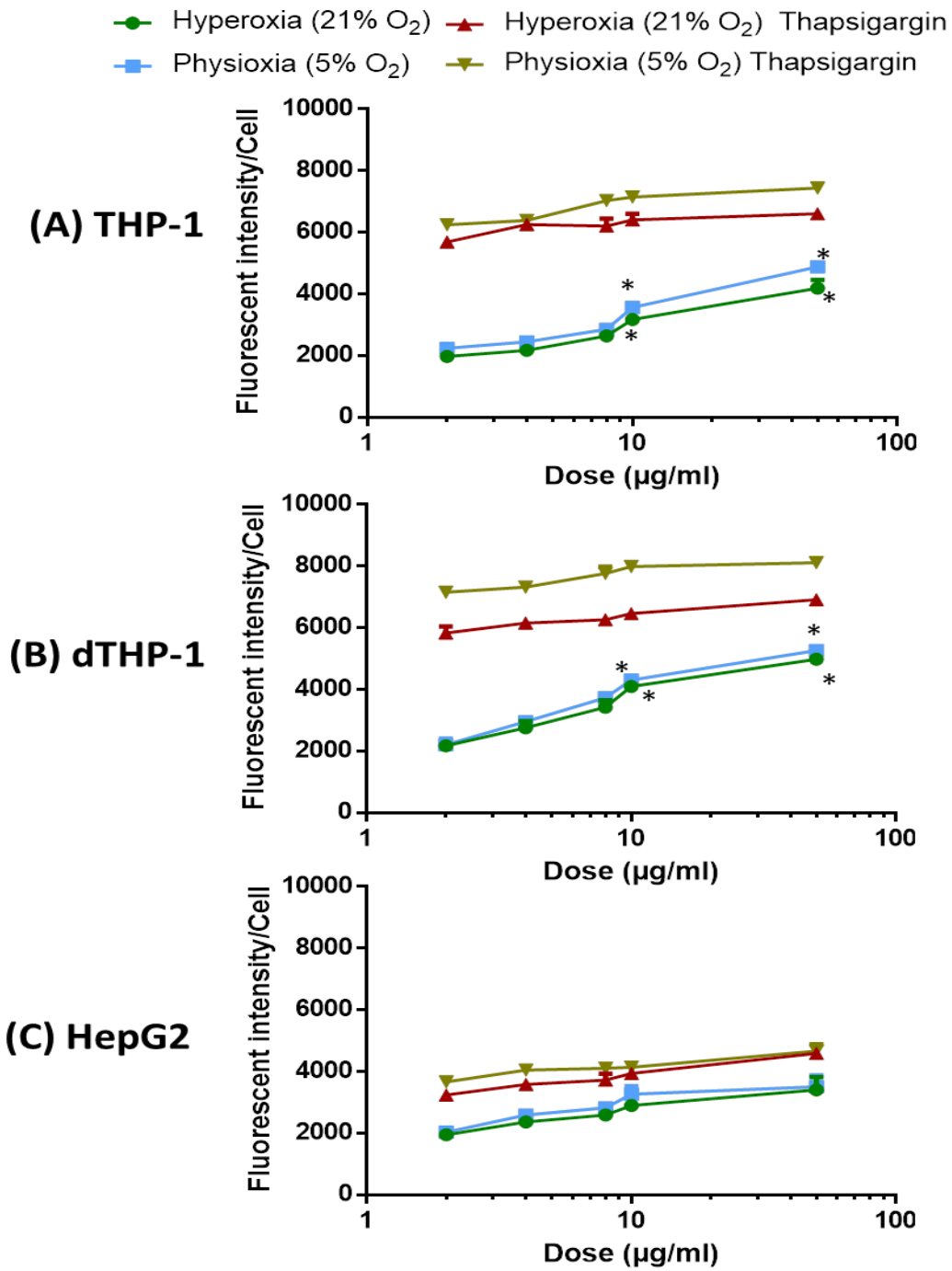

Figure 5.7: 30 min treatments with NM-104 in the distinct environments with and without Thapsigargin pre-treatment to determine the levels of Ca^{2+} release from the ER. This was performed in the distinct cell lines **(A)** THP-1 **(B)** dTHP-1 and **(C)** HepG2 and the different oxygen culture environments. *comparison with 0µg/ml #comparison between environments *P≤0.05* (n=9).

5.3.2.2.2 Intracellular Ca^{2+} responses to GPN/ MONPs treatment

After pre-treatment of the distinct cell lines, (namely, THP-1, dTHP-1 and HepG2) with the distinct MONPs for the period of 30min, GPN was administered as an injection at the time point of 20sec in each case. As is seen in **Figure 5.8**, initial measurements (0-20seconds) for each cell line indicated that each of the doses of the MONPs under study had a distinct baseline fluorescent intensity/cell. The fluorescent intensity measurements in that period resemble the results previously observed in **Figures 5.5-5.7**. **[**As is seen in **Figure 5.8** in the hyperoxic culture environment (21% O_2) exposures were carried in the full range of the NPs, for dSPIONs in concentrations of 0 µg/ml -100µg/ml, for NM-102 in concentration of 0 µg/ml -50µg/ml and for NM-104 in concentration of 0 µg/ml -50µg/ml. In the physioxic culture environment (5% O_2) exposures were carried only for 2 concentrations for each of the NPs, for dSPIONs in concentrations of 0 µg/ml, 10 µg/ml, 100µg/ml, for NM-102 in concentration of 0 µg/ml, 10 µg/ml and 50µg/ml and for NM-104 in concentration of 0 µg/ml, 10 µg/ml and 50µg/ml **(**the results are presented in **Appendix 2).**

After administration of GPN (50µM for THP-1, 100µM for dTHP-1 and 200µM GPN for HepG2) at 20 seconds the fluorescent intensity was increased, indicate that increases in cytosolic Ca^{2+} were identified in all cell lines and NPs. The results in both of the oxygen culture environments, all the cell lines and NPs showed elevation of cytosolic Ca^{2+} immediately after administration of GPN after 20s of measurements in a broadly similar manner (**Figure 5.8**). However variation of cytosolic Ca^{2+} elevation was identified between the cell lines and the distinct NPs but not between the different oxygen culture environments (**Figure 5.9**). The elevation intracellular Ca^{2+} was maintained for the period of 80 seconds after treatment in all the carried exposures.

Comparison of the response in elevation of intracellular Ca^{2+} immediately after treatment with GPN was carried out and can be seen in **Figure 5.9**. The difference of the elevation before treatment at 10s and after the administration of GPN at 20s, at both the top doses of each of the NPs and the negative control (0µg/ml), in each of the cell lines and the distinct cell culture environments was plotted and statistical comparison was carried out and can be seen in **Figure 5.9**. Both the negative control (0µg/ml) and positive control (0µg/ml + GPN) produced similar results in both oxygen culture environments and in all the

cell lines. The top doses of all the MONPs were able to induce a significant increase in the concentration of intracellular Ca^{2+} in immune cell lines, THP-1 and dTHP-1, when the results were compared with the negative control (0µg/ml) in each of the distinct cell lines. The positive control in all the cell lines had a lesser increase than the results observed after treatment with the NPs and GPN. Significantly greater than the positive control were found the results of THP-1 and dTHP-1 in all the environments. In dTHP-1, greater increase in the elevation of intracellular Ca^{2+} was identified in the physioxic oxygen culture environments (5% O_2) after treatment with dSPIONs (100µg/ml) and NM-104 (50µg/ml) in dTHP-1 (**Figure 5.9**).

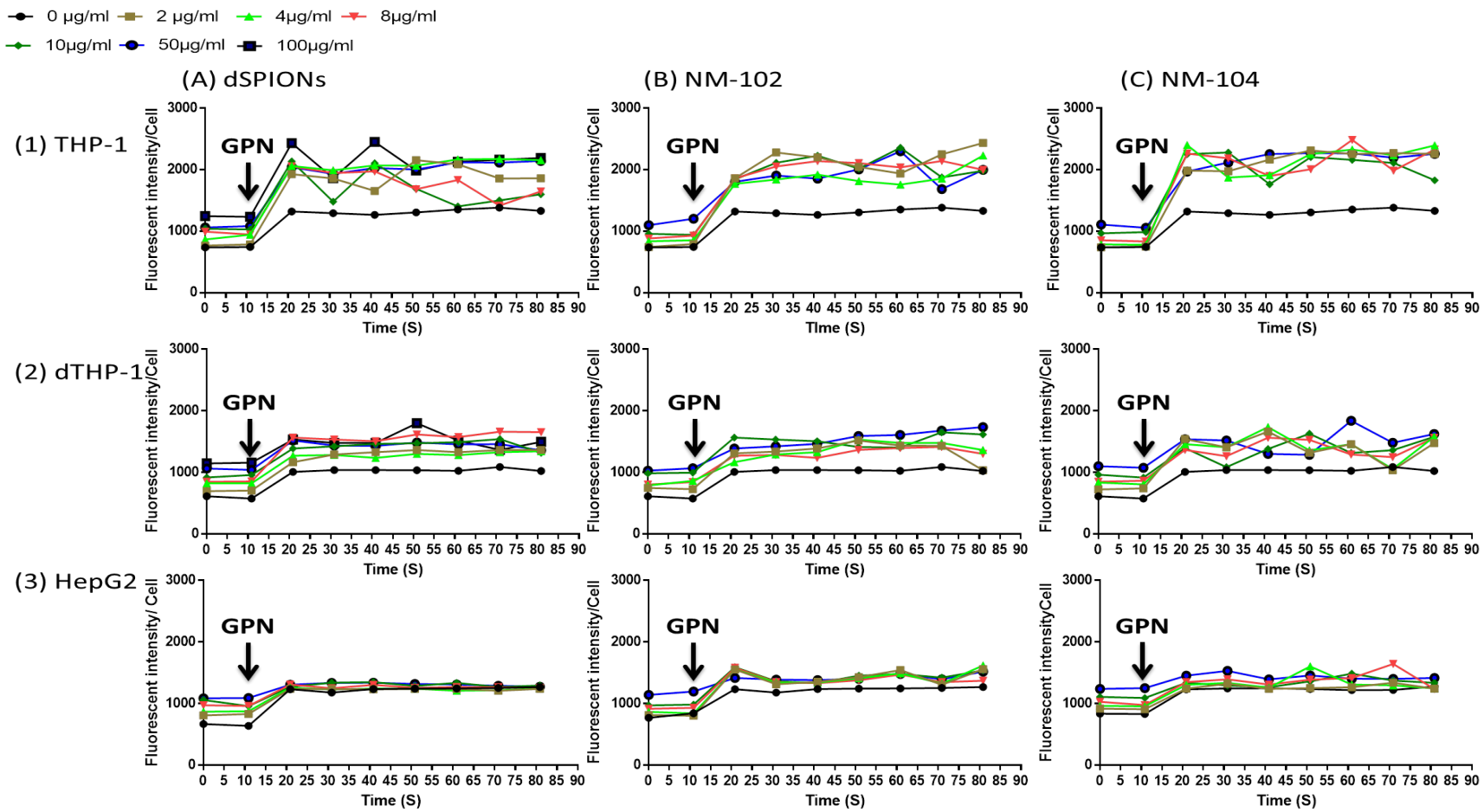

Figure 5.8: Continuous measurements of intracellular Ca^{2+} concentrations after treatments of the distinct metal oxide NM, namely, (A) dSPIONs, (B) NM-102 and (C) NM-104 and administration of GPN (at 20seconds) in the Hyperoxic environment. The continues measurements were carried for the period of 80s in the distinct cell lines under investigation, namely, **(1)** THP-1, **(2)** dTHP-1 and **(3)** HepG2. The black arrow at 10s shows the time GPN was administered to the cells. (n=9).

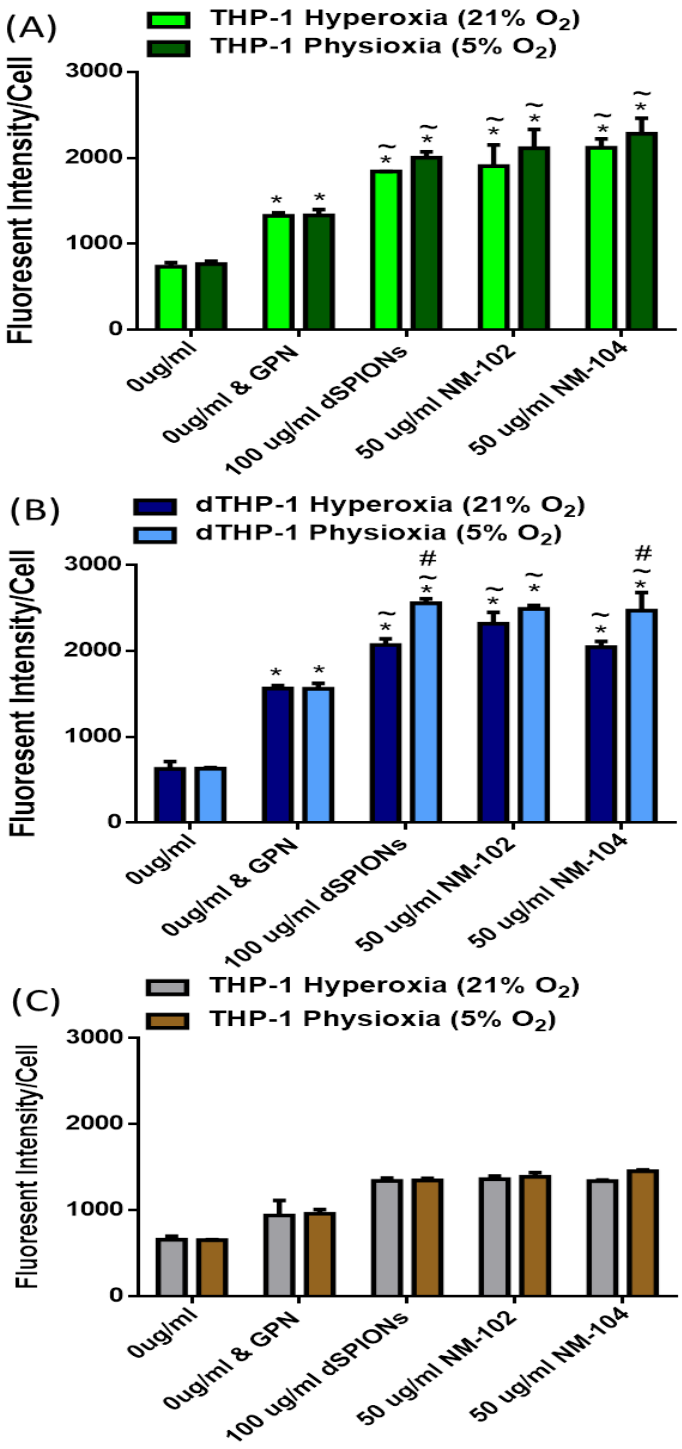

Figure 5.9: Comparison of measurements of intracellular Ca^{2+} concentrations after treatments of the different cell lines, namely, (A) THP-1, (B) dTHP-1 and (C) HepG2 to treatments with the distinct metal oxide NM (namely, dSPIONs, NM-102 and NM-104) and the administration of GPN. *comparison with 0µg/ml #comparison between environments ~comparison with the positive control 0µg/ml+GPN P≤0.05 (n=9)

5.3.2.3 Cytosolic Ca^{2+} levels after 5h treatments and Antioxidant (Trolox) pre-treatments

After 5h treatment in both oxygen culture environments with the higher doses of the NM under investigation, (namely, dSPIONs 100µg/ml, NM-102 50µg/ml and NM-104 50µg/ml) their ability to induce elevation in the concentration of Ca^{2+} in the cytosol was investigated. Given the reports in the literature regarding interactions between oxidative stress and Ca^{2+} signalling (**Section 1.5.1**), investigation was also carried when the cells were pre-treated with the antioxidant trolox (25mM).

As is seen in **Figure 5.10** baseline cytoplasmic Ca^{2+} concentrations showed no differences when THP-1 cells were pre-treated with trolox (0 µg/ml +trolox) when compared with the negative control. Similarly, no differences between the fluorescent intensity were identified in untreated THP-1 cells (negative control) in the different oxygen culture environments. As is seen in **Figure 5.10** concentrations underwent statistically significant elevations in a similar manner in the distinct oxygen culture environments after treatment of THP-1 cells with all the NP; statistically significant increases were also identified in fluorescence when the cells were treated with trolox prior to NP treatments. A visibly higher increase in fluorescent intensity after treatment with the NP was identified when the cells were not pre-treated with trolox, but the difference was found to be statistically significant when compared with the negative control but no significance when cells were pre-treated with trolox.

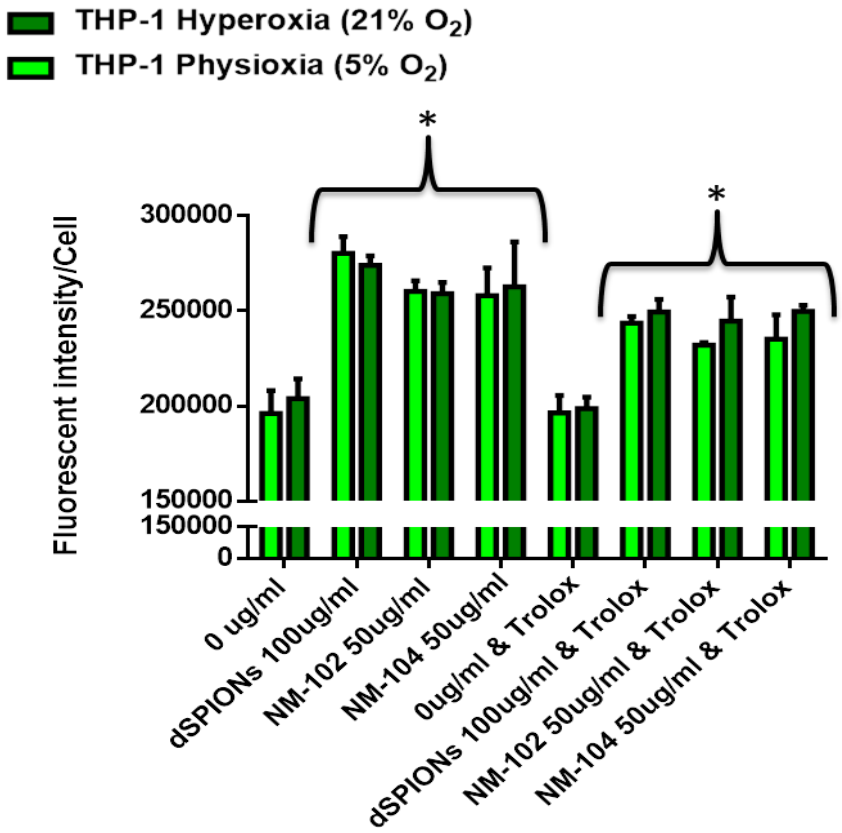

Figure 5.10: Elevation in cytosolic Ca^{2+} in THP-1 cells after pre-treatment with Trolox and then treatment with MONPs (dSPIONs 100µg/ml, NM-102 50µg/ml and NM-104 50µg/ml) in both hyperoxia (21% O_2) and physioxia (5% O_2). *comparison with negative controls (e.g. 0µg/ml and 0µg/ml +trolox) $P \leq 0.05$ (n=9)

As is seen in **Figure 5.11** Ca^{2+} concentrations were elevated in a similar significant manner in the distinct oxygen culture environments after treatment of dTHP-1 cells with the distinct NPs for 5h. In the different oxygen culture environments untreated dTHP-1 cells (negative control) didn't show difference in fluorescent intensity. The results for all NP treatments of trolox pre-treated cells 5h were found significant when compared with the negative control (0µg/ml+trolox). NP-induced increases were also identified in fluorescence when the cells were treated with trolox prior to NP treatments it was not found significant. A visibly higher increase in fluorescent intensity after treatment with the NP was identified when the cells were not treated with trolox compared to the cells treated with trolox although it was not found significant.

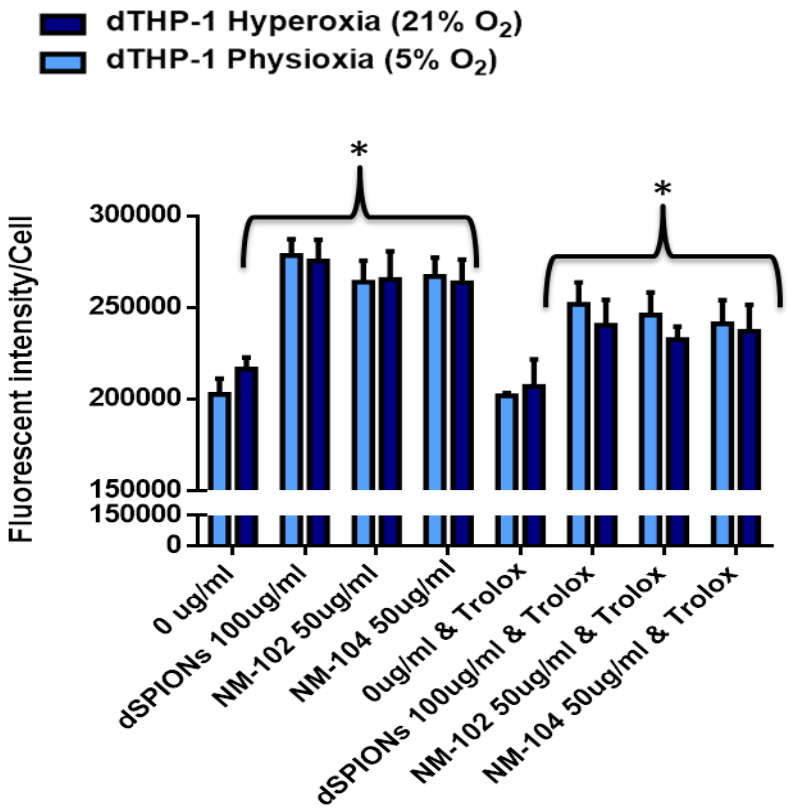

Figure 5.11: Elevation in cytosolic Ca^{2+} in dTHP-1 cells after pre-treatment with Trolox and then treatment with MONPs (dSPIONs 100µg/ml, NM-102 50µg/ml and NM-104 50µg/ml) in both hyperoxia (21% O_2) and physioxia (5% O_2). *comparison with negative controls (e.g. 0µg/ml and 0µg/ml +trolox) $P \leq 0.05$ (n=9)

In the different oxygen culture environments untreated HepG2 cells (negative control) did not show difference in fluorescent intensity (**Figure 5.12**). No differences were identified when the cells were pre-treated with trolox (0 µg/ml +trolox) when compared with the negative control. After treatment of HepG2 with the varied NPs for a period of 5h, fluorescent intensity that correlates to Ca^{2+} concentration was significantly elevated in both oxygen culture environments when compared with the negative control. The increase in fluorescent intensity after treatment with the NPs when the cells were treated with trolox had significant differences when compared with the observed results in the negative control+trolox.

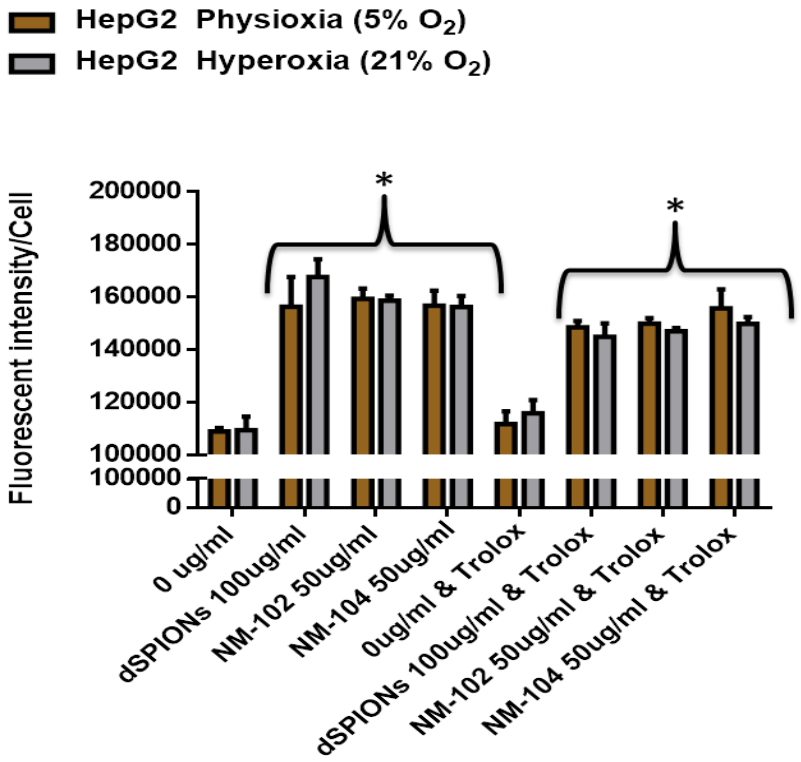

Figure 5.12: Elevation in cytosolic Ca^{2+} in THP-1 cells after pre-treatment with Trolox and then treatment with MONPs (dSPIONs 100µg/ml, NM-102 50µg/ml and NM-104 50µg/ml) in both hyperoxia (21% O_2) and physioxia (5% O_2). *comparison with negative controls (e.g. 0µg/ml and 0µg/ml +trolox) P≤0.05 (n=9)

5.3.2.4 Cytosolic Ca^{2+} levels after 24h treatments

The concentrations of cytosolic Ca^{2+} were investigated after treatment of the distinct cell lines with the various metal oxide NPs for the period of 24h. For this segment of the study higher concentrations were used only, namely, dSPIONs 100µg/ml, NM-102 50µg/ml and NM-104 50µg/ml. As is visible in the three graphs presented in **Figure 5.13** none of the NPs induced any elevation of intracellular Ca^{2+} (compared to negative control-untreated cells) in either of the oxygen culture environments. In addition, pre-treatment with trolox did not result in any significant changes compared to the responses of the non-pre-treated samples.

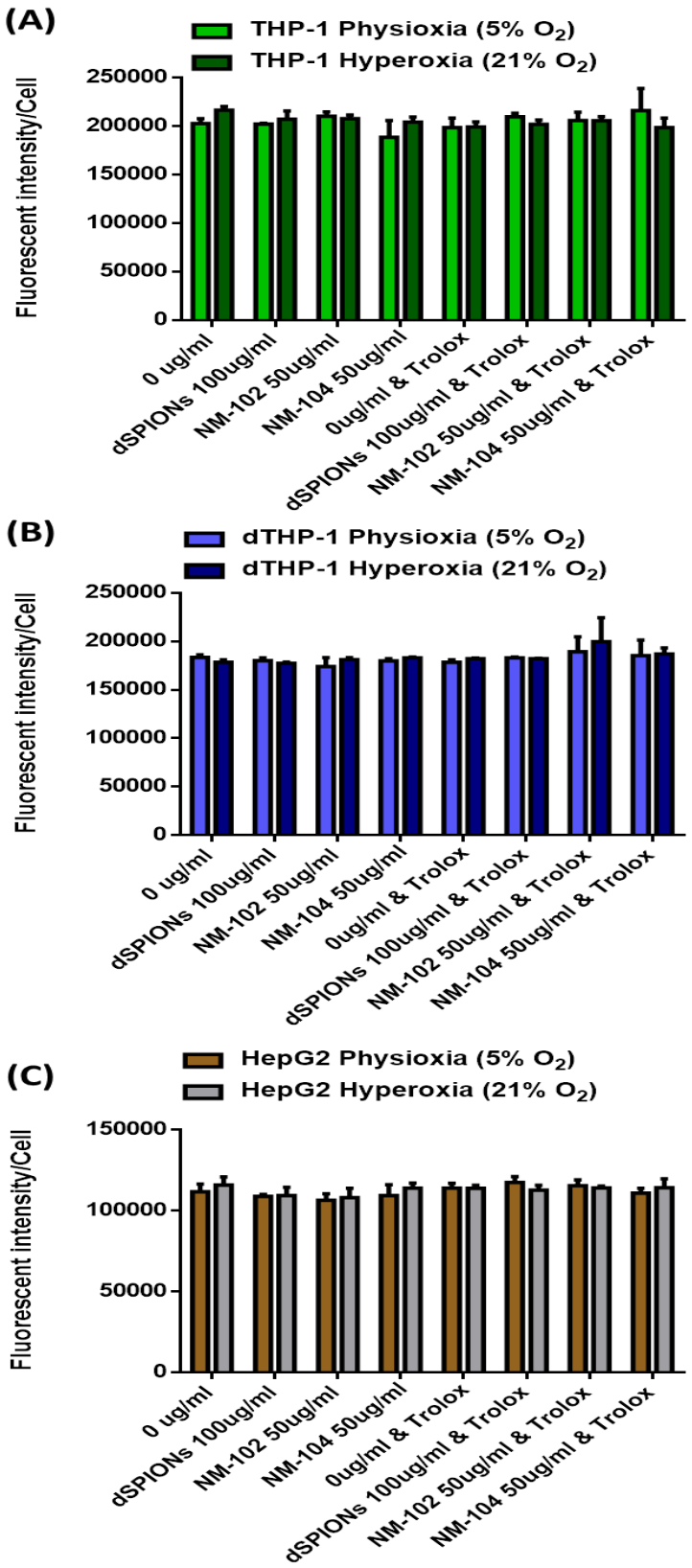

Figure 5.13: Ca^{2+} concentrations in the cytosol after treatment with MONPs for 24h in either the physioxic (5%O_2) or the hyperoxic environment (21% O_2) for (A) THP-1 (B) dTHP-1 and (C) HepG2 in the presence or absence of pre-treatment with trolox. (n=9)

5.3.3 Inflammatory cytokine quantification using an Enzyme-Linked Immunosorbent Assay (ELISA)

The effects the NM under investigation had on the production of IL-8 and TNF-α in the distinct cell lines, namely, HepG2, THP-1 and dTHP-1 were investigated with ELISA. Quantification of IL-8 and TNF-α was undertaken after treatment was carried out in both a hyperoxic (21% O_2) and a physioxic (5% O_2) environments.

5.3.3.1 Quantification of TNF-α

After treatment of all the cell lines with dSPIONs (0-100µg/ml) for 24h the concentration of TNF-α secreted in the medium was quantified using ELISA. As is seen in **Figure 5.14 (A)** concentration of TNF-α showed a dose dependent increase in all the cell lines and oxygen environments. Significant doses when compared to the negative control were identified in dTHP-1 and HepG2 in concentrations over 4µg/ml, in dTHP-1 significant were only the two top doses (50&100µg/ml). The concentration of TNF-α in the physioxic (5%O_2) environment had a significantly higher increase that in the hyperoxic (21%O_2) environment in all cell lines. Significant differences between the effects observed when the same concentrations of dSPIONS were administered in the distinct oxygen culturing environments were identified in THP-1 at concentrations of 8-100µg/ml, in dTHP-1 in concentrations 50 & 100µg/ml and in HepG2 in concentrations 8-100µg/ml.

Treatments of the distinct cell lines with anatase TiO_2 (NM-102) (0-50µg/ml) for the period of 24h were also investigated for the resulting production of TNF-α. As shown in **Figure 5.14 (B)** high concentration of NM-102 treatments resulted in significant dose dependent TNF-α increase in all the cell lines and environments (e.g. When the effect exerted for each dose was compared with the negative control (0 µg/ml significant results were identified in all the cell lines), in THP-1 when treated at concentrations of 4-50 µg/ml, in dTHP-1 when treated with 10 µg/ml and in HepG2 when treated with 10-50 µg/ml. In contrast to the dSPION data, similar results for NM-102 were observed in both environments in all the cell lines.

Finally, after treatment of all the cell lines with rutile TiO_2 (NM-104) (0-50µg/ml) for the period of 24h, the concentration in the production of TNF-α in the medium was quantified using ELISA. As is seen in **Figure 5.14 (C)** secreted concentration of TNF-α showed significant dose dependent increase in THP-1 (8-50µg/ml) and in dTHP-1 at 10&50 µg/ml (**Figure 5.14**). For NM-104 no differences were identified in TNF-α secretion between the distinct oxygen culturing environments for any of the cell lines and doses.

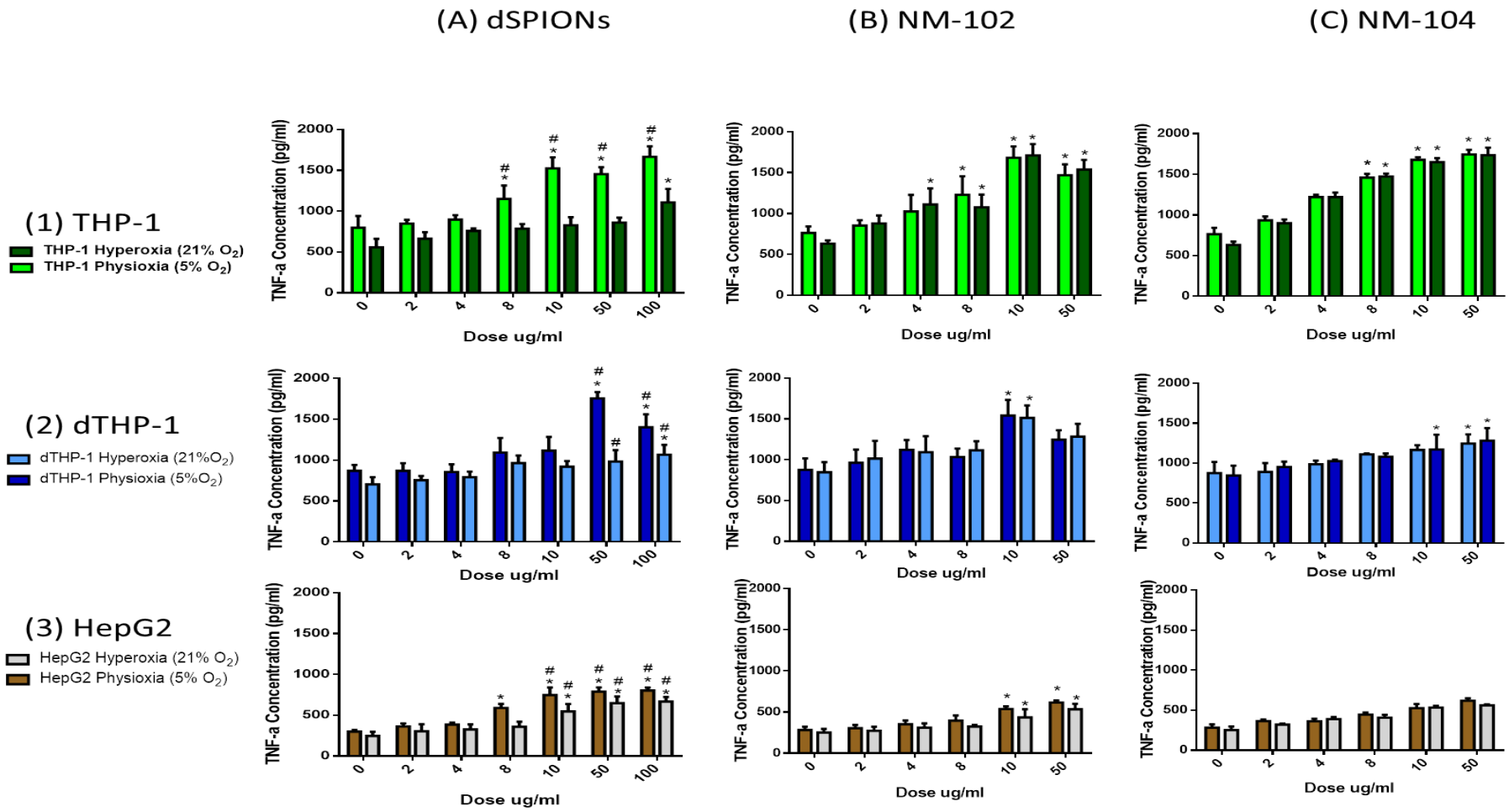

Figure 5.14: Quantification TNF-α production after treatment with MONPs [(A) dSPIONs (B) NM-102 (C) NM-104] in all the cell lines, namely, (1) THP-1, (2) dTHP-1 and (3) HepG2. ELISA experiments were completed in either hyperoxia (21%O_2) or Physioxia (5% O_2). *comparison with 0µg/ml #comparison between environments (n=3) P≤0.05

5.3.3.2 Quantification of IL-8

After treatment of all the cell lines with dSPIONs (0-100µg/ml) for the period of 24h the concentration of secteted IL-8 in the medium was quantified using ELISA. Data presented in **Figure 5.15(A)** indicate that there is a significant dose dependent increase in IL-8 secretion by all cell types following culture with dSPIONs in both hyperoxia and physioxia. Significant increases when compared to the negative control were identified in all cell lines at all concentrations over 4µg/ml. The concentration of IL-8 in the physioxic (5%O_2) environment underwent a significantly greater increases than were seen in the hyperoxic culture environment (21%O_2) in multiple cases. Specifically, significant differences between the effects was seen when the same dSPION concentrations were administered in the distinct oxygen culturing environments were identified in dTHP-1 at concentrations of 8 µg/ml and 10µg/ml, and in HepG2 in concentrations 8 µg/ml -50µg/ml. Although trends of larger magnitude responses were seen in THP-1 samples, these effects did not achieve statistical significance.

Treatments of the distinct cell lines with anatase TiO_2 (NM-102) (0 µg/ml -50µg/ml) for the period of 24h were investigated for the resulting production of IL-8. As is seen in **Figure 5.15 (B)** concentrations of IL-8 treatments underwent dose dependent increases in all the cell lines and environments. When the exerted effect for each dose was compared with the negative control (0 µg/ml) significant results were identified in all the cell lines in concentration over 8 µg/ml. With dTHP-1, when treated with 4 µg/ml NM-102 in the hyperoxic environment significant increases in Il-8 when compared with the negative control (0 µg/ml) were observed. Similar results were observed in both environments in the immune cell lines, THP-1 and dTHP-1, but increase in IL-8 in the physioxic environment was of larger magnitude than the corresponding increases at hyperoxia was observed when HepG2 were treated with NM-102 (8µg/ml).

After treatment of all the cell lines with rutile TiO_2 (NM-104) (0-50µg/ml) for 24h, the concentration of IL-8 secretion in the medium was quantified using ELISA. As is seen in **Figure 5.15 (C)** concentration of IL-8 showed a significant dose dependent increase in dTHP-1. The dose dependent increase was much greater in dTHP-1 with significant increase above control levels being identified in several concentrations over 4µg/ml and both oxygen culturing environments (**Figure 5.15 3A**). In contrast, no significant differences were identified between the effects by NM-104 in the distinct oxygen culture environments.

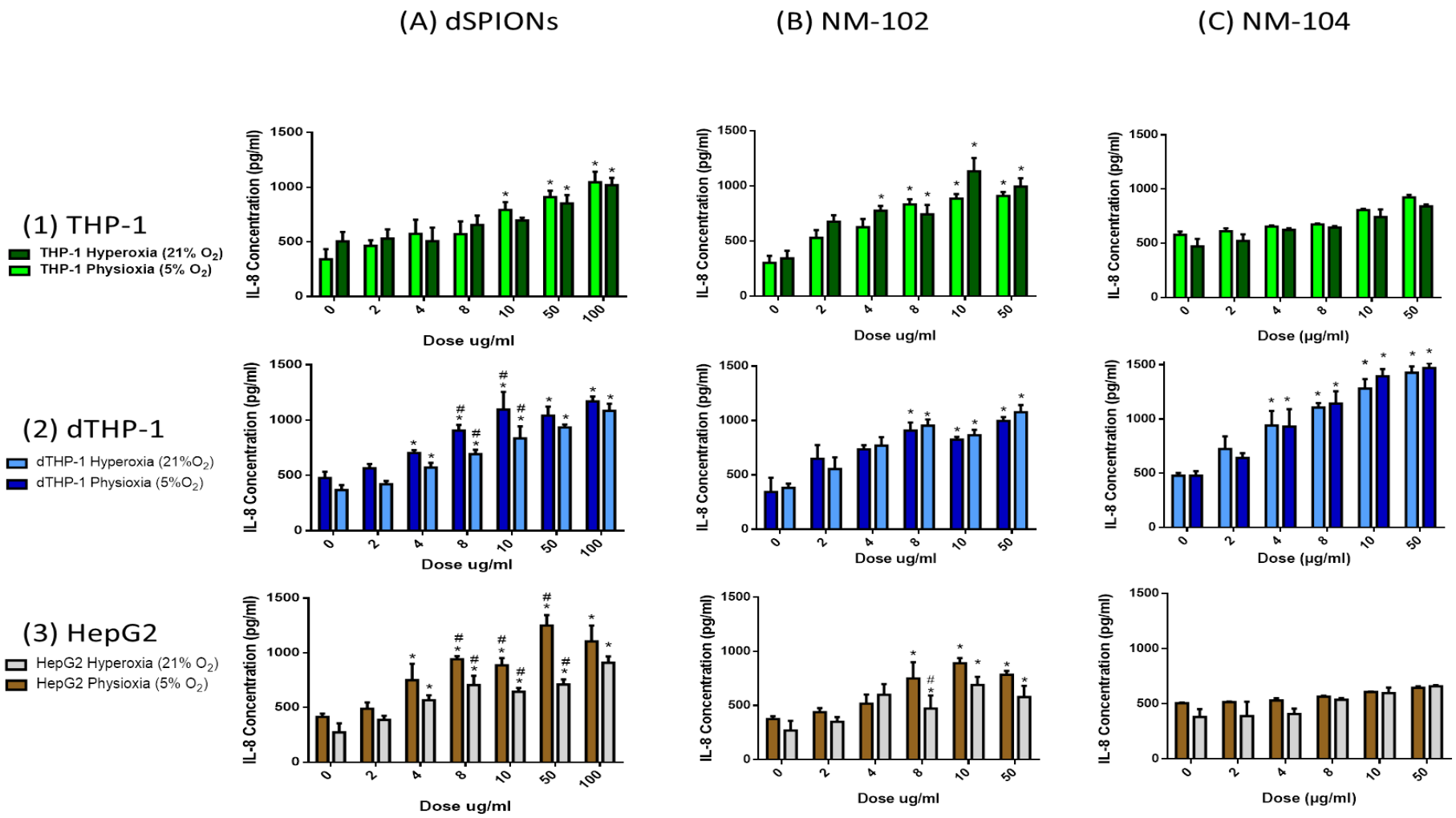

Figure 5.15: Quantification of IL-8 production after treatment with MONPs [(A) dSPIONs (B) NM-102 (C) NM-104] in all the cell lines, namely, (1) THP-1, (2) dTHP-1 and (3) HepG2. ELISA experiments were completed by samples completed in either hyperoxia (21%O_2) or Physioxia (5% O_2). *comparison with 0µg/ml #comparison between environments (n=3) P≤0.05

5.4 Discussion

In literature, the assessment of NP genotoxicity and cytotoxicity in vitro is generally undertaken in an ambient oxygen culturing environment (Hyperoxia 21% O_2). Although this has been proven to provide useful data, cells cultured in a more physiologically relevant oxygen culturing environment have previously been observed to closely express the cellular physiology identified *in vivo* (Costa *et. al.* 2017). Therefore, the purpose of this chapter was to characterize and compare the mechanisms of toxicity utilized by the distinct MONPs under investigation in this study; in both the commonly used hyperoxic culturing environment and the more physiologically relevant oxygen culturing environment (5% O_2).

5.4.2 Cellular antioxidants depletion and Oxidative stress

In order to determine if the ability of the different cell lines to regulate cellular levels of ROS was hindered after treatment with the distinct metal oxide NPs for the period of 5h, the depletion of the natural antioxidant Glutathione (GSH) was determined in both the hyperoxic (21% O_2) and physioxic (5% O_2) environments. As shown in **Figure 5.2** the untreated samples of the cell lines (i.e.negative controls) showed only non-significant differences in intracellular levels of GSH in the two different environments, whereas the effects after treatments with the different metal oxides showed significant impact on GSH levels in each of the cell lines when cultured in the distinct environments.

After treatment with dSPIONs, dose dependent depletions in the antioxidant GSH were identified. These results suggest that the greater the concentration of the metal oxide the greater its effect was on the redox status of the different cell lines. Importantly the magnitudes of these depletions were significantly greater (for THP-1 and HepG2) in the physioxic culture environment. From the results we conclude that at a cellular level dSPION were able to affect the ability of the cell to regulate ROS concentrations, and that this effect was significantly greater in the physioxic environment.

Investigation of GSH levels after treatment with either of the distinct TiO_2 polymoprhs showed similar results in the different cell lines and environments. As shown in **Figure 5.2B and C** both polymorphs induced dose dependent reductions in the concentration of GSH in all cell lines, but these reductions were found statistically significant only in the immune cell

lines, namely THP-1 and dTHP-1. The reductions identified in the physioxic environment when the immune cell lines were treated with NM-102 were significantly greater than the corresponding reduction seen in hyperoxia, while significantly greater reductions in the physioxic environment were only identified in THP-1 (not for dTHP-1 and HepG2) when the cell lines were treated with NM-104.

Thus it can be concluded that while there is some variation in general the dSPIONs induce greater oxidative stress in the physioxic culture environment (5%O_2). In addition, the TiO_2 polymorphs due to their physical characteristics interact in a distinct way with the different cell lines and thereby induce different amounts of oxidative stress.

5.4.3 Intracellular Ca^{2+} signalling

The effects of the distinct metal oxide NPs through the course of time on cytosolic $Ca2^{+}$ concentrations and hence intracellular signalling homeostasis in the distinct cell lines was investigated. Each of the chosen time periods, namely, immediate response (0h-5min), 30min, 5h and 24h were investigated in order to determine the relevant NP concentrations and also to correlate with other investigated parameters.

As shown in **Figure 5.3,** when treated with NPs cells concentrations of intracellular Ca^{2+} were elevated immediately after treatment with intracellular Ca^{2+} concentrations being maintained an elevated level for a period of at least 5min. This was evident after treatment with all NPs in all cell lines and environments in similar dose dependent manners. When the different cell lines were either at rest or treated with a positive control (e.g. Ca^{2+} ionophore A23187) the respective concentrations of intracellular Ca^{2+} exhibited no distinct differences between the different oxygen culture environments. However, after comparison was carried out, the NP-induced elevations were found to be of different extents in the different cell lines (dTHP-1>THP-1>HepG2), with the identified increase in intracellular Ca^{2+} being significantly greater in the physioxic culture environment than in the hyperoxic culture environment (**Figure 5.4**) when cells were treated with dSPIONs and NM-102 (while in NM-104 a similar discrepancy was evident but no statistical significance was identified). The results suggest that introduction of NPs in the cell culture was associated with an enhanced initial iCa^{2+} reaction in the physioxic environments.

Since intracellular Ca^{2+} concentrations were elevated for the period of 5 min; measurements were also carried after a 30min treatment with the MONPs. As shown in **Figures 5.5, 5.6 and 5.7** after a period of 30min of treatment with the distinct MONPs statistically significant dose dependent increases were identified in all cell lines and environments. No significant differences were identified between the responses seen in the distinct culture environments in any of the cell lines. In all cases the magnitude of the increase after treatment with the distinct metal oxides was greater in the immune cell lines (dTHP-1>THP-1>HepG2). Similarly, as shown in **Figures 5.10, 5.11 and 5.12** intracellular levels of Ca^{2+} were determined after 5h treatment with the different MONPs under investigation, and were found to undergo significant increase in all cases. The magnitudes of those identified increases were not found to be significantly different in either of the two culturing environments as shown in **Figure 5.13**.

Finally, concentrations of Ca^{2+} were also investigated after a treatment for the period of 24h. In all cases, concentrations of intracellular Ca^{2+} had returned back to the levels of cytosolic Ca^{2+} observed in the untreated cells.

Thus MONP-associated elevation in the concentrations of cytosolic Ca^{2+} for periods of up to 5h suggest that MONPs triggered intracellular Ca^{2+} signalling (and/or disrupted the normality of cellular Ca^{2+} homeostasis) in all three cell lines and environments. It should be also be noted that the changes in the elevation of Ca^{2+} had a distinct character which varied depending on the period of the treatment, and/or the nature of the cell line, and/or the levels within the oxygen culture environment.

5.4.3.1 Origins of the increase in intracellular Ca^{2+}

As the observed increase in cytosolic Ca^{2+} concentrations after a 30min treatment with the distinct MONPs could originate from the depletion of a variety of different cellular Ca^{2+} storage organelles, the levels of Ca^{2+} released from the ER and the acidic organelles was investigated.

After Fluo-4 loading into the cytoplasm, and pre-treatment of all the cell lines with thapsigargin (known to deplete the ER from Ca^{2+}, Doan *et. al.* 1994); as shown in **Figures 5.6** significantly higher Ca^{2+} dependent fluorescence was identified in the cytoplasm (and

therefore a greater release of Ca^{2+} from the ER) was identified in the physioxic environment (including the negative controls of all the cell lines). After a 30min treatment with the NPs NP-associated increases in cytosolic Ca^{2+} were significantly greater when the cells had not been pre-treated with thapsigargin suggesting that a proportion of the identified increase after NP treatments originates from the ER. However, the greater increase in the concentrations of cytosolic Ca^{2+} identified in cells treated both with high doses of the distinct MONPs and with thapsigargin (compared to those treated with thapsigargin alone) leads to the conclusion that high dose NP treatments result in the further release in Ca^{2+} from a different Ca^{2+} organelle (e.g. Acidic organelles), or addition from the extracellular environment. In order to determine the extent of Ca^{2+} addition from the extracellular environment in future work Ca^{2+} free PBS can be used instead of TC medium.

This aspect of determination of the origin of the increase identified in cytosolic Ca^{2+} commenced with the investigation of the acidic organelles with the use of GPN treatments. GPN is cleaved by the lysosomal enzyme cathepsin C which gives rise to osmotic stress and so ruptures lysosomal membranes; as a result lysosomal Ca^{2+} is released into the cytoplasm (Lloyd Evans *et. al.* 2008). After a 30min treatment with the distinct MONPs, continuous measurements of cytosolic Ca^{2+} concentrations were carried before and after injection with GPN. A MONPs dose dependent increase of cytosolic Ca^{2+} was identified in all samples prior to the administration of GPN (**Figures 5.5-5.9**). After administration of GPN the concentration of Ca^{2+} further increased in all doses in a similar extent in all NP doses. Previous observations on NP uptake and interaction (**Chapter 4**) would suggest that a greater amount of acidic organelles and hence lysosomal Ca^{2+} should be identified in the higher doses. These results allow the conclusion that partially the Ca^{2+} increase identified in the cytosol after treatment with MONPs originates from acidic organelles, and gives rise to the question if the acidic organelles remain intact after MONPs cellular internalization through phagocytosis.

5.4.3.2 Oxidative stress and Ca^{2+} signalling

As it was previously discussed, investigation in the concentrations of GSH suggests that the different MONPs induced changes in the cellular redox state of the distinct cell lines (**Figure 5.2**). In the literature induction of oxidative stress is interconnected with the elevation in

cytosolic Ca^{2+} concentrations (Miletto *et. al.* 2010, Gilardo *et. al.* 2015). Investigations to determine if the observed effects of depletion of GSH and elevation of cytosolic Ca^{2+} concentration after a treatment with the NPs for a 5h periods (**Figure 5.3 to 5.9**) are interconnected were therefore carried out by applying a pre-treatment to the cell lines with the antioxidant Trolox.

As shown in **Figure 5.10, 5.11 and 5.12** pre-treatments with the antioxidant trolox resulted in no significant reduction in the concentration of cytosolic Ca^{2+}. In contrast minor reductions in the magnitude of NP induced increases in the concentration of Ca^{2+} were identified in samples pre-treated with trolox; this reduction archieved statistical significance for HepG2 cells, but not for THP-1 and dTHP-1 cells. Such slight reductions in the NP exert increase of cytosolic Ca^{2+} observed after trolox pre-treatments would suggest that the identified increase in intracellular Ca^{2+} could be partially (but pherhaps not solely) due to the presence of oxidative stress.

5.4.4 Pro-inflammatory responses

The roles of mobilization and activation of the Ca^{2+} signalling and changes in the redox state of the cells in the production of IL-8 and TNF-α have been previously discussed in the literature (Watanabe *et. al.* 1996, yang *et. al.* 2015, Ermak & Davies, 2002). Therefore the ability of the MONPs under investigation to promote the activation of an immune response in THP-1, dTHP-1 and HepG2 was investigated by quantifying the changes in concentrations of inflammatory cytokines TNF-α and IL-8 released by cells following exposure to MONPs.

The extent in the production of TNF-α and IL-8 after treatment with the distinct MONPs was cell type dependent (dTHP-1>THP-1-HepG2). A significant dose dependent increase of TNF-α was identified in all cell lines and environments after treatments with dSPIONs. Environment dependency was identified when dSPIONs were used to treat the distinct cell lines; specifically significantly greater increases were identified in samples treated in the physioxic culture environment when compared with those treated in the hyperoxic culture environment. A dose dependent increase was identified in the production of IL-8 in all the cell lines and environments after treatment with dSPIONs. Significantly greater production

of IL-8 was identified in the physioxic culture environment only in THP-1 and HepG2 after treatment with dSPIONs.

Significant increases were identified in the production of TNF-α in all the cell lines after treatment with the TiO_2 polymorphs (NM-102 and NM-104), except after treatment of HepG2 with NM-104 where non-significant increases were observed. Dose dependent increase in the production of TNF-α were identified in both oxygen culture environments, with no evidence of an environmental specificity in any of the cell lines or NPs. Similar results were observed in the production of Il-8, with a dose dependent significant increase observed after treatment with the distinct TiO_2 polymorphs but no environmental specificity being identified.

The observed results regarding production of inflammatory cytokines in all cell lines and environments agree with the results observed in GSH reduction and intracellular Ca^{2+} increase. Specifically, given the literature reports linking the mechanisms alteration of cellular redox state and intracellular Ca^{2+} signalling after the treatment with the distinct MONPs could contribute to (or even be responsible for) the observed increase in the production of TNF-α and IL-8. More information about the mechanistic details linking the induction of oxidative stress (i.e GSH reduction), the alteration of iCa^{2+} and the production of pro-inflammatory responses can be found in **Section 1.5** and are further discussed in **Section 6.4**.

5.4.5 Summary and Conclusion of Chapter 5

From the results acquired we can now conclude that treatment with MONPs under investigation would lead to an alteration of the cellular redox state. This has been found to induce changes in intracellular Ca^{2+} signalling therefore it is plausible that MONPs-induced oxidative stress is responsible for the intracellular Ca^{2+} increase seen here (Ermak & Davies, 2002). The underlying mechanism of the Ca^{2+} immediate response observed (0-5min) and its compatibility with oxidative damage of Ca^{2+} handling proteins such as IP_3R requires further investigation (Bangashi et. al 2014). However, the results suggest that the alterations of Ca^{2+} signalling (after 5h treatment with MONPs) are not solely dependent on the presence of oxidative stress. Such synergistic alterations in cellular redox state and intracellular Ca^{2+} signalling could lead to the identified increase in the production of the inflammatory cytokines TNF-α and IL-8.

Intracellular Ca^{2+} signalling seems to have distinct behaviours in the two environments in the first 5 min of treatments, although no corresponding environment-specific differences were identified after treatments for extended periods of time (i.e. 30min-24h). Loss of Ca^{2+} from the ER occurred in greater extents in the physioxic culture environment in all samples including the negative controls of all the cell lines. Based on the results, at least a proportion of the increase identified in cytosolic Ca^{2+} after treatment with the MONPs originated from the ER. In addition, additional proportion of the increase after treatment with MONPs in the concentrations of cytosolic Ca^{2+} may originate from acidic organelles. Based on the results of this chapter, and results on uptake from **Chapter 4)** questions are raised about the integrity of acidic organelles after internalization of MONPs.

In conclusion, the results suggest distinct MONPs induced alterations in cellular signalling homeostasis (with regards to oxidative stress, iCa^{2+}) between the two environments, which may be the reason for the greater hazardous behaviour identified in the physioxic culture environment in dSPIONs.

Chapter 6: General Discussion

6.1 Fulfilment of the objectives of this Study

The applications of different NPs are greatly increasing in an unconstrained pace for the development of new and existing technologies. Therefore humanity's interaction with NPs will continually increase. Although NPs have proven to have numerous potential advantages, the health hazard associated with human exposure remains of heightened concern. Occupational exposure in the form of inhalation is of primary concern to human health, although systemic exposure through injections is of particularly high importance given the potential medical applications of NPs (Arora *et. al.* 2012). Primary exposure to NM's is mostly through the skin, gastrointestinal tract and most importantly the lungs (Papp et al. 2008). Although it is widely accepted that these are the primary exposure sites, distribution of particles via translocation through the bloodstream to other tissues is also observed as a secondary exposure (Eisner *et. al.* 2012). As a results identifying and understanding the ability of NPs to induce toxicity has been a pressing issue; accordingly the overreaching aim of the current study was to contribute to enhance understanding of NP induced toxicity.

6.1.1 Objectives and Summary of Chapter 3

Current research suggests that it is the unique physico-chemical properties of the NPs which make them so important for development of new medicine and technology. These unique physicochemical characteristics are what make NPs highly reactive with biological environments. Therefore, physico-chemical characterization of the materials under investigation prior to every nanotoxicological study is necessary. NP characterization conducted following their synthesis is deemed as the primary characterisation. Primary NP characteristics include size, morphology, surface area, composition/purity, surface charge, surface chemistry and potentially endotoxin contamination (Sayes and Warheit, 2009). Characterisation of the NPs secondary characteristics is conducted after their exposure to a test system (e.g. biological environment, experimental environment); these may include assessment of agglomeration state, suspension stability, dissolution and protein corona formation (Johnston et. al. 2012).

It has become increasingly evident that differences in NP properties, such as size/agglomeration status, surface charge, shape and chemical composition could affect their outcome of the toxicological endpoints (Öberdoster *et al.* 1992, Hall *et. al.* 2007). Additionally, identification of the characteristics allows avoidance of contradictions between studies that are investigating the same material. However, characterization of NPs under experimental conditions still faces significant challenges. The mostly commonly used technologies (such as DLS, NTA) used for evaluating NP secondary characteristics have the potential to be inaccurate or misused; therefore it is critical that suitable alternative techniques are identified (Hondow et al., 2012).

The determination of MONPs physico-chemical characteristics *in situ* was crucial to allow understanding of any adverse toxicological endpoints that may be observed when undertaking cyto-, immuno- and genotoxicity analysis. Therefore the assessment of the primary and secondary characteristic of the NPs used in this study, namely, dSPIONs, NM-102 and NM-104 was the matter of investigation in **Chapter 3**. In brief the key properties of all the MONPs under experimental conditions were that they tested positive for endotoxin presence, they had a near neutral (albeit slight negative) charge and had a hard protein corona consisting purely of BSA. Moreover, dSPIONs formed agglomerates in chain like structures that had a hydrodynamic diameter of 89nm. Both of the TiO_2 NPs were unstable in suspension; however agglomerates formed by NM-102 were larger than the agglomerates observed in NM-104. The characteristics investigated and the results obtained are described in detail in **Table 6.1.**

Table 6. 1: Summary of objectives and Results of Chapter 3, MONPs characterization. Characteristics investigated in the study include stability of the NPs in suspension, visible and using DLS and UV-Vis; hydrodynamic diameter and ζ-potential; size and chemical purity using SEM and EDX; the formation and composition of hard protein corona and endotoxin presence in NP suspension.

Objectives of Chapter 3	NPs	Results
1) Stability after dispersion in different diluents. (DMEM with 10%FBS, RPMI with 10% FBS, 0.05% BSA in Water)	**(A) dSPIONs**	**(A)** Visibly stable after dispersion in the different diluents used for the experiments
	(B) NM-102 **(C) NM-104**	**(B and C)** • Visibly unstable in suspension in all the diluents for periods of up to 24h. • Formation of sediment and stability seems to increase in lower NP concentrations.
2) Measurements of hydrodynamic diameter (HD) and ζ potential using DLS and NTA	**(A) dSPIONs**	**(A)** NTA and DLS provided similar results on the HD of dSPIONs at 89nm.
	(B) NM-102 **(C) NM-104**	• **(B) and (C)** hydrodynamic diameter reduced through time suggesting agglomeration and sedimentation of the NPs in the diluent. • NTA measurements could not provide valid results due to the nature of the technique and the instability of the NPs in diluents.
		(B) After 2h incubation HD=540nm and ζ potential = 14.6 +/- 2.1mV. **(C)** After 2h incubation HD= 284nm and ζ potential =12.4 +/- 3.2mV.
3) UV-Vis measurements for the determination of the concentration of TiO2 NPs after incubation in diluent.	**(A) NM-102** **(B) NM-104**	• Reduction in absorbance of light in both A and B suggested of a reduction in concentration of NPs remaining in suspension. • The concentration of NPs in suspension after 2h was calculated: **(A)** 97.08 µg/ml and **(B)** 93.88 µg/ml
(4) Measurements of size through SEM and chemical purity through EDX	**(A) NM-102** **(B) NM-104**	• Only minimal impurities were identified through EDX in both A and B. • The sizes of the NP agglomerates and aggregates varied although the majority resembled the measurements of HD identified of the two using DLS.
(5) Formation and identification of NP hard protein corona. Measured in DMEM with 10%FBS, RPMI with 10% FBS, 0.05% BSA in Water.	**All MONPs**	• In all the NPs and diluents under investigation only one protein was identified. Its safe to assume from the results that protein was also BSA. • Quantification suggests that the protein accumulates on the surface of all MONPs in a higher proportion in DMEM with 10%FBS, RPMI with 10% FBS.
(6) Endotoxin identification in NP Suspension	**All MONPs**	All MONPs tested positive for the presence of endotoxin.

6.1.2 Objectives and Summary of Chapter 4

Once the characteristics of the NPs were identified (**Table 6.1**) under experimental conditions a nanotoxicological assessment could be undertaken. Such investigations may be carried out using established *in vivo* techniques, although desire of implementations of the 3Rs initiative for the reduction, refinement and replacement of animal models use has led to a requirement for robust *in vitro* alternatives (Kota *et. al.* 2018, Joris et al., 2013). The current gold standard for regulation of NPs in the field is the application of 2D mono-culture based techniques for the assessment of cytotoxic, inflammatory and genotoxic responses following NP exposure normally carried out under humidified air supplemented with 5% CO2, resulting in an environment containing approximately 18.6% O_2. However as it was previously discussed, an important novel approach in the current study was to culture cells in a physiological resembling oxygen culture environment (5% O_2) *in vitro*, this would allow a more precise insight into MONPs toxicological profiles and cellular interaction *in vivo*.

An important parameter for the assessment of potential toxicity induced by NPs is the ability to determine interaction and uptake of NPs with the exposed cell systems (in this case THP-1, dTHP-1 and HepG2). These strongly depend on the physicochemical characteristics of the different MONPs, as identified and described in **Chapter 3.** Interaction of all the MONPs was identified in a cell type dependent manner (dTHP-1>THP-1>HepG2); however dSPIONs were the only NP whose interactions with cells expressed culture environment dependency. Under TEM NP uptake was identified with both TiO_2 NPs in all cell lines but not with dSPIONs. However in previous work conducted with the dSPIONs in our lab has provided uptake by THP-1 and dTHP-1 cells was observed using TEM (Evans *et. al.* 2017).

When the immune cell lines (THP-1 and dTHP-1) were treated with the different MONPs cytotoxicity was only identified by dSPIONs and only in the physioxic environment. When HepG2 were treated with dSPIONs DNA damage was only identified in the physioxic environment. The characteristics of the identified genotoxicity were further investigated for aneugenicity. NM-102 were able to produce a minor aneugenic response, details are shown on **Table 6.2**. Due to the presence of multiple centromeres in the micronuclei formed in HepG2 treated with NM-102, investigation on the effects on the mitotic spindle was carried

out with no positive results. All the objectives of **Chapter 4** and the results observed for each endpoint in the different culture environments are presented in **Table 6.2**.

Table 6. 2: Summary of objectives and Results of Chapter 4. Cellular uptake and interaction in the distinct environments was investigated prior to any toxicological studies. Cellular uptake was analysed by the ferrozine assay, flow cytometry and TEM imaging. Finally, the ability of MONPs to promote chromosomal DNA damage in HepG2 cells was quantified by the CBMN assay.

Objectives of Chapter 4	NP	Cell line	Hyperoxic Culture Environment	Physioxic Culture Environment
1) NP cellular Interaction and Uptake. Investigated using the ferrozine assay, Flow cytometry and TEM imaging.	**(A) dSPIONs**	**Immune cell lines (THP-1 , dTHP-1) and HepG2**	**(A)** Significant dose dependent increase in NP cell interaction was identified in the immune cell lines at 8µg/ml-100µg/ml when compared with the negative control.	**(A)** • Significant dose dependent increase in NP cell interaction was identified in the immune cell lines at 10µg/ml-100µg/ml and for HepG2 8µg/ml-100µg/ml when compared with the negative control. • Significantly greater results (compared with hyperoxia) were identified in THP-1 at 100µg/ml and in HepG2 50µg/ml and 100µg/ml.
	(B) NM-102		**B and C** exhibited • dose dependent increase in in all cell lines (dTHP1>THP-1>HepG2). • TEM imaging showed that the NPs were uptaken by both immune cell lines and HepG2 but were only located in cellular vesicles in the immune cell lines. No differences were identified between the culture environments.	
	(C) NM-104			
2) Cell viability Investigated using RPD% and RICC%	**(A) dSPIONs**	**Immune cell lines (THP-1 , dTHP-1) and HepG2**	**(A)** No reduction	**(A)** Significant reduction in cell proliferation was identified in both Immune cell lines when treated for 24h.
	(B) NM-102		**(B)** Reduction identified only in HepG2 50µg/ml	
	(C) NM-104		**(C)** Reduction identified only in HepG2 8µg/ml-50µg/ml	
3) Genotoxicity Investigated using CBMN	**(A) dSPIONs**	**HepG2**	**(A)** No increase in MN%	**(A)** • Significant increase in MN% at 8µg/ml-100µg/ml when compared with negative control. • Significant difference was identified at 50µg/ml and 100µg/ml when compared with hyperoxia.
	(B) NM-102		**(B)** Significant increase in MN% at 10µg/ml when compared with negative control	
	(C) NM-104		**(C)** No increase in MN%	
4) Aneugenicity Investigation Centromere staining	**(A) dSPIONs**	**HepG2**	**(A) Not applicable (no genotoxicity identified)**	**(A)** Clastogenic, centromere-negative Mn (%) remained in normal for the cell line.
	(B) NM-102		**(B)** Clastogenic, centromere-negative Mn (%) remained normal for the cell line in both environments.	
5) Investigation of the mitotic spindle	**(A) dSPIONs**	**HepG2**	No abnormalities in formation of the mitotic spindle following exposure.	
	(B) NM-102			

6.1.3 Objectives and Summary of Chapter 5

In **Chapter 5** the objective was to investigate the mechanism underlying the observed genotoxic and cytotoxic effects of the different MONPs that were previously identified in **Chapter 4**. This investigation and its respective endpoints, as presented in **Table 6.3 and Table 6.4**, were carried out in both a hyperoxic (21% O_2) environment and physioxic (5% O_2) environment. In order to identify what resulted in the distinct toxicity identified in the two environments, comparison of the respective results was carried out.

The MONPs used in this study (dSPIONs, TiO_2 polymorphs) have been previously observed to have the potential to elicit inflammatory responses, cause cytotoxicity, promote oxidative stress and instigate DNA damage (Singh et al., 2009, Hu et al., 2016, Arora et al., 2012, Shvetova et al., 2016). Therefore in this study the reduction in the presence of cellular antioxidant glutathione, and the production of pro-inflammatory chemokine IL-8 and cytokine TNF-α were investigated (**Table 6.3**). Changes in the concentration of iCa^{2+} following 0h to 24h exposure to the NPs were also investigated, with further investigations aiming to identify the respective involvements of different cellular calcium storage organelles (i.e. ER and lysosomes), and to determine if the identified disruptions in cellular Ca^{2+} homeostasis were the result of changes in the cellular redox state (**Table 6.4**).

The results suggest that the NPs (particularly dSPIONs) trigger distinct alterations in cellular signalling between the two environments, which may be the reason for the greater hazardous behaviour (e.g. genotoxicity/cytotoxicity) identified in the physioxic culture environment in dSPIONs. Given the evidence for disruption of lysosomal Ca^{2+} homeostasis is within (the results of this chapter, and results on uptake from **Chapter 4),** questions are raised about the integrity of acidic organelles after internalization of MONPs. Interestingly, the literature suggests that a synergistic alteration in cellular redox state and that intracellular calcium signalling (Forest *et al.* 2014, as observed in this chapter) could lead to the identified NP- associated increases in the production of the inflammatory cytokines TNF-α and IL-8.

Table 6.3: Summary of objectives and Results of Chapter 5. Cytokine IL-8 and TNF-α production were investigated in both oxygen culture environments using ELISA. Glutathione depletion was investigated in both oxygen culture environments in order to determine alterations in the cellular redox state.

Chapter 5 Objectives	NPs	Cell lines	Hyperoxic Culture Environment	Physioxic Culture Environment
(1) Il-8 and TNF-α production	**(A) dSPIONs**	**Immune cell lines (THP-1 , dTHP-1) and HepG2**	**(A)** Dose dependent significant increase was identified. Significant results were identified in all cell lines when compared with the negative control 0µg/ml.	**(A)** • Dose dependent significant increase was identified in all cell lines when compared with the negative control 0µg/ml. • Significant results were identified both in dTHP-1 and HepG2; when the response was compared to the same dose of the NPs in the hyperoxic environment.
	(B) NM-102		**(B)** Dose dependent increase in Il-8 production was identified in all cell lines and in both environments. No differences were identified in the different culture environments.	
	(C) NM-104		**(C)** Dose dependent increase was identified in all cell lines but was only found significant in dTHP-1. • The Increase showed no environment culture specificity, • Cell line specificity was identified dTHP-1>THP-1>HepG2	
(2) Glutathione depletion	**(A) dSPIONs**	**Immune cell lines (THP-1 , dTHP-1) and HepG2**	**(A)** Dose Dependent decrease in glutathione was identified in all the cell lines.	**(A)** Dose Dependent decrease in glutathione was identified in all the cell lines. • The decrease in Glutathione was greater in the physioxic culture environment. Significantly lower concentration in glutathion was found in HepG2 at 100µg/ml.
	(B) NM-102		**(B)** Dose dependent decrease was visible in all cell lines. No significant results were identified.	**(B)** Dose Dependent decrease in glutathione was identified in all the cell lines. • The decrease in Glutathione was greater in the physioxic culture environment. Significantly lower concentration in glutathione was found in dTHP-1 at 10µg/ml and 50µg/ml.
	(C) NM-104		**(C)** Dose dependent decrease was visible in all cell lines. Significant results were identified in the immune cell lines.	**(C)** Dose Dependent decrease in glutathione was identified in all the cell lines. • The decrease in Glutathione was greater in the physioxic culture environment. Significantly lower concentration in glutathione was found in dTHP-1 at 50µg/ml.

Table 6.4: Summary of objectives and Results of Chapter 5; intreacellular calcium signalling. Investigation of changes in intracellular calcium after treatment with the differenr in various time limits (0h-24h). Investigation of the effects MONPs had on ER and lysosomal calcium was carried out after 30min treatment with the MONPs. The effects of oxidative stress on intracellular calcium concentrations was also invetigated with the use of pretreatments with the antioxidant trolox.

Chapter 5: Intracellular Calcium Objectives	Cell line	Results
(1) Identify the extent in time the MONPs have an effect on intracellular calcium levels. Measurements were carried at 0-5min, 30min, 5h and 24h.	**Immune cell lines (THP-1 , dTHP-1) and HepG2**	**After pre-treatment with Thapsigargin and the different MONPs (A-C):** • All MONPs were able to increase the intracellular calcium concertation in both environments and all cell lines for the period of 0-5h. • The concentration of intracellular calcium gradually decreased through time. • Significantly greater increase in calcium was identified in the physioxic culture environment when compared with the hyperoxic environment. • Increase in intracellular calcium was cell dependent dTHP-1>THP-1>HepG2 • No NP specificity in the response was identified.
(2) Pre-treatment with Thapsigargin [non-competitive inhibitor of the sarco/endoplasmic reticulum Ca2+ ATPase (SERCA)]to determine if the identified increase in cytosolic calcium originates from the ER. Measurements were carried after a 30min treatment with NPs	**Immune cell lines (THP-1 , dTHP-1) and HepG2**	**After pre-treatment with Thapsigargin and the different MONPs :** • A dose dependent increase in cytosolic calcium was observed in both environments in all cell lines. • The increase was significantly greater in the higher doses of NPs in THP-1 and dTHP-1 when compared with 0μg/ml, the equivalent NP dose (μg/ml) without Thapsigargin and 0μg/ml + Thapsigargin • Significantly greater were the results observed in physioxia (5% O_2) when compared with hyperoxia (21% O_2) in THP-1 and dTHP-1. • No significant difference was identified in HepG2 between the two environments when treated with the MONPs
(3) Treatments with GPN (permeabilizes lysosomes by osmotic swelling) and release lysosomal calcium. Measurements were carried after a 30min treatment with NPs	**Immune cell lines (THP-1 , dTHP-1) and HepG2**	**After treatment with the different MONPs :** • A dose dependent increase in cytosolic calcium was observed in both environments in all cell lines. • The increase was significantly greater in the higher doses of NPs+GPN in THP-1 and dTHP-1 when compared with 0μg/ml, the equivalent NP dose (μg/ml) without GPN and 0μg/ml+GPN and • Significantly greater were the results observed in physioxia (5% O_2) when compared with hyperoxia (21% O_2) in THP-1 and dTHP-1 only with dSPIONs and NM-104. • No significant difference was identified in HepG2
(4) Antioxidant trolox pre-treatment. To determine the effects of cellular redox state have an effect on intracellular calcium. Measurements were carried after a 30min treatment with NPs	**Immune cell lines (THP-1 , dTHP-1) and HepG2**	• In all cell lines and environments a significant increase in the concentration of intracellular calcium was identified after 5h treatment with all the MONPs after both trolox and no trolox pre-treatments. • No significant decrease in calcium concentration was identified when the concentration of non-trolox were compared with trolox treated results.

6.2 Discussion of NP-Cell Interaction findings, and their Implications

The results of the study agree with the reported uptake capacity of the different cell lines. One of the major functions of monocytes-macrophages *in vivo* is the removal of foreign material from tissue. Therefore the higher interaction observed in THP-1 and dTHP-1 when treated with the different MONPs was consistent with the literature (Kopf et al., 2015). The identified hydrodynamic diameter (DLS) and size (SEM images) of the different MONPs (i.e. dSPIONs 89nm, NM-102 540nm, NM-104 255nm) suggest that they would have been capable of uptake by phagocytic mechanisms (Zhang *et al.* 2015). All of the NPs have shown to have a near neutral charge *in situ,* the slightly anionic charge may have contributed to the ability of THP-1 and dTHP-1 to internalise the different MONPs. Although in the literature it has been previously observed that macrophages preferably interact with negatively charge NPs (Fröhlich 2012, Greish *et. al.* 2012, Radomski *et. al.* 2012).

The hard protein corona identified in all the MONPs comprised of BSA only. The significantly greater of interaction and internalization by THP-1 and dTHP-1 suggests that this BSA has a positive impact on macrophages uptake. In literature is suggested that BSA allows an increase in interaction and uptake, hence BSA is commonly used as a NP coating. BSA used as coating for SPIONs and CuO when they were compared with the equivalent uncoated NPs showed increased uptake in RAW264.7 macrophages (Wilhelm et al., 2003, Zhang et al., 2016). The formation of a BSA-corona was found to assist the NPs to attach on different macrophage scavenger protein including the glycoprotein receptors gp30 and gp18 (Fleischer and Payne, 2014).

Similarly to the results observed in the monocyte/macrophage cell types, HepG2 cells showed shown increased interaction in the physioxic environment only with dSPIONs, in the data observed with the Ferrozine assay. However after investigation under TEM no visible evidence of uptake (and hence intracellular located NPs) was identified after treatments with dSPIONs in the physioxic environment for the period of 24h which appeared to contradict the results of the Ferrozine assay. In contrast, internalised TiO_2 NPs were observed via TEM, the prominent difference between dSPIONs and the other two MONPs is the larger agglomerate HD and size formed by NM-102 and NM-104. This greater size of the

TiO_2 NPs may have increased the likelihood of it being taken up by HepG2 by endocytic mechanisms (Conner and Schmid, 2003).

To summarise the uptake and interaction of the different MONPs in the different immune cell lines (THP-1 and dTHP-1) was greater than in HepG2 (dTHP-1>THP-1>HepG2). The results observed are consistent with the expected response of the cell types, with the immune cell lines exhibiting higher interaction and uptake than the epithelial cells (HepG2) due to their increased phagocytic abilities (Aderem and Underhill 1999, Behzadi et al., 2017). As it was previously mentioned the observed uptake was likely aided by the size range, surface charge and protein corona of the test NPs.

Interesting is the smaller in agglomerate size and hydrodynamic diameter dSPIONs showed increased uptake and interaction in the physioxic culture environment. This is a matter of utmost importance given that increase in uptake and interaction can further affect the toxicity dSPIONs have exhibited. Due to the size identified in dSPIONs this might be due to an improved scavenger receptor-mediated endocytic activity, as was previously identified in a physioxic representative environment on LSECs (Martinez *et. al.* 2008). Therefore, it is suggested that further investigation is undertaken on the extent certain uptake pathways are activated and utilized in the different environments. To achieve this certain pathway inhibitors of the different endocytic uptake mechanisms for dSPIONs in all the cell lines and environments can be used, such inhibitors can be found in an article published in 2014 by Kuhnand colleagues. However, it has to be taken into account that the measurements for dSPIONs and for TiO_2 NPs were acquired using different techniques. Flow cytometry based techniques due to their nature allow single cell measurements in contrast to the ferrozine assay, which is a bulk cell measurement with lower sensitivity.

6.3 Evaluation of the Cytotoxicity and Genotoxicity of the NPs under investigation

The next step of this study was to assess the genotoxicity and cytotoxicity of the different MONPs under both a physioxic and a hyperoxic environment in THP-1, dTHP-1 and HepG2 cells. The study produced interesting data, particularly the observation that dSPIONs only induced chromosomal damage and cytotoxicity in the physioxic environment. As previously mentioned, dSPIONs were observed to have a greater interaction with the different cell lines in the physioxic culture environment and also to induce greater toxicity in all cell lines when cultured in the physioxic culture environment. In literature the majority of the studies have been conducted in a hyperoxic culture environment; accordingly these results would suggest that the scientific field may potentially be underestimating the (geno)toxicity induced by NPsNumerous studies conducted in the hyperoxic environment have demonstrated the inability of dSPIONs (dextran-Fe_3O_4) to induce cytotoxic or genotoxic effects (e.g. Singh *et al.* 2012); this is in contrast to the present study in which it was shown that results between the hyperoxic and physioxic environment are different, with a significantly genotoxic result being observed in physioxia. It is of particular interest that the dSPIONs used for this study have been previously demonstrated to degrade forming Fe^{2+}/Fe^{3+}, this effect occurs at a faster rate when exposed to a more acidic environment such of that of an endosome (Singh *et. al.*, 2012). With that information in mind, these results arouse curiosity on whether the increased interaction/uptake identified in the physioxic environment is associated with increased trafficking via the endocytic pathway, and whether this would in turn lead to elevated presence of free iron radicals, and ultimately the observed toxicity.

The ability of the distinct Titanium dioxide polymorphs to induce cytotoxic and genotoxic behaviours was investigated in both a hyperoxic and physioxic environment. In contrast to dSPIONs, both Titanium dioxide NPs induced an almost identical behaviour in the two environments. No toxicity was identified in the immune cell lines, but both Titanium dioxide polymoprhs were able to reduce the cellular viability in HepG2, interestingly only anatase (NM-102) was able to increase the frequency of MN indication after treatment. After centromere staining non-significant abnormalities were identified only with NM-102 treatments, with multiple centromeres being identified in the micronuclei. TiO_2 has been

previously shown to be capable of damaging cell division by deregulating the PLK1 protein which supports the maturation of the centrosome in late G2/early prophase among other mitotic processes, and that similar mechanisms may be underlining TiO_2 genotoxic effects identified in the current study (Huang et al., 2009).

The results of this study agree with the results of a recent study which reported that anatase titanium dioxide caused less severe necrosis and lysosomal membrane permealization than rutile titanium dioxide (Li *et. al.* 2017). In contrast anatase Titanium dioxide NPs were previously found to have a greater toxic potency than rutile Titanium dioxide NP, this was due to an increased surface reactivity of anatase Titanium dioxide that results in a greater ability to induce ROS accumulation, which governs their cytotoxic and inflammatory potential (Johnston *et. al.* 2009). In a more recent study the two polymorphs have been shown to have the same agglomerate size and solubilty have exhibited similar levels of reactive oxygen species (Yu *et al.* 2017). In the same study by Yu and colleagues the distinct toxicity of the polymorphs was attributed to Anatase Titanium dioxide NPs having a greater impact on mitochondrial dysfunction than rutile NPs; whereas the Rutile Titanium dioxide NPs cause more severe lysosomal membrane permeabilization than anatase Titanium dioxide NPs (Yu *et al.* 2017).Thus Yu and colleagues may point towards damage to lysosomal integrity (as triggered by endocytosed TiO_2 NPs) as the predominant mechanisms underlying the NM-102 induced cytotoxicity and genotoxicity seen in this study. However, the observed results in this study for the two polymorphs are not solely associated with their crystalline structure, the results also depend on their distinct size, agglomeration status and solubility therefore direct comparison with previous studies cannot be conducted.

In conclusion the most interesting finding of this aspect of the thesis is the significant change in genotoxic behaviour identified in dSPIONs in the physioxic culture environment. In order to elicit the mechanism underlying the observed toxicity, and to explore what other alteration; happen in the cellular behaviour after treatment with the different MONPs the redox state of the cells alongside with the alteration of intracellular calcium signalling and finally the production of pro-inflammatory cytokines were investigated in **Chapter 5**.

6.4 Elucidation of Cellular signalling mechanics triggered following NP exposure

As extensively discussed previously generation of excessive amount of reactive oxygen species (ROS) is the most frequent pathway NPs have for the induction of toxic actions (Manke *et al.* 2013). Induction of oxidative stress via excessive ROS levels was reported to lead to oxidative DNA damage and micronucleus formation in different metal oxide NP's (Singh *et al.*2012, Shukla *et al.* 2011). Therefore investigation of the depletion of the cellular antioxidant glutathione was carried out in order to identify changes in the cellular redox state after treatment with the different MONPs. After treatment with dSPIONs, dose dependent depletions in the antioxidant GSH were identified. These results suggest that the greater the concentration of the MONPs the greater its effect was on the redox status of the different cell lines. The magnitudes of these depletions were significantly greater (for THP-1 and HepG2) in the physioxic culture environment when compared with the hyperoxic culture environment. The NP, cell line and dose specificity seen in the hyperoxic environment was similar to that described and observed in the literature, but importantly the impact of the impact of the MONPs in the oxygen culture environment has not been previously described (Khanna *et. al.* 2015).

Investigation of GSH levels after treatment with either of the distinct TiO_2 polymoprhs showed similar results in the different cell lines and environments. Both polymorphs induced similar dose dependent reductions in the concentration of GSH in all cell lines. The reductions were found to be statistically significant only in the immune cell lines, namely THP-1 and dTHP-1. The reductions identified in the physioxic environment when the immune cell lines were treated with NM-102 were significantly greater than the corresponding reductions seen in hyperoxia, but significantly greater reductions in the physioxic environment were only identified in THP-1 (not for dTHP-1 and HepG2) when the cell lines were treated with NM-104. Thus it can be concluded that the polymorphs (presumably due to their physical characteristics) interact in a distinct way with the different cell lines in the different environments, and thereby induce different amounts of oxidative stress. Specifically, we conclude that in a cellular level dSPION and NM-102 were able to affect the ability of the cell to regulate ROS concentrations, and that this effect was significantly greater in the physioxic environment. However, when cells were treated with

NM-104 significantly greater reductions in the physioxic environment were only identified in THP-1 (not for dTHP-1 and HepG2).

The observed induction of oxidative stress (identified through reduction of GSH) generally correspond with the respective extent of DNA damage being identified. Thus, the results provide evidence that the different MONPs (due to their physico-chemical characteristics) interact in a distinct way with the different cell lines in the varying environments; which in turn results in a distinct induction of oxidative stress and toxicity. The results agree with previous observations identified in the literature, although the difference in the two oxygen culture environments arouses curiosity and requires therefore further investigation (Yu *et al.* 2017, Evans *et al.* 2017).

It was previously suggested that treatments with different NPs (e.g. TIO_2, quantum dot NPs, ZnO) via the production of oxidative stress may give rise to the expression of pro-inflammatory responses via the activation of intracellular calcium signals (Ermack and Davies 2002, Clift et al. 2010, Huang et al. 200,9 Chen et al., 2012b). In this study experiments also suggested that NPs could induce elevation of cytosolic calcium immediately after treatment for up to 5h, with the cytosolic calcium returning to the baseline by 24h. In the literature, induction of oxidative stress is interconnected with the elevation in cytosolic calcium concentrations (Miletto et al. 2010, Gilardo et al 2015). Therefore, investigations to determine if the observed effects of depletion of GSH and elevation of cytosolic calcium concentration after a treatment with the NPs for a 5h period are interconnected were therefore carried out by applying a pre-treatment to the cell lines with the cellular antioxidant Trolox. Pre-treatments with the antioxidant trolox resulted in no significant reduction in the concentration of cytosolic calcium. A minor reduction in the magnitude of NP induced increase in the concentration of calcium was identified in pre-treated with trolox Hepg2, THP-1 and dTHP-1 cells after treatment with all MONPs. Such slight reductions in the NP triggered increase of cytosolic calcium observed after trolox pre-treatments would suggest that the identified increase in intracellular calcium could be partially but not solely due to the presence of oxidative stress. These results suggest that the observed alteration of the intracellular calcium signalling may be at least partly due to different reasons. In order to investigate and identify the reason of the increase in cytosolic

calcium and why it is independent from oxidative stress, the effects on key calcium organelles had to be investigated.

Oxidative stress causes calcium influx into the cytoplasm from the extracellular environment and from iCa^{2+} storage organelles such as the endoplasmic reticulum (ER, or the lysosomes. Investigation of the origins in the increase of cytosolic calcium would also allow us to hypothesise how the Ca^{2+} storage organelles may contribute to the observed cytotoxicity and inflammation. The greater increase in the concentrations of cytosolic calcium identified in cells treated with the distinct MONPs when the cell lines were pre-treated with thapsigargin (compared to those treated with thapsigargin alone) leads to the conclusion that NP treatments result in the further release in calcium from a different calcium organelle (e.g. acidic organelles such as the lysosomes), or addition from the extracellular environment. In order to determine the extent of calcium addition from the extracellular environment in future work calcium free PBS can be used instead of TC medium. This will allow to determine if the identified response identified in cytosolic calcium concentrations involved extracellular calcium via the activation of voltagegated calcium channels and transient receptor potential (TRP) channels, as it was previously identified with SiO_2 NPs in smooth muscle cells (Dubes *et. al.* 2017).

Determination of the origin of the increase identified in cytosolic calcium commenced with the investigation of the acidic organelles with the use of GPN treatments. After a 30min treatment with the distinct MONPs continuous measurements of cytosolic calcium concentrations were carried before and after injection with GPN. A MONPs dose dependent increase of cytosolic calcium was identified in all samples prior to the administration of GPN. After administration of GPN the concentration of calcium further increased in all doses in a similar extent in all NP only doses. Previous observations on NP uptake and interaction (**Chapter 4**) would suggest that a greater amount of acidic organelles and hence lysosomal calcium should be identified in the higher doses. However, such larger magnitude increases were not evoked by GPN in NP-treated samples, these results allow to the conclusion that partially the calcium increase identified in the cytosol after treatment with MONPs originates from acidic organelles, and gives rise to the question as to whether the acidic organelles remain intact after MONP cellular internalization through phagocytosis.

In the literature induction of transcription factor activation and pro-inflammatory cytokine expression have been reported to result by both the presence of oxidants and calcium signalling events (Brown, Donaldson and Stone 2002, Stone et al. 2000). There is also the risk that inflammatory mediators may promote or aid in the promotion of DNA damage in the form of chromosomal fragmentation, DNA adduct formation and point mutations (Magdolenova et al., 2014b, Evans et al., 2016). The results of this study showed that all the MONPs under investigation were able to induce the production of both TNF-α and IL-8 in a dose dependent manner in both culture environments. Interestingly, only dSPIONs induced a greater increase in the production of TNF-α and IL-8 in the physioxic culture environment than what was observed in the hyperoxic culture environment . These results agree with the environment specific results observed for the impact of dSPIONs on DNA damage, the change in the redox state of the cells and the alterations of intracellular calcium signalling.

Although alteration of calcium signalling and redox state of the cells could be the reason for the identified increase in production of excess TNF-α and IL-8, the presence of endotoxin in the suspensions of the different MONPs has to be pointed out. Presence of LPS (endotoxin) is well known elicit an immune response, and it has previously been stated that NPs can only induce an immune response if they are contaminated with endotoxin (Fadeel et al., 2012). This is due to the fact that presence of endotoxin was reported to induced production of the cytokines as a downstream consequence of the NP/endotoxin interaction with TLR4 (Janssens and Beyaert, 2002). Although previous studies refuted that theory and demonstrated that uncontaminated NPs can cause cellular pro-inflammatory cytokine production (Dobrovolskaia and McNeil, 2013, Xu et al., 2016, Evans et al. 2016). The probability of contamination during and following synthesis of NPs is extremely high, and thus it can be argued that investigation of NP toxicity should be seen in the context of both the presence of LPS and the physicochemical characteristics of the NPs under investigation.

Therefore, based on the observed results and previous reports in the literature it is hypothesised that a synergistic outcome (of MONPs treatments) of changes on both the redox state of the cells (identified in this study from the results produced in the depletion of GSH) and alterations of calcium signalling may lead to the production of excess TNF-α and IL-8. The alteration of intracellular calcium signalling has been shown to be through the

effect MONPs have on both the ER Ca^{2+} concentrations and lysosomal Ca^{2+} concentrations. Functional links between ER Ca^{2+} stores and lysosomal Ca^{2+} stores have been previously observed by Kilpatrick and colleagues, which suggested membrane contact sites between endosomes and the ER emerge as Ca^{2+}-dependent hubs for signalling (Kilpatrick *et. al.* 2017). Interesting is that the results of the different endpoints investigated in this chapter agree with the results on the dSPION-cell interaction, cytotoxicity and genotoxicity that were found to be significantly greater in the physioxic culture environment in **Chapter 4**.

6.5 Suggestions for Future Research

The current study has numerous limitations and so it is appropriate at this stage to evaluate those limitations and provide some suggestions for future studies that may address these limitations. A greater increase in interaction and uptake was identified only in dSPIONs in the physioxic environment, the only metal oxide with that chemical composition, with spherical shape and agglomerate size smaller than 100nm in this study. However further investigation on the uptake pathways affected in the different cell culture environments, and hence if there is increased presence of dSPIONs in the acidic organelles, certain pathway inhibitors of the different endocytic uptake mechanisms for dSPIONs in all the cell lines and environments can be used (Kuhn *et. al.* 2014). We can also assume that since a greater interaction and uptake is observed, a greater accumulation of NPs in the acidic organelles, which from the results of this study the integrity, is questioned. Increase in cytosolic calcium and activation of the NRLP3 inflammasome have been found to occur after the damage of calcium organelles alongside the increase in concentrations of cathepsin-β such as the lysosomes (Jo et al. 2016). To further support this hypothesis in a study by Laskar and colleagues, dSPION have been found to result in the upregulation of lysosomal cathepsin-β which was then associated with secretion of both pro- and anti-inflammatory cytokines (Laskar *et al.* 2012).

Therefore initiation of the NRLP3 inflammasome could be the mechanism of the observed toxicity of MONPs. Although, initiation of the inflammasome is suggested to be the result of different parameters, which may include:

- The change in redox status of the cells (already measured through changes in the concentration of the antioxidant GSH).
- Increase in cytosolic calcium (from different organelles i.e. ER, Lysosomes).
- Bursting of acidic organelles (to be further investigated from the increase in cathepsin β).
- Measurement of Caspase 1 activity, an essential component of the inflammasome.
- Direct interaction and activation of the TLR and triggering of downstream signalling (e.g. Nf-κB) by the distinct MONPs.

Similarly in previous studies it was suggested, with regard to NPs inducing an inflammatory response following cellular internalisation, that TiO_2 NPs MWCNTs cause IL-1β production via the initiation of NLRP3 inflammasome assembly and caspase 1 activation (Sun et al., 2013, Sun et al., 2015, Jo et al. 2016). NP-induced oxidative stress provides an additional mechanism of pro-inflammatory cytokine production via ROS induction of NF-kB activated inflammatory pathways (Evans et. al. 2016). Various NPs in the literature have demonstrated the ability to induce a similar inflammatory response to that shown by the test materials in this study. Nano polymer rods for instance cause TNFα and IL-8 activation in THP-1 macrophages, which was shown to be dependent on the test NM shape (Chen et al., 2016). Additionally, as direct interaction of the MONPs with toll like receptors (TLR) signalling cascades is also suggested, it should be noted that in previous studies graphene oxide has been demonstrated to promote TLR4 and TLR9 signalling cascades and subsequent immune activation the CT26 colon cancer cells (Chen et al. 2014). In a more recent study TLRs' activation in THP-1 cells by clinically relevant and promising NPs, such as Fe_3O_4, TiO_2, ZnO, CuO, Ag_2O, and AlOOH was investigated. The study went on to prove that the NPs under investigation caused an increase of TLR-4 and -6 expression, which was comparable with the LPS-induced level (Vasilichin *et. al.* 2020). This further supports the hypothesis of the activation of the NRLP3 inflammasome.

A schematic presented in **Figure 6.1** summarises the findings of this study and also hypothesises other effects the different MONPs could have after treatment of the cells. This is striking that the NLRP3-activating parameters on the list were either directly observed in the current study, or are plausible companion effects to the phenomena observed in the current study. This allows the understanding on the mechanism of the induced toxicity identified but also suggests of future work that has to be investigated.

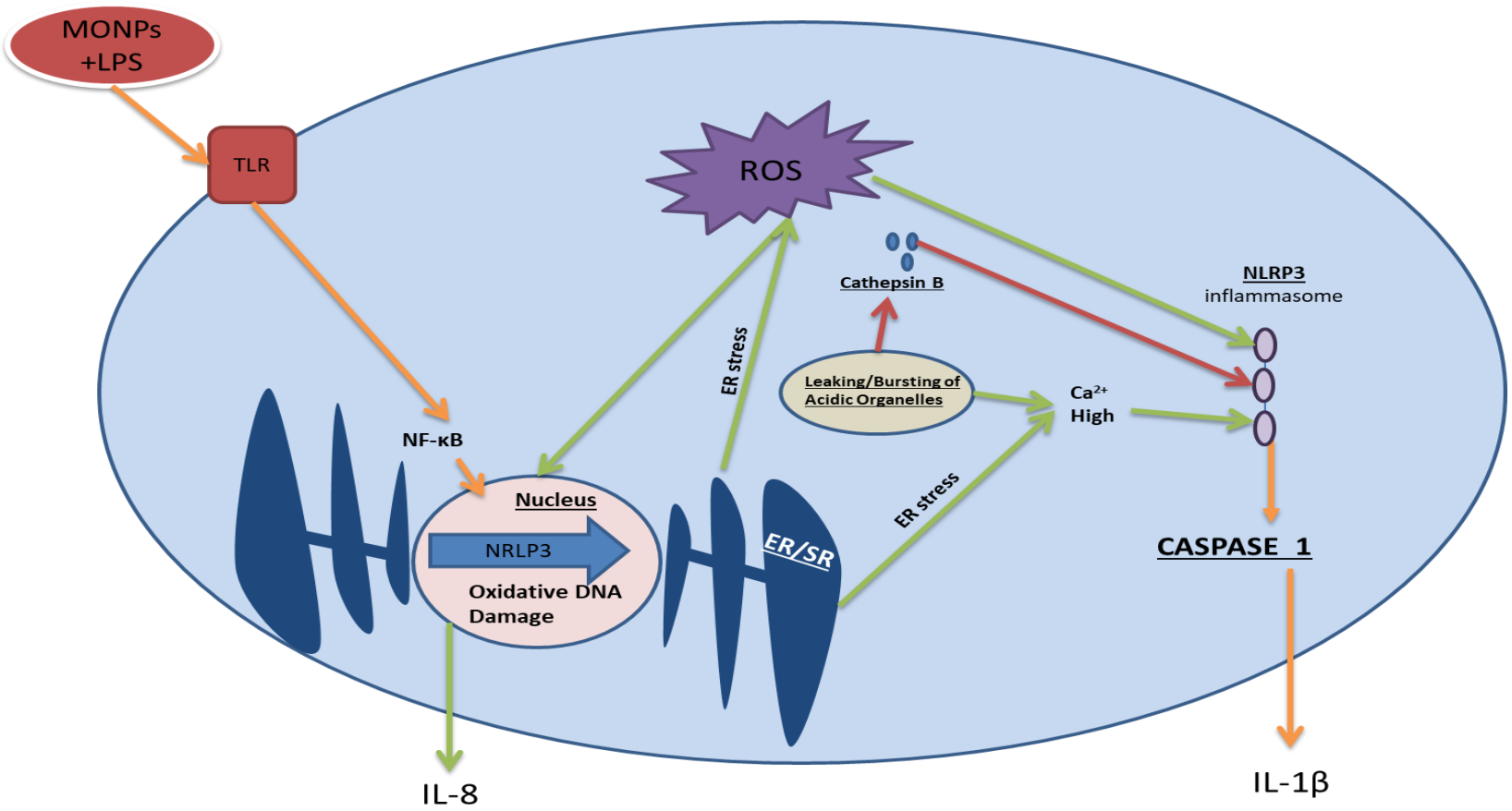

Figure 6. 1: Suggested mechanism for the induction of DNA damage. Actions supported by the results provided in this study are seen in **green arrows** (e.g. Change in cellular redox state, calcium signalling and IL-8 production). Results produced by other studies that support the hypothesis of the activation of the NRLP3 inflammasome are seen in **orange arrows**. Such experiments include Increase in Caspase 1 activity avital component of the inflammasome. Direct interaction of the different MONPs with the TLR and production of NF-κB. Further study required to support the hypothesis of the activation of the NRLP3 can be seen in **red arrows** and is the bursting of acidic organelles and release of will of cathepsin β.

6.6 General Conclusion

The aim of this study was to assess the respective impact of anatase TiO_2 (NM-102), rutile TiO_2 and dSPIONs upon monocytes (THP-1), macrophages (dTHP-1) and hepatocarcinoma (HepG2) cells in both an *in vivo*-resembling physioxic environment *(5%O_2, 5%CO_2)* and a hyperoxic cell culture conditions *(21%O_2, 5%CO_2),* and also to identify the mechanism underlying those impacts. All MONPs were found to interact with the cell lines (with the following sensitivity; dTHP-1>THP-1>HepG2) under both oxygen-content culture environments. However, dSPIONs showed a greater cell interaction in the physioxic culturing environment when compared to the hyperoxic culture environment, suggesting NP dependent uptake is altered in the lower-oxygen content environment. The observed levels of NP-cell interaction corresponded with the results for cytotoxicity and genotoxicity, where the greater the amount of NP-cell interaction, the higher the identified hazardous cytotoxicity or genotoxicity effect. Further investigation of the mechanisms underlying the MONPs toxicity allowed the identification of NP-induced changes in the cellular redox state and increase in cytosolic calcium levels that again were greater in extent in the physioxic culture environment than under hyperoxic conditions. Interestingly the results suggest that the alterations of calcium signalling are not solely dependent on the presence of oxidative stress suggesting that other sequence of NP exposure may also disrupt intracellular calcium homeostasis. As lysosomes are a main cellular calcium store, from which calcium can potentially leak into the cytosol, questions are raised about the integrity of acidic organelles after internalization of MONPs. The synergistic alterations in cellular redox state and intracellular calcium signalling could lead to the identified increase in the production of the inflammatory cytokines TNF-α and IL-8. Environment-specific biological interaction and impacts with regard to NP uptake, genotoxic effects, and consequence on cellular signalling mechanisms were only observed with dSPIONs, while TiO_2 induced similar effects in both environments. These results suggest that changes in magnitude of NP uptake and alterations in cellular homeostasis in the physioxic environment may contribute to enhanced dSPION toxicity. In conclusion, the results suggest distinct alterations in cellular signalling between the two environments, which may be the reason for the greater hazardous behaviour identified in the physioxic culture environment in dSPIONs.

Chapter 7: References

1. Aderem A, Underhill D M (1999) Mechanisms of phagocytosis in macrophages Annu. Rev. Immunol. 17 593–623,

2. Adler, V.; Yin, Z.; Tew, K. D.; Ronai, Z.(1999) Role of redox potential and reactive oxygen species in stress signaling. Oncogene 18: 6104–6111.
3. Ahamed M, Alhadlaq HA, Alam J, Khan MA, Ali D, Alarafi S. (2013) Iron oxide NP-induced oxidative stress and genotoxicity in human skin epithelial and lung epithelial cell lines. Curr Pharm Des 2013;19:6681–90.
4. Alberts B, Johnson A, Lewis J, Raff M, Roberts K, Walter P. (2002). Molecular Biology of the Cell, 4th ed. Garland Science.
5. Almeida JP, Chen AL, Foster A Drezek R (2011). In vivo biodistribution of NPs.*Nanomedicine* 6(5): 815-835.
6. Anzai Y, Piccoli CW, Outwater EK, *(2003)* Radiology for the group evaluation of neck and body metastases to nodes with ferumoxtran 10-enhanced MR imaging: Phase III safety and efficacy study. *Radiology* 228(3): 777-788.
7. Apopa PL, Qian Y, Shao R, Guo NL, Schwegler-Berry D, Pacurari M, Porter D, Shi X, Vallyathan V, Castranova V (2009) Iron oxide NPs induce human microvascular endothelial cell permeability through reactive oxygen species production and microtubule remodeling. Part Fibre Toxicol 6:1.

8. Arias, L., Pessan, J., Vieira, A., Lima, T., Delbem, A. and Monteiro, D., 2018. Iron Oxide Nanoparticles for Biomedical Applications: A Perspective on Synthesis, Drugs, Antimicrobial Activity, and Toxicity. *Antibiotics*, 7(2), p.46.

9. ASHARANI, P. V., HANDE, M. P. & VALIYAVEETTIL, S. 2009. Anti-proliferative activity of silver NPs. BMC cell biology, 10, 65.
10. Ashley, R. and Williams, A.J. 1990. Divalent cation activation and inhibition of single Ca^{2+} release channels from sheep cardiac sarcoplasmic reticulum. The Journal of General Physiology 95(5), pp. 981-1005.
11. Auffan M, Decome L, Rose J, Orsiere T, De Meo M, Briois V, Chaneac C, Olivi L, Berge-Lefranc J-L, Botta A. (2006). In vitro interactions between DMSA-coated maghemite NPs

and human fibroblasts: A physicochemical and cyto-genotoxical study. Environ Sci Technol 40:4367–4373.

12. Baoum A, Dhillon N, Buch S, Berkland C. (2010) Cationic surface modification of PLG NPs offers sustained gene delivery to pulmonary epithelial cells. J Pharm Sci. 99:2413–2422.

13. Baranowska-Wójcik, E., Szwajgier, D., Oleszczuk, P. and Winiarska-Mieczan, A., 2019. Effects of Titanium Dioxide Nanoparticles Exposure on Human Health—a Review. *Biological Trace Element Research*, 193(1), pp.118-129.
14. Barritt, G. 2000. Ca^{2+} Signalling in Liver Cells. Ca^{2+}: The Molecular Basis of Ca^{2+} Action in Biology and Medicine 1, pp. pp 73-94.
15. Behzadi, S., Serpooshan, V., Tao, W., Hamaly, M., Alkawareek, M., Dreaden, E., Brown, D., Alkilany, A., Farokhzad, O. and Mahmoudi, M., 2017. Cellular uptake of nanoparticles: journey inside the cell. *Chemical Society Reviews*, 46(14), pp.4218-4244.

16. Benmerah A., Lamaze C. (2007) Clathrin-coated Pits: Vive La Différence? Traffic, 8:970–982.

17. Bernardi P1, Rasola A.2007. Ca^{2+} and cell death: the mitochondrial connection. Subcell Biochem.
18. Berridge MJ, Lipp P and Bootman MD (2000) The versatility and universality of Ca^{2+} signalling. Nature Reviews Molecular Cell Biology 1: 11–21.
19. Berridge, M. 1998. Neuronal Ca^{2+} Signaling. Neuron 21(1), pp. 13-26.
20. Berridge, M., Bootman, M. and Roderick, H. 2003. Ca^{2+}: Ca^{2+} signalling: dynamics, homeostasis and remodelling. Nature Reviews Molecular Cell Biology 4(7), pp. 517-529.
21. Berridge, M.J., Bootman, M.D., Lipp, P., 1998. Ca^{2+}—a life and death signal. Nature 395, 645–648.
22. Bers, D. 2002. Cardiac excitation–contraction coupling. Nature 415(6868), pp. 198-205.

23. Bhattacharya K, Davoren M, Boertz J, Schins RP, Hoffmann E, Dopp E.(2009). Titanium dioxide NPs induce oxidative stress and DNA-adduct formation but not DNA-breakage in human lung cells. Part Fibre Toxicol 6:17.

24. Bigini P, Diana V, Barbera S, Fumagalli E, Micotti E, Sitia L, Paladini A, Bisighini C, De Grada L, Coloca L (2012) Longitudinal tracking of human fetal cells labeled with super paramagnetic iron oxide NPs in the brain of mice with motor neuron disease.
25. Bonner J.C (2007) Lung fibrotic responses to particle exposure. Toxicologic Pathology, 35:1, 148–153.
26. Bootman, M., Rietdorf, K., Collins, T., Walker, S. and Sanderson, M. 2013. Ca^{2+}-Sensitive Fluorescent Dyes and Intracellular Ca^{2+} Imaging. Cold Spring Harbor Protocols 2013(2), pp. pdb.top066050-pdb.top066050.
27. Bootman, Martin D; Rietdorf, Katja; Hardy, Holly; Dautova, Yana; Corps, Elaine; Pierro, Cristina; Stapleton, Eloise; Kang, Esther; and Proudfoot, Diane (October 2012) Ca^{2+} Signalling and Regulation of Cell Function. In: eLS. John Wiley & Sons, Ltd: Chichester. DOI: 10.1002/9780470015902.a0001265.pub3
28. Borm P.J.A, Robbins D, Haubold S, Kuhlbusch T, Fissan H, Donaldson K, Schins R.P.F, Stone V, Kreyling W, Lademann J, Krutmann J, Warheit D, Oberdorster E. (2006) The potential risks of NPs: a review carried out for ECETOC (review) Part. Fibre Toxicol. 3, 11.
29. Bourrinet P, Bengele HH, Bonnemain B, Dencausse A, Idee J-M, Jacobs PM, Lewis JM. (2006) Preclinical safety and pharmacokinetic profile of ferumoxtran-10, an ultrasmall superparamagnetic iron oxide magnetic resonance contrast agent. Invest Radiol 41:313–324.
30. Brown SC, Kamal M, Nasreen N, Baumuratov A, Sharma P, Antony VB(2009) Influence of shape, adhesion and simulated lung mechanics on amorphous silica NP toxicity. Adv Powder Technol. 18:69–79.
31. Brown, D. (2004). Ca^{2+} and ROS-mediated activation of transcription factors and TNF-cytokine gene expression in macrophages exposed to ultrafine particles. AJP: Lung Cellular and Molecular Physiology, 286(2), pp.344L-353.
32. Brown, D., Donaldson, K. and Stone, V. (2002). Role of Ca^{2+} in the Induction of TNF Expression by Macrophages on Exposure to Ultrafine Particles. Annals of Occupational Hygiene, 46(Suppl. 1), pp.219-222.

33. Burdakov, D. 2005. Physiological Changes in Glucose Differentially Modulate the Excitability of Hypothalamic Melanin-Concentrating Hormone and Orexin Neurons In Situ. Journal of Neuroscience 25(9), pp. 2429-2433.
34. Burgos J.S. (2005) Involvement of the Epstein-Barr virus in the nasopharyngeal carcinoma pathogenesis Med. Oncol. 22, 113-121.
35. Buyukhatipoglu K, Clyne AM (2011) Superparamagnetic iron oxide NPs change endothelial cell morphology and mechanics via reactive oxygen species formation. J Biomed Mater Res A 96:186–195.
36. Buzea C, Pacheco I, Robbie K. (2007) NPs and NPs: sources and toxicity. Biointerphases. 2:MR17–MR71.
37. Carafoli, E. 1974. The release of Ca^{2+} from heart mitochondria by sodium. Journal of Molecular and Cellular Cardiology 6(4), pp. 361-371.
38. Carafoli, E. 2003. Timeline: The Ca^{2+}-signalling saga: tap water and protein crystals. Nature Reviews Molecular Cell Biology 4(4), pp. 326-332.
39. Castilho, R.F., Carvalho-Alves, P.C., Vercesi, A.E., Ferreira, S.T., 1996. Oxidative damage to sarcoplasmic reticulum $Ca(^{2+})$-pump induced by Fe^{2+}/H2O2/ascorbate is not mediated by lipid peroxidation or thiol oxidation and leads to protein fragmentation. Mol. Cell Biochem. 159, 105–114.
40. Castranova V, Huffman L.J, Judy D.J (1998) Enhancement of nitric oxide production by pulmonary cells following silica exposure. Environmental Health Perspectives,106: 5,1165–1169.
41. Cavalli S, Carbajo D, Acosta M (2012) Efficient γ-amino-proline-derived cell penetrating peptide–superparamagnetic iron oxide NP conjugates via aniline-catalyzed oxime chemistry as bimodal imaging nanoagents. *Chem. Commun.* 48: 5322-5324.
42. Champion JA, Mitragotri S. (2009) Shape induced inhibition of phagocytosis of polymer particles. Pharm Res. 26:244–249.
43. Chen T, Shukoor MI, Wang R, (2011) Smart multifunctional nanostructure for targeted cancer chemotherapy and magnetic resonance imaging. *ACS Nano* 5(10):7866–7873.
44. CHEN, E. Y., GARNICA, M., WANG, Y. C., CHEN, C. S. & CHIN, W. C. 2011. Mucin secretion induced by titanium dioxide NPs. PloS one, 6, e16198.

45. CHEN, E. Y., GARNICA, M., WANG, Y. C., MINTZ, A. J., CHEN, C. S. & CHIN, W. C. 2012a. A mixture of anatase and rutile TiO(2) NPs induces histamine secretion in mast cells. Particle and fibre toxicology, 9, 2.
46. CHEN, Z., YIN, J. J., ZHOU, Y. T., ZHANG, Y., SONG, L., SONG, M., HU, S. & GU, N. 2012b. Dual enzyme-like activities of iron oxide NPs and their implication for diminishing cytotoxicity. ACS nano, 6, 4001-12.

47. Chithrani BD, Chan WCW. (2007). Elucidating the mechanism of cellular uptake and removal of protein-coated gold NPs of different sizes and shapes. Nano Lett 7:1542–1550.
48. Chithrani BD, Ghazani AA, Chan WCW. (2006). Determining the size and shape dependence of gold NP uptake into mammalian cells. Nano Lett 6:662–668.

49. Christensen K, Myers J, Swanson J (2002), pH-dependent regulation of lysosomal Ca^{2+} in macrophages, J. Cell. Sci. 115 599–607.

50. Clemente-Casares X, Santamaria P (2014) Nanomedicine in autoimmunity. *Immunol Lett*. 158: 167–174.

51. Clift, M., Boyles, M., Brown, D. and Stone, V. (2009). An investigation into the potential for different surface-coated quantum dots to cause oxidative stress and affect macrophage cell signalling in vitro. Nanotoxicology, 4(2), pp.139-149.

52. Conner SD, Schmid SL. (2003). Regulated portals of entry into the cell. Nature 422:37–44.

53. Cook, S. and Lockyer, P. 2006. Recent advances in Ca^{2+}-dependent Ras regulation and cell proliferation. Cell Ca^{2+} 39(2), pp. 101-112.
54. Crabtree GR, Olson EN. NFAT signaling: choreographing the social lives of cells. Cell. 2002;109:S67–S79

55. Crist RM, Grossman JH, Patri AK, Stern ST, Dobrovolskaia MA, Adiseshaiah PP, (2013) Common pitfalls in nanotechnology: lessons learned from NCI's nanotechnology characterization laboratory. Integr Biol (Camb). 5:66–73.

56. CROMPTON, M., MOSER, R., LUDI, H. and CARAFOLI, E. 1978. The Interrelations between the Transport of Sodium and Ca^{2+} in Mitochondria of Various Mammalian Tissues. Eur J Biochem 82(1), pp. 25-31.

57. D'Arienzo A, Scaglione G, Bennato R(2001)The prognostic value, in active ulcerative colitis, of an increased intensity of colonic perivisceral fat signal on magnetic resonance imaging with ferumoxil. *Am. J. Gastroenterol*. 96(2): 481–486.

58. De Koninck, P. and Schulman, H. 1998. Sensitivity of CaM Kinase II to the Frequency of Ca^{2+} Oscillations. Science 279(5348), pp. 227-230.

59. Decuzzi P, Pasqualini R, Arap W, Ferrari M. (2009) Intravascular delivery of particulate systems: does geometry really matter? Pharm Res. 26:235–243.

60. Degnan AJ, Patterson AJ, Tang TY, Howarth SP, Gillard JH. (2012) Evaluation of ultrasmall superparamagnetic iron oxide-enhanced MRI of carotid atherosclerosis to assess risk of cerebrovascular and cardiovascular events: Followup of the ATHEROMA trial. *Cerebrovasc. Dis*. 34(2): 169–173.

61. Delva E., J.M. Jennings J.M., Calkins C.C. (2008) Pemphigus vulgaris IgG-induced desmoglein-3 endocytosis and desmosomal disassembly are mediated by a clathrin-and dynamin-independent mechanism. J Biol Chem, 283:18303–18313.

62. Destouches D, Page N, Hamma-Kourbali Y (2011) A simple approach to cancer therapy afforded by multivalent pseudopeptides that target cell-surface nucleoproteins. *Cancer Res.* 71(9): 3296–3305.

63. Dilnawaz F, Singh A, Mohanty C, Sahoo SK. (2011) Dual drug loaded superparamagnetic iron oxide NPs for targeted cancer therapy. *Biomaterials* 31(13), 3694–3706

64. DiMaio D, Liao J.B. (2006) Human papillomaviruses and cervical cancer Adv. Virus. Res. 66, 125-159.

65. Doherty GJ, McMahon HT. (2009). Mechanisms of endocytosis. Annu Rev Biochem 78:857–902.

66. Dolmetsch, R. 2003. Excitation-Transcription Coupling: Signaling by Ion Channels to the Nucleus. Science Signaling 2003(166), pp. pe4-pe4.

67. Dolmetsch, R. E., Xu, K. & Lewis, R. S. Ca^{2+} oscillations increase the efficiency and specificity of gene expression. Nature 392, 933–936 (1998).
68. Dolmetsch, R., Lewis, R., Goodnow, C. and Healy, J. 1997. Differential activation of transcription factors induced by Ca^{2+} response amplitude and duration. Nature 386(6627), pp. 855-858.

69. Donaldson K, Stone V 2003 Current hypotheses on the mechanisms of toxicity of ultrafine particles Ann. Ist. Super Sanita. 39, 405-410.
70. Donaldson K, Stone V, Tran C, Kreyling W, Borm P.J.A. (2004) Nanotoxicology Occup. Environ. Med. 6, 727-728.

71. Dubes, V., Parpaite, T., Ducret, T., Quignard, J., Mornet, S., Reinhardt, N., Baudrimont, I., Dubois, M., Freund-Michel, V., Marthan, R., Muller, B., Savineau, J. and Courtois, A., 2017. Calcium signalling induced by in vitro exposure to silicium dioxide nanoparticles in rat pulmonary artery smooth muscle cells. *Toxicology*, 375, pp.37-47.
72. Duffin, R., Tran, C., Clouter, A., Brown, D., MacNee, W., Stone, V. and Donaldson, K. (2002). The Importance of Surface Area and Specific Reactivity in the Acute Pulmonary Inflammatory Response to Particles. Annals of Occupational Hygiene, 46(Suppl. 1), pp.242-245.

73. Duguet E (2006) Magnetic NPs and their applications in medicine. Nanomed. 1(2):157–68.

74. Dunne, J. F. Time window analysis and sorting. Cytometry 12: 597–601, 1991. Gee, K., Brown, K., Chen, W., Bishop-Stewart, J., Gray, D. and Johnson, I. 2000. Chemical and physiological characterization of fluo-4 Ca^{2+}-indicator dyes. Cell Ca^{2+} 27(2), pp. 97-106.
75. Dupont G, Combettes L, Bird GS and Putney JW (2011) Ca^{2+} oscillations. Cold Spring Harbor Perspectives in Biology 3: a004226

76. Dwivedi S, Siddiqui MA, Farshori NN, Ahamed M, Musarrat J, Al- Khedhairy AA. (2014) Synthesis, characterization and toxicological evaluation of iron oxide NPs in human lung alveolar epithelial cells. Colloids Surf B Biointerfaces 122:209–215.
77. Eaton JW, Qian M. (2002) Molecular bases of cellular iron toxicity. Free Radic Biol Med 32:833–840.

78. El Badawy AM, Silva RG, Morris B, Scheckel KG, Suidan MT, Tolaymat TM. (2010) Surface charge dependent toxicity of silver NPs. Environ Sci Technol. 45:283–287.

79. Elliott, S.J., Meszaros, J.G., Schilling, W.P., 1992. Effect of oxidant stress on Ca^{2+} signaling in vascular endothelial cells. Free Rad. Biol. Med. 13, 635–650.

80. El-Sayed Ivan H, Huang Xiaohua, El-Sayed Mostafa A. (2006) Selective laser photo-thermal therapy of epithelial carcinoma using anti-EGFR antibody conjugated gold NPs. Cancer Letters: 239,129–135.

81. Ermak, G., Morgan, T.E., Davies, K.J.A., 2001. Chronic overexpression of the calcineurin inhibitory gene DSCR1 (Adapt78) is associated with Alzheimer disease. J. Biol. Chem. 42, 38787–38794.

82. Ermak, G.; Davies, K. J. (2002) Ca^{2+} and oxidative stress: from cell signaling to cell death. Mol. Immunol. 38:713–721.

83. Etheridge ML, Campbell SA, Erdman AG, Haynes CL, Wolf SM, McCullough J.(2013) The big picture on nanomedicine: the state of investigational and approved nanomedicine products. Nanomed Nanotechnol Biol Med. 9:1–14.

84. Evans, S., Clift, M., Singh, N., Wills, J., Hondow, N., Wilkinson, T., Burgum, M., Brown, A., Jenkins, G. and Doak, S., 2019. In vitro detection of in vitro secondary mechanisms of genotoxicity induced by engineered nanomaterials. *Particle and Fibre Toxicology*, 16(1).

85. Fan C, Gao W, Chen Z, *(2011)* Tumor selectivity of stealth multi-functionalized superparamagnetic iron oxide NPs. *Int. J. Pharm.* 404(1-2), 180–190.

86. Fearnley, C., Roderick, H. and Bootman, M. 2011. Ca^{2+} Signaling in Cardiac Myocytes. Cold Spring Harbor Perspectives in Biology 3(11), pp. a004242-a004242.

87. Feng, X. and Yang, J., 2016. Lysosomal Calcium in Neurodegeneration. *Messenger*, 5(1), pp.56-66.

88. Ferguson PM, Feindel KW, Slocombe A (2013) Strongly magnetic iron NPs improve the diagnosis of small tumours in the reticuloendothelial system by magnetic resonance imaging. *PLoS One* 8: e56572.

89. Ferrari M. (2005) Cancer nanotechnology: opportunities and challenges. Nat Rev Cancer 5:161–71.
90. Ferrari M. (2008) Nanogeometry: beyond drug delivery. Nat Nanotechnol. 3:131–132. Ferreira L, Karp JM, Nobre L, Langer R (2008) New opportunities: The use of nanotechnologies to manipulate and track stem cells. *Cell Stem Cell* 3(2): 136–146.
91. Feske, S., Gwack, Y., Prakriya, M., Srikanth, S., Puppel, S., Tanasa, B. and Hogan, P. *et. al.* 2006. A mutation in Orai1 causes immune deficiency by abrogating CRAC channel function. Nature 441(7090), pp. 179-185.
92. Fiskum, G. and Lehninger, A. 1979. Regulated release of Ca^{2+} from respiring mitochondria by Ca^{2+}/2H+ antiport. J. Biol. Chem. 254, p. 6236
93. Fixemer, T., Wissenbach, U., Flockerzi, V. and Bonkhoff, H. 2003. Expression of the Ca^{2+}-selective cation channel TRPV6 in human prostate cancer: a novel prognostic marker for tumor progression. Oncogene 22(49), pp. 7858-7861.
94. Flavell, S.W. and Greenberg, M.E. (2008) Signaling mechanisms linking neuronal activity to gene expression and plasticity of the nervous system. Annu. Rev. Neurosci. **31**, 563–590.
95. Fohlman J, Friman G. (1993) Is juvenile diabetes a viral disease? Ann. Med. 25, 569-574.
96. Forest V, Pailleux M, Pourchez J, Boudard D, Tomatis M, Fubini B, Sennour M, Hochepied JF, Grosseau P, Cottier M. Toxicity of boehmite nanoparticles: impact of the ultrafine fraction and of the agglomerates size on cytotoxicity and pro-inflammatory response. Inhal Toxicol. 2014;26:545–553.
97. Freitas MLL, Silva LP, Azevedo RB, Garcia VAP, Lacava LM, Grisolia CK, Lucci CM, Morais PC, Da Silva MF, Buske N (2002). A double-coated magnetite-based magnetic fluid evaluation by cytometry and genetic tests. J Magn Magn Mater 252:396–398.
98. FUTREAL, P., WOOSTER, R. and STRATTON, M. 2005. Somatic Mutations in Human Cancer: Insights from Resequencing the Protein Kinase Gene Family. Cold Spring Harbor Symposia on Quantitative Biology 70(0), pp. 43-49.

99. Gaglia JL, Guimaraes AR, Harisinghani M (2010) Noninvasive imaging of pancreatic islet inflammation in type 1A diabetes patients. *J. Clin. Invest*. 121(1):442–445.

100. Gaido, M.L., Cidlowski, J.A., 1991. Identification, purification, and characterization of a Ca^{2+}-dependent endonuclease (NUC18) from apoptotic rat thymocytes. NUC18 is not histone H2B. J. Biol. Chem. 266, 18580–18585.

101. Galione A (2011) NAADP receptors. Cold Spring Harbor Perspectives in Biology 3: a004036.

102. Galione, A. and Churchill, G. 2002. Interactions between Ca^{2+} release pathways: multiple messengers and multiple stores. Cell Ca^{2+} 32(5-6), pp. 343-354.

103. Galione, A., Morgan, A., Arredouani, A., Davis, L., Rietdorf, K., Ruas, M. and Parrington, J. (2010). NAADP as an intracellular messenger regulating lysosomal Ca^{2+}-release channels. *Biochm. Soc. Trans.*, 38(6), pp.1424-1431.

104. Gao H, Shi W, Freund LB. 2005. Mechanics of receptor-mediated endocytosis. Proc Natl Acad Sci U S A 102:9469–9474.

105. Garnet M C, Kallinteri P (2006) Nanomedicines and nanotoxicology: some physiological principles Occ. Med. 56 307-311

106. Geiser M, Rothen-Rutishauser B, Kapp N, Schürch S, Kreyling W, Schulz H, Semmler M, Hof VI, Heyder J, Gehr P. (2005). Ultrafine particles cross cellular membranes by nonphagocytic mechanisms in lungs and in cultured cells. Environ Health Perspect 113:1555–1560.

107. George S, Lin S, Ji Z, Thomas CR, Li L, Mecklenburg M (2012) Surface defects on plate-shaped silver NPs contribute to its hazard potential in a fish gill cell line and zebrafish embryos. ACS Nano. 6:3745–3759.

108. Gilardino, A., Catalano, F., Ruffinatti, F., Alberto, G., Nilius, B., Antoniotti, S., Martra, G. and Lovisolo, D. (2015). Interaction of SiO2 NPs with neuronal cells: Ionic mechanisms involved in the perturbation of Ca^{2+} homeostasis. The International Journal of Biochemistry & Cell Biology, 66, pp.101-111.

109. Goldstein JL, Brown MS, Anderson RGW, Russell DW, Schneider WJ. (1985). Receptor-mediated endocytosis: Concepts emerging from the LDL receptor system. Ann Rev Cell Biol 1:1–39.

110. Golovina, V. and Blaustein M. P. 1997. Spatially and Functionally Distinct Ca^{2+} Stores in Sarcoplasmic and Endoplasmic Reticulum. Science 275(5306), pp. 1643-1648.

111. Goonasekera, S. and Molkentin, J. 2012. Unraveling the secrets of a double life: Contractile versus signaling Ca^{2+} in a cardiac myocyte. Journal of Molecular and Cellular Cardiology 52(2), pp. 317-322.

112. Graier, W., Hoebel, B., Paltauf-Doburzynska, J. and Kostner, G. (1998). Effects of Superoxide Anions on Endothelial Ca^{2+} Signaling Pathways. Arteriosclerosis, Thrombosis, and Vascular Biology, 18(9), pp.1470-1479.

113. Gratton SE, Ropp PA, Pohlhaus PD, Luft JC, Madden VJ, Napier ME (2008) The effect of particle design on cellular internalization pathways. Proc Nat. Aca. Sci USA 105:11613–8.

114. Greish K, Thiagarajan G, Herd H, Price R, Bauer H, Hubbard D, Burckle A, Sadekar S, Yu T, Anwar A. 2012Size and Surface Charge Significantly Influence the Toxicity of Silica and Dendritic Nanoparticles. Nanotoxicology. 6:pp713–723.

115. Griffiths, E.J., Ocampo, C.J., Savage, J.S., Rutter, G.A., Hansford, R.G., Stern, M.D., Silverman, H.S., 1998. Mitochondrial Ca^{2+} transporting pathways during hypoxia and reoxygenation in single rat cardiomyocytes. Cardiovasc. Res. 39, 423–433.

116. Grove J, Marsh M. (2011). The cell biology of receptor-mediated virus entry. J Cell Biol 195:1071–1082.

117. Grover, A.K., Samson, S.E., 1988. Effect of superoxide radical on Ca^{2+} pumps of coronary artery. Am. J. Physiol. 255, C297–C303.

118. Grover, A.K., Samson, S.E., Fomin, V.P., 1992. Peroxide inactivates Ca^{2+} pumps in pig coronary artery. Am. J. Physiol. 263, H537– H543.

119. Grynkiewicz Grzegorz,Poenie Martin, Tsien Roger (1985) A new generation of Ca^{2+} Indicators with greatly improved Fluorescence properties. The journal of biological Chemistry. 260 (6):3440-3450.

120. Grynkiewicz, G., M. Poenie, AND R. Y. Tsien. A new generation of Ca21 indicators with greatly improved fluorescence properties. J. Biol. Chem. 260: 3440–3450, 1985.

121. Guichard Y, Schmit J, Darne C, Gat_e L, Goutet M, Rousset D, Rastoix O, Wrobel R, Witschger O, Martin A (2012) Cytotoxicity and genotoxicity of nanosized and microsized titanium dioxide and iron oxide particles in Syrian hamster embryo cells. Ann Occup Hyg 56: 631–644.

122. Gunter, T.E., Buntinas, L., Sparagna, G.C., Gunter, K.K., 1998. The Ca^{2+} transport mechanisms of mitochondria and Ca^{2+} uptake from physiological-type Ca^{2+} transients. Biochim. Biophys. Acta 1366, 5– 15.

123. Hachani R, Lowdell M, Birchall M, Thanh NT. (2013) Tracking stem cells in tissue-engineered organs using magnetic NPs. Nanoscale. 5:11362–11372.

124. Hall JB, Dobrovolskaia MA, Patri AK, McNeil SE (2007) Characterization of NPs for therapeutics. Nanomedicine (London). 2:789–803.

125. Hanahan, D. & Weinberg, R. A. The hallmarks of cancer. Cell 100, 57–70 (2000)

126. Hanini A, Schmitt A, Kacem K, Chau F, Ammar S, Gavard J (2011)Evaluation of iron oxide NP biocompatibility. Int J Nanomed 6:787–794.

127. Hardie, R. 2006. TRP channels and lipids: from Drosophila to mammalian physiology. The Journal of Physiology 578(1), pp. 9-24

128. Hardman R. (2006) A toxicologic review of quantum dots: toxicity depends on physicochemical and environmental factors. Environ Health Perspect. 114:165–172.

129. Harisinghani MG, Barentsz J, Hahn PF (2003) Noninvasive detection of clinically occult lymphnode metastases in prostate cancer. *N. Engl. J. Med*. 348, 2491–2499.

130. He C, Hu Y, Yin L, Tang C, Yin C. (2010) Effects of particle size and surface charge on cellular uptake and biodistribution of polymeric NPs. Biomaterials 31:3657–3666.

131. He X, Young, Schwegler-Berry S, Chisholm W.P, Fernback J.E, Ma Q (2011), Multiwalled carbon nanotubes induce a fibrogenic response bystimulating reactive oxygen species production, activating NF-κB signaling, and promoting fibroblast-to-myofibroblast transformation. Chemical Research in Toxicology, 24:12, 2237–2248.

132. Herbig ME, Assi F, Textor M, Merkle HP.(2006) The cell penetrating peptides pVEC and W2-pVEC induce transformation of gel phase domains in phospholipid bilayers without affecting their integrity. Biochemistry 45(11):3598-609.

133. Hetzel D, Strauss W, Bernard K, Li Z, Urboniene A, Allen LF (2014) A Phase III, randomized, open-label trial of ferumoxytol compared with iron sucrose for the treatment of iron deficiency anemia in patients with a history of unsatisfactory oral iron therapy. *Am. J. Hematol*. 89(6): 646-650.

134. Hildebrand H, Kuhnel D, Potthoff A, Mackenzie K, Springer A, Schirmer K. (2010) Evaluating the cytotoxicity of palladium/magnetite nano-catalysts intended for wastewater treatment. Environ Pollut 158:65–73.

135. Ho N, Gullberg M, Chatila T. Activation protein 1-dependent transcriptional activation of interleukin 2 gene by Ca^{2+}/calmodulin kinase type IV/Gr. J Exp Med. 1996;184:101–112.

136. Hofer, A. and Machen, T. 1993. Technique for in situ measurement of Ca^{2+} in intracellular inositol 1,4,5-trisphosphate-sensitive stores using the fluorescent indicator mag-fura-2. Proceedings of the National Academy of Sciences 90(7), pp. 2598-2602.

137. Hogan, P. Chen, L., Nardone, J. and Rao, A. 2003. Transcriptional regulation by Ca^{2+}, calcineurin, and NFAT. Genes & Development 17(18), pp. 2205-2232.

138. Hondow Nicole, Harrington John, Brydson Rick, Doak Shareen, Singh Neenu, Manshian Bella, Brown Andy (2010) STEM mode in the SEM: A practical tool for nanotoxicology. Nanotoxicology, 1–13.

139. Hong SC, Lee JH, Lee J, Kim HY, Park JY, Cho J, Lee J, Han D-W (2011) Subtle cytotoxicity and genotoxicity differences in superparamagnetic iron oxide NPs coated with various functional groups. Int J Nanomed 6:3219–3231.

140. Hu Y, Litwin T, Nagaraja AR, Kwong B, Katz J, Watson N, Irvine DJ.(2007) Cytosolic delivery of membrane-impermeable molecules in dendritic cells using pH-responsive core-shell NPs. Nano Lett. (10):3056-64.

141. Huang Y, Wu C, and Aronstam R (2010) Toxicity of transition metal oxide NPs: recent insights from in vitro Studies," Materials 3:10,4842–4859.

142. Huang YF, Liu H, Xiong X, Chen Y, Tan W. 2009. NP-mediated IgEreceptor aggregation and signaling in RBL mast cells. J Am Chem Soc 131: 17328–17334.

143. Huang, J. B., Kindzelskii, A. L., Clark, A. J. & Petty, H. R.(2004) fication of channels promoting Ca^{2+} spikes and waves in HT1080 tumor cells: their apparent roles in cell motility and invasion. Cancer Res. 64, 2482–2489.

144. Inoue K I, Takano H, Yanagisawa R, Hirano S, Ichinose T, Shimada A, Yoshikawa T (2006) The role of toll-like receptor 4 in the airway inflammation induced by diesel exhaust particles Arch. Toxicol. 80 275279

145. Ispas C, Andreescu D, Patel A, Goia DV, Andreescu S, Wallace KN. (2009)Toxicity and developmental defects of different sizes and shape nickel NPs in zebrafish. Environ Sci Technol. 43:6349–6356.

146. Itzhaki R.F, Wozniak M.A, Appelt D.M, Balin B J. (2004) Infiltration of the brain by pathogens causes Alzheimer's disease Neurobiol. Aging. 25, 619-627.

147. Jain, S., Coulter, J., Butterworth, K., Hounsell, A., McMahon, S., Hyland, W., Muir, M., Dickson, G., Prise, K., Currell, F., Hirst, D. and O'Sullivan, J., 2014. Gold nanoparticle cellular uptake, toxicity and radiosensitisation in hypoxic conditions. *Radiotherapy and Oncology*, 110(2), pp.342-347.

148. Jarrett R. F. (2006) Viruses and lymphoma/leukaemia J. Pathol. 208 176–186.

149. Jiang J, Oberdorster G, Biswas P. (2009) Characterisation of size, surface charge and agglomeration state of NP dispersions for toxicological studies. J Nanopart Res 11:77–89.

150. Jiang W, Kim BY, Rutka JT, Chan WC (2008) NP-mediated cellular response is size-dependent. Nat Nanotechnol. (3):145-50.

151. Jiang X, Qu W, Pan D, Ren Y, Williford JM, Cui H (2013) Plasmid-templated shape control of condensed DNA-block copolymer NPs. Adv Mater. 25:227–232.

152. Johannsen M, Gneveckow U, Taymoorian K (2007) Morbidity and quality of life during thermotherapy using magnetic NPs in locally recurrent prostate cancer: Results of a prospective phase I trial. *Int. J. Hyperth.* 23(3): 315–323.

153. Johnston H.J, Hutchison G, Christensen F.M, Peters S, Hankin S and Stone V (2010), "A review of the in vivo and in vitro toxicity of silver and gold particulates: particle attributes and biological mechanisms responsible for the observed toxicity," CriticalReviewsinToxicology,40:4, 328–346.

154. Kahl, C. and Means, A. 2003. Regulation of Cell Cycle Progression by Ca^{2+}/Calmodulin-Dependent Pathways. Endocrine Reviews 24(6), pp. 719-736.

155. Kajander E.O. and Çiftçioglu N. (1998) Nanobacteria: an alternative mechanism for pathogenic intra- and extracellular calcification and stone formation Proc. Natl. Acad. Sci. 95, 8274-8279.

156. Kaneko, M., Matsumoto, Y., Hayashi, H., Kobayashi, A., Yamazaki, N., 1994. Oxygen free radicals and Ca^{2+} homeostasis in the heart. Mol. Cell Biochem. 135, 99–108.

157. Kang HW, Josephson L, Petrovsky A, Weissleder R, Bogdanov A Jr(2002). Magnetic resonance imaging of inducible E-selectin expression in human endothelial cell culture. *Bioconjug. Chem.* 13(1): 122–127.

158. Karlsson HL, Gustafsson J, Cronholm P, Möller L (2009) Size-dependent toxicity of metal oxide particles—a comparison between nano- and micrometer size. Toxicol Lett. 188:112–118.

159. Karussis D, Karageorgiou C, Vaknin-Dembinsky A, Gowda-Kurkalli B, Gomori JM, Kassis I, Bulte JW, Petrou P, Ben-Hur T, Abramsky O, Slavin S (2013) Safety and immunological effects of mesenchymal stem cell transplantation in patients with multiple sclerosis and amyotrophic lateral sclerosis. *Arch. Neurol.* 67(10): 1187–1194.

160. Kasamatsu H., Nakanishi A. (1998) How do animal DNA viruses get to the nucleus? Annu Rev Microbiol, 52: 627–686.

161. Kelly, K. A. Very early detection of changes associated with cellular activation using a modified flow cytometer. Cytometry 12: 464–468, 1991

162. Kennedy J.M, Wilson D, Barakat A.I (2009) Uptake and inflammatory effects of NPs in a human vascular endothelial cell line. Research Report, 136:3–32.

163. Khalil I.A., Kogure K., Akita H. (2006) Uptake pathways and subsequent intracellular trafficking in nonviral gene deliveryPharmacol Rev, 58: 32–45.

164. Khan J. A., Pillai B, Das T. K., Singh Y.,Maiti S. (2007)Molecular effects of uptake of gold NPs in HeLa cells. ChemBioChem 8, 1237.

165. Khanna, P., Ong, C., Bay, B. and Baeg, G., 2015. Nanotoxicity: An Interplay of Oxidative Stress, Inflammation and Cell Death. *Nanomaterials*, 5(3), pp.1163-1180.

166. Kim JE, Shin JY, Cho MH (2012) Magnetic NPs: an update of application for drug delivery and possible toxic effects. Arch Toxicol. 86(5):685-700.

167. Kim TH, Kim M, Park HS, Shin US, Gong MS, Kim HW. (2012) Size-dependent cellular toxicity of silver NPs. J Biomed Mater Res A. 100:1033–1043.

168. Kittelson D.B. (2001) Recent measurements of NP emission from engines Current Research on Diesel Exhaust Particles, Japan Association of Aerosol Science and Technology, Tokyo, Japan.

169. Kizilel S, Nazli C, Ergenc, Acar, HY (2012) RGDSfunctionalized polyethylene glycol hydrogel-coated magnetic iron oxide NPs enhance specific intracellular uptake by HeLa cells. *Int. J. Nanomedicine* 7: 1903-1920.

170. Knaapen A.M, Borm P.J.A, Albrecht C, Schins R.P.F (2004) Inhaled particles and lung cancer, partA: mechanisms. International Journal of Cancer,109:6, 799–809.

171. Kobzik L (1995) Lung macrophage uptake of unposonized environmental particulates. Role of scavenger-type receptors J. Immunol. 155 367-376

172. Koch, G. 1990. The endoplasmic reticulum and Ca^{2+} storage. Bioessays 12(11), pp. 527-531.

173. Kol A, Santini M. (2004) Infectious agents and atherosclerosis: current perspectives and unsolved issues Ital. Heart J. 5, 350-357.

174. Konczol M, Ebeling S, Goldenberg E, Treude F, Gminski R, Gier_e R, Grob_ety B, Rothen-Rutishauser B, Merfort I, Mersch- Sundermann V. 2011. Cytotoxicity and

genotoxicity of sizefractionated iron oxide (magnetite) in A549 human lung epithelial cells: role of ROS, JNK, and NF-jB. Chem Res Toxicol 24: 1460–1475.

175. Kondo E, Saito K, Tashiro Y (2012) Tumour lineagehoming cell-penetrating peptides as anticancer molecular delivery systems. *Nat. Commun.* 3: 951.

176. Kota, S., Hou, S., Guerrant, W., Madoux, F., Troutman, S., Fernandez-Vega, V., Alekseeva, N., Madala, N., Scampavia, L., Kissil, J. and Spicer, T., 2018. A novel three-dimensional high-throughput screening approach identifies inducers of a mutant KRAS selective lethal phenotype. *Oncogene*, 37(32), pp.4372-4384.

177. Kuhn, D., Vanhecke, D., Michen, B., Blank, F., Gehr, P., Petri-Fink, A. and Rothen-Rutishauser, B., 2014. Different endocytotic uptake mechanisms for nanoparticles in epithelial cells and macrophages. *Beilstein Journal of Nanotechnology*, 5, pp.1625-1636.

178. Kunzmann A, Andersson B, Vogt C, Feliu N, Ye F, Gabrielsson S, Toprak MS, Buerki-Thurnherr T, Laurent S, Vahter M, *et. al.* (2011) Efficient internalization of silica-coated iron oxide NPs of different sizes by primary human macrophages and dendritic cells. Toxicol Appl Pharmacol 253:81–93.

179. Kusters J.G, van Vliet A.H, Kuipers E.J. (2006) Pathogenesis of Helicobacter pylori infection Clin. Microbiol. Rev. 19, 449-490.

180. Kuum, M., Veksler, V. and Kaasik, A. (2015). Potassium fluxes across the endoplasmic reticulum and their role in endoplasmic reticulum Ca^{2+} homeostasis. *Cell Ca^{2+}*, 58(1), pp.79-85.

181. Lead JR. (2009). Environmental and Human Health Impacts of Nanotechnology. Wiley-Blackwell, Chippenham, UK.

182. Lehen'Kyi, V., Flourakis, M., Skryma, R. and Prevarskaya, N. 2007. TRPV6 channel controls prostate cancer cell proliferation via Ca^{2+}/NFAT-dependent pathways. Oncogene 26(52), pp. 7380-7385.

183. Leroueil P. R., Berry S. A., Duthie K., Han G. , Rotello V. M., McNerny D. Q., Baker J. R., Orr B. G., M. Holl M. B. (2008) The Interaction of Polycationic Organic Polymers with Biological Membranes. Nano Lett. 8, 420.

184. Levrero M. (2006) Viral hepatitis and liver cancer: the case of hepatitis C Oncogene 25, 3834-3847.

185. Li J.J, Muralikrishnan S., Ng C.T, Yung L.Y, Bay B.H (2010) “NP-induced pulmonary toxicity,”Experimental Biology and Medicine 235:9,1025–1033.

186. Li L, Mak K Y, Shi J, Koon HK, Leung CH, Wong CM, Leung CW, Mak CSK, Chan NMM, Zhong W (2012) Comparative in vitro cytotoxicity study on uncoated magnetic NPs: effects on cell viability, cell morphology, and cellular uptake. J Nanosci Nanotechnol 12:9010–9017.

187. Li N, Xia T, and Nel A. E (2008) “The role of oxidative stress in ambient particulate matter-induced lung diseases and its implications in the toxicity of engineered NPs,” Free RadicalBiologyandMedicine, 44:9,1689–1699.

188. Lioudyno, M., Kozak, J., Penna, A., Safrina, O., Zhang, S., Sen, D. and Roos, J. *et. al.* 2008. Orai1 and STIM1 move to the immunological synapse and are up-regulated during T cell activation. Proceedings of the National Academy of Sciences 105(6), pp. 2011-2016.

189. Lipp P, Niggli E. 1993. Ratiometric confocal Ca^{2+}-measurements with visible wavelength indicators in isolated cardiac myocytes. Cell Ca^{2+} 14: 359–372

190. Liu G, Li D. S, Pasumarthy M. K, Kowalczyk T. H., Gedeon C. R.,Hyatt S. L., Payne J. M., Miller T. J., Brunovskis P., Fink T. L., Muhammad O., Moen R. C., Hanson R. W., Cooper M. J.,(2003) NPs of Compacted DNA Transfect Post-Mitotic Cells J. Biol.Chem. 278, 32578.

191. Liu Y, Li W, Lao F, Liu Y, Wang L, Bai R(2011) Intracellular dynamics of cationic and anionic polystyrene NPs without direct interaction with mitotic spindle and chromosomes. Biomaterials. 32:8291–8303.

192. Liu, J., Farmer, J.D., Lane, W.S., *et. al.*, 1991. Calcineurin is a common target of cyclosporin–cyclosporin A and FKBP–FK506 complexes. Cell 66, 807–815

193. Lloyd-Evans, E., Morgan, A., He, X., Smith, D., Elliot-Smith, E., Sillence, D., Churchill, G., Schuchman, E., Galione, A. and Platt, F. (2008). Niemann-Pick disease type C1 is a sphingosine storage disease that causes deregulation of lysosomal Ca^{2+}. *Nature Medicine*, 14(11), pp.1247-1255.

194. Lloyd-Evans, E., Waller-Evans, H., Peterneva, K. and Platt, F. (2010). Endolysosomal Ca^{2+} regulation and disease. *Biochm. Soc. Trans.*, 38(6), pp.1458-1464.

195. Lnch, D.R., Dawson, T.M., 1994. Secondary mechanisms in neuronal trauma. Curr. Opin. Neurol. 7, 510–516.

196. Lo, Y. Y.; Wong, J. M.; Cruz, T. F. 1996 Reactive oxygen species mediate cytokine activation of c-Jun NH2-terminal kinases. J. Biol. Chem. 271:15703–15707;

197. Lopez-Lorente AI, Simonet BM, Valcarcel M. 2013. Qualitative detection and quantitative determination of single-walled carbon nanotubes in mixtures of carbon nanotubes with a portable Raman spectrometer. Analyst 138: 2378–2385.

198. Lorge E, Hayashi M, Albertini S, Kirkland D (2008) Comparison of different methods for an accurate assessment of cytotoxicity in the *in vitro* micronucleus test. Mutation Research 655: 1–3.

199. Lu F, Wu S-H, Hung Y, Mou C-Y. (2009) Size effect on cell uptake in well-suspended, uniform mesoporous silica NPs. Small 10:1–6.

200. Luyts K, Napierska D, Nemery B, Hoet PHM. (2013) How physico-chemical characteristics of NPs cause their toxicity: complex and unresolved interrelations. Environ Sci Process Impacts. 15:23–38.

201. Lyons S, O'Neal J, Sontheimer H.(2002) Chlorotoxin, a scorpion-derived peptide, specifically binds to gliomas and tumors of neuroectodermal origin. *Glia* 39: 162–173.

202. M. Fenech M, Chang W.P, M. Kirsch-Volders M, Holland N, Bonassi S, Zeiger E. (2003) HUMN project: detailed description of the scoring criteria for the cytokinesis-block micronucleus assay using isolated human lymphocyte cultures Mutation Research 534 :65–75.

203. Maccioni F, Bruni A, Viscido A (2006) MR imaging in patients with Crohn disease: Value of T2- versus T1- weighted gadolinium-enhanced MR sequences with use of an oral superparamagnetic contrast agent. *Radiology* 238(2): 517–530.

204. Magdolenova Z, Drlickova M, Henjum K, Rund_en-Pran E, Tulinska J, Bilanicova D, Pojana G, Kazimirova A, Barancokova M, Kuricova M (2013) Coating-dependent induction of cytotoxicity and genotoxicity of iron oxide NPs. Nanotoxicology

205. Mahmoudi M, Simchi A, Milani A S, Stroeve P.(2009) Cell toxicity of superparamagnetic iron oxide NPs. J Colloid Interface Sci. 336:510–518.

206. Mahon E, Hristov DL, Dawson KA. (2012) Stabilising fluorescent silica NPs against dissolution effects for biological studies. Chem Commun 48:7970–7972.

207. Maier-Hauff K, Ulrich F, Nestler D (2011) Efficacy and safety of intratumoral thermotherapy using magnetic iron-oxide NPs combined with external beam radiotherapy on patients with recurrent glioblastoma multiforme. *J. Neurooncol.* 103(2): 317–324.

208. Malcuit, C., Kurokawa, M. and Fissore, R. (2005). Ca^{2+} oscillations and mammalian egg activation. J. Cell. Physiol., 206(3), pp.565-573.

209. Malek TR. (2008) The biology of interleukin-2. Annu Rev Immunol. 26:453–479.

210. Malvindi MA, De Matteis V, Galeone A, Brunetti V, Anyfantis GC, Athanassiou A, Cingolani R, Pompa PP (2014) Toxicity assessment of silica coated iron oxide NPs and biocompatibility improvement by surface engineering.

211. Manke, A., Wang, L. and Rojanasakul, Y., 2013. Mechanisms of Nanoparticle-Induced Oxidative Stress and Toxicity. *BioMed Research International*, 2013, pp.1-15.

212. Marin, J., Encabo, A., Briones, A., Garcia-Cohen, E.C., Alonso, M.J., 1999. Mechanisms involved in the cellular Ca^{2+} homeostasis in vascular smooth muscle: Ca^{2+} pumps. Life Sci. 64, 279–303.

213. Martin AL, Bernas LM, Rutt BK, Foster PJ, Gillies ER (2008) Enhanced cell uptake of superparamagnetic iron oxide NPs functionalized with dendritic guanidines. *Bioconjug. Chem.* 19(12): 2375–2384.

214. Matter, N., Ritz, M.F., Freyermuth, S., Rogue, P., Malviya, A.N., 1993. Stimulation of nuclear protein kinase C leads to phosphorylation of nuclear inositol 1,4,5-trisphosphate receptor and accelerated Ca^{2+} release by inositol 1,4,5-trisphosphate from isolated rat liver nuclei. J. Biol. Chem. 268, 732–736.

215. McMahon HT, Boucrot E. 2011. Molecular mechanism and physiological functions of clathrin–mediated endocytosis. Nat Rev Mol Cell Biol 12:517–533.

216. Meindl, C., Kueznik, T., Bösch, M., Roblegg, E. and Fröhlich, E. (2015). Intracellular Ca^{2+} levels as screening tool for NP toxicity. J. Appl. Toxicol., 35(10), pp.1150-1159.

217. Mellstrom, B., Savignac, M., Gomez-Villafuertes, R. and Naranjo, J.R. (2008) Ca^{2+}-operated transcriptional networks: Molecular mechanisms and in vivo models. Physiol. Rev. 88, 421–449

218. Mercer J, Helenius A. 2009. Virus entry by macropinocytosis. Nat Cell Biol 11:510–520.

219. Merrifield C. J (2004) Seeing is believing: imaging actin dynamics at single sites of endocytosis. Trends Cell Biol 14: 352–358.

220. Merrifield C. J, Perrais D, Zenisek D (2005) Coupling between clathrin-coated-pit invagination, cortactin recruitment, and membrane scission observed in live cells. Cell 121: 593–606.

221. Mesarosova M, Kozics K, Babelova A, Regendova E, Pastorek M, Vnukov_a D, Buliakova B, Razga F, Gabelova A. (2014). The role of reactive oxygen species in the genotoxicity of surfacemodified magnetite NPs. Toxicol Lett 226:303–313.

222. Meyer, M.; Schreck, R.; Baeuerle, P. (1993) A. H2O2 and antioxidants have opposite effects on activation of NF-kappa B and AP-1 in intact cells: AP-1 as secondary antioxidant-responsive factor. EMBO J. 12:2005–2015.

223. Meyer, T., Wensel, T. and Stryer, L. 1990. Kinetics of Ca^{2+} channel opening by inositol 1,4,5-trisphosphate. Biochemistry 29(1), pp. 32-37.

224. Miranda H.C, Nunes S.O, Calvo E.S, Suzart S, Itano E.N, Watanabe M.A. (2006)Detection of Borna disease virus p24 RNA in peripheral blood cells from Brazilian mood and psychotic disorder patients J. Affect. Disord. 90, 43-47.

225. Monopoli Marco, Pitek Andrzej, Lynch Iseult, Dawson Kenneth (2013) Formation and Characterization of the NP–Protein Corona. NP Interfaces in Biology, 1025:137-155.

226. Naqvi S, Samim M, Abdin M, Ahmed FJ, Maitra A, Prashant C, Dinda AK (2010) Concentration-dependent toxicity of iron oxide NPs NPs mediated by increased oxidative stress. Int J Nanomed 5:983–989.

227. Nel A, Xia T, Madler L, Li N (2006) Toxic potential of materials at the nanolevel. Science. 311:5761, 622–627.

228. Neshatian, M., Chung, S., Yohan, D., Yang, C. and Chithrani, D., 2015. Uptake of Gold Nanoparticles in Breathless (Hypoxic) Cancer Cells. *Journal of Biomedical Nanotechnology*, 11(7), pp.1162-1172.

229. Ng A W, Bidani A, Heming T A (2004) Innate host defense of the lung: effects of lung-lining fluid pH Lung 182 297-317

230. Nielsen, S. and Petersen, O. 1972. Transport of Ca^{2+} in the perfused submandibular gland of the cat. The Journal of Physiology 223(3), pp. 685-697.

231. Oberdörster G, Maynard A, Donaldson K (2005) Principles for characterizing the potential human health effects from exposure to NPs: elements of a screening strategy. Particleand Fibre Toxicology,2:8.

232. Oberdörster G, Oberdörster E, Oberdörster J. (2005) Nanotoxicology: an emerging discipline evolving from studies of ultrafine particles Environ. Health. Perspect. 113, 823-839.

233. Palecanda A, Kobzik L 2000 Alveolar macrophage-environmental particle interaction: analysis by flow cytometry Methods 21 241-247

234. Panyam J, Labhasetwar V (2003) Biodegradable NPs for drug and gene delivery to cells and tissue. Adv Drug Deliv Rev. 55(3):329-47.

235. Parekh AB, Putney JW., Jr Store-operated Ca^{2+} channels. Physiol Rev. 2005;85:757–810

236. Park J B (2003) Phagocytosis induces superoxide formation and apoptosis in macrophages Exp. Mol. Med. 35 325-335

237. Park Y-H, Bae HC, Jang Y, Jeong SH, Lee HN, Ryu W-I (2013) Effect of the size and surface charge of silica NPs on cutaneous toxicity. Mol Cell Toxicol. 9:67–74.

238. Parton R.G, Simons K. (2007) The multiple faces of caveolae. Nat Rev Mol Cell Biol, 8: 185–194.

239. Pastan IH, Willingham MC. (1981). Receptor-mediated endocytosis of hormones in cultured cells. Annu Rev Physiol 43:239–250.

240. Patel LN, Zaro JL, Shen W-C. (2007) Cell penetrating peptides: Intracellular pathways and pharmaceutical perspectives. Pharmaceut Research. 24:1977–1992.

241. Patel, S. and Cai, X. (2015). Evolution of acidic Ca2+ stores and their resident Ca2+ -permeable channels. Cell Calcium 57, 222–230.

242. Patel, S. and Docampo, R. (2010). Acidic Ca^{2+} stores open for business: expanding the potential for intracellular Ca^{2+} signaling. *Trends in Cell Biology*, 20(5), pp.277-286.

243. Patri, A.; Dobrovolskaia, M.; Stern, S.; McNeil, S.; Amiji, M.(2006); Preclinical characterization of engineered NPs intended for cancer therapeutics. Nanotechnology for cancer therapy. CRC Press p. 105-138

244. Payne AR, Berry C, Kellman P (2011) Bright-blood T(2)-weighted MRI has high diagnostic accuracy for myocardial hemorrhage in myocardial infarction: A preclinical validation study in swine. *Circ. Cardiovasc. Imaging* 4(6): 738–745.

245. Pelkmans L., PüntenerD. , Helenius A. (2002) Local actin polymerization and dynamin recruitment in SV40-induced internalization of caveolae. Science, 296: 535–539.

246. Peters A, Veronesi B, Calderon-Garciduenas L, Gehr P, Chen L C, Geiser M, Reed W, Rothen, Rutishauer B, Schurch S, Schultz H (2006) Translocation and potential neurological effects of fine and ultrafine particles. A critical update Part. Fibre Toxicol. 3:13.

247. Petersen, O. and Tepikin, A. (2008). Polarized Ca^{2+} Signaling in Exocrine Gland Cells. Annual Review of Physiology, 70(1), pp.273-299.

248. Petersen, O.H., Gerasimenko, O.V., Gerasimenko, J.V., Mogami, H. and Tepikin, A.V. (1998) The Ca^{2+} store in the nuclear envelope. Cell Ca^{2+} 23, 87–90.

249. Philipp, S., Strauss, B., Hirnet, D., Wissenbach, U., Mery, L., Flockerzi, V. and Hoth, M. 2003. TRPC3 Mediates T-cell Receptor-dependent Ca^{2+} Entry in Human T-lymphocytes. Journal of Biological Chemistry 278(29), pp. 26629-26638.

250. Pierce, A., Barron, N., Linehan, R., Ryan, E., O'Driscoll, L., Daly, C. and Clynes, M. 2008. Identification of a novel, functional role for S100A13 in invasive lung cancer cell lines. European Journal of Cancer 44(1), pp. 151-159.

251. Piraux H, Hai J, Verbeke P (2013) Transferrin receptor-1 iron-acquisition pathway - Synthesis, kinetics, thermodynamics and rapid cellular internalization of a holotransferrin-maghemite NP construct. *Biochim. Biophys. Acta - Gen. Subj.* 1830(8), 4254–426 .

252. Porter A E, Muller K, Skepper J, Midgley P, Welland M (2006) Uptake of C60 by human monocyte macrophages, its localization and implications for toxicity: studied by high resolution electron microscopy and electron tomography Acta Biomater. 2 409-419.

253. Powers KW, Brown SC, Krishna VB, Wasdo SC, Moudgil BM, Roberts SM. (2006) Characterization of nanoscale particles for toxicological evaluation. Research strategies for safety evaluation of NPs. Part VI. Toxicol Sci. 90:296–303.

254. Powers, KW.; Palazuelos, M.; Brown, SC.; Roberts, SM. (2009) Characterization of NPs for toxicological evaluation. Nanotoxicology From In Vivo and In Vitro Models to Health Risks. 2009. p. 1-27.

255. Provenzano R, Schiller B, Rao M, Coyne D, Brenner L, Pereira BJ (2009) Ferumoxytol as an intravenous iron replacement therapy in hemodialysis patients. *Clin. J. Am. Soc. Nephrol*. 4(2): 386–393.

256. Pryor W.A, Stone K, Cross C.E, Machlin L, Packer L (1993) "Oxidants in cigarette smoke: radicals, hydrogen peroxide, peroxy-nitrate, and peroxy-nitrite,"Annals of the new York Academy of Sciences,686,12–28.

257. Pucadyil T.J. , Schmid S.L. (2009) Conserved functions of membrane active GTPases in coated vesicle formation. Science, 325: 1217–1220.

258. Putney JW., Jr Capacitative Ca^{2+} entry: sensing the Ca^{2+} stores. J Cell Biol. 2005;169:381–382.

259. Radomski A, Jurasz P, Alonso-Escolano D, Drews M, Morandi M, Malinski T, Radomski MW. Nanoparticle-induced Platelet Aggregation and Vascular Thrombosis. 2005. Br J Pharmacol. 146:pp882–893.

260. Rahman, I.; MacNee, W. (1998) Role of transcription factors in inflammatory lung diseases. Thorax 53:601–612.

261. Rahman, I.; MacNee, W. Regulation of redox glutathione levels and gene transcription in lung inflammation: therapeutic approaches. (2000) Free Radic. Biol. Med. 28:1405–1420.

262. Rappoport J. (2008) Focusing on clathrin-mediated endocytosis. Biochem J, 412: 415–423.

263. Ratner, BD.; Hoffman, AS.; Schoen, FJ.; Lemons, JE. (2004) Biomaterials science: an introduction to materials in medicine. Academic Press.

264. Reichert JM, Valge-archer VE. (2007) Antibody cancer therapeutics. *Nat. Rev. Drug Discov.* 6: 349–356.

265. Reimer Peter and Balzer Thomas (2003) Ferucarbotran (Resovist): a new clinically approved RES-specific contrast agent for contrast-enhanced MRI of the liver: properties, clinical development, and applications. Eur Radiol 13:1266–1276.

266. Richards JM, Shaw C, Lang NN, *et. al.* In vivo mononuclear cell tracking using superparamagnetic particles of iron oxide: Feasibility and safety in humans. *Circ. Cardiovasc. Imaging* 5(4): 509–517.

267. Riemer Jan, Hoepken H. Hans, Czerwinska Hania, Robinson Stephen, Dringen Ralf (2004) Colorimetric ferrozine-based assay for the quantitation of iron in cultured cells. Analytical Biochemistry 331: 370–375.

268. Risom L, Møller P,and Loft S (2005) Oxidativestress-inducedDNA damage by particulate air pollution," Mutation Research 592:1-2,119–137.

269. Rivet CJ, Yuan Y, Borca-Tasciuc D-A, Gilbert RJ (2012) Altering iron oxide NP surface properties induce cortical neuron cytotoxicity. Chem Res Toxicol 25:153–161.

270. Rizzuto R, Marchi S, Bonora M *et. al.* (2009) $Ca(^{2+})$ transfer from the ER to mitochondria: When, how and why. Biochimica et Biophysica Acta 1787: 1342–1351.

271. Rizzuto, R. 2006. Microdomains of Intracellular Ca^{2+}: Molecular Determinants and Functional Consequences. Physiological Reviews 86(1), pp. 369-408.

272. Rizzuto, R., Bernardi, P., Pozzan, T., 2000. Mitochondria as all-round players of the Ca^{2+} game. J. Physiol. 529 (1), 37–47.

273. Rizzuto, R., Pinton, P., Carrington, W., Fay, F.S., Fogarty, K.E., Lifshitz, L.M., Tuft, R.A., Pozzan, T., 1998. Close contacts with the endoplasmic reticulum as determinants of mitochondrial Ca^{2+} responses. Scienc 280, 1763–1766.

274. Roderick, H. and Cook, S. 2008. Ca^{2+} signalling checkpoints in cancer: remodelling Ca^{2+} for cancer cell proliferation and survival. Nature Reviews Cancer 8(5), pp. 361-375.

275. Rodrigues, M.A., Gomes, D.A., Leite, M.F., Grant, W., Zhang, L., Lam, W., Cheng, Y.C., Bennett, A.M. and Nathanson, M.H. (2007) Nucleoplasmic Ca^{2+} is required for cell proliferation. J. Biol. Chem. 282, 17061–17068

276. Rohn, T.T., Hinds, T.R., Vincenzi, F.F., 1993. Ion transport ATPases as targets for free radical damage. Protection by an aminosteroid of the Ca^{2+} pump ATPase and Na+/K+ pump ATPase of human red blood cell membranes. Biochem. Pharmacol. 46, 525–534.

277. Rojas-Chapana Jose´ A, Correa-Duarte Miguel, Zhifeng Ren, Krzysztof Kempa,‡ and Giersig Michael (2004) Enhanced Introduction of Gold NPs into Vital Acidothiobacillus ferrooxidans by Carbon Nanotube-based Microwave Electroporation. Nano Lett. 4, 985.

278. Rosenberger, S., Thorey, I., Werner, S. and Boukamp, P. 2006. A Novel Regulator of Telomerase: S100A8 MEDIATES DIFFERENTIATION-DEPENDENT AND CA^{2+}-INDUCED INHIBITION OF TELOMERASE ACTIVITY IN THE HUMAN EPIDERMAL KERATINOCYTE LINE HaCaT. Journal of Biological Chemistry 282(9), pp. 6126-6135.

279. Rossi AM, Tovey SC, Rahman T, Prole DL and Taylor CW (2012) Analysis of IP(3) receptors in and out of cells. Biochimica et biophysica acta 1820: 1214–1227.

280. Roveri, A., Coassin, M., Maiorino, M., Zamburlini, A., van Amsterdam, F.T., Ratti, E., Ursini, F., 1992. Effect of hydrogen peroxide on Ca^{2+} homeostasis in smooth muscle cells. Arch. Biochem. Biophys. 297, 265–270.

281. Sadeghiani N, Barbosa LS, Silva LP, Azevedo RB, Morais PC, Lacava ZGM. (2005). Genotoxicity and inflammatory investigation in mice treated with magnetite NPs surface coated with polyaspartic acid. J Magn Magn Mater 289:466–468.

282. Sakaguchi, M., Miyazaki, M., Takaishi, M., Sakaguchi, Y., Makino, E., Kataoka, N. and Yamada, H. *et. al.* 2003. S100C/A11 is a key mediator of Ca^{2+} -induced growth inhibition of human epidermal keratinocytes. J Cell Biol 163(4), pp. 825-835.

283. Santella, L., Carafoli, E., 1997. Ca^{2+} signaling in the cell nucleus. FASEB J. 11, 1091–1109.

284. Sapsford KE, Algar WR, Berti L (2013) Functionalizing NPs with biological molecules: Developing chemistries that facilitate nanotechnology. *Chem. Rev.* 113(3): 1904–2074.

285. Sayes CM, Liang F, Hudson JL, Mendez J, Guo W, Beach JM (2006) Functionalization density dependence of single-walled carbon nanotubes cytotoxicity in vitro. Toxicol Lett 161:135–42.

286. Scherer, N.M., Deamer, D.W., 1986. Oxidative stress impairs the function of sarcoplasmic reticulum by oxidation of sulfhydryl groups in the Ca^{2+}-ATPase. Arch. Biochem. Biophys. 246, 589–601.

287. Schins R.P.F (2002) Mechanisms of genotoxicity of particles and fibers,"Inhalation Toxicology 14:1,57–78.

288. Schneider, G., Oswald, F., Wahl, C., Greten, F., Adler, G. and Schmid, R. 2002. Cyclosporine Inhibits Growth through the Activating Transcription Factor/cAMP-responsive Element-binding Protein Binding Site in the Cyclin D1 Promoter. Journal of Biological Chemistry 277(46), pp. 43599-43607.

289. Shander A, Cappellini MD, Goodnough LT. (2009) Iron overload and toxicity: The hidden risk of multiple blood transfusions. Vox Sang 97:185–197.

290. Sharifi S, Behzadi S, Laurent S, Forrest M.L, Stroeve P, Mahmoudi M. (2011)Toxicity of NPs. *Chem. Soc. Rev. 41:* 2323 .

291. Sheng, M., McFadden, G., Greenberg, M.E., 1990. Membrane depolarization and Ca^{2+} induce c-fos transcription via phosphorylation of transcription factor CREB. Neuron 4, 571–582.

292. Shvedova A.A, Pietroiusti A, Fadeel B, Kagan V.E (2012) "Mechanisms of carbon nanotube-induced toxicity: focus on oxidativestress,"Toxicology and Applied Pharmacology, 261: 2,121–133.

293. Sies H (1991) Oxidative stress: introduction. Oxidative Stress Oxidants and Antioxidants, 15–22, Academic Press, London, UK.

294. Singh N, Jenkins GJS, Nelson BC, Marquis BJ, Maffeis TGG, Brown AP, Williams PM, Wright CJ, Doak SH. (2012) The role of iron redox state in the genotoxicity of ultrafine superparamagnetic iron oxide NPs. Biomaterials 33:163–170.

295. Singh SP, Rahman MF, Murty USN, Mahboob M, Grover P. (2013) Comparative study of genotoxicity and tissue distribution of nano and micron sized iron oxide in rats after acute oral treatment. Toxicol Appl Pharmacol 266:56–66.

296. Sioutas C, Delfino R J, Singh M (2005) Exposure Assessment for Atmospheric Ultrafine Particles (UFPs) and Implications in Epidemiologic Research Environ. Health Res. 113 947-955.

297. Sjoblom, T., Jones, S., Wood, L., Parsons, D., Lin, J., Barber, T. and Mandelker, D. *et. al.* 2006. The Consensus Coding Sequences of Human Breast and Colorectal Cancers. Science 314(5797), pp. 268-274.

298. Slamon DJ, Clark GM, Wong SG, Levin WJ, Ullrich A, McGuire WL.(1987) Human breast cancer: Correlation of relapse and survival with amplification of the HER-2/neu oncogene. *Science* 235(4785), 177–182.

299. Smith A.E, Helenius A. (2009). How viruses enter animal cells. Science 304:237–242

300. Smith K.R, Klei L, Barchowsky A (2001) Arsenite stimulates plasma membrane NADPH oxidase in vascular endothelial cells. American Journal of Physiology. 280 (3):442– 449.

301. Soenen SJH, De Cuyper M. (2009) Assessing cytotoxicity of (iron oxidebased) NPs: An overview of different methods exemplified with cationic magnetoliposomes. Contrast Media Mol Imaging, 4:207–219.

302. Soenen SJH, De Cuyper M. 2010. Assessing iron oxide NP toxicity in vitro: Current status and future prospects. Nanomedicine 5:1261–1275.

303. Sohaebuddin S, Thevenot P, Baker D, Eaton J, Tang L. (2010) NP cytotoxicity is composition, size, and cell type dependent. Part Fibre Toxicol. 7:22.

304. Stone, D. M. Brown, N. Watt, M. Wil, V. (2000). ULTRAFINE PARTICLE-MEDIATED ACTIVATION OF MACROPHAGES: Intracellular Ca^{2+} Signaling and Oxidative Stress. Inhalation Toxicology, 12(sup3), pp.345-351.

305. Stone, V., Shaw, J., Brown, D., MacNee, W., Faux, S. and Donaldson, K. (1998). The role of oxidative stress in the prolonged inhibitory effect of ultrafine carbon black on epithelial cell function. Toxicology in Vitro, 12(6), pp.649-659.

306. Stone, V., Tuinman, M., Vamvakopoulos, J., Shaw, J., Brown, D., Petterson, S., Faux, S., Borm, P., MacNee, W., Michaelangeli, F. and Donaldson, K. (2000). Increased Ca^{2+} influx in a monocytic cell line on exposure to ultrafine carbon black. *Eur Respir J*, 15(2), p.297.

307. Stroh A, Zimmer C, Gutzeit C, Jakstadt M, Marschinke F, Jung T, Pilgrimm H, Grune T. (2004) Iron oxide particles for molecular magnetic resonance imaging cause transient oxidative stress in rat macrophages. Free Radic Biol Med 36:976–984.

308. Subramanian, K. and Meyer, T. (1997) Ca^{2+}-induced restructuring of nuclear envelope and endoplasmic reticulum Ca^{2+} stores. Cell 89, 963–971

309. Sukhanova, A., Bozrova, S., Sokolov, P., Berestovoy, M., Karaulov, A. and Nabiev, I., 2018. Dependence of Nanoparticle Toxicity on Their Physical and Chemical Properties. *Nanoscale Research Letters*, 13(1).

310. Sun Y, Martin A. C, Drubin D. G (2006) Endocytic internalization in budding yeast requires coordinated actin nucleation and myosin motor activity. Dev Cell 11: 33–46.

311. Suzuki, Y.J., Ford, G.D., 1991. Inhibition of $Ca(^{2+})$-ATPase of vascular smooth muscle sarcoplasmic reticulum by reactive oxygen intermediates. Am. J. Physiol. 261, H568–H574.

312. Svensen N, Walton JG, Bradley M (2012) Peptides for cellselective drug delivery. *Trends Pharmacol. Sci.* 33(4): 186–192.

313. Takuwa, N., Zhou, W., Kumada, M. & Takuwa, Y. Ca^{2+}-dependent stimulation of retinoblastoma gene product phosphorylation and p34cdc2 kinase activation in serum-stimulated human fibroblasts. J. Biol. Chem. 268, 138–145 (1993)

314. Thannickal V.J and Fanburg B.L (2000) Reactive oxygen species in cell signaling, American Journal of Physiology, 279: 6, 1005-1028.

315. Thannickal, V. J.; Fanburg, B. L. (2000) Reactive oxygen species in cell signaling. Am. J. Physiol. Lung Cell. Mol. Physiol. 279:L1005– L1028.,

316. Thastrup, O., Cullen, P., Drobak, B., Hanley, M. and Dawson, A. (1990). Thapsigargin, a tumor promoter, discharges intracellular Ca^{2+} stores by specific inhibition of the endoplasmic reticulum Ca2(+)-ATPase. Proceedings of the National Academy of Sciences, 87(7), pp.2466-2470.

317. Thebault, S (2006) Differential role of transient receptor potential channels in Ca^{2+} entry and proliferation of prostate cancer epithelial cells. Cancer Res. 66, 2038–2047.

318. Thibodeau GA, Patton KT,(2003) Anatomy and physiology, Fifth edition Mosby Inc., St. Luis.

319. Thomas D, Tovey SC, Collins TJ, Bootman MD, Berridge MJ, Lipp P. 2000. A comparison of fluorescent Ca^{2+} indicator properties and their use in measuring elementary and global Ca^{2+} signals. Cell Ca^{2+} 28: 213– 223.

320. Tourdias T, Roggerone S, Filippi M (2012) Assessment of disease activity in multiple sclerosis phenotypes with combined gadolinium- and superparamagnetic iron oxide-enhanced MR imaging. *Radiology* 264(1): 225–233.

321. Tse, F., Tse, A. and Hille, B. 1994. Cyclic Ca^{2+} changes in intracellular stores of gonadotropes during gonadotropin-releasing hormone-stimulated Ca^{2+} oscillations. Proceedings of the National Academy of Sciences 91(21), pp. 9750-9754.

322. Tsien RY, Pozzan T, Rink TJ. 1982. T-cell mitogens cause early changes in cytoplasmic free Ca^{2+} and membrane potential in lymphocytes. Nature 295: 68–71

323. Vadhan-Raj S, Strauss W, Ford D (2014) Efficacy and safety of IV ferumoxytol for adults with iron deficiency anemia previously unresponsive to or unable to tolerate oral iron. *Am. J. Hematol*. 89(1): 7– 12.

324. Valko M, Rhodes C.J, Moncol J, Izakovic M, Mazur M (2006) Free radicals, metals and antioxidants in oxidative stress induced cancer. Chemico Biological Interactions,160:1, 1–40.

325. Vallyathan V. and Shi X. (1997) The role of oxygen free radicals in occupational and environmental lung diseases. Environmental Health Perspectives 105, 165–177.

326. van Abel, M., Hoenderop, J. and Bindels, R. 2005. The epithelial Ca^{2+} channels TRPV5 and TRPV6: regulation and implications for disease. Naunyn-Schmiedeberg's Archives of Pharmacology 371(4), pp. 295-306.

327. Vasilichin, V., Tsymbal, S., Fakhardo, A., Anastasova, E., Marchenko, A., Shtil, A., Vinogradov, V. and Koshel, E., 2020. Effects of Metal Oxide Nanoparticles on Toll-Like Receptor mRNAs in Human Monocytes. *Nanomaterials*, 10(1), p.127.

328. Vellinga MM, Vrenken H, Hulst HE(2009) Use of ultrasmall superparamagnetic particles of iron oxide (USPIO)-enhanced MRI to demonstrate diffuse inflammation in the normal-appearing white matter (NAWM) of multiple sclerosis (MS) patients: An exploratory study. *J. Magn. Reson. Imaging*. 29, 774–779.

329. Venkatachalam, K., Ma, H., Ford, D. and Gill, D. 2001. Expression of Functional Receptor-coupled TRPC3 Channels in DT40 Triple Receptor InsP3 knockout Cells. Journal of Biological Chemistry 276(36), pp. 33980-33985.

330. Vig, M. 2006. CRACM1 Is a Plasma Membrane Protein Essential for Store-Operated Ca^{2+} Entry. Science 312(5777), pp. 1220-1223.

331. Vigor KL, Kyrtatos PG, Minogue S (2020) NPs functionalized with recombinant single chain Fv antibody fragments (scFv) for the magnetic resonance imaging of cancer cells. *Biomaterials* 31(6): 1307–1315.

332. Villereal, M. 2006. Mechanism and functional significance of TRPC channel multimerization. Seminars in Cell & Developmental Biology 17(6), pp. 618-629.

333. Vines, A., McBean, G. and Blanco-Fernández, A. (2010). A flow-cytometric method for continuous measurement of intracellular Ca^{2+} concentration. *Cytometry*, 77A(11), pp.1091-1097.

334. Wadia JS, Dowdy SF (2002) Protein transduction technology. *Curr. Opin. Biotechnol.* 13: 52–56.

335. Walker, D., Sun, T., Macneil, S. and Smallwood, R. 2006. Modeling the Effect of Exogenous Ca^{2+} on Keratinocyte and HaCat Cell Proliferation and Differentiation Using an Agent-Based Computational Paradigm. Tissue Engineering 12(8), pp. 2301-2309.

336. Wang L, Mercer R.R, Rojanasakuletal Y (2010) Directfibrogenic effects of dispersed single-walled carbon nanotubes on human lung fibroblasts. Journal of Toxicology and Environmental Health. 73:5-6, 410–422.

337. Wankhede M, Bouras A, Kaluzova M, Hadjipanayis CG (2012) Magnetic NPs: An emerging technology for malignant brain tumor imaging and therapy. *Expert Rev. Clin. Pharmacol*. 5(2):173–186.

338. Weissleder R (2006) Molecular imaging in cancer. Science. 312(5777):1168-71.

339. Whitehead KA, Langer R, Anderson DG (2009) Knocking down barriers: advances in siRNA delivery. Nat Rev Drug Discov. 8(2):129-38.

340. Whitfield, J. F. Ca^{2+} signals and cancer. Crit. Rev. Oncog. 3, 55–90 (1992).

341. Wilhelm, D.; Bender, K.; Knebel, A.; Angel, P. 1997 The level of intracellular glutathione is a key regulator for the induction of stress-activated signal transduction

pathways including Jun Nterminal protein kinases and p38 kinase by alkylating agents. Mol. Cell. Biol. 17:4792–4800.

342. Wilson M.R, Lightbody J.H, Donaldson K, Sales J, and Stone V (2002) Interactions between ultrafine particles and transition metals in vivo and in vitro. Toxicology and Applied Pharmacology,184:3,172–179.

343. Wood, L. D. *et. al.* The genomic landscapes of human breast and colorectal cancers. Science 318, 1108–1113 (2007).

344. Wu J, Sun J (2011) Investigation on mechanism of growth arrest induced by iron oxide NPs in PC12 cells. J Nanosci Nanotechnol 11:11079–11083.

345. Wu L, Cao Y, Liao C, Huang J, Gao F (2010) Diagnostic performance of USPIO-enhanced MRI for lymphnode metastases in different body regions: A metaanalysis. *Eur. J. Radiol*. 80(2): 582–589.

346. Wust P, Hildebrandt B, Sreenivasa G (2012) Hyperthermia in combined treatment of cancer. *Lancet Oncol*. 3(8), 487–497.

347. Xia T, Kovochich M, Brant J. (2006) Comparison of the abilities of ambient and manufactured NPs to induce cellular toxicity according to an oxidative stress paradigm. NanoLetters,6: 8, 1794–1807.

348. Xie J, Xu C, Kohler N, Hou Y, Sun S (2007)Controlled PEGylation of Monodisperse Fe3O4 NPs for Reduced Non-Specific Uptake by Macrophage Cells. Advance Materials.19:20, 3163–3166.

349. Xu Y, Tillman TS, Tang P. (2009). Pharmacology: Principles and Practice, 1st ed. Academic, San Diego, CA, USA.

350. Xu, K.Y., Zweier, J.L., Becker, L.C., 1997. Hydroxyl radical inhibits sarcoplasmic reticulum $Ca(^{2+})$-ATPase function by direct attack on the ATP binding site. Circ. Res. 80, 76–81.

351. Yang C-Y, Hsiao J-K, Tai M-F, Chen S-T, Cheng H-Y, Wang J-L, Liu H-M. (2011) Direct labeling of hMSC with SPIO: the long-term influence on toxicity, chondrogenic differentiation capacity, and intracellular distribution. Mol Imaging Biol 13:443–451.

352. Yilmaz A, Dengler MA, van der Kuip H *(2012)* Imaging of myocardial infarction using ultrasmall superparamagnetic iron oxide NPs: A human study using a multi-parametric cardiovascular magnetic resonance imaging approach. *Eur. Hear. J*. 34(6): 462–475.

353. Yu J, Patel SA, Dickson RM.(2007) In vitro and intracellular production of peptide-encapsulated fluorescent silver nanoclusters. Angew Chem Int Ed Engl. 46(12):2028-30.

354. Yu, Q., Wang, H., Peng, Q., Li, Y., Liu, Z. and Li, M., 2017. Different toxicity of anatase and rutile TiO 2 nanoparticles on macrophages: Involvement of difference in affinity to proteins and phospholipids. *Journal of Hazardous Materials*, 335, pp.125-134.

355. Yuan H, Zhanga S. 2010. Effects of particle size and ligand density on the kinetics of receptor-mediated endocytosis of NPs. Appl Phys Lett 96:033704.

356. Yuan, J., Zeng, W., Huang, G., Worley, P. and Muallem, S. 2007. STIM1 heteromultimerizes TRPC channels to determine their function as store-operated channels. Nature Cell Biology 9(6), pp. 636-645.

357. Zhang T, Qian L, Tang M, Xue Y, Kong L, Zhang S, Pu Y. (2012) Evaluation on cytotoxicity and genotoxicity of the L-glutamic acid coated iron oxide NPs. J Nanosci Nanotechnol 12: 2866– 2873.

358. Zhang, S., Yeromin, A., Zhang, X., Yu, Y., Safrina, O., Penna, A. and Roos, J. *et. al.* 2006. Genome-wide RNAi screen of Ca^{2+} influx identifies genes that regulate Ca^{2+} release-activated Ca^{2+} channel activity. Proceedings of the National Academy of Sciences 103(24), pp. 9357-9362.

359. Zhang, S., Yu, Y., Roos, J., Kozak, J., Deerinck, T., Ellisman, M. and Stauderman, K. *et. al.* 2005. STIM1 is a Ca^{2+} sensor that activates CRAC channels and migrates from the Ca^{2+} store to the plasma membrane. Nature 437(7060), pp. 902-905.

360. Zhao M, Kircher MF, Josephson L, Weissleder R (2002) Differential conjugation of tat peptide to superparamagnetic NPs and its effect on cellular uptake. *Bioconjug. Chem.* 13(4): 840–844.

361. Zhivotovsky, B., Wade, D., Gahm, A., Orrenius, S., Nicotera, P., 1994. Formation of 50 kbp chromatin fragments in isolated liver nuclei is mediated by protease and endonuclease activation. FEBS Lett. 351, 150–154.

362. Zhu M-T, Wang B, Wang Y, Yuan L, Wang H-J, Wang M, Ouyang H, Chai Z-F, Feng W-Y, Zhao Y-L (2011) Endothelial dysfunction and inflammation induced by iron oxide NP exposure: Risk factors for early atherosclerosis. Toxicol Lett 203:162–171.

363. Zhu M-T, Wang Y, Feng W-Y, Wang B, Wang M, Ouyang H, Chai Z-F (2010) Oxidative stress and apoptosis induced by iron oxide NPs in cultured human umbilical endothelial cells. J Nanosci Nanotechnol 10:8584–8590.

364. Ziental, D., Czarczynska-Goslinska, B., Mlynarczyk, D., Glowacka-Sobotta, A., Stanisz, B., Goslinski, T. and Sobotta, L., 2020. Titanium Dioxide Nanoparticles: Prospects and Applications in Medicine. *Nanomaterials*, 10(2), p.387.

365. Zorko M, Langel Ü (2005) Cell-penetrating peptides: Mechanism and kinetics of cargo delivery. Adv. Drug Deliv:57, 529–545.

366. K., Αραι, N., 1994. Calcineurin activates transcription from the GM-CSF promoter in synergy with either protein kinase C or NF-kappa B/AP-1 in T cells. Biochem. Biophys. Res. Commun. 199, 1064–1072.

Appendix 1: Use of UV-Vis Results for calculation of NP concentration in Suspension

As is seen in **Figure 1** the MatLab script developed to calculate the concentration of the two TiO_2 polymorphs is presented. The results collected by DLS for the hydrodynamic diameter of the NPs; in addition to the UV-Vis results for absorbance of the NPs in suspension at 0h, 2h and 24h; were used to determine the concentration of the NPs in suspension. When the analytical relations between the extinction efficiency (q_{ext}) and diameter, acquired by other techniques such as dynamic light scattering (DLS) or electron microscopy (EM) (e.g. Transmission EM or Scanning EM), are established, a determination of the particle concentration (c) was accomplished by applying the Mie's theory (Paramelle *et. al.* 2014).

```
%% SCATTERING BY A titanium dioxide NANOPARTICLE USING MIE THEORY

%% inputs
%n_m optical index of the medium
%lambda0 wavelength in nm
%r0 radius of the particle in nm
%N=5 maximum n-pole
function [Qext,Qsca,Qabs]=MieScattering2(lambda0,r0,n_m)

%% parameters
n_An=indexRead(lambda0,'An'); %any function that returns the optical index of Anatase (An)/Rutile (Ru)
m=n_An/n_m;
k=2*pi*n_m/lambda0;
x=k*r0;
z=m*x;
N=round(2+x+4*x^(1/3))

%% computation
j=(1:N);
sqr=sqrt(pi*x/2);
sqrm=sqrt(pi*z/2);
phi=sqr.*besselj(j+0.5,x);
xi=sqr.*(besselj(j+0.5,x)+i*bessely(j+0.5,x));
phim=sqrm.*besselj(j+0.5,z);
phi1=[sin(x), phi(1:N-1)];
phi1m=[sin(z), phim(1:N-1)];
y=sqr*bessely(j+0.5,x);
y1=[-cos(x), y(1:N-1)];
phip=(phi1-j/x.*phi);
phimp=(phi1m-j/z.*phim);
xip=(phi1+i*y1)-j/x.*(phi+i*y);
aj=(m*phim.*phip-phi.*phimp)./(m*phim.*xip-xi.*phimp);
bj=(phim.*phip-m*phi.*phimp)./(phim.*xip-m*xi.*phimp);
Qsca=sum( (2*j+1).*(abs(aj).*abs(aj)+abs(bj).*abs(bj)) );
Qext=sum( (2*j+1).*real(aj+bj) );
Qext=Qext*2*pi/(k*k);
Qsca=Qsca*2*pi/(k*k);
Qabs=Qext-Qsca;
```

Figure 1: A screenshot of the text script that was used in Matlab. This was based on theoretical and practical physics from previous work done with Au and Ag NPs (Paramelle *et. al.* 2014).

Appendix 2: Additional results acquired in physioxia for i(Ca^{2+}) signalling

1. Cytosolic Ca^{2+} immediate response to MONPs treatments

Immediate response to the exposure of the distinct MONPs was investigated in all the cell lines. As is seen **Figure 2** in the physioxic culture environment (5% O_2) exposures were carried only for 2 concentrations for each of the NPs, for dSPIONs in concentrations of 0, 10, 100µg/ml, for NM-102 or NM-104 in concentration of 0 µg/ml, 10 µg/ml and 50µg/ml.

A dose dependent elevation of intracellular Ca^{2+} immediately after administration of the NPs (which occurred after 30s of measurements) was identified with a variation of intracellular Ca^{2+} elevation between the different cell lines and the distinct NPs. The elevation of intracellular Ca^{2+} was maintained for the period of 5min after treatment in all the experiments. The results presented here were used for comparison of the immediate response of the different cell lines, to the highest concentration of the different MONPs used for treatment in the different oxygen culture environments (seen in **Figure 5.4**)

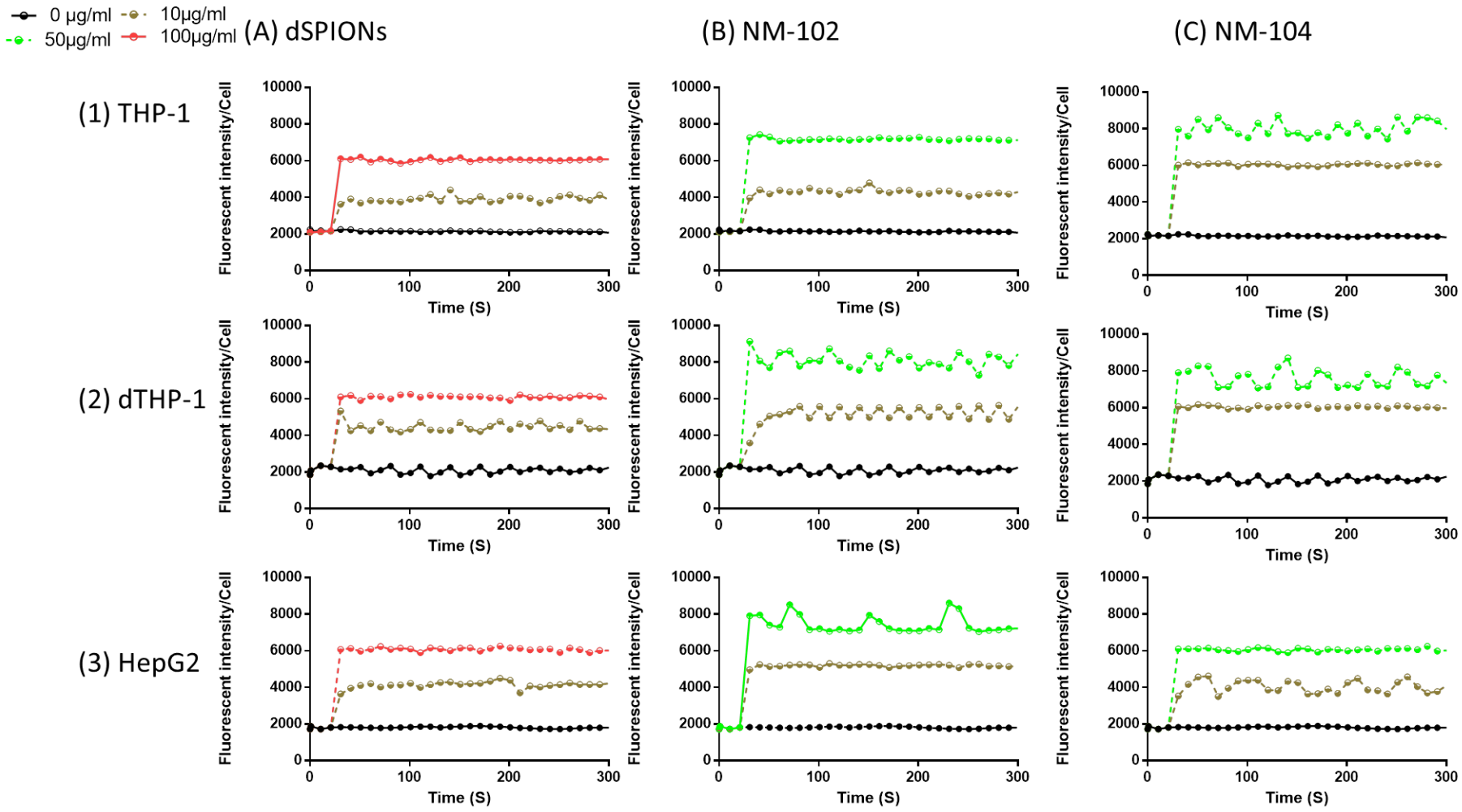

Figure 2: Immediate response of intracellular Ca^{2+} concentrations to treatments of the distinct metal oxide NM, namely, (A) dSPIONs, (B) NM-102 and (C) NM-104 in the Physioxic environment. Continuous measurements were carried for the period of 300s (5min), woth the NPs being injected after 10s, in the distinct cell lines under investigation, namely, (1) THP-1, (2)dTHP-1 and (3) HepG2. (n=9).

2. Intracellular Ca^{2+} responses to GPN/ MONPs treatment

After pre-treatment of the distinct cell lines, (namely, THP-1, dTHP-1 and HepG2) with the distinct MONPs for the period of 30min, GPN was administered as an injection at the time point of 20sec in each case. In the physioxic culture environment (5% O_2) exposures were carried only for 2 concentrations for each of the NPs, for dSPIONs in concentrations of 0 µg/ml, 10 µg/ml, 100µg/ml, for NM-102 in concentration of 0 µg/ml, 10 µg/ml and 50µg/ml and for NM-104 in concentration of 0 µg/ml, 10 µg/ml and 50µg/ml **(Figure 3).**

As with the results observed in the hyperoxic environment the administration of GPN (50µM for THP-1, 100µM for dTHP-1 and 200µM GPN for HepG2) at 20 seconds let to the increase in fluorescent intensity, indicate that increases in cytosolic Ca^{2+} were identified in all cell lines and NPs. The increase was broadly similar both oxygen culture environments as is seen in **Section 5.3.2.2.2**, all the cell lines and NPs showed elevation of cytosolic Ca^{2+} immediately after administration of GPN after 20s of measurements. Interesting was that variation of cytosolic Ca^{2+} elevation was identified between the cell lines and the distinct NPs. The elevation intracellular Ca^{2+} was maintained for the period of 80 seconds after treatment in all the carried exposures.

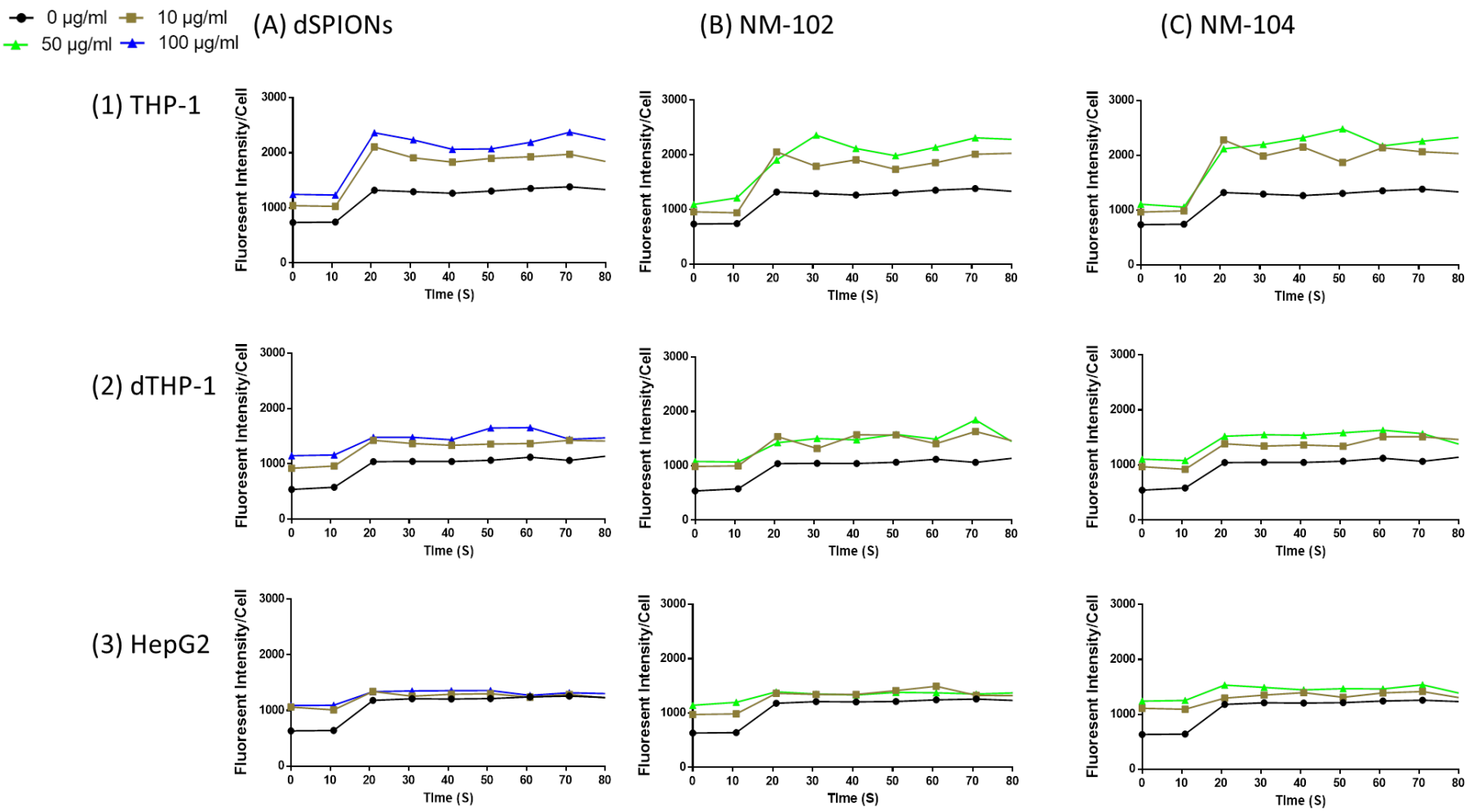

Figure 3: Continuous measurements of intracellular Ca^{2+} concentrations after treatments of the distinct metal oxide NM, namely, (A) dSPIONs, (B) NM-102 and (C) NM-104 and administration of GPN (at 20seconds) in the Physioxic environment. The continuous measurements were carried for the period of 80s in the distinct cell lines under investigation, namely, **(1)** THP-1, **(2)** dTHP-1 and **(3)** HepG2. The black arrow at 10s shows the time GPN was administered to the cells. (n=9).